COMPRESSIVE CREEP BEHAVIOR OF NEXTEL™ 720/ALUMINA CERAMIC MATRIX COMPOSITE AT 1200°C IN AIR AND IN STEAM ENVIRONMENT

THESIS

Neil R. Szymczak, Ensign, USN

AFIT/GAE/ENY/07-J20

DEPARTMENT OF THE AIR FORCE
AIR UNIVERSITY

AIR FORCE INSTITUTE OF TECHNOLOGY

Wright-Patterson Air Force Base, Ohio

The views expressed in this thesis are those of the author and do not reflect the official policy or position of the United States Navy, United States Air Force, Department of Defense, or the United States Government.

AFIT/GAE/ENY/07-J20

COMPRESSIVE CREEP BEHAVIOR OF NEXTEL™ 720/ALUMINA CERAMIC MATRIX COMPOSITE AT 1200°C IN AIR AND IN STEAM ENVIRONMENT

THESIS

Presented to the Faculty

Department of Aeronautics and Astronautics

Graduate School of Engineering and Management

Air Force Institute of Technology

Air University

Air Education and Training Command

In Partial Fulfillment of the Requirements for the

Degree of Master of Science in Aeronautical Engineering

Neil R. Szymczak, B.S.O.E.

Ensign, USN

June 2007

AFIT/GAE/ENY/07-J20

COMPRESSIVE CREEP BEHAVIOR OF NEXTEL™ 720/ALUMINA CERAMIC MATRIX COMPOSITE AT 1200°C IN AIR AND IN STEAM ENVIRONMENT

Neil R. Szymczak, B.S.O.E.

Ensign, USN

Approved:

//SIGNED//	
Dr. Marina Ruggles-Wrenn (Chairman)	Date
//SIGNED//	
Dr. Robert Canfield (Member)	Date
//SIGNED//	
Dr. Som Soni (Member)	Date

Abstract

The aerospace community continues to push the envelope in engineering aircraft that fly higher, faster, and safer while operating with a greater degree of efficiency. To meet these operational requirements innovative aerospace components must be designed to operate in aggressive environments. This research will investigate the ultimate compressive strength and the compressive creep behavior of Nextel^{TM} 720/Alumina ceramic matrix composite at 1200°C in air and 100% steam environments. The effects of creep loading history on the tensile and compressive material behavior will also be examined. The primary strengths of the N720/A composite are its oxide/oxide composition which inherently resists oxidation and a porous matrix which enables crack deflection producing enhanced matrix damage tolerance.

Mechanical testing showed a significant decrease in the compressive performance of N720/A when exposed to steam environment. Conversely, N720/A specimens tested in compressive creep in air experienced an increase in compressive performance. SEM analysis showed that densification of the α-alumina matrix occurred in both test environments. In air densification sinters the matrix resulting in a strengthening effect. Whereas, in steam environment analysis shows the addition of hydrogen induces hydrothermal softening of the matrix resulting in a significant loss of the compressive performance of N720/A.

Acknowledgments

I would like to thank the following people for their assistance during the course of my thesis; my faculty advisor Dr. Marina Ruggles-Wrenn for her guidance and support throughout the course of this work, thesis sponsors Dr. Ruth Sikorski (AFRL/PRTS) and Dr. Charles Cross (AFRL/PRTS) for supporting my research effort, Captain Jason Braun for sharing his thesis advice and knowledge of experimental procedures, Barry Page for his help with experimental arrangements, Sean Miller and Chris Zickefoose for their technical experience in SEM and optical analysis, Ensign Dan Solfelt and Ensign Patrick Laffey for their valued friendship and helpful advice during my research, and most of all my truly loving and support fiancé.

Neil R. Szymczak

Table of Contents

Page

List of Figures

Page

Page

Page

Page

Page

Page

Page

Page

Page

Page

Page

Page

Page

Page

Page

Page

Page

Page

Page

Page

Page

Page

List of Tables

Page

COMPRESSIVE CREEP BEHAVIOR OF NEXTEL™ 720/ALUMINA CERAMIC MATRIX COMPOSITE AT 1200°C IN AIR AND IN STEAM ENVIRONMENT

I. Introduction

For thousands of years composite materials have been used to enhance the quality of human life. During the primitive age straw was added to clay to produce reinforced bricks. Now, in the twenty-first century we see the application of composites in everyday life, ranging from roadways formed of steel and aggregate reinforced Portland cement to fiberglass bathtubs and cultured marble countertops [75]. With a greater understanding of composites advances are not limited to such simple applications, but rather extend to great feats of engineering.

Perhaps, the engineering field that stands to gain the most from the use of composites is the aerospace industry. The unique demands of aircraft design are stringent. A material must exhibit high durability and consistent performance while undergoing prolonged and repeated use. Additionally, it must be lightweight to maximize the capacity and efficiency of aeronautic components. Attributes such as high strength to weight ratio, low life cycle cost, maintainability, and reliability make composites ideal for use in aerospace applications [16:4-9].

In fact the aerospace industry has been benefiting from the use of composites since the early 1950's when Boeing introduced the 707, one of the most reliable jetliners

in the world [7]. Since then several aircraft have been composed almost entirely of composites, for example the Air Force B-2 Spirit [16:7]. Today, composites continue to be used in the manufacturing of the most modern aircraft designs. Airbus A380, the world's largest jetliner, recently introduced in 2005, is comprised of 25% composites by weight [74].

Although composites have advanced aerospace technology by providing lightweight durable materials, in the past they have lacked strong performance under elevated temperature. Materials such as ceramic matrix composites (CMC) and carbon/carbon composites have been developed to meet the ultra-high temperature requirements of future jet turbine designs. As of late these materials have sparked the most interest in the engineering community due to their proven reliability, low weight, and promising performance under high temperature.

Testing has shown that these materials do in fact provide enhanced durability under elevated temperatures. However, some shortcomings were discovered. When exposed to oxidizing environments such as steam these newer composites degraded at a much higher rate. This prompted the development of all-oxide CMCs which resist oxidation in typical operating environments, but display less favorable mechanical behavior than non-oxide counterparts [63:1]. Nextel^{TM} 720/Alumina (N720/A) composite, is the latest effort in correcting the oxidation problem encountered by CMCs with non-oxide fibers. The objective of this investigation is to examine the compressive creep characteristics of N720/A CMC at 1200°C in air and steam environments. Furthermore, it is important to examine the effects of creep loading history on the tensile and compressive material behavior of N720/A, in order to better design CMC material

systems that resist oxidation, and exhibit superior strength under severe temperature conditions.

II. Background

2.1 Ceramic Matrix Composites

2.1.1 Composites

The concept of a composite is simple. Place two substances together, that generally have opposite strengths, and create a single material that benefits from both. Fundamentally, a composite is a material that combines two chemically or physically distinct phases into one form. As displayed in Figure 1, the continuous phase is called the matrix while the distributed phase is referred to as reinforcement. The latest addition to the field of composites are CMCs. In the past, monolithic high performance ceramics have displayed incredible strength and hardness at high temperatures. However, poor performance was revealed when monolithic ceramics were subjected to tensile and compressive loading. Even worse, these ceramics had a tendency to fail without warning in a catastrophic manner under mechanical and thermal loading; making these types of materials unlikely candidates for use in the aerospace industry [14:1-4].

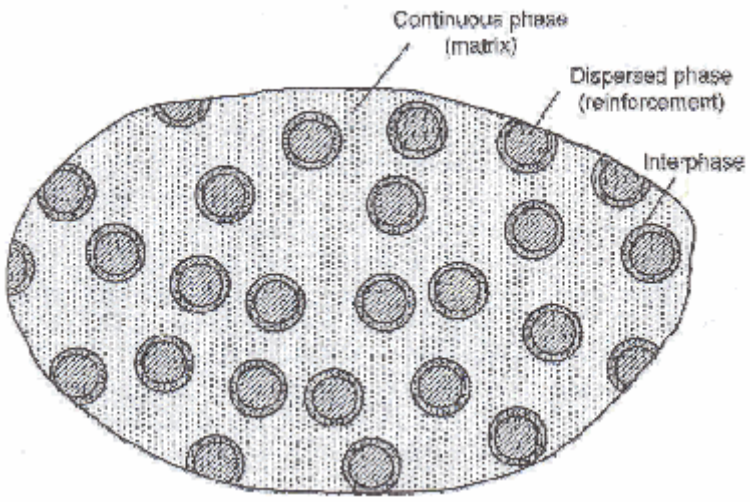

Figure 1. Composite Phases [16:1].

As a result of these previous findings a method for harnessing the capability of ceramics to withstand incredible heat was engineered in the form of ceramic matrix composites. The primary goal of CMC was to make ceramics fail "gracefully", meaning to show signs of deformation before failure while also increasing the threshold of mechanical loading [14:4]. Ceramics are the prime candidate materials because they are the only substance that can reliably operate above temperatures of 1100°C. Polymers and metals have the advantage of deforming plastically before failure, however, Figure 2 shows that ceramics have the capacity to withstand much higher temperatures. Due to the heat resistant quality of ceramics they are ideal for applications in demanding environments such as operating environments of rocket nozzles, heat exchangers, automobile engines and cutting tools [14:5].

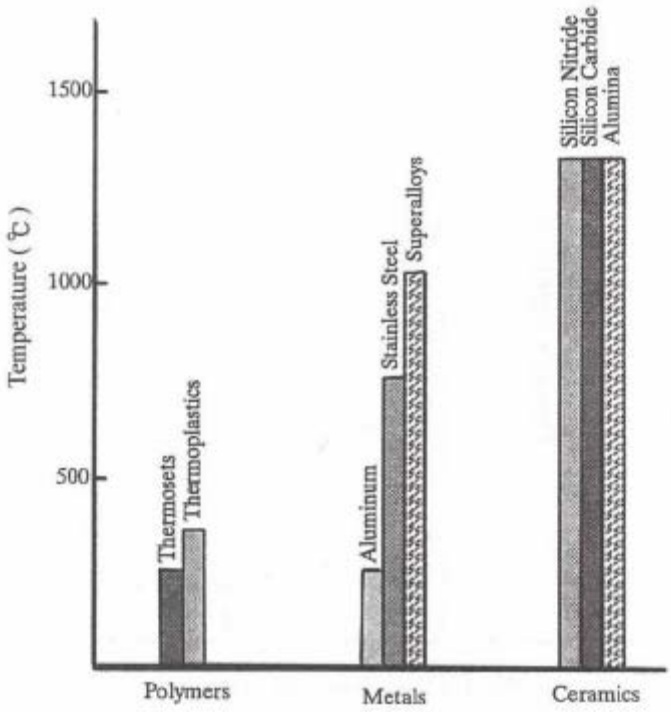

Figure 2. Maximum Material Service Temperatures [14:5].

In nature ceramics exist in both crystalline and non-crystalline form (i.e. general ceramics vs. glass). Ceramics are held together by mostly ionic bonds and some covalent bonds. Some common crystal bonding structures include: simple cubic, close-packed cubic, and hexagonal closed packed. Ceramic characteristic strength and brittleness can be attributed to these bonding configurations [14:11-13]. However, with the addition of fibers the high temperature resistance of ceramics can be complemented by higher fracture toughness of a CMC. Fibers can provide energy dissipating qualities such as fiber matrix debonding, loading to crack deflection, and subsequent fiber pullout [14:7]. These attributes greatly enhance the potential of CMCs by significantly increasing damage tolerance.

2.1.2 Fibers

The primary purpose of reinforcement is to strengthen the matrix by enhancing its mechanical loading characteristics. The reinforcement phase can be situated in several orientations. Some reinforcements are distributed in particle form as whiskers or as short fibers measuring only a few mm in length. Long fibers are called continuous because they run the entire length of the composite material. Continuous fibers sometimes labeled as filaments or monofilaments are laid out in the matrix in bundles of fiber called tows. When comparing different composites the number of fibers in each tow may vary. Tows are then twisted among each other to provide strength in the form of bundles of tows referred to as yarn [27:3].

Fibers can be arranged in several different architectures throughout the matrix. The two primary types of architectures are woven and laminate. Woven fibers are

interlaced among each other in a variety of methods such as a plain weave or satin weave. On the other hand, laminate fibers are simply laid on top of one another in the matrix in an organized fashion. The difference between these two fiber architectures involves the freedom of fibers to move during mechanical loading and the overall porosity of the resulting composite. Composites reinforced with woven fibers tend to be more porous than laminates due to the space created by interlocking the tows; the more favorable configuration depends on the intended application of the material. These architectures are important because fibers provide the majority of tensile strength in CMC materials.

Ceramic fibers have proven to be exceptionally reliable at high temperatures and under substantial loading. However, fibers will frequently be exposed to oxidizing environments when used in aerospace applications. This was a problem for non-oxide fiber material, which heavily degrades in mechanical loading capacity when oxidation occurs. Fiber coatings were added in an attempt to prevent oxidation. However, some of these coatings breakdown at high temperatures rendering them ineffective; additionally they add cost to the fabrication process making them an unsatisfactory design solution. The current solution to the oxidation process is to manufacture all-oxide CMCs that resist oxidation even in the most aggressive environments. Review of mechanical properties shows that oxide fibers typically perform worse than non-oxide fibers [41:6]. The most recent effort to solve the oxidation problem while maintaining the strength characteristics of non-oxide fibers is Nextel^{TM} 720/Alumina composite; the material featured in this research.

2.1.3 Matrix

The matrix is the continuous phase that provides the shape of the material. The primary functions of the matrix are to transfer load between fibers, separates fibers to prevent adjacent tows from failing, and to protect and house the fibers from environmental attack [5:7]. A clear illustration of the fiber/matrix relationship is depicted in concrete reinforced with steel bars (rebar). Concrete is very strong in compression but lacks strength in tension. In some applications concrete will experience tensile loadings therefore it is cast with rebar to allow for this design criteria. Much like a CMC, the combination of two constituent materials provides a concrete that has multidimensional capabilities.

In order for a material to qualify as an acceptable matrix it must meet several criteria. Ceramic matrix material should form a mechanical or frictional bond with the reinforcement and should not react chemically with the fibers during fabrication or service. Additionally, the matrix should not damage the reinforcement and it should provide resistance to creep, fatigue, and impact loading, while exhibiting high toughness [14:44]. Generally, fiber used as reinforcement should have the same or similar coefficient of thermal expansion as the selected matrix, to prevent undue internal stress in the material when exposed to extremely high temperature. This is why ceramic fibers typically reinforce ceramic matrix materials. Although very few matrix materials meet all of these requirements, composite materials are always engineered to exhibit the most desirable characteristics.

Some common ceramic matrix materials include α-alumina (Al_2O_3), mullite ($3Al_2O_3$-$2SiO_2$), Boron Nitride (BN), Boron Carbide, and Carbon [14:35-38]. Most of

these ceramic compounds have low density, high melting point, and a high degree of hardness which make them ideal for use in various CMCs. α-Alumina is the most stable ceramic in a variety of environments such as air, oxygen, and argon. Although α-alumina is not the most heat resistant ceramic material it has a high melting point of 2050°C [14:35]. The CMC featured in this research takes advantage of an α-alumina matrix to operate effectively at high temperatures.

One of the most important aspects of an effective matrix/fiber relationship is the connection between the two phases often referred to as the interface of the composite. Contrary to intuition, experimentation has shown that having a weak fiber-matrix interface is more advantageous than having a strong fiber-matrix interface. The reason this is structurally beneficial is due to crack deflection. When a crack forms it is better for it to propagate between the fiber through the matrix, rather than propagating through both matrix and fiber; causing the composite to fail catastrophically [23:607]. The crack deflection mechanism provides CMCs with higher fracture toughness and the benefit of exhibiting delayed failure rather than catastrophic failure. Figure 3 shows both types of interface and different types of fracture mechanisms.

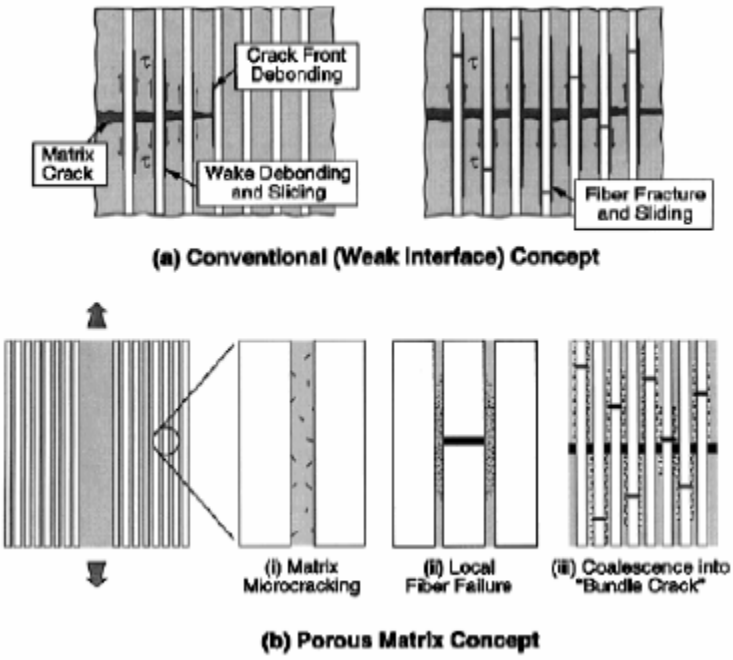

Figure 3. Schematics of the Damage Processes that Enable Damage Tolerance in a) Conventional Dense-Matrix Weak-Interface CMC and b) Porous Matrix CMCs Without Fiber Coatings [79:15].

Similar to fibers, ceramic matrix material can be categorized as either oxide or non-oxide compounds. As with fiber selection, choosing ceramic matrix materials that are already oxidized is preferred to non-oxide materials. At high temperatures and in oxidizing environments, non-oxide matrix material is susceptible to degradation and a loss of mechanical properties. Matrix materials such as α-alumina and mullite are the most commonly used oxide substances in the fabrication of CMCs. When exposed to various loading scenarios it is important that both the fiber and the matrix resist oxidation in order to maintain the structural integrity and durability of a component. When monolithic ceramics are paired with reinforcing fibers of similar properties and structure, a brittle material can be transformed into a composite with a high damage tolerance

capable of providing strength at the ultra-high temperatures commonly encountered in aerospace applications [4:565].

2.1.4 All Oxide CMCs

Oxide-oxide ceramic matrix composites are materials composed of oxide fibers surrounded by an oxide matrix. The ability to resist oxidation is an inherent quality of all-oxide CMCs. Not only is it important for a CMC to resist oxidation on its exterior surface it is crucial that if a crack forms and the oxidizing environment reaches the interior the fiber has a similar oxidation resistance. This is the reason that CMCs that combined oxide and non-oxide materials did not exhibit environmental durability required for a material expected to operate under loading at extreme temperatures in an oxidizing environment for prolonged periods of time [27:10].

There are two ways to provide for crack deflection and to achieve damage tolerance in a CMC. The first method relies on a weak fiber-matrix interface, frequently accomplished by using fiber coating. The second design philosophy accepts the strong fiber-matrix interface and achieves crack deflecting behavior by means of a finely distributed porosity in the matrix. This research involves N720/A, a porous matrix CMC, designed to exhibit inherent oxidation resistance and high strength as well as stiffness.

2.1.5 Fabrication of CMCs

The manufacturing process of a CMC is one of the most crucial steps in the life cycle of the material. In order to benefit from the unique design and exceptional attributes of CMCs in aggressive environments, fabrication must be consistent and

precise. The first step in the processing of a CMC is appropriate selection of a fiber and matrix combination. There are a number of different conventional methods for fabricating the matrix material; some of these include sintering, injection molding, hot isostatic pressing (HIP), chemical vapor deposition (CVD), and reaction forming [14:20-22]. In general the following steps apply to the processing of the matrix material. The matrix starts in a powder form and is prepared for the ensuing process. The powder is then formed into a desired shape by using a binder called a green body. The green body is then sintered at high temperatures to densify the material; sometimes a combination of hot pressing is involved. Finally, the sintered material is formed into a desired shape for use in a component [14:20].

Much like matrix materials, fibers are processed with a similar type of precision to ensure that the finished product has desirable reinforcement qualities. Such attributes include high theoretical density (low porosity), small grain size for low temperature applications, large grain size for high temperature applications, and high purity [14:64]. These traits heavily rely on the fabrication method and the type of material used. The Nextel^{TM} 720/Alumina CMC featured in this research benefits from fibers that are comprised of 85% α-alumina (Al_2O_3) and 15% mullite (SiO_2) by weight and are fabricated by the 3M Corporation in the following basic steps. An organic basic salt solution is used as a precursor. Then the organic material is driven out by decomposing or volatilization. In order to maintain the design characteristics it is important to ensure that no defects such as cracks or blisters form as the organic material is being driven away. Next the fibers are fired at 1400°C under carefully controlled conditions. Finally, the fibers will undergo a straightening treatment at lower temperatures [14:69]. It is

important to note that because this material is fired/sintered at such a high temperature it will develop larger grain size ideal for use at elevated temperatures, making this type of fiber a good candidate for use in aerospace components.

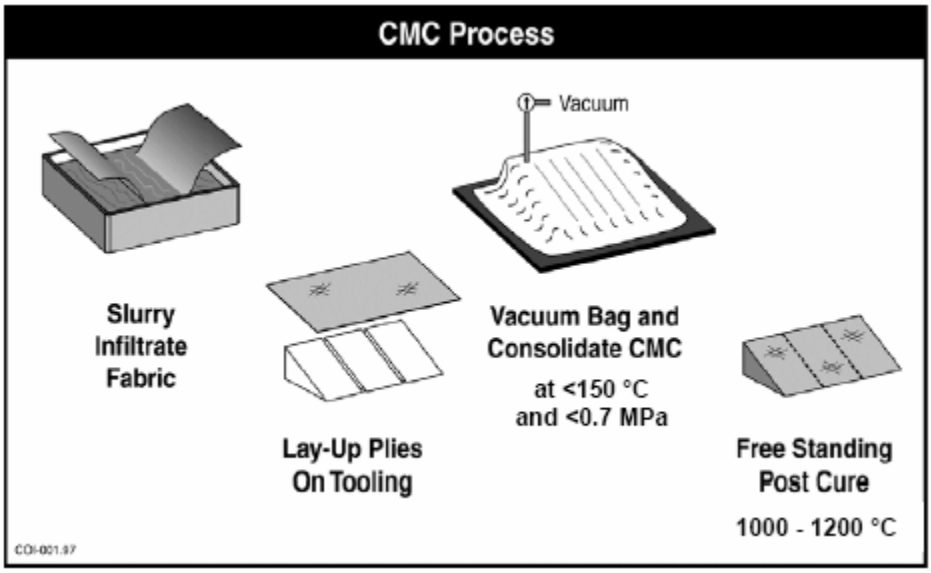

Figure 4. Representative steps of fabric-based CMC manufacturing process [31].

Once both the matrix and reinforcement materials are fabricated individually they can be combined together in any number of desired orientations with continuous or whisker reinforcement. The fibers are laid-up in the unconsolidated matrix and the final process involves consolidating the matrix into its finished form. Figure 4 illustrates the process by which fiber and matrix are combined to make a CMC.

2.2 Aerospace Applications

Ceramic matrix composites possess several qualities which make them desirable for use in aerospace applications. Such qualities include fracture strength, toughness, temperature resistance, oxidation resistance, and reliability. The unique requirements of aerospace engineering include designing components that will increase the performance and efficiency of aircraft while reducing the cost of operation and maintenance without sacrificing reliability [14:399]. During the late twentieth century CMCs started appearing in several civilian and military aircraft. As fabrication becomes cheaper and material properties are established, ceramic matrix composites will become more prevalent in the structural and mechanical components of modern aircraft.

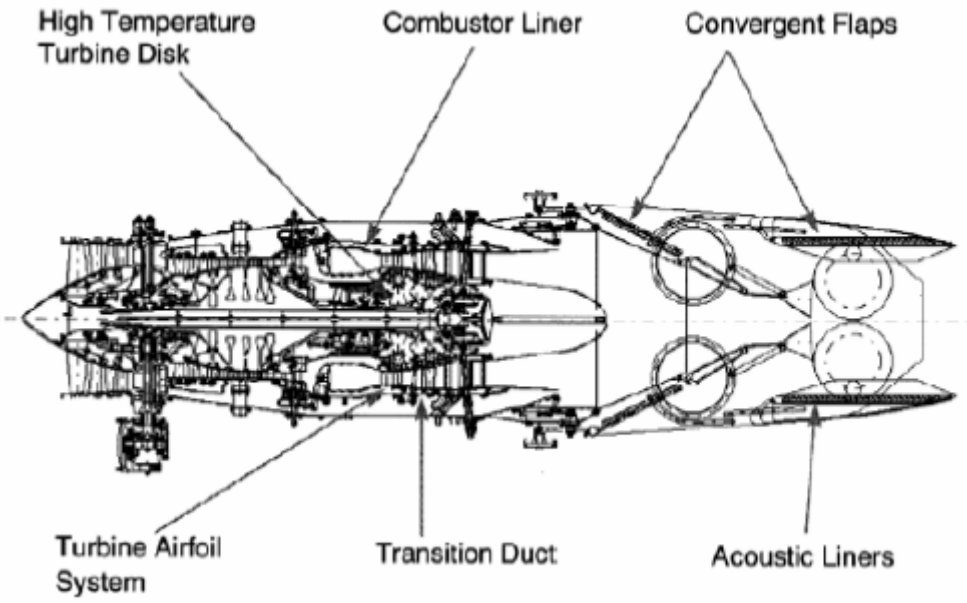

Figure 5. Potential Engine CMC Applications [52:492].

CMCs are ideal for use in aerospace platforms such as satellites, space vehicles, and turbine engines. Components that typically operate at very high temperatures will

certainly benefit the most from the advancements made in composites. Nearly all components found in turbine engines will have the potential to be constructed using CMC materials. Figure 5 labels some specific components found in turbine engines that will benefit from the advancement of CMC materials. Other components include nozzle flaps, exhaust nozzles, combustor, turbine vanes, and blisks (bladed disks) [52]. If these components are manufactured using environment specific CMC material, engines which normally operate with cooling systems will be able to operate without cooling at temperatures of 1400°C without sacrificing performance or safety [5:17,41:50]. Additionally, oxidation resistance will be provided by all-oxide materials. The future of the aerospace industry will be undoubtedly optimized by the incredible capability and versatility that these materials can provide.

2.3 Failure Mechanisms

In order to effectively characterize the performance of specific ceramic matrix composites it is important to understand how failure occurs on the macroscopic level. Under mechanical loading CMCs fail when the ultimate strength of one of the two phases is reached. Whether the matrix fails first or the fiber fails depends on the type of loading the material undergoes. Previous research has shown that the matrix generally fails first when a CMC is exposed to tensile loading. On the other hand when similar CMCs are loaded in compression the fibers tend to fail first resulting in a very distinctive fracture surface.

Due to the fact that this research focuses on the compressive creep behavior of N720/A CMC, further discussion of compressive failure mechanisms is necessary. There

are three basic modes of failure when a CMC is exposed to compression; the first involves longitudinal splitting of the fiber-matrix interface. This type of failure is characterized by a shearing of the fibers and matrix usually due to a weak interface. This failure mode illustrated in Figure 6, is common among CMCs with a fiber coating (weak interface) [27].

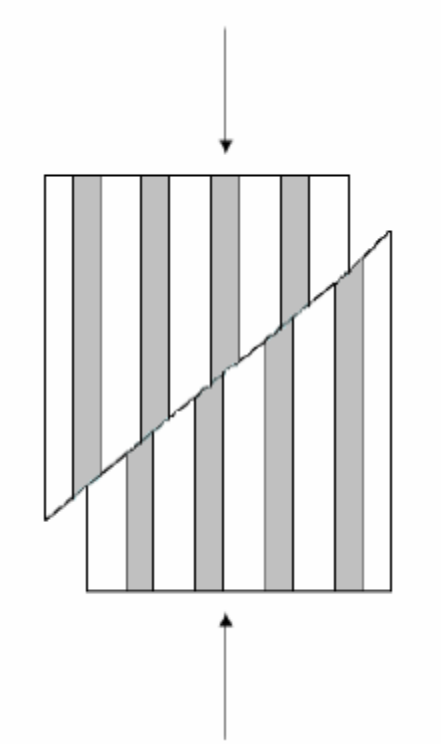

Figure 6. Schematic of Shear Failure Mode of Unidirectional Composite Under Longitudinal Compression [27].

The second mode of failure is referred to as fiber buckling or kinking. This type of failure occurs when the fibers bend under loading forming kink bands. Typically, the kink bands form at angles between 20°-30° relative to the plane normal to the direction of the fibers. This mode eventually causes the fibers to fail, therefore eliminating the CMC's ability to carry load.

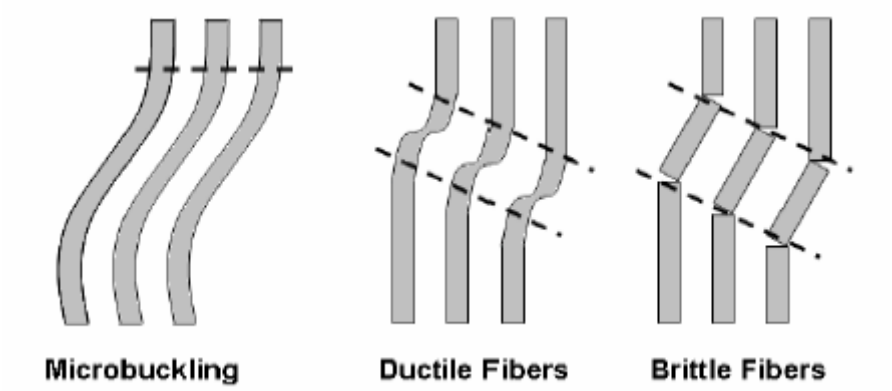

Figure 7. Schematic of Microbuckling, which Leads to Excessive Deformation in Ductile Fibers or Fracture Planes in Brittle Fibers [27].

The third mode of failure is called "crushing." This occurs when the axial strain within the composite attains a value equal to the critical crushing strain of the fibers. Interestingly, technological advancements in fiber fabrication and implementation have provided fibers with increased axial performance. Therefore crushing failure mode rarely occurs due to the fact that fiber buckling will happen first.

2.4 Previous Work

Recently, much research concerning ceramic matrix composites has been conducted to determine their structural integrity when exposed to mechanical loading, high temperature, and aggressive environments. Two of the most advanced CMCs previously investigated are Nextel^{TM} 610/Alumina with monazite coated fibers and Nextel^{TM} 720/Alumina. Both materials have been thoroughly tested in multiple loading scenarios to provide data concerning which materials perform best under different loading histories. Such scenarios include subjecting N720/A and N610/M/A to tension, compression, and cyclic loading while at a wide range of high temperatures. Valuable information on both types of CMC was collected and analyzed.

Harlan investigated the effect of 100% steam and laboratory air environments on the tensile creep performance of N720/A at 1200°C and 1330°C. Monotonic tensile tests were performed in order to determine the ultimate tensile strength of the N720/A at both temperatures. As a result several stress levels were selected for use in creep tests at high temperatures. This research concluded that while tensile creep resistance was good at 1200°C in laboratory air, the presence of steam significantly degraded creep resistance, especially at 1330°C [22,60].

Mehrman investigated the effect of hold times at maximum load on fatigue performance of N720/A at 1200°C as well as the effects of load history on the retained durability. This research showed that material performance is degraded significantly in the presence of steam. Testing also revealed that prior fatigue in air environment resulted in an order of magnitude increase in creep life [41:83-84,42]

Hetrick investigated the effect of frequency on the fatigue response of N720/A at 1200°C in both air and steam environments. This study focused on the frequencies of 0.1 and 10 Hz. The research showed a considerable decrease in fatigue performance when tested in steam as opposed to in laboratory air. It was revealed that specimens tested at 0.1 Hz exhibited shorter fatigue lives and smaller strains at failure than those tested at 10 Hz. It was also interesting to note that a higher degree of fiber pullout and a more fibrous failure surface occurred in specimens tested at 10 Hz. These observations, led to the conclusion that the fiber-matrix interface was weakening significantly at the higher frequency level [25:71,59].

2.4.1 Off-Axis Behavior of CMCs

The previously mentioned research endeavors were all concerned with an on-axis testing of specific CMC material. This means that loading was directed along the 0° fibers. However, there has been much interest in exploring how these CMCs would respond to an off-axis loading scenario such as can be imposed on a composite with a ±45° fiber orientation. The value of such testing is easy to see when considering that under operational conditions the highest loads are not always applied in the direction of the reinforcing fibers.

A study conducted by Siegert evaluated the tensile creep performance of N720/A with a ±45° fiber orientation at 1200°C in laboratory air and steam. Creep-rupture tests were completed in all environments at stress levels of 45, 40, 35, and 15 MPa. The ultimate tensile strength of N720/A with a ±45° fiber orientation was 55 MPa with an elastic modulus of 45 GPa and a failure strain of 0.265%. As expected, testing showed that an increase in creep stress level caused a decrease in creep life. The material was found to perform best in air followed by steam and then argon, disproving the theory that N720/A performs best in non-oxidizing environments. Specimens tested at stress levels $\leq$35 MPa exhibited strong creep performance, all achieving creep run-out set to 100 hr at 1200°C [62,65]. Furthermore, Scanning Electron Microscope investigation showed a correlation between coordinated fiber bundle failure and decreased creep life.

2.4.2 Compression

Previously, little importance was placed on investigating the compressive behavior of CMC materials. In fact this research effort is the first formal attempt to

assess the compressive properties of Nextel^{TM} 720/Alumina ceramic matrix composite. This study focuses on compressive properties and the compressive creep behavior of N720/A. In an earlier study Jackson reported on the compressive creep behavior of N610/M/A, also a porous matrix CMC. However, there are several very important features of these two CMCs that differ substantially and have the potential to greatly affect the compressive creep behavior of each material.

A primary difference between N610/M/A and N720/A is the interface. The N610/M/A has monazite fiber coating which provides a weak interface between the fiber and the matrix. Conversely, the N720/A relies on a porous matrix for crack deflection. Another difference between the two materials is the fiber architecture. The N610/M/A uses a laminate fiber architecture which means layers of fiber and matrix are constructed on top of one another. On the other hand the N720/A CMC is constructed using woven 0°/90° fiber fabric layers. The structural difference paired with the interface distinction may cause N720/A to perform in a different manner than the N610/M/A CMC.

As previously mentioned Jackson determined the compressive properties and studied compressive creep behavior of N610/M/A at both 900°C and 1100°C. This CMC is fabricated with unidirectional layers in a symmetric cross-ply $(0°/90°/0°/90°)_s$ orientation and was tested on-axis. This research revealed that the monazite coating resulted in the loss of compressive strength at both investigated temperatures. The creep behavior was unaffected by the monazite coating at 900°C. However, at 1100°C, greater creep strains were accumulated by the monazite-containing composite. It is important to note that all specimens tested at various stress levels between 50 and 95 MPa achieved creep run-out set to 100 hr [27:91-92,28].

2.5 Thesis Objective

The objective of this thesis is to explore the compressive creep behavior of Nextel^{TM} 720/Alumina at 1200°C in air and steam environments. Additionally it will be imperative to establish information concerning the ultimate compressive strength of N720/A at 1200°C. This research will be conducted with the mission of establishing limitations on the use of this material in high-temperature aerospace applications.

III. Material and Specimen

3.1 Nextel™ 720/Alumina Ceramic Matrix Composite

Nextel™ 720/Alumina is the CMC material featured in this research. N720/A CMC has no interface between the fiber and matrix and relies on a porous matrix for flaw tolerance. Extensive research into the tensile behavior of N720/A CMC has resulted in favorable and promising findings. Compressive behavior at elevated temperatures must be investigated to completely understand the capabilities and limitations of this material.

3.1.1 Nextel™ 720 Fiber

Fiber found in N720/A is manufactured by Minnesota Mining and Manufacturing Company (3M™). This fiber is composed of 85%Al_2O_3 and 15%SiO_2 by weight in the form of α-alumina (41 vol %) and mullite (59 vol %) [45]. These fibers are distributed along the entire length and width of the matrix material in a continuous manner with a 0°/90° orientation. At the microscopic level the structure of N720/A is quite intricate. α-Al_20_3 appears in the fiber in the form of small elongated grains with sizes less than 0.1 μm. In addition mullite and Al_2O_3 both appear in larger mosaic crystals with grain sizes up to 0.5 μm [77].

These fibers are designed to give N720/A the ability to withstand tensile loading at high temperatures. The N720/A fiber exhibits better creep performance than any other commercially available polycrystalline oxide fiber [77]. One of the reasons why N720/A fiber demonstrates better creep performance than other fibers is due to the absence of non-crystalline phases in the fibers. It is interesting to note that creep performance of

α-alumina is inversely proportional to grain size [75]. The exact process by which the N720/A fiber is fabricated is proprietary, however it does follow the basic steps of the sol gel process previously discussed.

3.1.2 Alumina Matrix

Nextel^{TM} 720/Alumina CMC material employs a porous α-alumina matrix. The alpha form of alumina is thermodynamically stable and has a high melting point of 2050°C. In the form of a monolithic ceramic, α-alumina is very strong with a strength range of 300 to 900 MPa depending on grain size. Its Young's modulus is 380 GPa. However, it is very brittle. Therefore the addition of fibers is extremely beneficial to its characteristics [14:13,40].

A fine grained α-alumina structure is generally desirable at low temperatures because at low temperatures, both strength and toughness increase with decreasing grain size. However, in this CMC a larger grain size α-alumina was used to satisfy the need for the CMC to perform at aerospace turbine temperatures. A commercial mainstay in ceramics is α-alumina reinforced by zirconia to increase toughness. Zirconia particles change the molecular structure of α-alumina by increasing its volume and creating a hexagonal closed packed orientation [14:35]. This research will primarily focus on the microstructure of the porous matrix, specifically the densification of the porous matrix and its effects on compressive creep behavior.

3.2 Specimen Development

3.2.1 Material Processing

The micrograph displayed in Figure 8 shows the fiber-matrix interface of an as-processed virgin specimen. The granular substance surrounding the circular fibers is an α-alumina matrix which exhibits a porous nature. Due to the fact that N720/A composite employs a strong bond between fiber and matrix, the inherent porosity of α-alumina is essential to providing crack deflection around fibers. During fabrication it is important for the material to be manufactured with precision, so as to ensure the structural design is comprised of the appropriate material constituents. The physical properties of the N720/A composite used in this investigation are displayed in Table 1.

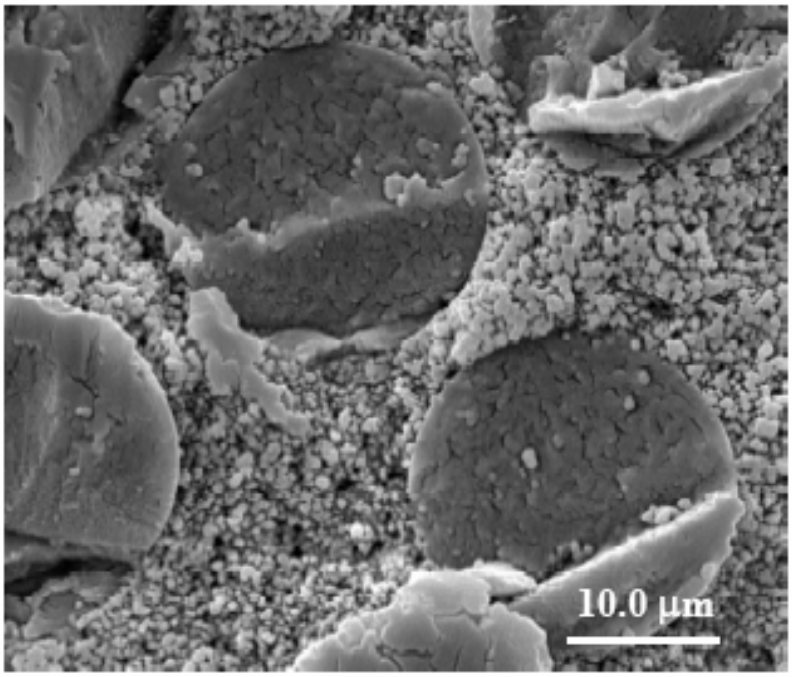

Figure 8. Micrograph of as-processed virgin N720/A composite. Porous nature of matrix is apparent [37].

Table 1. Characteristic Properties of N720/A Panel.

	Fiber vol (%)	Matrix vol (%)	Porosity (%)	Density (g.cc)
6656-3	46.6	31	22.3	2.83

The ceramic matrix composite material studied in this research was Nextel™ 720/Alumina (N720/A), manufactured by Composite Optics, Inc. (COI) Ceramics, a division of ATK Space Systems. The composite was supplied in a form of a 5.2 mm thick panel comprised of 24 0°/90° woven layers, with fibers woven in an 8 harness satin weave.

Test specimens were cut using abrasive water-jet machining to specifications shown in Figure 9. Plexiglas sheets sandwiched the panels during cutting to reduce fraying at the edges of the specimens. After machining, the specimens were cleaned to remove any residual debris from the water jet machining. The cut specimens were placed into an ultrasonic bath of deionized water for 20 min., then soaked in 200-proof ethyl alcohol for 20 min., and finally, dried in an Omegalux LMF- 3550 Bench top Muffler Furnace at 250 °C for 2 hours.

3.2.2 Specimen Geometry

Due to the unique demands of this research the specimens were cut in a rectangular shape as opposed to the dog bone shape usually employed in tensile tests. The reason for this change was to minimize the chance of buckling. For each specimen to provide valuable information it must fail in pure compression. With a wider and thicker cross section, and special care taken when aligning the test machine and mounting

the specimen, buckling was easily avoided. In the past, anti-buckling devices have been used to remedy this problem, however this is not a practical solution at 1200°C.

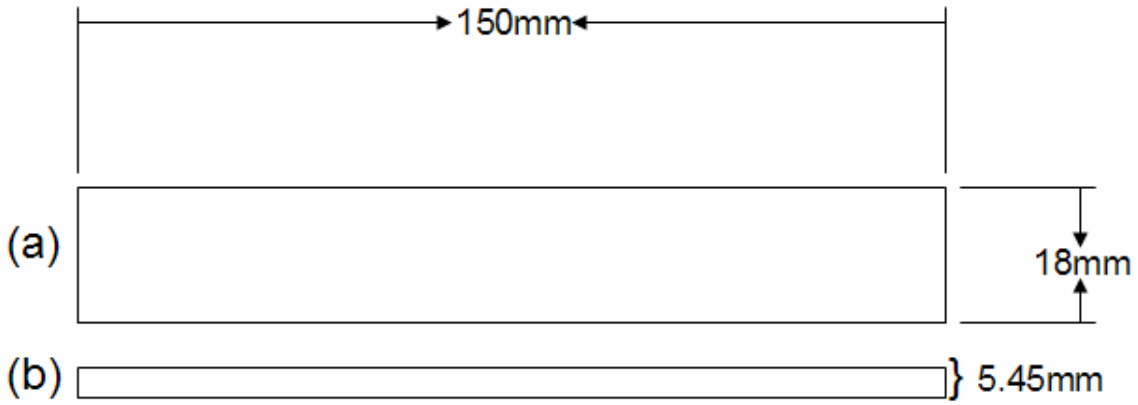

Figure 9. Test Specimen: (a) top view, (b) side view.

3.2.3 Specimen Tabbing

Before a specimen could be tested it had to be properly prepared to withstand grip pressure. Fiberglass tabs were bonded to the grip section of the specimens with M-Bond 200 adhesive. The tabs protected the specimen surface from being damaged by the grip wedges.

IV. Experimental Arrangements and Test Procedures

4.1 Testing System and Components

There were several components used in this research in order to test specimens under load, at extremely high temperatures, and in different environments. The components used include a servo hydraulic testing machine, a digital controller with associated software, extensometer, high temperature ovens, steam generator, chiller, and susceptor. All of these components were used in each compressive creep test with the exception of the susceptor and steam generator, which were only used for testing in steam environment.

Figure 10. MTS 810 Test Station.

The primary system used in this research was the servo hydraulic machine manufactured by Material Testing Systems (MTS) Corporation. The axial 810 Material

Testing System with a 25 kN (5.5 kip) capacity shown in Figure 10, was used for compression to failure tests and compressive creep tests. This system was equipped with hydraulic wedge grips which were used to apply a pressure of 10 MPa to the grip points of the specimen.

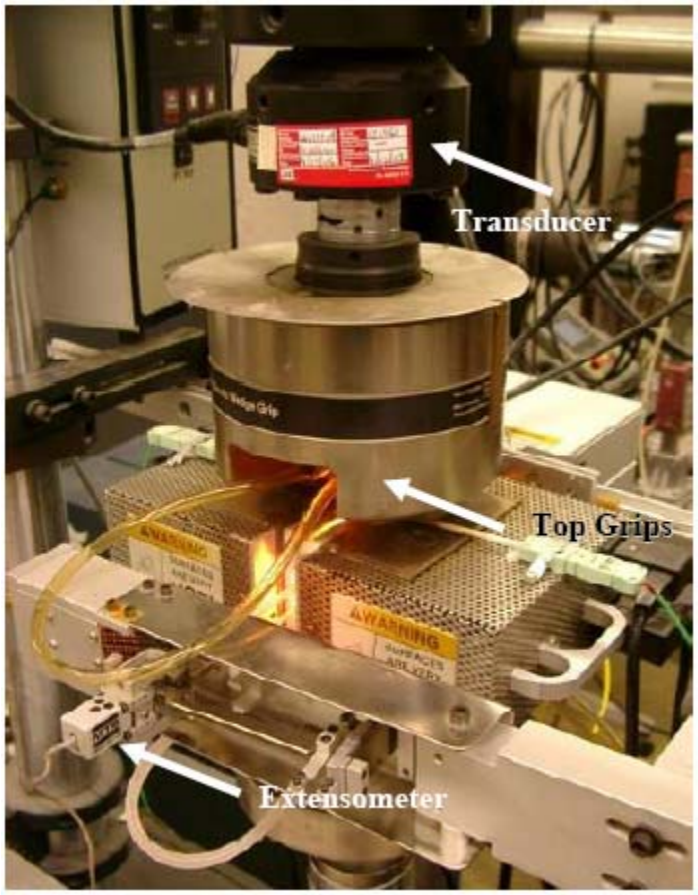

Figure 11. Test System Close-up.

The controller used in this research was the TestStar II digital controller displayed in Figure 12. This controller was used to generate input signals and was able to store large amounts of data. Throughout each test several signals of information were sent to a file designated by the specimen name. These signals included force, force command, displacement, displacement command, temperature in each oven, strain, and time.

Multipurpose Testware (MPT) was the software used to program test histories and for data acquisition. The software allows the user to create specific programs for testing in different control modes.

Figure 12. MTS Temperature Controller.

During testing it was imperative to measure the strain experienced by the specimen. The component used to measure strain levels is the called the extensometer. Displayed in Figure 13, the extensometer used in this research was an MTS axial high-temperature low contact force extensometer of 12.5-mm gage length. By using two alumina extension rods, 3.5 mm in diameter and 151 mm in length the extensometer was protected during high-temperature tests. The tips of the rods are sharp to ensure firm contact with the specimen; if the extensometer were to slip test results would be inconclusive. The extensometer is placed behind a heat shield and air-cooled.

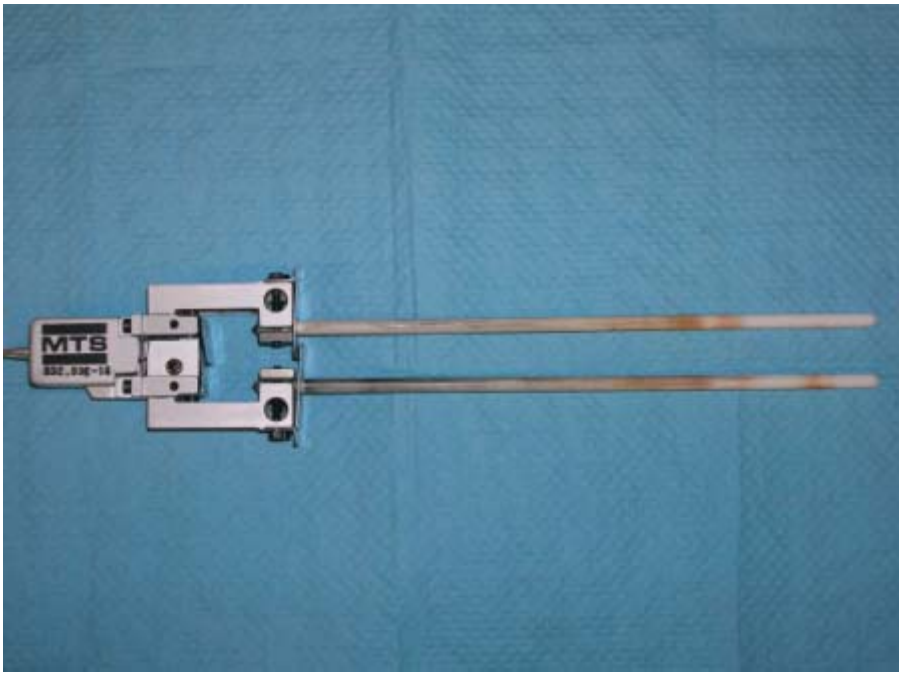

Figure 13. MTS Extensometer.

The component used to heat the specimen to the desired temperature was the oven. Shown in Figure 14, the oven is comprised of several parts. It is surrounded by an extremely heat resistant alumina casing which seals completely around the specimen. The heating elements are small devices located inside the alumina casing which convert electricity to heat. Thermocouples in the oven provide the digital controller with closed-loop feedback that ensured the oven was running at a consistent temperature. The thermocouples used in this experimentation are S-type thermocouples which were routinely used during testing at 1200°C.

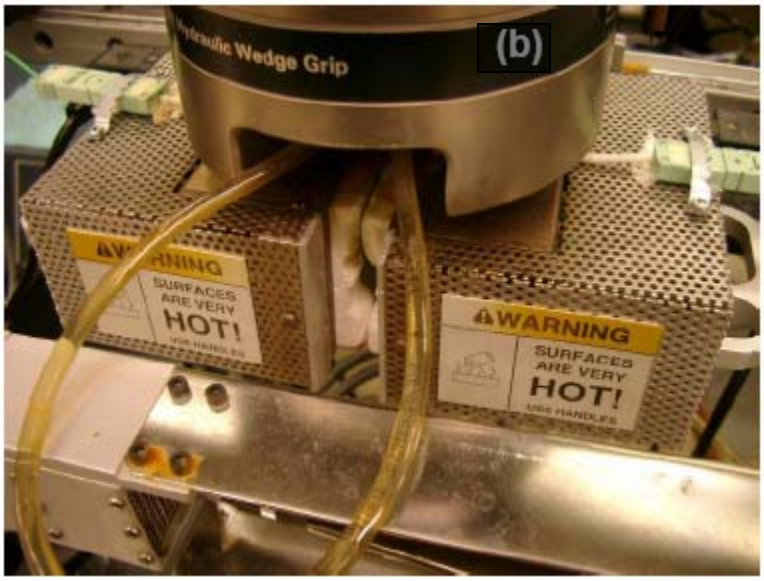

Figure 14. AMTECO Hot-Rail Furnace/Oven.

For testing in steam, continuous steam environment was provided by an AMTECO HRFS-STMGEN Steam Generation System displayed in Figure 15. Tests in steam employed the alumina susceptor, a cylinder with end caps, which fits inside the furnace. The specimen gage-section is located inside the susceptor, with the ends of the specimen passing through slots in the susceptor. Steam is introduced through a feeding tube in a continuous stream with a slight positive pressure, expelling the dry air and creating 100% steam environment inside the susceptor. The portion of the specimen enclosed in the susceptor is surrounded with steam environment. During testing it was important to monitor distilled water levels in the steam generator system to ensure steam was being produced. This set-up was very effective in simulating steam environment.

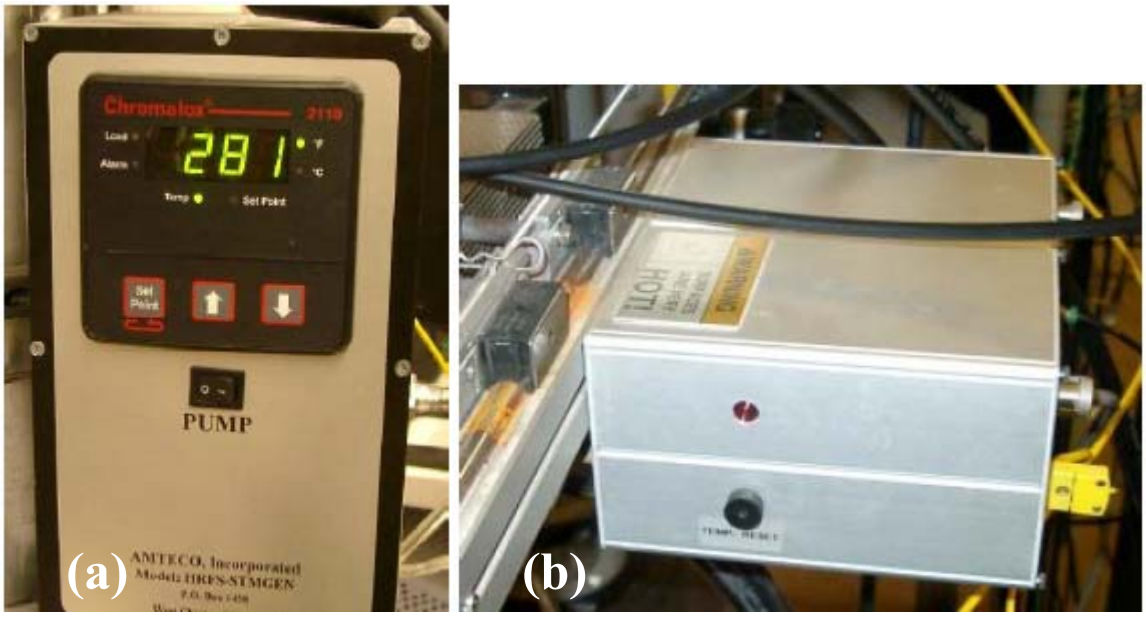

Figure 15. Steam System: (a) pump and temperature controller, (b) heating unit.

Hydraulic wedge grips were employed in all tests. Grips displayed in Figure 14 are exposed to the intense heat created by the oven during testing, but are only rated to operate at a temperature of 400°C. To remedy this problem a Neslab model HX-75 chiller was used to cool the grips. By flowing cold water through tubes running through machined holes in each grip wedge the temperature was prevented from harming any parts of the servo hydraulic grip system. The chiller was filled with distilled water to prevent corrosion and was able to cool the water to 14°C.

The final piece of equipment necessary to conduct testing in different environments was the alumina susceptor. The susceptor , shown in Figure 16 was used only when conducting tests in steam. There are several openings in the susceptor, one in the rear to allow for a feeding tube and two in the front to allow the extensometer rods to

contact the specimen. The feeding tube was connected to the steam generation system to provide the appropriate test environment.

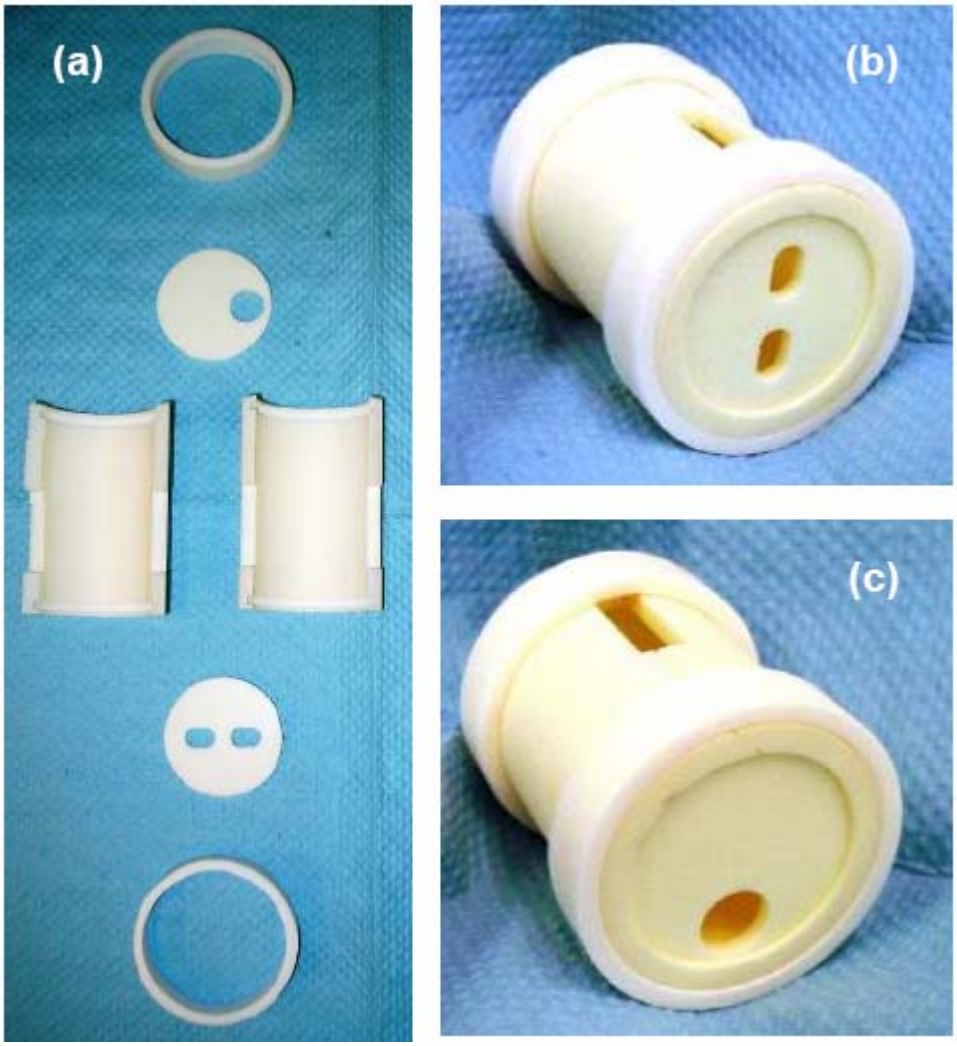

Figure 16. Alumina susceptor: (a) disassembled, (b) front view, (c) rear view.

When all of the aforementioned components are combined the result is an excellent system for testing CMC materials. In previous research this set-up has proven reliable in all types of testing such as tension, compression, and cyclic loading scenarios. This system was used heavily in compression during this experimentation. When testing in compression, it is important to take care in identifying limits for the machine. The

placement of the oven between the servo-hydraulic grips is precarious due to the fact that if failure occurs the oven could be damaged. By setting limits in the computer software program called interlocks, the Teststar II digital controller was able to monitor the location of the grips ensuring that damage to the oven was avoided.

4.2 Temperature Calibration

Before testing could commence the temperature controllers were calibrated to ensure the desired temperature was actually achieved. In order to accurately simulate potential operating environments it was important to measure the surface temperature of the specimen. Due to the fact that two ovens are used simultaneously to elevate the temperature around the specimen the setting of each individual temperature controller must be determined.

To establish the appropriate settings two S-type thermocouples were attached to the specimen with a cement adhesive. The thermocouples were connected to an OMEGA HH202A portable two channel temperature sensor, which provided a read-out of the specimen temperature. The temperature calibration specimen is displayed in Figure 17. The specimen was placed in the grips and force control was selected and set to zero force during temperature calibration. Command temperature was then automatically elevated to a pre-selected level at a slow rate to reduce the chance of overshooting the end point. After the temperature settled, manual adjustments were made in order to reach the desired temperature of the specimen.

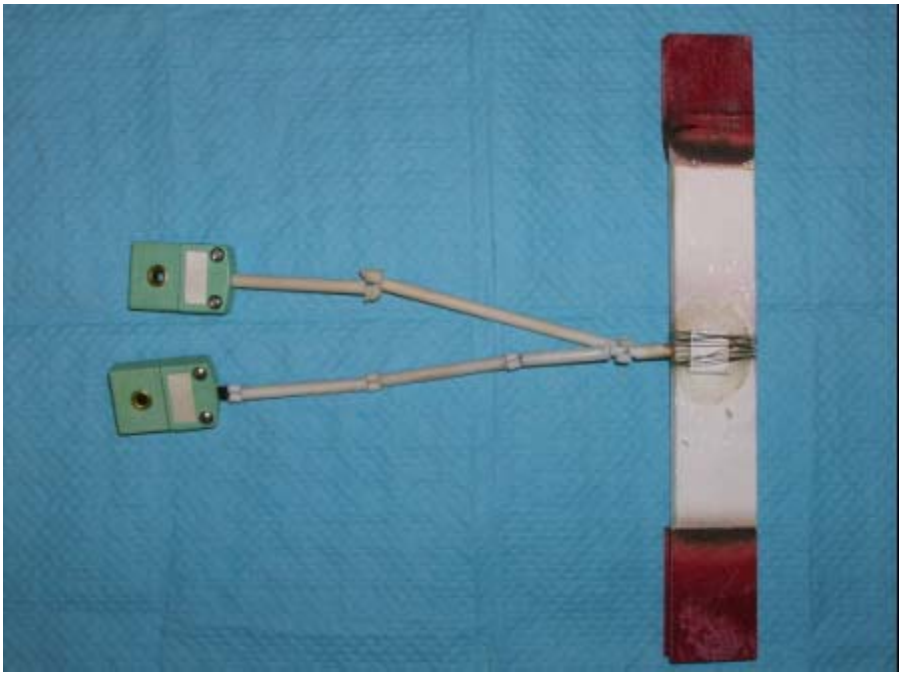

Figure 17. Temperature Calibration Specimen.

Once this temperature was reached the ovens were allowed to dwell for approximately 30 minutes to ensure settling occurred. Throughout the calibration process an independent high temperature probe was used to verify the readings displayed on the sensor. Once these values were obtained they could continue to be used for future testing of these specimens at the same temperature. It is important to note that if the size or shape of the specimen changes its thermal characteristics will change making it necessary to repeat the temperature calibration process. Temperature calibration was conducted in each environment. For example when calibrating the ovens in air to reach a temperature of 1200°C the right oven was set at 997°C and the left oven was set at 999°C. While in steam, temperature settings had to be a significantly higher due to the cooling effect of moisture. In steam the right oven was set to 1187°C and the left oven was set to 1181°C.

4.3 Test Procedures

This research focused primarily on compressive creep behavior of N720/A composite in two environments at elevated temperature. Several test procedures had to be constructed in order to thoroughly examine and classify the reasons for specific behavior exhibited by the material. These tests included compression to failure of a virgin specimen, long term creep tests in both air and steam environment, and compression or tension tests on specimens that achieved creep run-out. Each procedure was individually programmed in the Multipurpose Testware (MPT) software station manager, carefully inspected for flaws, and locked into the controller. The controller maintained excellent command of the system through a feedback loop and successfully carried out each test under full automation. In all tests the specimen was heated to 1200°C in 15 minutes and held at 1200°C for an additional 30 minutes prior to testing.

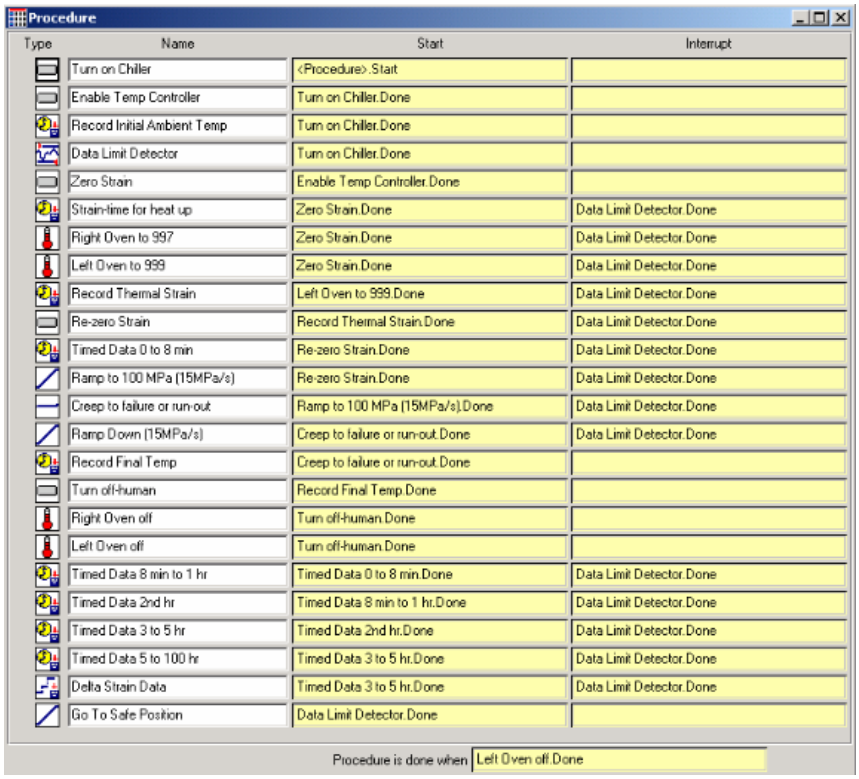

Figure 18. Sample MPT Test Procedure.

4.3.1 Compression to Failure

In order to evaluate the data collected throughout this research it was important to establish compressive properties of Nextel^{TM} 720/Alumina composite at 1200°C. This was accomplished in compression tests to failure conducted in displacement control with the rate of -0.05 mm/s. Very valuable information was collected from this type of test, such as the ultimate compressive strength, strain at failure, time to failure, and the coefficient of thermal expansion. Several compression to failure tests were completed to ensure the repeatability of the data. It is important to note that compression to failure tests were conducted in both air and steam environments.

4.3.2 Creep Rupture Tests

The next series of tests involved long term creep rupture tests lasting up to 100 hours. Creep tests were carried out in both air and steam environments at stress levels of -40, -60, -80, and -100 MPa. All creep tests were conducted in force control. In compressive creep-rupture tests specimens were loaded to the desired creep stress level at the stress rate magnitude of 15 MPa/s. Creep run-out was defined as 100 h at a given creep stress. Much like compression to failure tests, valuable information was collected from creep rupture tests. Information such as compressive modulus, creep rates, and creep curves were determined.

4.3.3 Post-Creep Testing

After long-term creep tests were performed, it was important to see how the specimen that achieved run-out was affected by exposure to sustained mechanical loading

at elevated temperature and to evaluate any changes in modulus, strength, and stress-strain behavior. Post-creep tests were conducted in compression or tension, and were carried out to failure. Much like compression to failure tests, post creep tests were run in displacement control at a rate magnitude of 0.05 mm/s.

4.4 Post-Failure Analysis

While the data collected during actual testing was valuable in illustrating the mechanical performance and retained properties of individual specimens, it did not reveal the mechanisms behind the mechanical response of the material. In order to elucidate important factors affecting material behavior it was necessary to take a closer look at the composite microstructure and specimen fracture surfaces. This was done by using an optical microscope and a scanning electron microscope (SEM).

4.4.1 Specimen Preparation for Microscopy

Although the optical microscope required no specimen preparation for effective viewing, the SEM was preparation intensive. The SEM relies on the transfer of electrons from an above mounted aperture to the specimen being viewed. Therefore, it was necessary to ground the specimen and provide it with a conductive coating [1]. The specimen was cut just below the fracture surface using an MTI Corporation EC400 CNC Dicing/Cutting and 3.5 in. impregnated diamond blade. It was then secured to an aluminum platform using silver paste to satisfy the grounding condition.

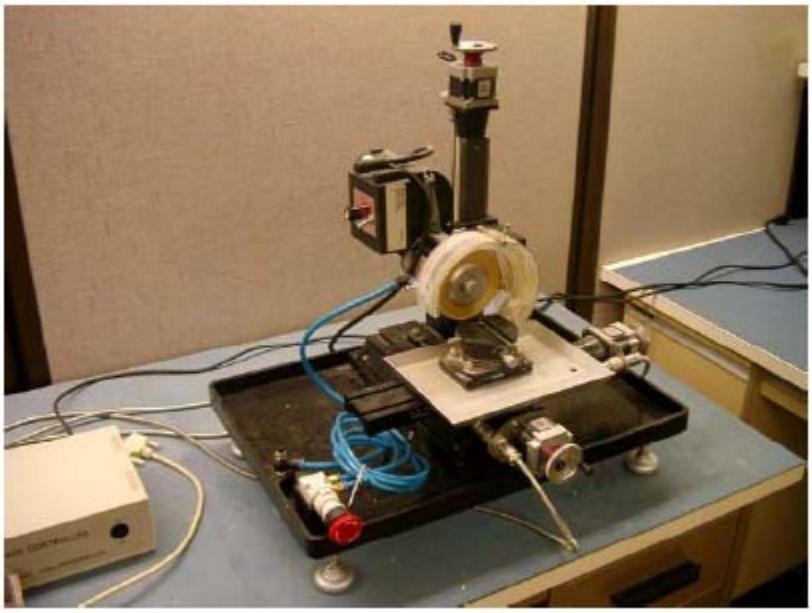

Figure 19. CNC Saw.

Next, the mounted specimen was placed in a SPI-MODULE Control and Carbon Coater to coat the non-conductive surface of N720/A with a conductive carbon coating. This was achieved by creating a vacuum around the specimen purging it of all air and then sending current through carbon rope, effectively transferring carbon atoms to the fracture surface.

Figure 20. SPI Carbon Coating System.

4.4.2 Optical Microscopy

After each test was completed and the specimen achieved failure, the fracture surface was examined using the optical microscope. Typically, each specimen yielded two fracture surfaces and each fracture surface required four photographs to fully document its characteristics. Each fracture surface was different, however, fracture surfaces of specimens which were exposed to similar environments and loadings histories showed significant resemblance.

Figure 21. Zeiss Optical Microscope.

A simple procedure was used to capture clear and detailed optical micrographs. The procedure included five steps. (1) The procedure involved selecting appropriate lighting at the 3200K setting so as to not overexpose areas of the specimen. (2) A z-stack function was performed to capture images at different depth levels throughout the specimen. (3) The z-stack images were then overlaid using a geometric alignment function to create a three dimensional picture. (4) In order to adjust the z-stack images on top of one another an extended focus was performed to perfectly align and focus each level of the image. (5) Finally, the image was sharpened to define individual fibers and matrix cracking and then smoothed in a gauss format to provide the optimal micrograph.

4.4.3 Scanning Electron Microscope Analysis

The scanning electron microscope is a sophisticated tool used to capture high resolution images at magnifications much greater than the human eye or even an optical microscope can achieve. Due to its unique manner of creating images the SEM is ideal for capturing fracture surfaces, especially those with complex damage zones. The SEM operates by thermionically emitting electrons from a tungsten cathode and accelerating them towards an anode. The energy exchange between the electron beam and the sample result in the emission of electrons and electromagnetic radiation which can be detected and used to form an image [1].

Figure 22. FEI Quanta Scanning Electron Microscope (SEM) and EDAX X-Ray Analysis System.

V. Results and Discussion

The following chapter provides a comprehensive discussion of all tests completed during this investigation. This study focused on the compressive creep behavior of Nextel^{TM} 720/Alumina at 1200°C in both air and steam environments. Additionally, compressive properties of N720/A at 1200°C were established. Furthermore, the effect of steam on the compressive creep performance of N720/A at elevated temperature was evaluated. Retained properties of specimens that achieved creep run-out in both environments were evaluated. The effect of load rate on the compressive characteristic properties and stress-strain behavior of N720/A was assessed. Once these results are presented, an in depth analysis of composite microstructure and damage and failure mechanisms is presented. The objective of the microstructure investigation is to identify mechanisms behind degraded compressive creep performance in steam. Note that this is the first investigation into the compressive behavior of N720/A at 1200°C, therefore comparison with prior work is limited. Table 2 summarizes all tests performed during this study.

Table 2. Test Matrix

Specimen	Loading Type	Environment	Max. Stress Magnitude (MPa)
UCS-1	Compression to failure	Air	130
UCS-2	Compression to failure	Air	132
UCS-3	Compression to failure	Air	122
UCS-4	Compression to failure	Steam	115
UCS-5	Compression to failure	Aged 25h Steam	99
AC-1	Creep	Air	100
AC-2	Creep	Air	80
AC-3	Creep	Air	60
SC-1	Creep	Steam	100
SC-2	Creep	Steam	60
SC-3	Creep	Steam	40
LRA	Compression	Air	108
LRS	Compression	Steam	54
AC-1a.	Post Creep	Air	123
AC-2a.	Post Creep Tension	Air	133
AC-3a.	Post Creep	Air	137

(UCS=ultimate compressive strength AC=air creep SC=steam creep LR=load rate)

5.1 Thermal Expansion

Each test in this investigation was performed at 1200°C. In order to achieve this temperature the specimen and associated testing equipment were required to heat to this temperature and dwell at temperature for a period of between 45 minutes to 1 hour. During heat-up the N720/A CMC experienced significant thermal expansion. Thermal expansion is defined as the event when a material increases in volume when exposed to increasing temperature. In each test, data was recorded during temperature ramp-up in order to determine thermal strain (ε_{th}). The coefficient of thermal expansion (α) was calculated by fitting a curve to the linear portion of the ε-T curve. The coefficient of thermal expansion in steam was higher than that in air temperature heat-up sequences.

Strain and temperature data was collected for all specimens. Table 3 summarizes the recorded values for thermal strain and the coefficients of thermal expansion.

Table 3. Thermal strain and coefficients of linear thermal expansion for the N720/A composite in steam and air environments.

Specimen	Thermal Strain (%)	Coefficient of Linear Thermal Expansion (10^{-6} K^{-1})
UCS-1	no strain data	N/A
UCS-2	no strain data	N/A
UCS-3	0.752	7.61
*UCS-4	0.977	9.92
*UCS-5	0.943	9.98
AC-1	0.756	8.53
AC-2	0.740	7.73
AC-3	0.712	7.55
*SC-1	1.028	9.84
*SC-2	1.00	9.99
*SC-3	0.997	9.99
LRA	0.788	8.33
*LRS	1.053	9.93

(*) Temperature Ramp Conducted in Steam Environment.

5.2 Monotonic Compression Tests

Nextel™ 720/Alumina CMC material system has been researched exhaustively in prior efforts to examine tensile, fatigue, and off-axis behavior in several environments at varying temperatures. However, this investigation is the first effort to explore the compressive characteristics of N720/A. Monotonic compression tests were conducted in both laboratory air and steam environments.

Compression to failure was performed in laboratory air to establish the ultimate compressive strength and the compressive elastic modulus of N720/A at 1200°C. For the purpose of this investigation ultimate compressive strength (UCS) is defined as the stress

level at which a specimen fails under loading. Results reveal an ultimate compressive strength magnitude of 122 MPa and a compressive modulus of 68.8 GPa. After these baseline values were established the effects of environment, creep, and load rate on the strength, modulus, and failure strain of the N720/A CMC material system were assessed.

The effect of steam on the compressive properties and behavior of N720/A was investigated in two compressive tests. A compression-to-failure test was performed in steam in order to evaluate short-term effect of steam environment. Results indicate that short-term exposure to steam reduces the ultimate compressive strength by 5.73% to 115 MPa, whereas the effect of steam on the compressive modulus is more pronounced showing a 15.84% decrease. While steam environment takes little time to have an effect on the compressive strength and stiffness of N720/A, prolonged exposure shows an even greater impact. The specimen aged for 25 hours at 1200°C in steam prior to the compressive test to failure loading showed an 18.9% reduction in strength as well as a 36.5% decrease in compressive modulus. Figure 23 shows compressive stress-strain curves obtained in laboratory air and in steam for the as-processed material as well as the compressive stress-strain curve obtained for the specimen subjected to 25 h of prior aging at 1200°C in steam.

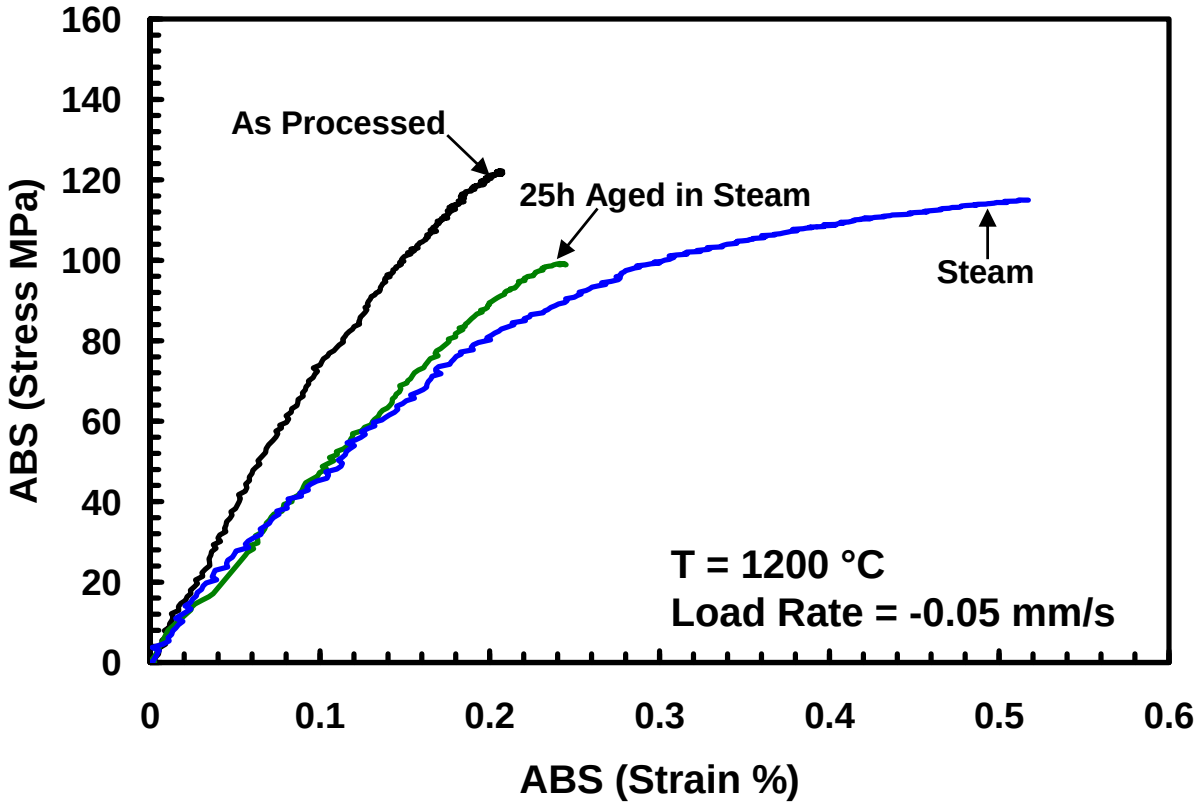

Figure 23. Compressive stress-strain curves for as-processed N720/A specimens tested at 1200°C in air and in steam and for N720/A specimen subjected to prior aging for 25h at 1200°C in steam and failed at 1200°C in steam.

It is seen that steam environment is detrimental to the compressive properties of N720/A. Compressive behavior of a 0°/90° composite is matrix-dominated; CMCs rely on the matrix to carry the load. Hence this reduction in strength and modulus indicates that the presence of steam has a degrading effect on the α-alumina matrix. A further discussion as to the mechanisms behind this degradation is substantiated by extensive microstructural investigation provided in later sections.

The effect of loading rate on the compressive properties and stress-strain behavior of N720/A was explored in both air and steam environments. The MTS servo hydraulic set-up was programmed to perform a compression to failure test in load control, at a rate

of -0.0025 MPa/sec. At this rate in both air and steam environments specimens achieved compressive failure at a much lower stress magnitude than those tested at a faster rate. When compared to the as-processed specimen the moduli of specimens tested at the slower load rate in air and in steam were significantly reduced. It is also interesting to note that failure strain in steam is increased by roughly 900% when load rate is reduced. Steam environment continues to degrade the compressive performance of N720/A independent of loading scenario. Figure 24 shows a comparison of the stress-strain behavior of N720/A specimens when tested to failure in displacement control versus slow rate load control.

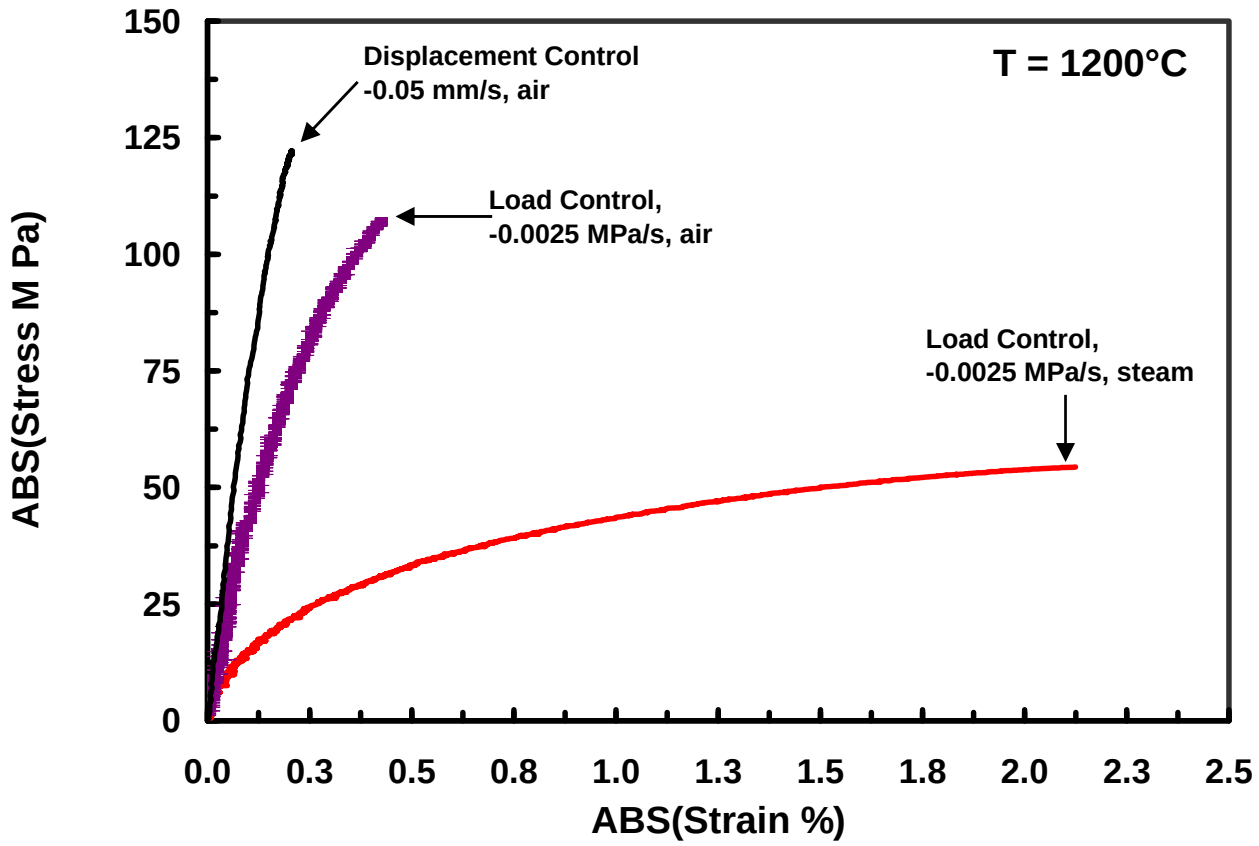

Figure 24. Compressive stress-strain curves obtained for N720/A specimens tested at 1200°C in air in displacement control at -0.05 mm/s and in load control at -0.0025 MPa/s in both steam and air environments.

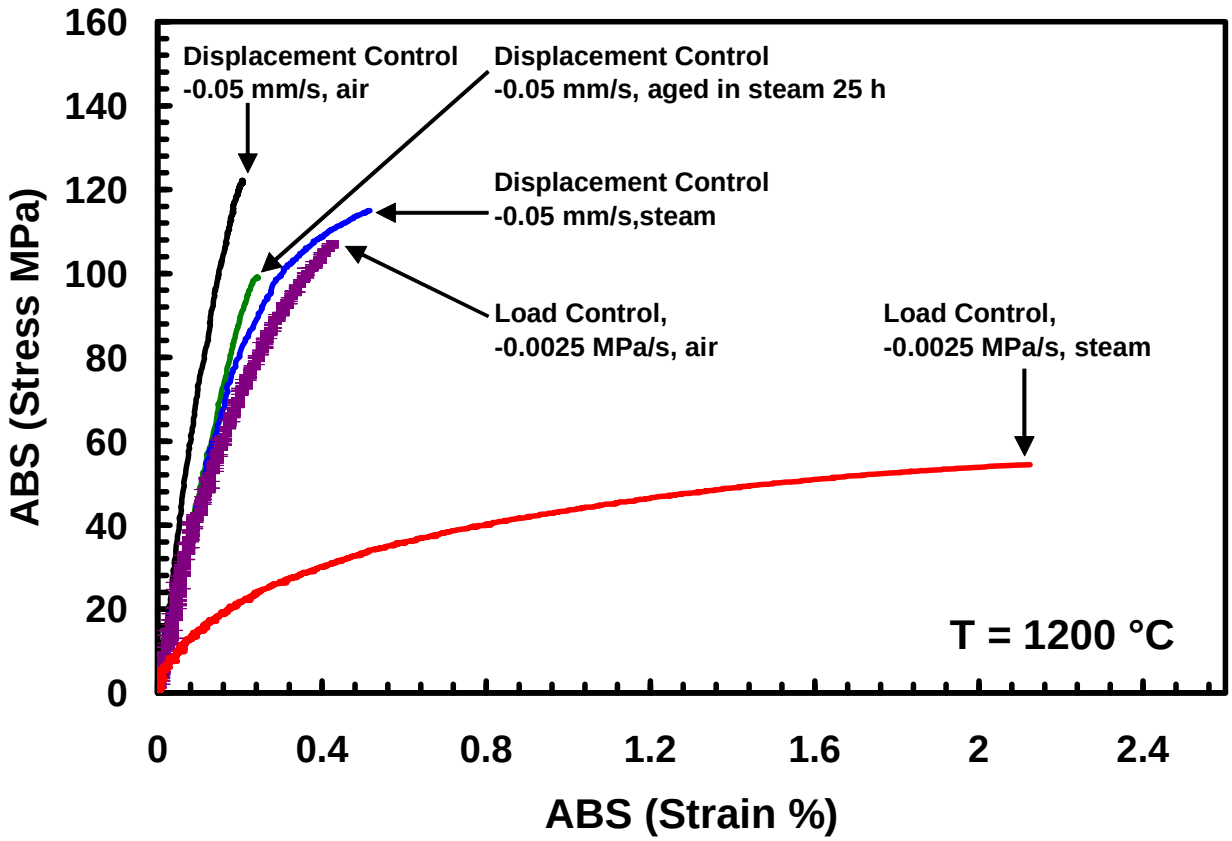

Figure 25. Compressive stress-strain curves for N720/A specimens tested in compression to failure at 1200°C in: (1) displacement control: in air, in steam, and following aging in steam for 25 h, (2) load control: in air and in steam.

The graph shown in Figure 25 compares the stress-strain behavior of all N720/A specimens tested in compression to failure at 1200°C. The shape of the load control in steam stress-strain curve is particularly interesting, because its stress-strain behavior deviates the most noticeably from as-processed behavior, of any of the other curves. Comparison of the load control in steam curve and the displacement control aged in steam for 25 h curve, shows that in both cases steam is detrimental to the modulus and compressive strength of as-processed N720/A. However, the combination of exposure to steam under increasing load at 1200°C as seen in the load control curve, results in the

most catastrophic change in the compressive performance of N720/A composite. Sustained loading during exposure to steam at 1200°C is the exact scenario which specimens undergo when exposed to a steam creep environment. Therefore this finding will be important in a later discussion of the compressive creep performance of N720/A in steam at 1200°C.

It is also important to discuss test duration in order to understand how much time elapsed prior to failure of each specimen. In tests conducted in displacement control at a rate of -0.05 mm/s failure occurred rapidly. Test duration for the compression to failure test of N720/A at 1200°C in air was approximately 16.0 seconds. Test duration for the compression to failure test of N720/A at 1200°C in steam was approximately 13.0 seconds. Test duration for the compression to failure test of N720/A at 1200°C following 25 h of aging in steam was approximately 8.0 seconds. Conversely, tests conducted in load control at a stress rate of -0.0025 MPa/s failed slowly. Test duration for the slow compressive load rate to failure of N720/A at 1200°C in air was approximately 12 hours and 12 minutes. Test duration for the slow compressive load rate to failure of N720/A at 1200°C in steam was approximately 5 hour and 47 minutes. Table 4 shows the associated compressive properties of tests conducted in compression to failure.

Table 4. Summary of compressive properties for the N720/A composite

Specimen	**Test Environment**	**Compressive Strength Magnitude (MPa)**	**Compressive Modulus (GPa)**	**Failure Strain (%) Magnitude**
UCS-3	Air	122	68.8	0.207
UCS-4	Steam	115	57.9	0.523
UCS-5	Aged 25h Steam	99	43.7	0.244
LRA	Air	108	25.75	0.420
LRS	Steam	54	8.95	2.12

5.3 Creep Rupture Tests in Air

Three creep rupture tests were performed in the laboratory air environment. After attaining a reliable value for the ultimate compressive strength of N720/A several creep stress levels were selected. These values were approximately 80%, 65%, and 50% of the ultimate compressive stress level of -122 MPa, yielding stress levels of -100, -80, and -60 MPa. The test specimen was held at creep stress for 100 h or until failure occurred. All specimens tested in air achieved the creep run-out of 100 h. Figure 26 illustrates the creep behavior of N720/A at several creep stress levels in laboratory air at 1200°C.

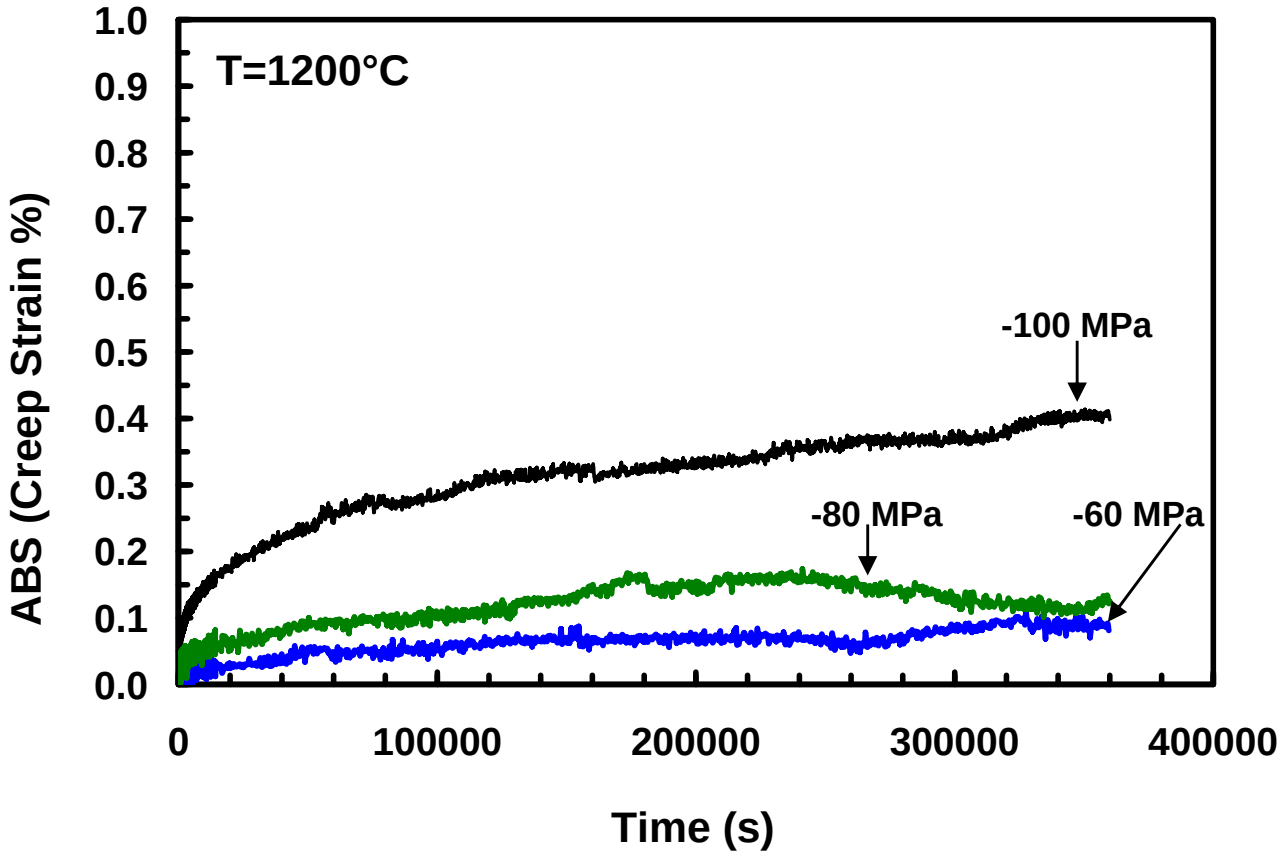

Figure 26. Compressive creep curves for N720/A CMC at 1200°C in air.

In previous work investigating Nextel™ 720/Alumina CMC tensile fatigue and creep behaviors were the focus of the study. Because in tension, the behavior of the composite is fiber-dominated, prior work focused on fiber-dominated behavior and properties. However, in compression the composite behavior is matrix-dominated. The matrix is carrying essentially the entire load in compression. It is seen that at 1200°C in air, N720/A exhibits primary and secondary creep regimes when subjected to sustained compressive loading. Note that creep strain magnitudes accumulated at creep stresses of -60 and -80 MPa are lower than the failure strain magnitude reached in compression tests to failure. Conversely, creep strain magnitude accumulated in the -100 MPa creep test exceeds the failure strain magnitude produced in compression tests to failure. As expected, creep strain accumulation increased with increasing creep stress. Table 5 summarizes the results of compressive creep tests at 1200°C in air.

Table 5. Summary of Compressive Creep Tests at 1200°C in Air.

Specimen	**Creep Stress (MPa)**	**Creep Strain (%)**	**Time to Rupture (s)**
AC-1	-100	-0.404	360,000 (Run-out)
AC-2	-80	-0.140	360,000 (Run-out)
AC-3	-60	-0.095	360,000 (Run-out)

5.4 Creep Rupture Tests in Steam

The effect of steam on creep performance was investigated by performing three creep tests at similar stress levels to those executed in air. However, from the start of this sequence of testing the results of creep tests in steam environment differed significantly

from those obtained in air environment. The first creep test in steam was performed at -100 MPa. The failure occurred after a mere 6.5 seconds. It became quite clear that the presence of steam would significantly reduce the life of N720/A in compressive creep at 1200°C. Therefore the two subsequent creep tests were performed at -40 and -60 MPa; lower stress magnitudes. Figure 27a shows the compressive creep curves obtained for N720/A at 1200°C in steam environment on a full test scale. Figure 27b shows a close-up of the creep curve obtained at -100 MPa at 1200°C in steam on a truncated test scale.

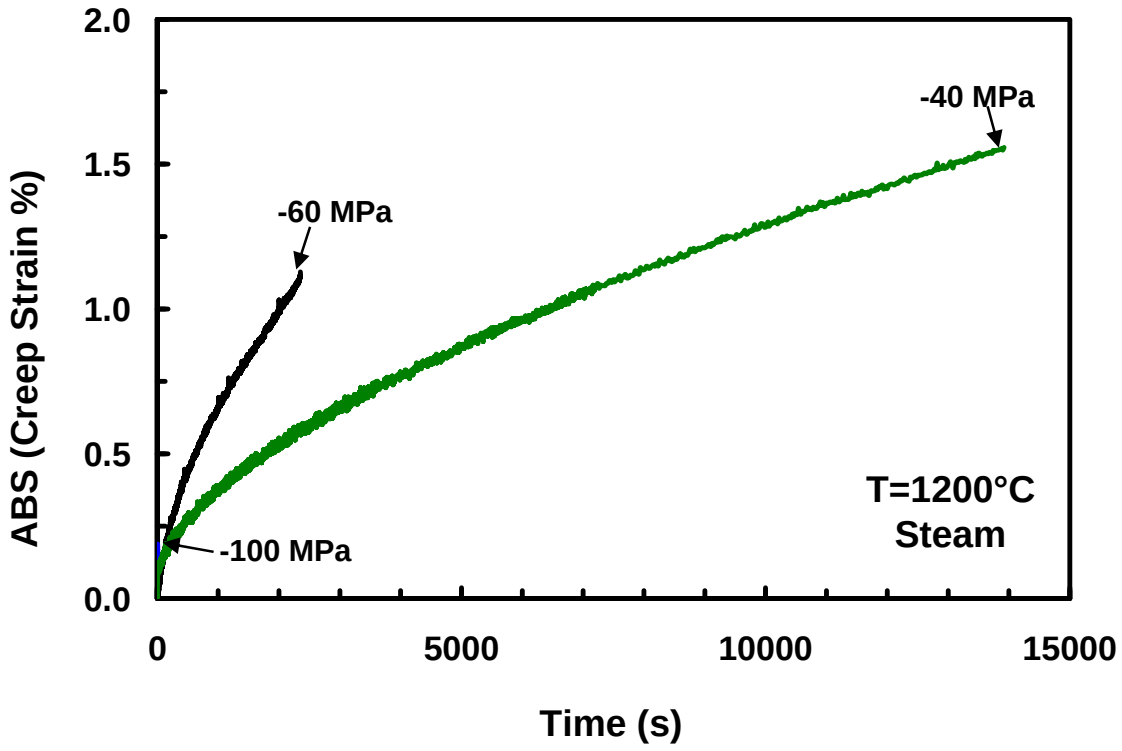

Figure 27a. Full scale: compressive creep curves for N720/A CMC at 1200°C in steam.

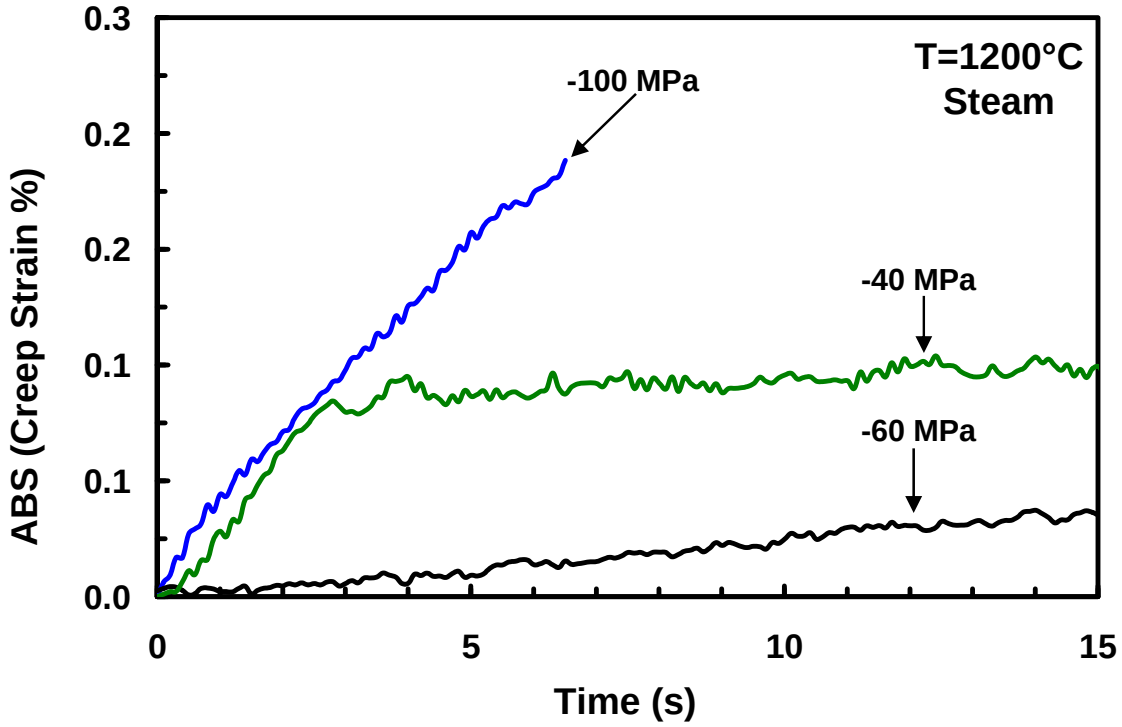

Figure 27b. Truncated scale: compressive creep curves for N720/A CMC at 1200°C in steam.

Creep testing in steam was initiated after creep tests in air were completed. Due to the fact that all creep tests in air achieved run-out it seemed that similar behavior in steam might be observed. However, none of the specimens tested in creep in steam environment survived 100 h at creep stress. In fact all specimens tested in creep in steam failed rapidly compared to the specimens tested in creep in air. The longest creep lifetime in steam of approximately 4 h was achieved by the specimen tested at -40 MPa. It is also interesting to note that specimens tested at lower creep stress magnitudes accumulated higher creep strains at failure. This is due to a reduction in creep rate magnitude at lower creep stress magnitudes. Specimens tested at lower creep stress magnitude, creep at a significant rate but not at a catastrophic rate, such as experienced

by the specimen tested at -100MPa. The cause of this rapid failure is a direct result of the addition of steam to the experimental conditions. Hence, the presence of steam has a deteriorating effect on the creep performance of the α-alumina matrix of the N720/A CMC which dominates the material response under compressive loading. The following section will discuss the influence of steam and stress levels on the creep rate of N720/A subjected to compressive creep loading. Table 6 summarizes the data collected in creep tests performed in steam.

Table 6. Summary of Compressive Creep Tests at 1200°C in Steam.

Specimen	Creep Stress (MPa)	Creep Strain (%)	Time to Rupture (s)
SC-1	-100	-0.188	6.5
SC-2	-60	-1.128	2355
SC-3	-40	-1.577	13920

5.5 Compressive Creep Rate and Time to Creep Rupture of N720/A

Comparison of creep data at 1200°C in air and in steam environments obtained in testing leads to a very definitive conclusion about the effect of steam on the compressive creep performance of N720/A. Steam is detrimental to the compressive creep performance, to the point where catastrophic failure occurs rendering this CMC material system ineffective. In order to quantify the degree to which the presence of steam affects compressive creep resistance of N720/A, creep rates were calculated to determine at what rate compressive strain is accumulated in the material under sustained loading in steam and air environments. Table 7 shows creep rates and associated test environments as well as creep stress levels. All creep rate magnitudes in steam are higher than those recorded

in air. A catastrophically high creep rate magnitude of 0.018 s^{-1} with a corresponding life of only 6.5 seconds was observed at -100 MPa in steam. Specimens subjected to creep at -40 and -60 MPa also produced creep strain rate magnitudes that were an order of magnitude higher than those produced in air at the same creep stress levels. These high creep rate magnitudes suggest that the matrix is strongly affected by the presence of steam. Failure of all specimens tested in steam occurs in less than four hours, while all specimens tested in air achieved creep run-out of 100 h. A further investigation as to the mechanisms causing these early failures in steam is presented in the next section where the behavior of α-alumina matrix is discussed.

Table 7. Minimum Creep Rates for N720/A Specimens Tested at 1200°C in Air and in Steam.

Specimen	**Creep Stress (MPa)**	**Test Environment**	**Strain Rate (s^{-1})**
AC-1	-100	Air	-2.95E-7
AC-2	-80	Air	-9.024E-8
AC-3	-60	Air	-8.336E-8
SC-1	-100	Steam	-1.8E-2
SC-2	-60	Steam	-2.879E-6
SC-3	-40	Steam	-6.09E-7

It is also interesting to compare the compressive creep rates of N720/A obtained in this study with the tensile creep rates obtained in prior efforts. Figure 28 compares the creep rates produced in this investigation and those obtained in tensile creep tests by Harlan [22,60]. Results in Figure 28 suggest that steam has the same degrading effect on the tensile as on compressive creep performance of N720/A. However, in the case of tensile creep the effect seems less pronounced. In the case of tensile creep, the relationship between the minimum creep rate and creep stress can be described by a

power law. On the other hand, in steam the minimum creep rate magnitude increases drastically as the creep stress magnitude exceeds 60 MPa. This leads to the conclusion that steam has a greater effect on the compressive creep performance of N720/A than on its tensile creep performance. These findings are significant because this CMC material will undoubtedly be subjected to sustained compressive loading in degrading environments when used in real aerospace engine components.

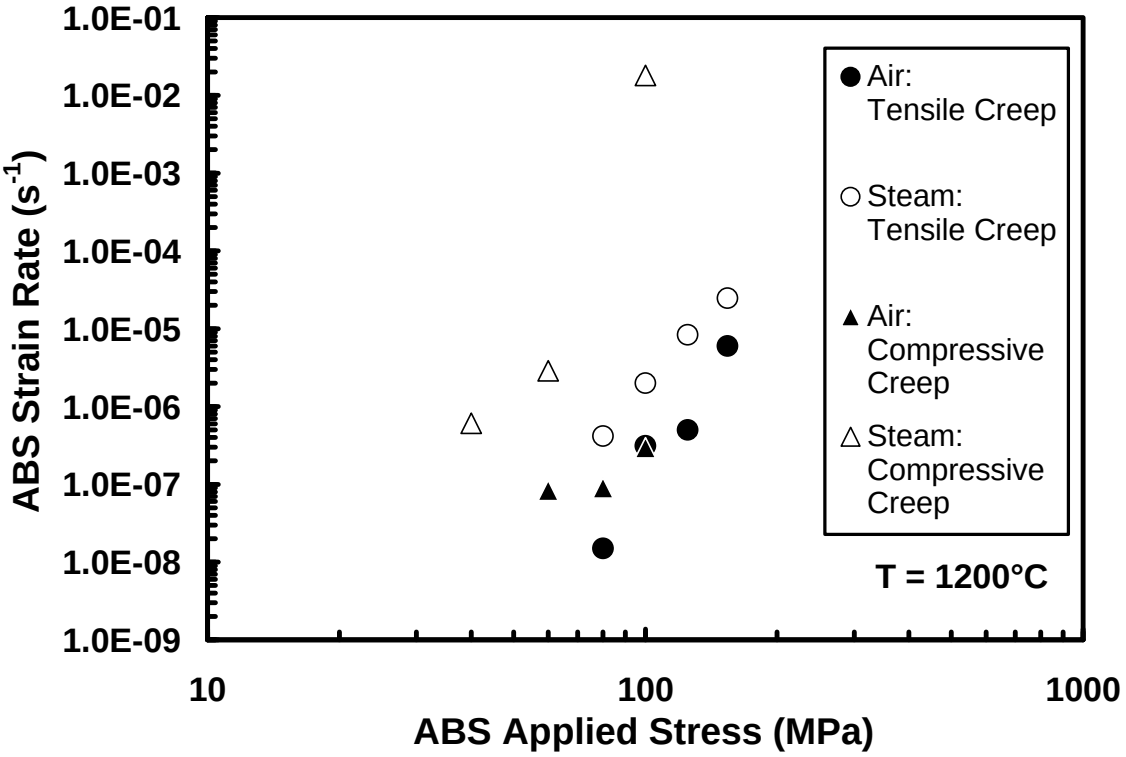

Figure 28. Minimum creep rate magnitude vs. applied stress magnitude for N720/A composite at 1200°C in air and in steam. Tensile data form Harlan [22,60].

Additional evidence substantiating the conclusion that steam has a detrimental effect on the compressive creep performance of N720/A is provided by time to rupture data. Specimens tested in steam exhibit a much shorter creep life duration than

specimens tested in air at identical stress levels. Another method of quantifying the degree to which the presence of steam affects compressive creep resistance of N720/A, is to record and analyze creep lifetimes of specimens tested in air and steam environments. Figure 29 graphically represents the time to rupture for each specimen at its associated stress level in each environment.

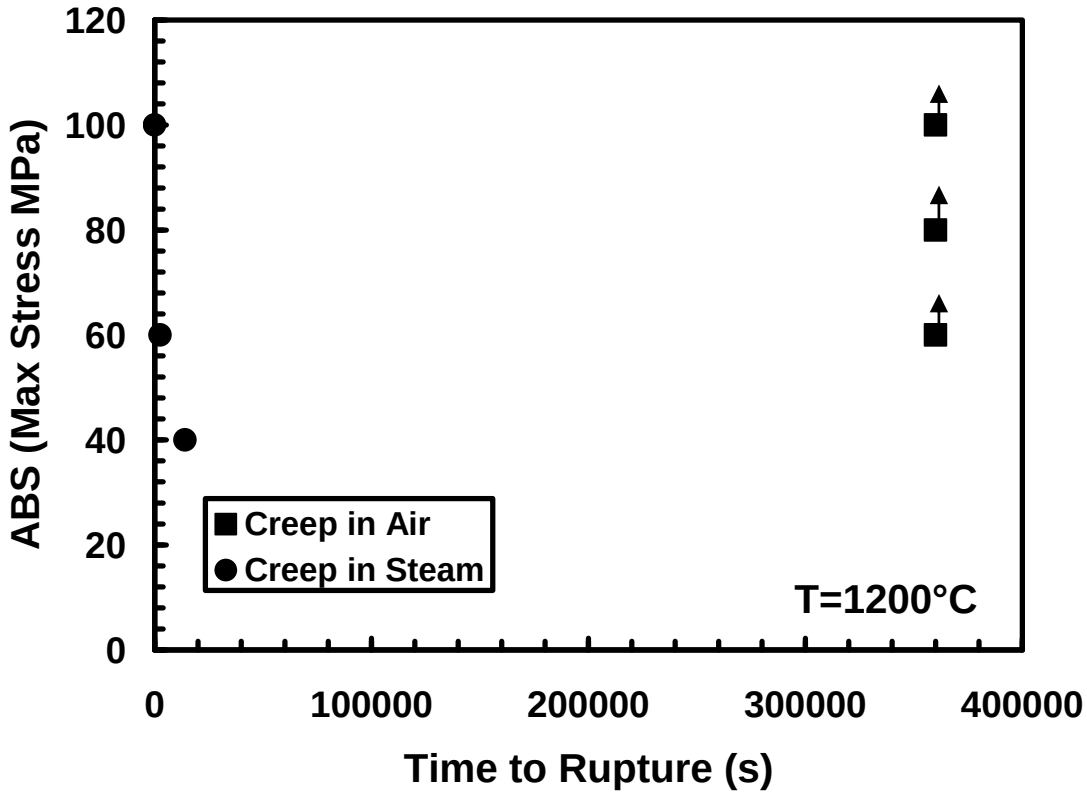

Figure 29. Stress rupture plot: creep lifetimes of all N720/A specimens tested in air and in steam at 1200°C.

Additionally, Table 8 shows the time to rupture for each specimen and associated test environments as well as creep stress levels. Notice that all specimens subjected to creep in air achieve run-out of 100 h, while all specimens subjected to creep in steam fail in less than 4 hours. These creep lifetimes correspond to the catastrophically high creep rate magnitudes observed in steam especially at the higher stress levels. These short creep lifetimes suggest that matrix performance is negatively affected by the presence of steam.

Table 8. Time to rupture of specimens tested in creep loading at 1200°C in air and in steam.

Specimen	**Creep Stress (MPa)**	**Test Environment**	**Time to Rupture (s)**
AC-1	-100	Air	Run-out
AC-2	-80	Air	Run-out
AC-3	-60	Air	Run-out
SC-1	-100	Steam	6.5
SC-2	-60	Steam	2355
SC-3	-40	Steam	13920

5.6 Effect of Steam on Compressive Creep Rupture Behavior

As a matrix material α-alumina is a candidate constituent in CMCs for high temperature application due to its stability at elevated temperatures. Additionally, as an oxide material it exhibits inherent oxidation resistance, a valuable property especially when being considered for use in aerospace applications where corrosive water vapor is likely to be present during normal operation. However, results of compressive creep testing at 1200°C in a steam environment show a significant decrease in performance as compared to laboratory air environment. This poses an important question; if oxidation is

not responsible for this decrease in performance, what aspect of water vapor is causing such degradation in compressive creep resistance?

Several previous studies have explored the effect of steam on polycrystalline α-alumina subjected to creep at 1200°C [35]. These research efforts have concluded that it is not the oxygen in steam that has a degrading effect on the α-alumina matrix, rather the presence of hydrogen is to blame. Previous results have shown that the presence of hydrogen leads to a significant reduction in yield stress. Furthermore, presence of hydrogen lowers the mechanical strength of polycrystalline α-alumina with different grain sizes [35:566].

Creep studies performed on polycrystalline α-alumina at temperatures above 1200°C that focused on fine grained materials indicated that the main deformation mechanism is diffusion-controlled grain boundary sliding. It was also shown [35] that the presence of hydrogen induces hydrothermal softening of α-alumina and changes in the deformation mechanism. These phenomena are attributed to the penetration of hydrogen defects into α-alumina. Results reported in literature [35] reveal that hydrogen defects can be introduced in to α-alumina to depths of mm by diffusion from water vapor. The two kinds of hydrogen defects were reported to be: (1) interstitial protons in the bulk and (2) molecular clusters likely located near surfaces and grain boundaries. Results in reference (35) demonstrate that the yield stress of α-alumina was reduced by the presence of hydrogen by a factor of 6 for fine grained α-alumina. In this case weakening is associated with a change in the predominant deformation mechanism, from dislocation glide to grain boundary sliding and cracking. In summary, the presence of hydrogen

induces a hydrothermal softening of α-alumina and changes the deformation mechanisms, resulting in a reduction in mechanical performance [35:573].

The conclusions drawn by previous studies are clearly illustrated and confirmed by the early failures and high creep rates experienced by N720/A subjected to compressive creep in steam environment. Further examination of specimens failed in the aforementioned scenarios is carried out using optical and SEM microscopy techniques.

5.7 Retained Properties

Creep testing was performed on six N720/A specimens. However, only the specimens tested in air achieved creep run-out. To evaluate the retained properties of these pre-crept specimens it was essential to test them in compression to failure and to determine the retained modulus, failure strain, and retained strength. Specimens which achieved run-out in creep tests at -60 and -100 MPa were subjected to compression tests to failure. Conversely, the specimen tested in creep at -80 MPa was subjected to a tensile test to failure in order to evaluate the effects of prior compressive creep on tensile properties and stress-strain behavior.

Post-creep testing revealed that prior compressive creep significantly affected the retained properties. Retained compressive strength is increased after 100 h in creep loading at -60 and -100 MPa. The specimen subjected to creep at -60 MPa showed a rather significant increase in strength of 12.3%. However, both specimens exhibited a reduction in compressive modulus. Results of retained mechanical properties of N720/A specimens subjected to prior creep at 1200°C in air are shown in Table 9.

Table 9. Retained Properties of N720/A CMC specimens subjected to prior creep in air at 1200°C.

Specimen	Creep Stress (MPa)	Retained Strength (MPa)	Retained Modulus (GPa)	Initial Modulus (GPa)	Failure Strain (%)	Strength Retention (%)	Modulus Retention (%)
AC-1a.	-100	-123	45.4	68.8	-0.218	100.8	66.0
AC-2a.*	-80	+133	60.0	75.1	-0.301	70.0	79.9
AC-3a.	-60	-137	49.7	66.0	-0.249	112.3	75.3

(*) Post creep testing in tension.

It appears that the porous matrix could be the source of the increase in compressive strength. When the specimen is held under sustained compressive load for a prolonged period of time, matrix porosity is likely to decrease, causing matrix coarsening and densification. This process makes the matrix inherently stronger and therefore able to carry significantly higher loads than in the as-processed condition. Figure 30 illustrates the effect of prior compressive creep on the retained compressive properties of N720/A composite.

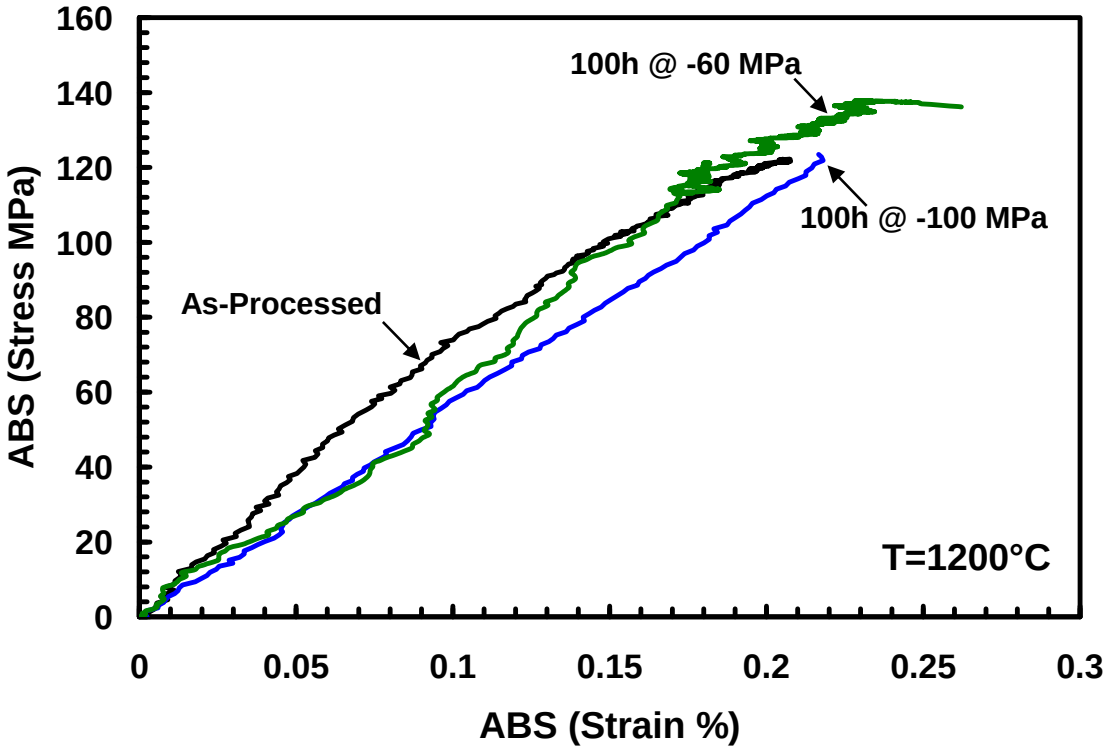

Figure 30. Effect of prior compressive creep at 1200°C in air on the compressive stress-strain behavior of N720/A CMC at 1200°C in air.

Although this research focuses primarily on the compressive creep behavior of N720A, it was important to assess how prior compressive creep affected tensile stress-strain behavior. The specimen subjected to creep at -80 MPa was subjected to tension to failure after achieving creep run-out. Although prior compressive creep caused an increase in compressive strength, it significantly degraded the tensile properties. Tensile modulus was reduced by 20.1% while the tensile strength suffered a greater reduction of 30%. The densification of the porous matrix plays the opposite role under tensile loading. As the porosity is reduced the matrix loses its ability to provide for crack deflection and to prevent brittle failure. While fiber performance is critical to the performance of the CMC in tensile loading, a minimum level of finely distributed matrix

porosity is equally critical to crack deflecting behavior and damage tolerance. Matrix densification leads to decrease in damage tolerance and brittle failure. Evidence of this phenomenon is provided by the fracture surface. The fracture surface reveals planes of coordinated fiber failure. This finding indicates that cracks were not deflected around fibers. The composite fractured in a brittle manner like a monolithic ceramic. Following sections will discuss this observation using optical micrographs for substantiation. Figure 31 illustrates the reduced performance of N720/A in tension following 100 h of compressive creep at 1200°C in air.

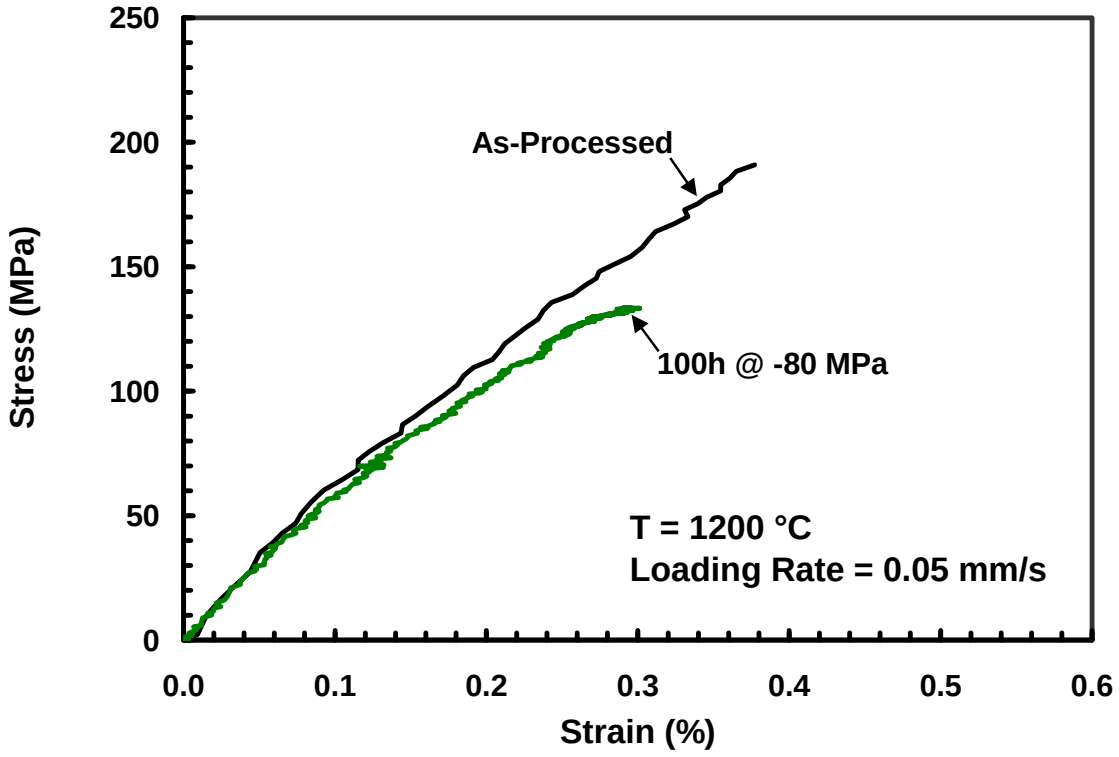

Figure 31. Effect of prior compressive creep at 1200°C on tensile stress-strain behavior of N720/A CMC at 1200°C.

5.7.1 Compressive Creep Behavior of Polycrystalline Alumina

The retained properties obtained in this study for specimens subjected to prior compressive creep at 1200°C in air and in steam were somewhat unexpected. Prior compressive creep in air at 1200°C caused a noticeable increase in the compressive strength of this particular material system. To understand why such an increase in compressive strength is observed it is essential to understand that the matrix is responsible for carrying most of the compressive load experienced by N720/A composite. Therefore the behavior of the matrix dictates strengthening of this CMC in compression.

The matrix material used in the fabrication of Nextel^{TM} 720/Alumina composite is a slightly porous polycrystalline α-alumina. A previous study investigated the behavior of α-alumina under compressive load in aggressive temperature environments [6]. This previous research effort focused on the behavior of α-alumina, alone. However, it is reasonable to assume the introduction of fibers should not change α-alumina properties significantly, especially in compressive loading. It was reported [6] that at low temperature and/or low applied stresses, deformation in α-alumina occurs by grain boundary sliding. In this case increased densification is observed in the samples subjected to compressive creep, compared to the as-sintered material [6:2807].

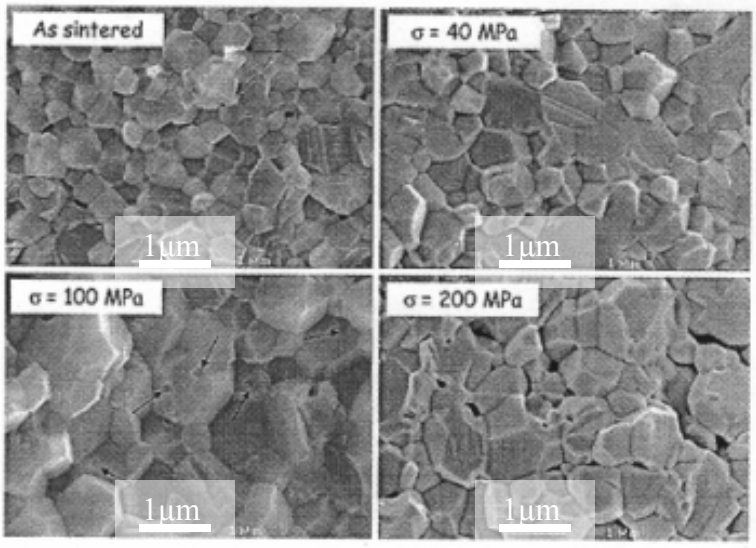

Figure 32. α-Alumina microstructure after being subjected to creep loading at various stress levels; comparison of grain size [6].

This study showed that specimens subjected to prior compressive creep at high temperature exhibited grain growth during high temperature deformation. Aforementioned grain growth under various stress levels is illustrated in Figure 32 [6]. To evaluate the stress influence on grain size, the average grain size after creep tests was compared to a reference sample put in the creep furnace, without load, at the same time. At 1200°C when the applied stress is between 40 and 100 MPa the resultant microstructure after creep is coarser compared to that of the as-sintered material, very few residual pores are observed [6:2814]. These findings confirm the theory that the porous α-alumina undergoes additional sintering and coarsening under compressive load at elevated temperature, resulting in a loss of matrix porosity and a densification of the N720/A CMC material system, leading to an increase in compressive strength.

It is important to note that this previous research [6] clearly defines low temperature and low applied stress as a range of values. The temperatures between 1150°C and

1200°C are defined as low. Applied stresses between 0 and 100 MPa are defined as low as well [6:2818]. While it is apparent that these temperatures and stresses are quite aggressive, for the purposes of a relative discussion of the compressive behavior of α-alumina under load at elevated temperature these definitions are important.

5.8 Composite Microstructure

Throughout this discussion of results, data and theories have been provided to serve as an explanation for what occurred in each specimen from an objective and quantitative standpoint. The experimental results present a fairly clear picture of the material behavior under monotonic and sustained compressive loading at 1200°C in air and in steam. However, it is important and also considerably more difficult to identify the microstructure mechanisms responsible for the observed mechanical behaviors. Inspecting the composite microstructure of selected specimens with both the optical microscope and SEM will allow for a deeper understanding to what mechanisms were activated during loading, at elevated temperature, in steam or air environment. Phenomenon such as grain growth under load and densification of the matrix are explored at the microscopic level. The goal of this exercise is to understand why certain failure mechanisms occur, why steam environment is so detrimental, and to fully evaluate the performance of N720/A in compressive loading scenarios.

5.8.1 Optical Microscopy

Viewing optical images of the Nextel™ 720/Alumina fracture surfaces is useful for establishing the basic appearance of fracture surfaces obtained under specific conditions. These micrographs capture the entire fracture surface revealing important features concerning the topography of each specimen failure. All tests in this investigation were conducted at 1200°C. Therefore fracture surfaces are only environment and load type dependent. Although some of the fracture surfaces presented in figures on the following pages look very different there is a basic similarity between N720/A specimens failed in compression at 1200°C. This similarity is a distinctive angled fracture surface which indicates shearing of the fibers. See the side views in Figures 33(b), 35(a), and 35(b).

It is important to note that the N720/A CMC employs a woven fiber architecture. The reinforcement is composed of 0°/90° fibers which are woven into an 8 harness satin weave fabric. This is much different from CMC materials studied in the past that had a laminate structure with the 0° and 90° fibers included in separate unidirectional layers of the material. This difference has a significant influence on the performance of the material as well as on the appearance of the fracture surfaces.

The images in Figure 33 show fracture surface of an as-processed N720/A CMC specimen subjected to compression to failure at 1200°C in a laboratory air environment. The image in Figure 33(a) reveals a long damage zone measuring 45 mm. The weave is exposed showing that it played a role in resisting the failure under compressive loading. The failure mechanism usually associated with compression failure is buckling and kinking of the fibers which ultimately leads to fiber fracture. However, the failure

mechanism observed in this compression to failure specimen is shearing of the fibers and matrix. The fracture is not extremely clean; however, there is a distinct stair-step pattern which is easily seen in Figure 33b. The side view also reveals that some delamination occurred during failure. This failure mode is common among dense matrix CMCs with a fiber coating (weak interface). It is important to note that only 9.0 seconds elapsed before the specimen in Figure 33 failed at a compressive stress of 122 MPa.

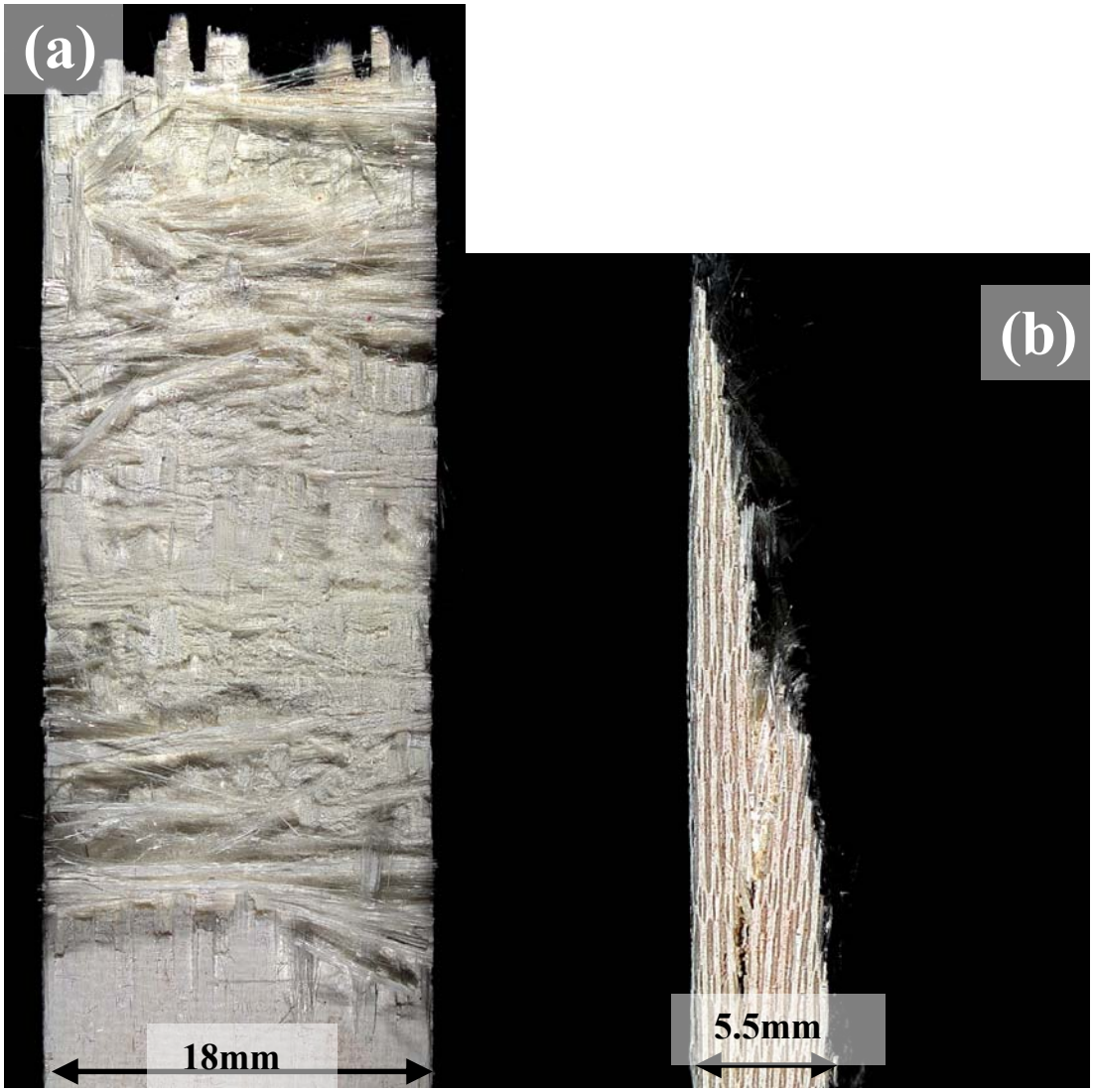

Figure 33. Fracture surfaces of N720/A specimen tested in compression to failure at 1200°C in laboratory air: (a) top view, (b) side view.

Presented in Figure 34 are fracture surfaces of specimens failed in compression after being subjected to 100 h of compressive creep loading in laboratory air environment at 1200°C. These fracture surfaces are very similar to those observed in compression to failure tests of as-processed N720/A, displayed in Figure 33. This is not surprising when considering that even after sustained loading at elevated temperature the retained properties of this material are similar to those of the as-processed CMC.

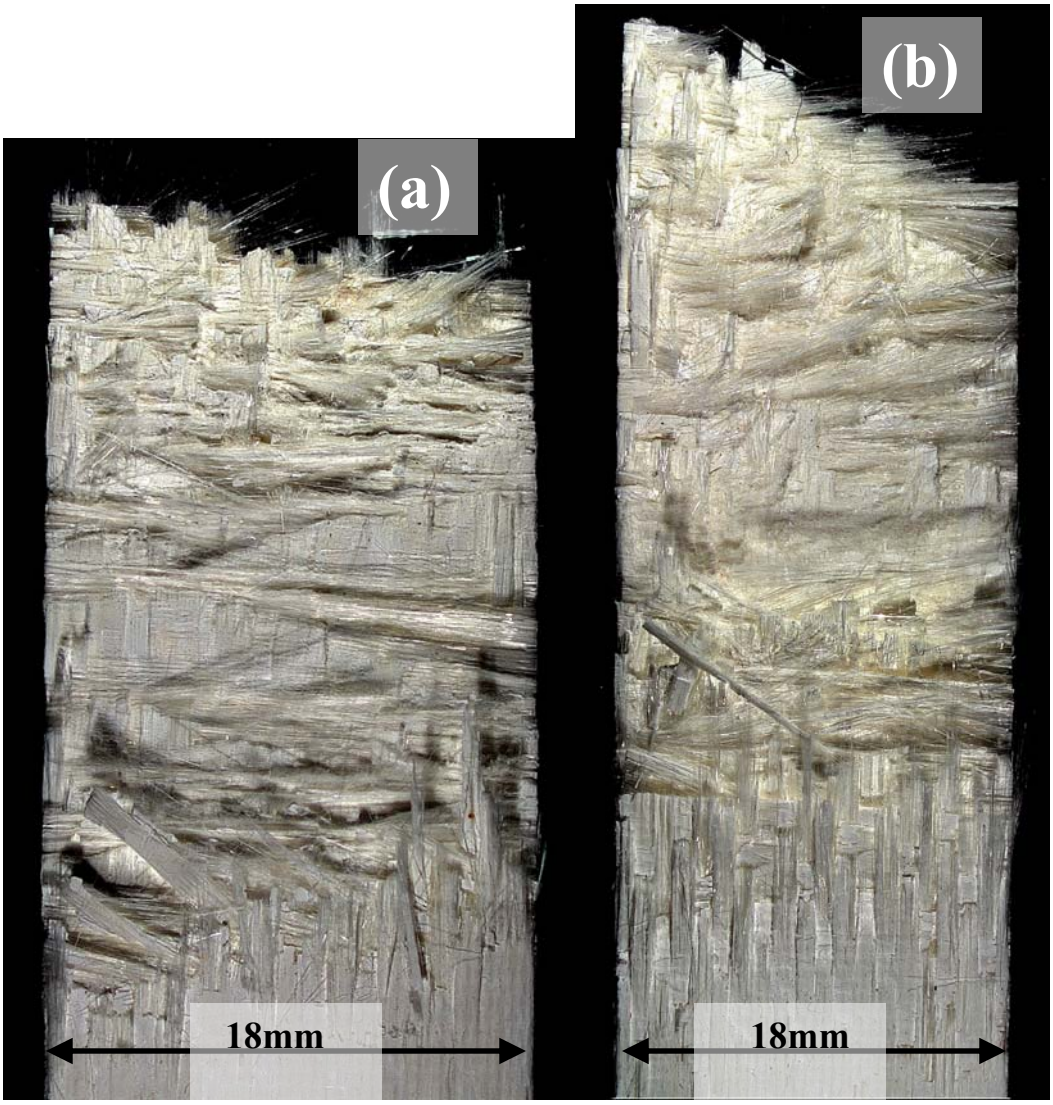

Figure 34. Fracture surfaces of N720/A specimens subjected to compressive creep tests at 1200°C in air: (a) -60 MPa, (b) -100 MPa.

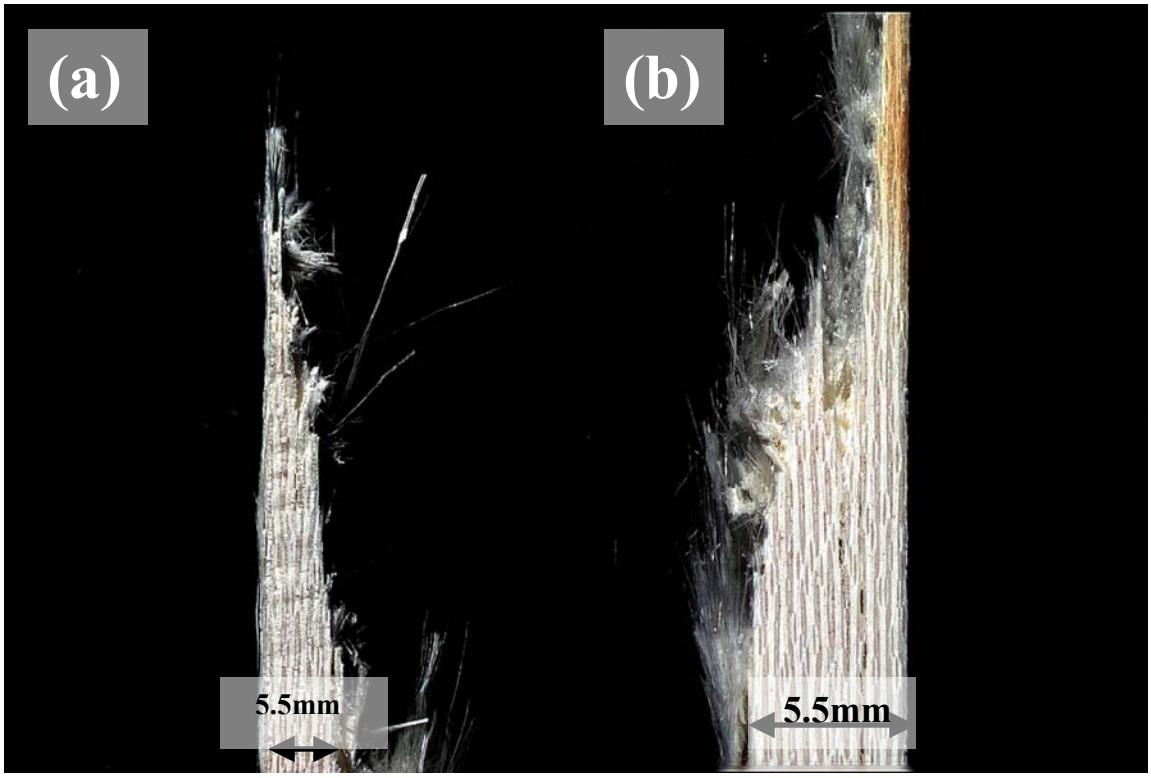

Figure 35. Fracture surfaces of N720/A specimens subjected to compressive creep tests at 1200°C in air: (a) -60 MPa side view and (b) -100 MPa side view.

The specimen tested in creep at -100 MPa exhibits a fracture surface similar to that obtained for the as-sintered material. This specimen also retained its strength; data indicates it failed at 123 MPa which is 100.8% of the as-processed compressive strength. The fracture surface indicates that the woven reinforcement resists failure but ultimately succumbs to a shearing force producing a stair-step fracture surface. Additionally, the side view provided in Figure 35, indicates there is some delamination much like what was observed in the as-processed compression to failure specimen.

When N720/A CMC is exposed to a steam environment, its compressive performance degrades significantly. An earlier explanation suggested that the presence of hydrogen caused this decrease in performance of the α-alumina matrix material. Figure 36 shows fracture surfaces obtained in all compressive creep tests performed in

steam at 1200°C. All three fracture surfaces show a significantly denser matrix, however data obtained during this investigation suggests that in steam this matrix coarsening/densification does not translate into matrix strengthening. In this case the dense matrix appearance is an indication of both grain growth and hydrothermal softening of α-alumina yielding a decreased compressive performance. It is important to note that none of these specimens achieved creep run-out of 100 h and consequently failed in creep loading.

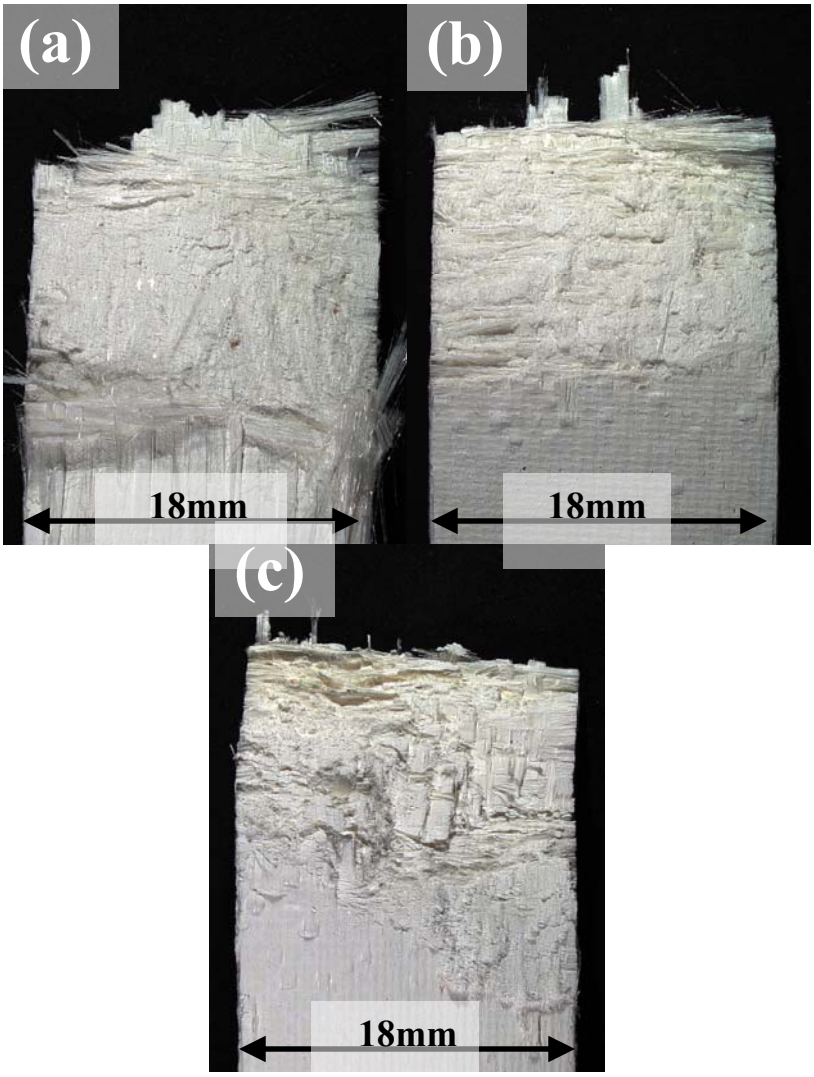

Figure 36. Fracture surfaces of N720/A specimens subjected to compressive creep tests at 1200°C in steam: (a) -100 MPa, (b) -60 MPa, (c) -40 MPa.

The most noticeable difference between the fracture surfaces produced in creep tests conducted in steam and those produced in air is the length of the damage zone. Specimens tested in creep in steam produced much shorter damage zones. Accompanying this shorter fracture zone is a denser appearance indicated by a coalescence of failure for both fibers and matrix. The stair-step topography of the fracture surface seen in creep tests performed in air is not present in the fracture surfaces obtained in steam due to the fact that steam "softens" the matrix, making it adhere more readily to the fibers. As a result of matrix coarsening and densification coordinated fiber fracture is observed. The side views in Figure 37 show the "smooth" nature of the fracture surfaces obtained in steam. Brushiness that characterizes failure surfaces obtained in compression of N720/A in laboratory air is not present in the fracture surfaces produced in steam. Although minor cracking is present in the 40 MPa specimen, only very little delamination is observed in the fracture surface of N720/A specimen tested in creep at -40 MPa in steam. This is due to the fact that the matrix is weakened and fails at a lower load.

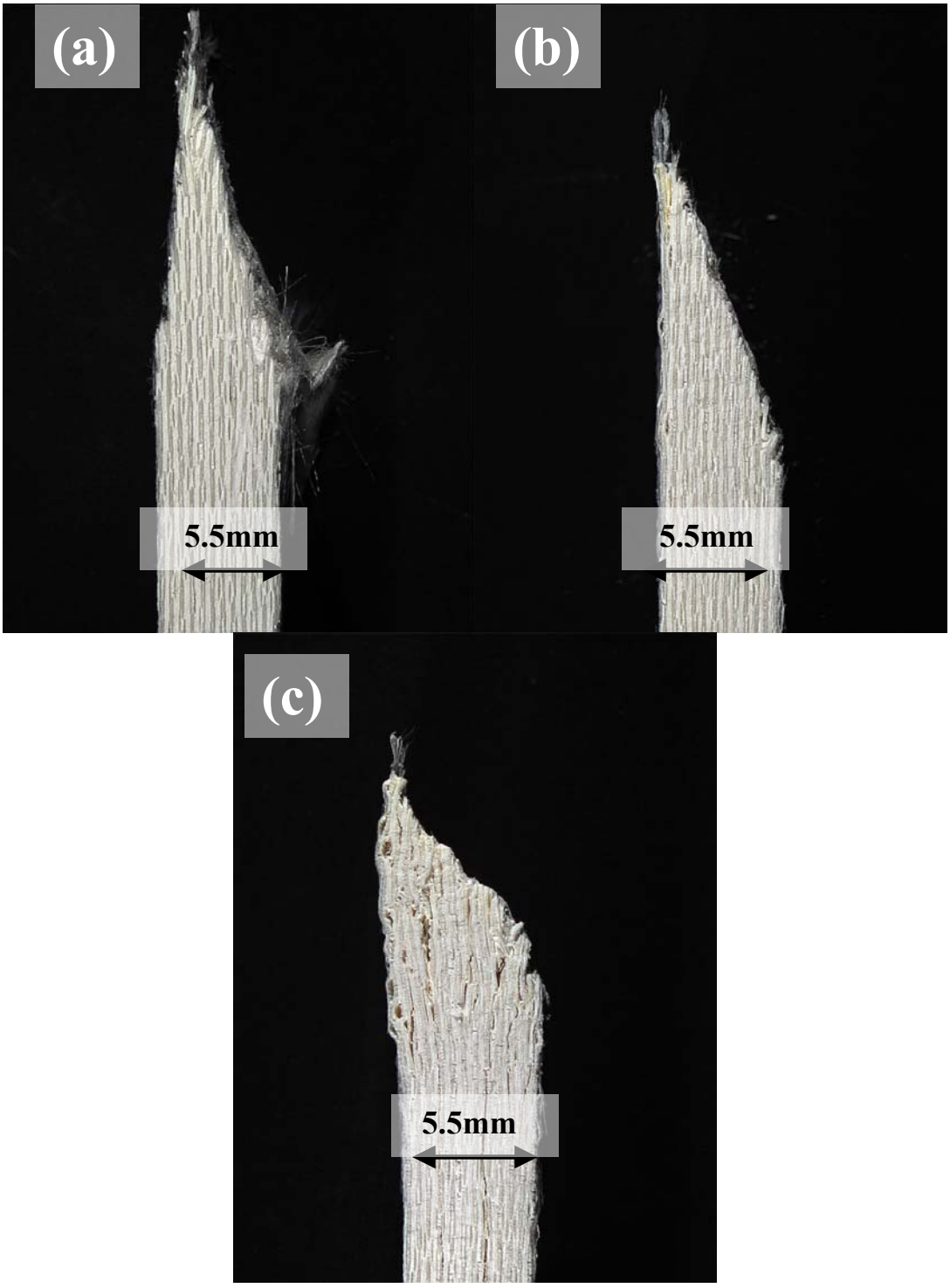

Figure 37. Damage Zones: compression to failure of N720/A specimens failed in creep in steam at 1200°C: (a) -100 MPa side view, (b) -60 MPa side view, (c) -40 MPa side view.

Figure 38 displays the fracture surfaces of the specimens used to explore the effect of loading rate on the compressive performance of N720/A in both air and steam environments. These specimens were subjected to monotonic compression tests at -0.0025 MPa/s, a much slower loading rate than that experienced by specimens tested in displacement control. Examination of these fracture surfaces reveals that they follow the same pattern in fracture topography as do the specimens tested in different environments.

The specimen tested in a laboratory air environment at a load rate of -0.0025 MPa/s exhibits similar characteristics to the as-processed sample tested in air at -0.05 mm/s. The damage zone of the specimen tested at -0.0025 MPa/s is only slightly shorter. The surface is very brushy with fibers separating from bundles. A clear stair-step appearance is observed indicating shearing was the failure mechanism as opposed to buckling or kinking of the fibers. On the other hand, the fracture surface of the specimen tested in steam looks much like those obtained for specimens subjected to creep loading in steam. The "smooth" appearance of the damage zone and the short length of the break all indicated that matrix densification paired with hydrothermal weakening were contributing factors to the failure mechanism. It is also interesting to note that mechanical loading in the presence of steam causes more degradation to the N720/A CMC material system than either loading or environment acting individually. The specimen failed in steam produced a compressive strength of only 54 MPa, a mere 44.3% of the compressive strength produced by the as-processed composite.

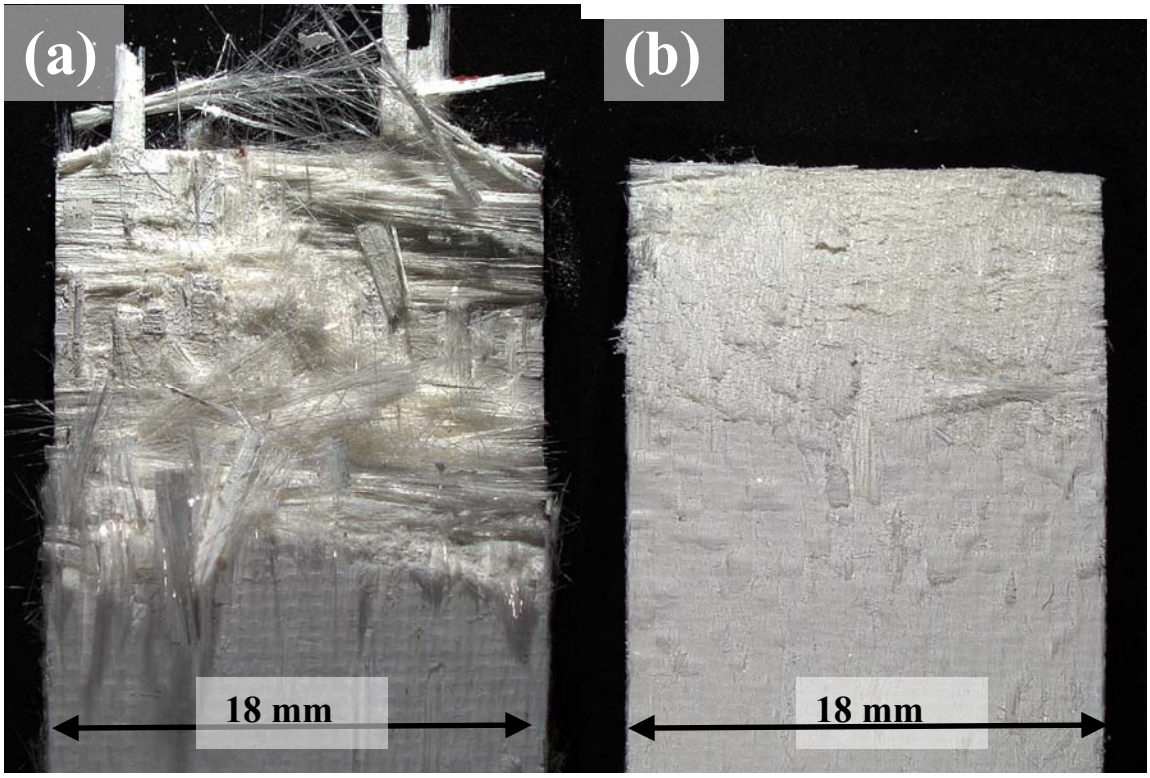

Figure 38. Fracture surfaces of N720/A specimens tested in monotonic compression at the rate of -0.0025 MPa/s at 1200°C: (a) air and (b) steam.

After creep testing was completed, it became very apparent that the presence of steam played a substantial role in the performance of N720/A under compressive loading. Concerns about the length of time required for steam to have a degrading effect and if the presence of steam alone could degrade the material system were presented. In order to answer these questions two loading scenarios were carried out. The first involved a compression to failure test in steam environment at 1200°C. The second scenario exposed N720/A to a steam environment at 1200°C at zero load for 25 h, then subjected this specimen to compression to failure after aging in steam. The two fracture surfaces in the Figure 39 provide some insight into the effect of prior aging at 1200°C in steam on the failure mechanisms of this CMC.

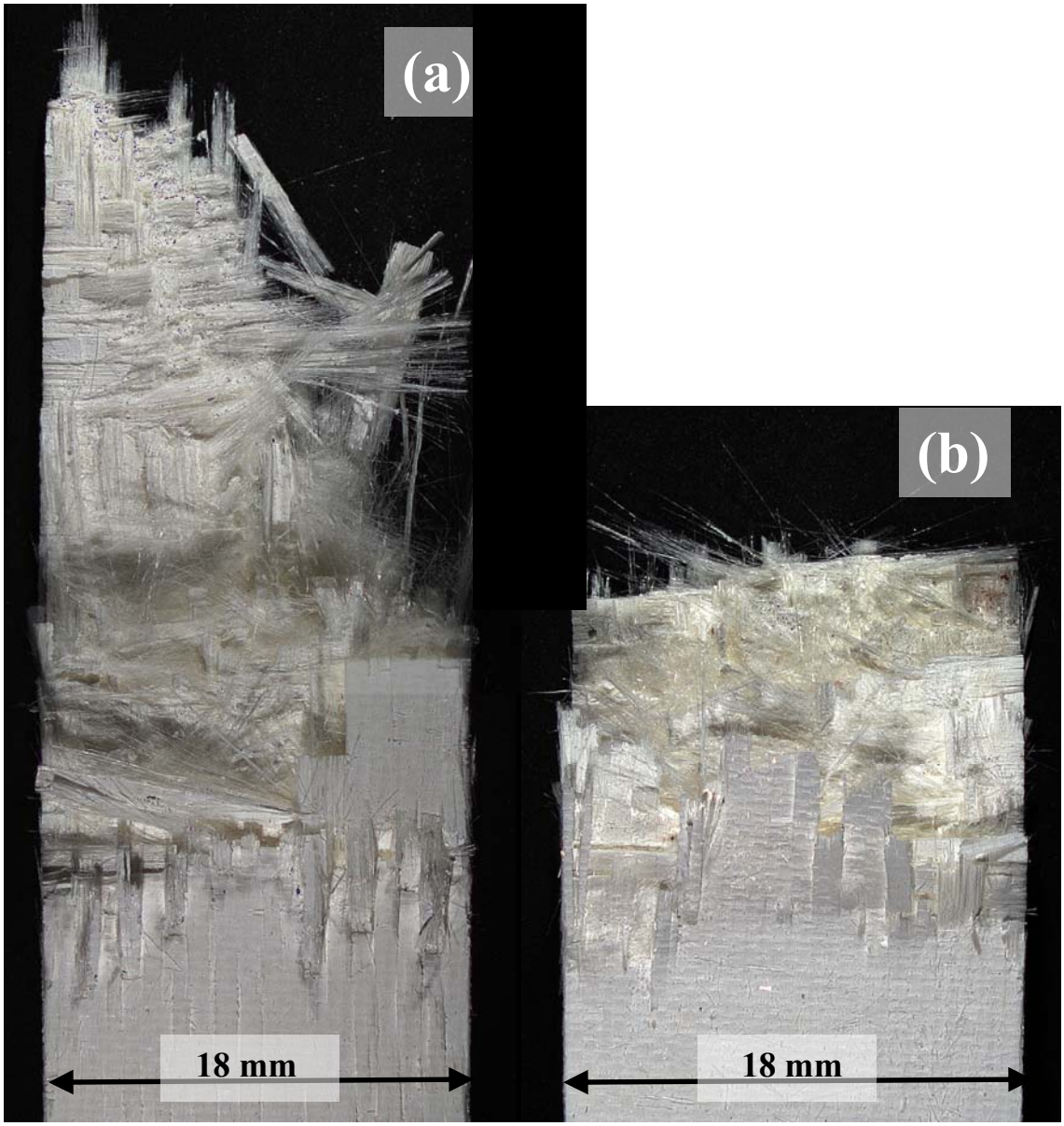

Figure 39. Fracture Surfaces: compression to failure of N720/A specimens failed at a displacement rate of -.05 mm/s at 1200°C: (a) steam and (b) aged for 25 hours in steam.

The fracture surface of the specimen tested in compression to failure in steam looks similar to that obtained in compression to failure test in air. The fracture surface has a brushy appearance. Additionally, the stair-step topography is observed indicating that fiber shearing is the damage mechanism responsible for failure. Results of the two tests reveal similar values of compressive modulus and strength as well.

The fracture surface of the specimen aged in steam for 25 h prior to compression to failure is much different from those produced in creep tests and in compression to failure tests conducted in steam for the N720/A material system. It appears to be a "hybrid" fracture surface exhibiting both fractures typically seen in air and those observed in specimens tested in steam. Although the fracture surface appears to have a brushy appearance the length of the damage zone is significantly reduced. The α-alumina matrix appears to have densified only slightly, this is indicated by uncorrelated fiber fracture. Data reveals that prior aging has a more degrading effect on the compressive strength and modulus than the presence of steam does during a compression to failure test. Ultimate compressive strength drops to -99 MPa and the modulus is reduced by 36.5%.

To identify the mechanism behind the strength and modulus degradation it is necessary to examine the fracture surface of the specimen tested at the slow rate of -0.0025 MPa/s in steam environment. The fracture surface is presented in Figure 38(b). Examination of the fracture surface reveals that the specimen failed through shearing of the matrix and fibers as one coordinated mass. This coordinated mass was created by the compressive load which caused a reduced porosity in the α-alumina matrix as well as matrix coarsening and densification. While steam environment causes coarsening and densification of the α-alumina matrix and the presence of hydrogen results in hydrothermal softening both mechanisms acting in concert, degrade compressive performance of N720/A CMC to a much greater extent than each mechanism would if acting alone.

5.8.2 Scanning Electron Microscopy

While inspection of fracture surfaces provided by optical microscopy can be valuable in assessing the general appearance and topography of individual specimens, SEM micrographs allow a closer view of the composite microstructure. The SEM micrographs are particularly useful in studying composites where interaction between matrix and fiber is essential in understanding composite performance. In this investigation the SEM permitted observation of specimen characteristics at up to 13000x magnifications. Areas of interest included the matrix, pulled-out fibers, and fiber still embedded in matrix. When examining matrix, points of interest include remaining matrix porosity, shape of matrix aggregate, and grain size. These attributes are valuable in demonstrating the impact of environment and loading scenarios on composite microstructure.

Specimens selected for observation with SEM included a virgin N720/A sample, a specimen tested in compression to failure in air, a specimen tested in creep at 60 MPa in air, a specimen tested in creep at 60 MPa in steam, a specimen tested in compression to failure at -0.0025 MPa/s in steam, and a specimen tested in compression to failure in steam in displacement control. This group of fracture surfaces was selected to best represent the overall effect of loading and environment on the compressive creep performance of N720/A at 1200°C.

The first point of interest is grain size of the matrix material. A prior discussion concerning the behavior of α-alumina matrix summarized the findings of a previous investigation [6] in which grain growth was observed during compressive creep testing. The images displayed in Figure 40 show the matrix grain size of an as-processed

specimen as well as the grain size of a specimen tested in compression to failure in air. Micrographs in Figure 40 show little change in grain size.

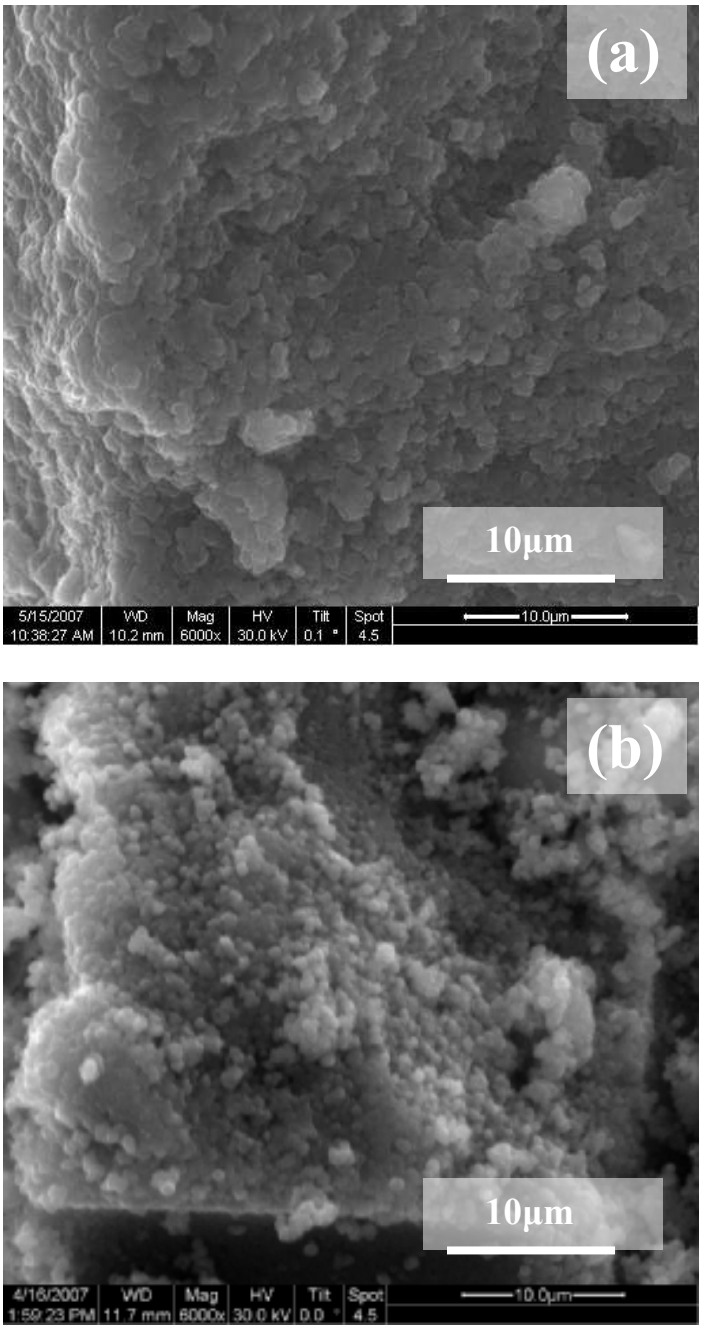

Figure 40. Fracture surfaces that exhibit grain growth in the α-alumina matrix of N720/A specimens (a) virgin specimen, (b) compression to failure in air at 1200°C.

The micrographs in Figure 41 display matrix grain size for specimens subjected to compressive creep in both air and steam at 60 MPa. While the specimen tested in air does not exhibit significant increase in matrix grain size, matrix grain growth is evident for the specimen tested in steam.

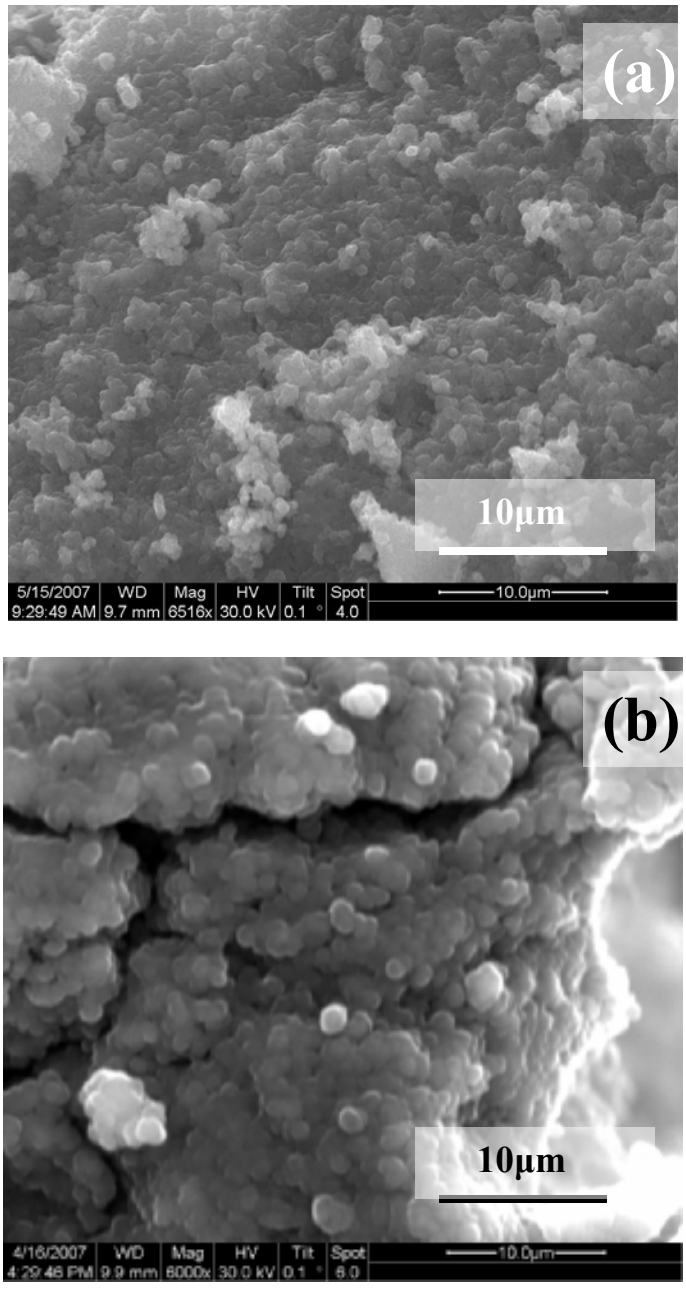

Figure 41. Fracture surfaces that exhibit grain growth in the α-alumina matrix of N720/A specimens at 1200°C (a) subjected to prior creep in air at 60 MPa, (b) subjected to prior creep in steam at 60 MPa.

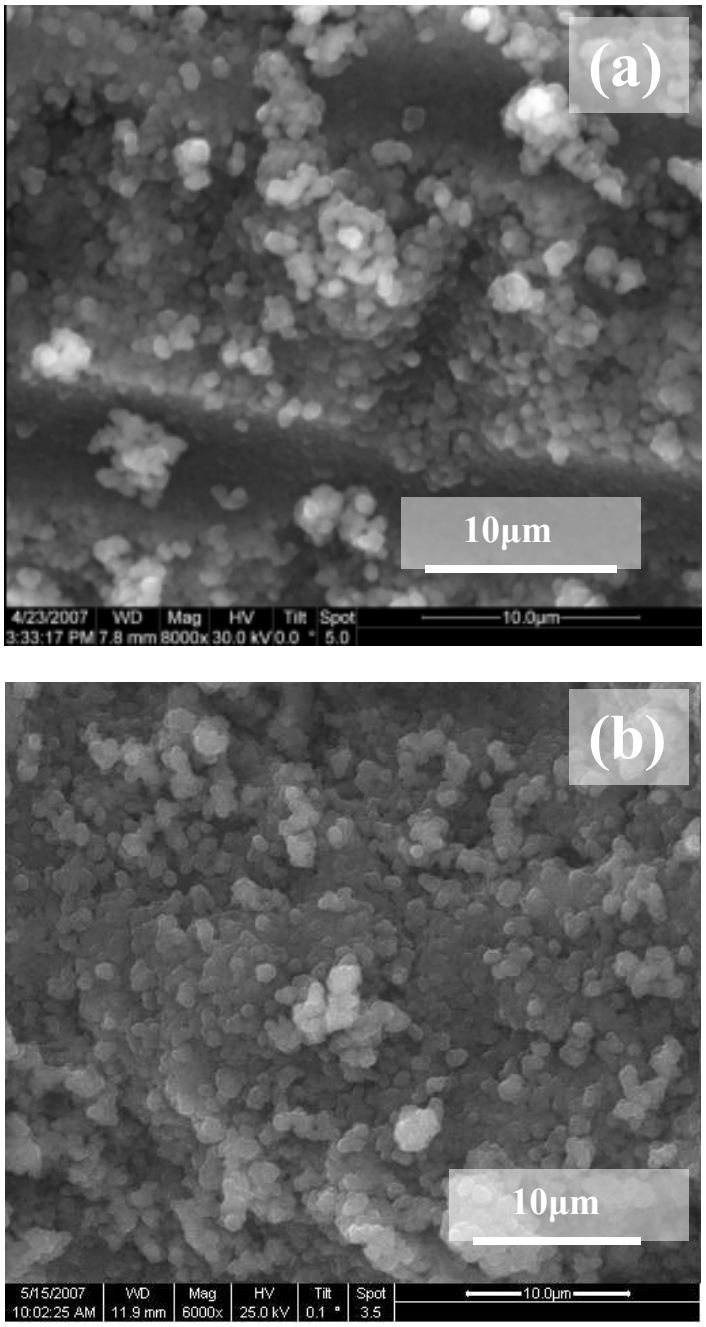

Figure 42. Fracture surfaces that exhibit grain growth in the α-alumina matrix of N720/A specimens at 1200°C (a) compression to failure at -.0025 MPa/s in steam, (b) subjected to 25 hours aging in steam and then failed in compression.

While specimens exposed to prior creep loading in laboratory air experienced an increase in compressive strength, the presence of steam considerably degraded compressive performance. Results presented earlier demonstrate that specimens tested in compression to failure in steam produced lower values of elastic modulus and compressive strength and larger failure strains than the specimens tested in air. Close observation of the micrographs in Figures 41(b), 42(a), and 42(b) show that all specimens subjected to compressive tests to failure conducted in steam exhibit significant grain growth in the matrix. It would seem that the same matrix strengthening that was observed in air would be experienced by the specimens tested in the steam environment. However, each specimen tested in steam exhibited early failure and a short lifetime. The introduction of hydrogen from the steam environment is responsible for corroding the α-alumina and degrading its performance. This occurrence has been termed "hydrothermal softening," a phenomenon during which interaction of elevated temperature and the presence of hydrogen soften the matrix making it more malleable and easily deformed. SEM micrographs provided on the following pages support this conclusion.

The second microstructural feature of interest are matrix troughs formed by the pulled-out fibers. This type of surface topography was not anticipated before testing commenced. However, examination under the SEM high vacuum mode revealed matrix troughs in all specimens tested in this research investigation. It is recognized that in the case of a porous-matrix conjugate no matrix holes or troughs would be observed on the fracture surface. In dense-matrix CMCs with "weak" interfaces, the fiber pull-out results in formation of matrix holes, where broken fibers slide out of the matrix. However, in the porous-matrix composite, the pull-out of fibers does not leave matrix sockets, but

causes fragmentation of the intervening matrix in the region of strain localization. The presence of matrix troughs on the fracture surface seen in Figure 43 indicates the loss of matrix porosity and an increase in matrix coarsening and densification. This densification process is attributable to additional sintering of the matrix. It is important to understand that α-alumina matrix used in this composite, is a porous material. Without support of fibers the α-alumina matrix material would move freely and would not maintain shape. Formation of matrix troughs illustrates that the matrix has been densified to the point at which it holds its shape without the support of any other constituent. The troughs (indentations) created by the pulled-out fibers indicate that the porous α-alumina has been densified by exposure to elevated temperature and compressive load.

The images displayed in Figure 40 show matrix troughs. Matrix troughs were observed in each specimen, with those observed in specimens subjected to creep tests and/or steam environment being more pronounced.

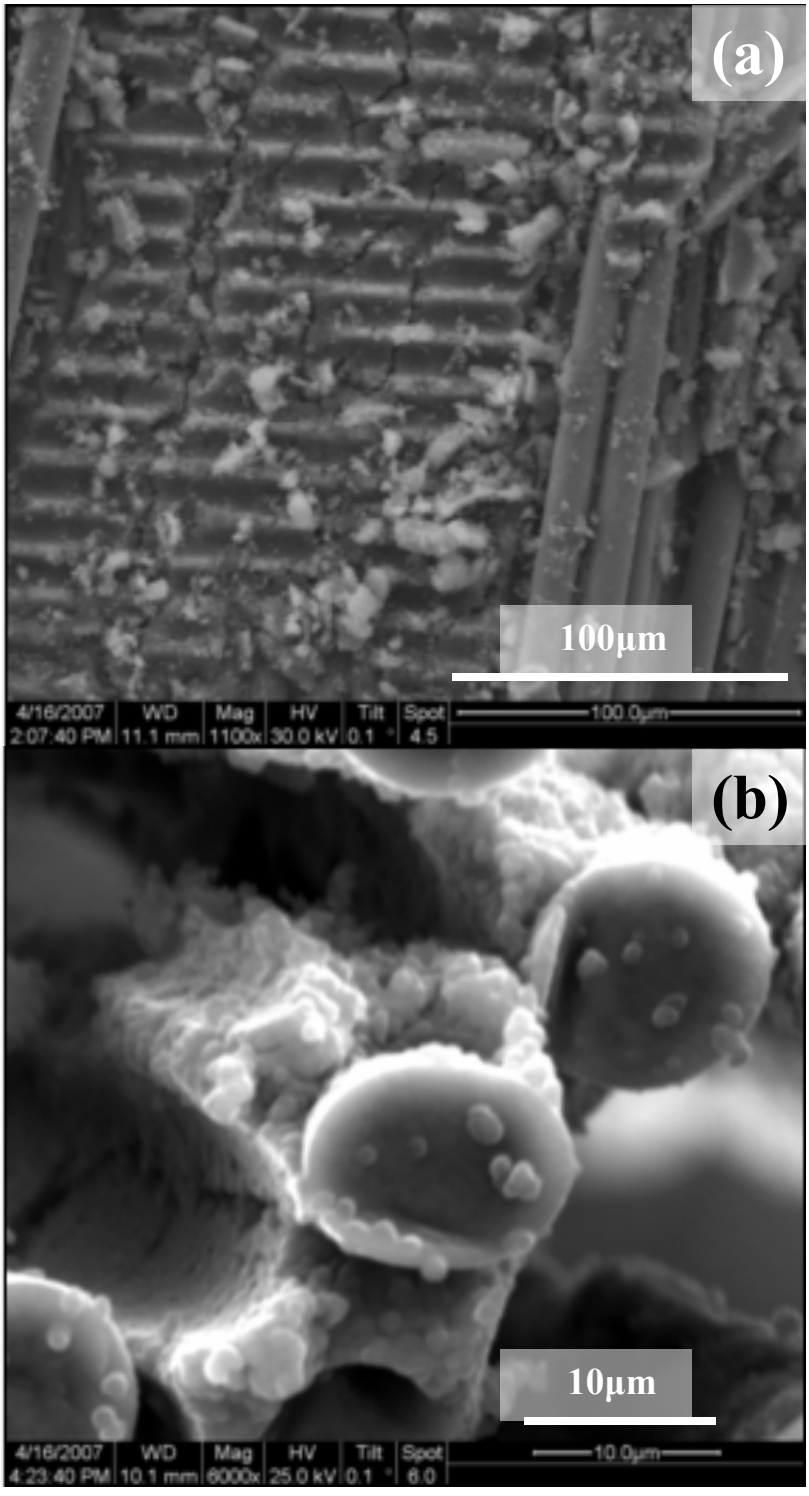

Figure 43. Fracture surfaces of N720/A specimens tested at 1200°C in: (a) compression to failure in air, (b) creep in steam at 60 MPa. Matrix troughs are apparent.

The micrograph in Figure 43(b) shows a close-up view of a group of fibers with one fiber missing. However, the matrix material which previously separated the fibers still maintains the shape it had when the fiber was lying in its trough. This image is an example of a matrix trough. The micrographs presented in Figure 44 show matrix troughs left by the 90° fibers. The fracture surface of the specimen tested in air at 60 MPa exhibits very clean and tight matrix troughs. Conversely, the specimen tested at low load rate in steam exhibits a considerable amount of matrix debris on the fracture surface in addition to the matrix troughs. This result suggests that matrix densification occurs at a faster rate under sustained loading than under a monotonically increasing load. It is important to recognize that in air, matrix densification occurs, which leads to matrix strengthening. Conversely, in steam matrix weakening is observed.

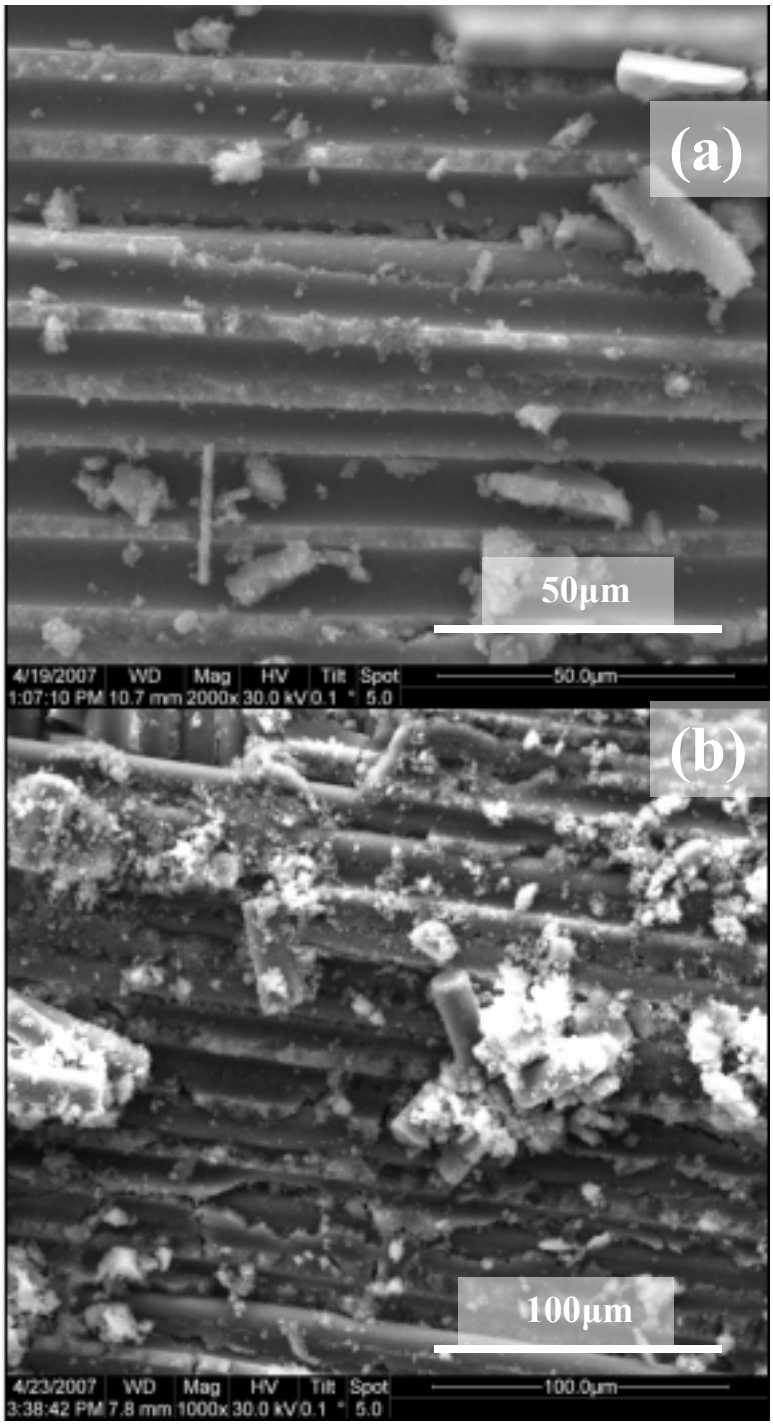

Figure 44. Fracture surfaces of N720/A specimens tested at 1200°C in: (a) creep in air at 60 MPa, (b) compression to failure at -0.0025 MPa/s in steam.

The micrograph shown in Figure 45 shows a matrix mass which previously supported 0° fibers in a specimen aged in steam for 25 hours and then failed in compression. The micrograph reveals matrix troughs as well as several of the 0° fibers that are still intact and holding onto the matrix despite the condition of the damage zone. This not only signifies that the matrix has densified but that hydrothermal softening resulting from exposure to steam indeed took place allowing the matrix to hold onto fiber fragments. The next sequence of micrographs reveals the effect of steam on failure and damage mechanisms and the compressive performance of N720/A.

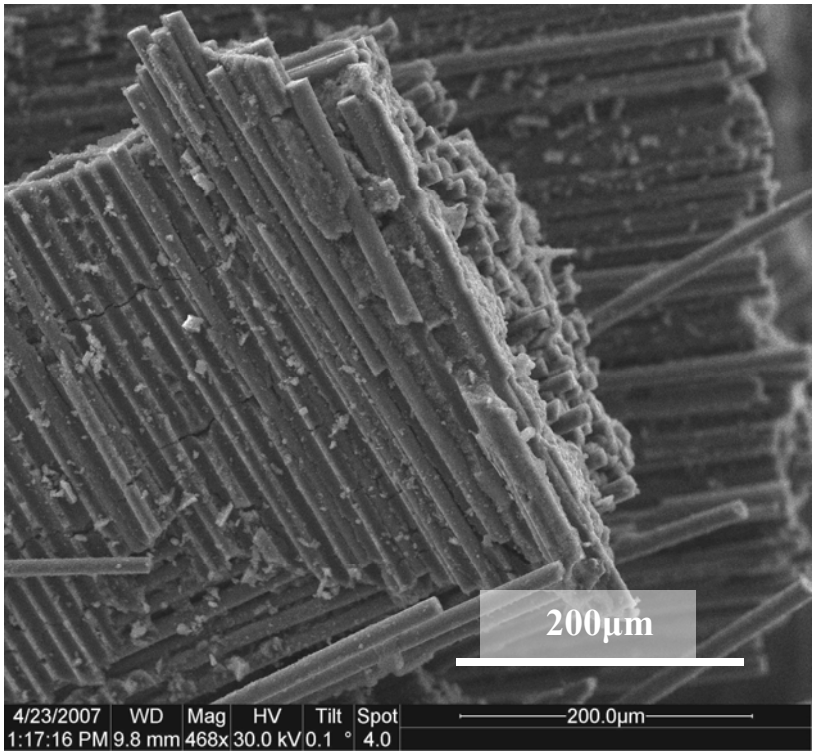

Figure 45. Fracture surface of an N720/A specimen subjected to 25 hours aging at 1200°C in steam, then tested in compression to failure at 1200°C in steam.

Throughout this research investigation when comparing fracture surfaces produced in steam to those produced in air, significant differences in appearance of the general topography were observed. The specimens tested in air generally had a brushy and fibrous fracture surface, whereas the fracture surfaces produced in steam are dominated by coordinated fiber failure.

Figure 46 shows the pull-out of fiber bundles in a specimen aged at 1200°C in steam for 25 h prior to testing and in a specimen failed in laboratory air. Both appear to be brushy, as is typical for specimens failed rapidly in a short-time test conducted in displacement control. However, the fiber bundles of the specimen aged in steam appear much more organized and tightly grouped together than those of the specimen tested in air. The presence of steam at elevated temperature exposes N720/A CMC to hydrogen, which has a softening effect on the matrix. As a result the matrix becomes coarser and more malleable causing large pieces of matrix to adhere to the fibers and to hold fiber bundles together. Finally, when the fibers begin to fail instead of splitting and fracturing separately, fiber bundles adhere and deform together. Conversely, in air these fiber bundles are more likely to separate and yield a very brushy appearance. Because specimens tested in both air and steam environments exhibited densification as indicated by matrix troughing, the hydrothermal softening must be responsible for the decrease in compressive performance of N720/A in steam.

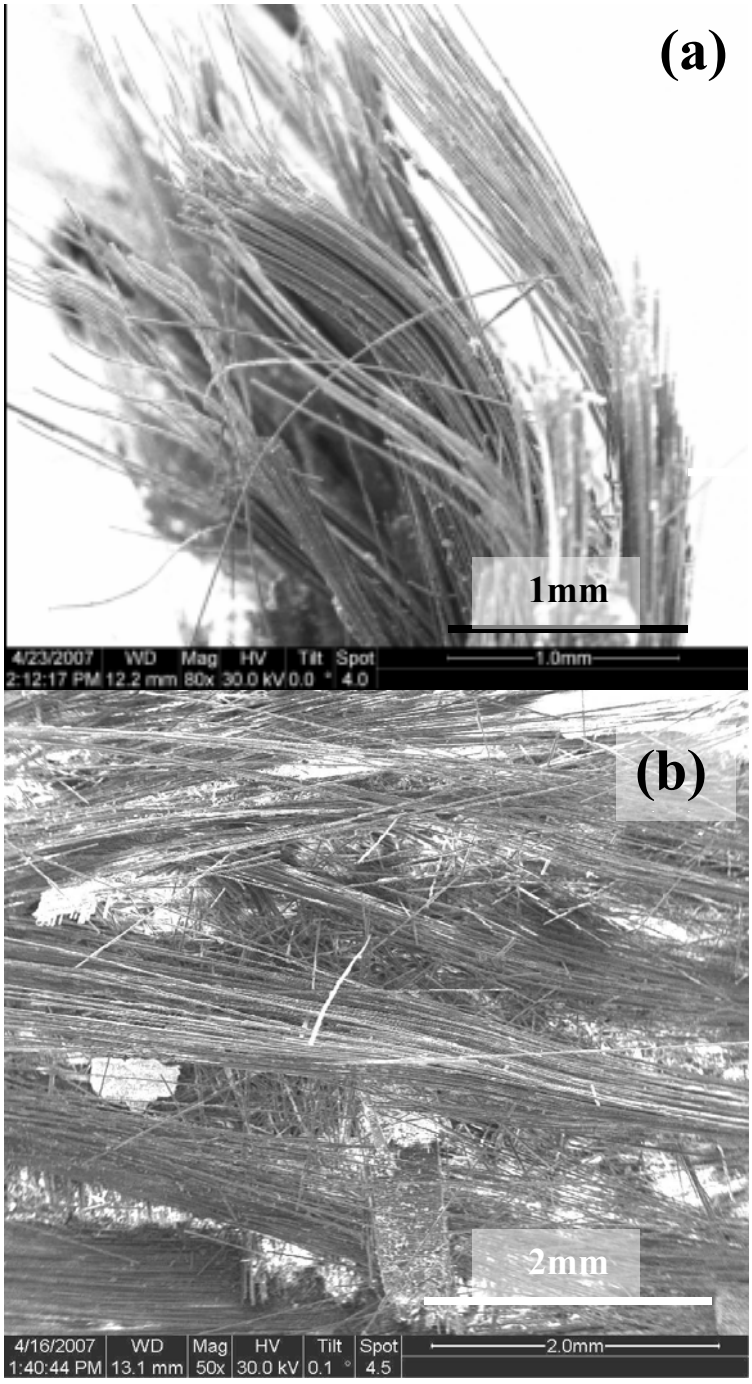

Figure 46. Fracture surfaces of N720/A specimens (a) subjected to 25 h aging at 1200°C in steam and then failed in compression, (b) compression to failure in air.

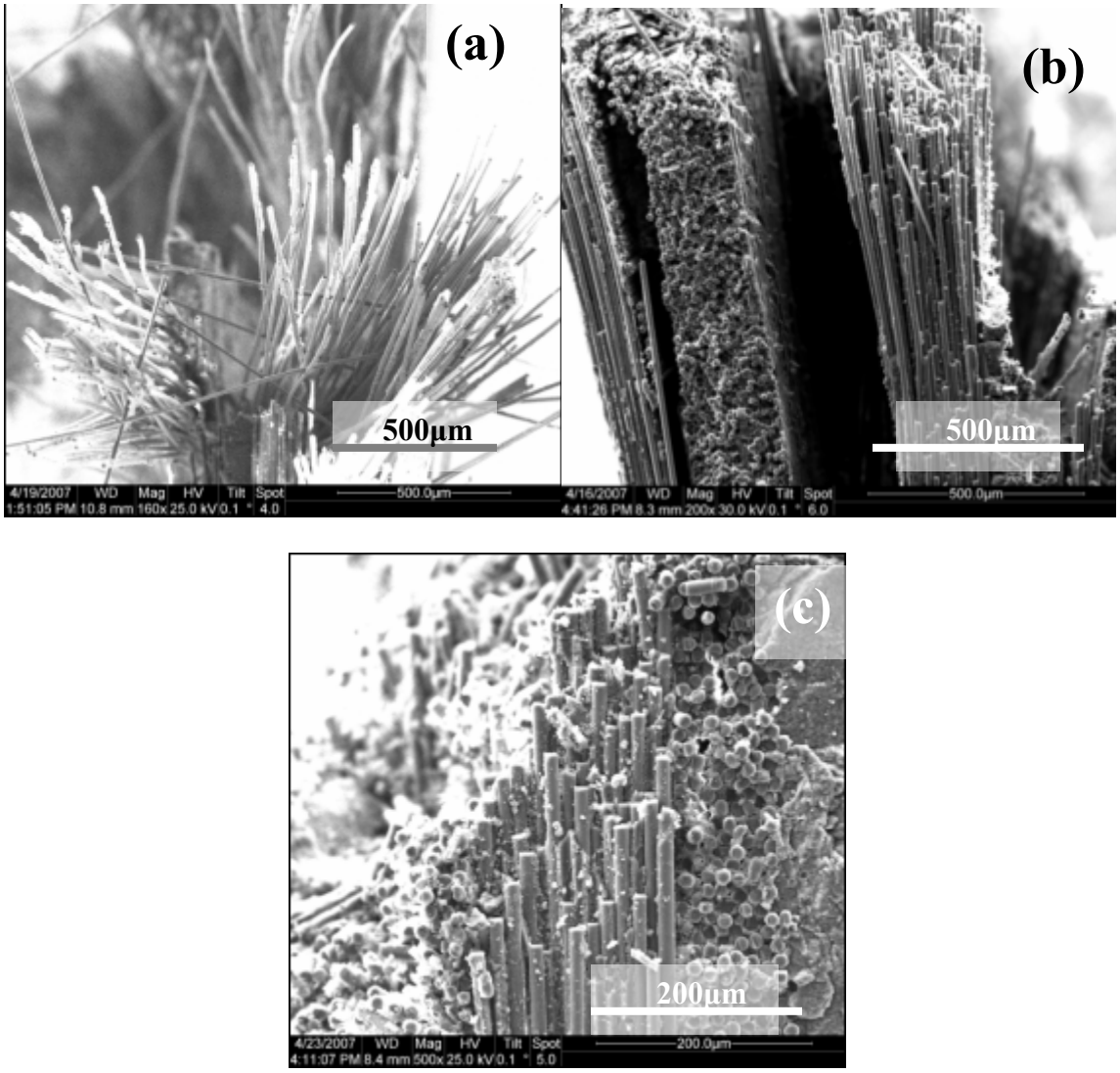

Figure 47. Fracture surfaces of N720/A specimens tested at 1200°C in: (a) creep in air at 60 MPa, (b) creep in steam at 60 MPa, (c) compression to failure at -0.0025 MPa/s in steam.

The images in Figure 47 further emphasize the difference in microstructure observed of specimens tested in air and those tested in steam. The specimen tested in air exhibits fiber pull-out where individual filaments are clearly discernable. Conversely fracture surfaces obtained in steam show areas of coordinated fiber fracture, where entire bundles appear to have fractured at once. Furthermore, considerable delamination is seen in specimens tested in steam. However, the fibers in each individual layer stay closely

packed. This is a strong indication that matrix altered by the hydrothermal softening does indeed keep individual fibers close together during loading.

Additionally, the image in Figure 38(b) of the specimen failed in the load-controlled test in steam environment shows the "smoothest" fracture surface of all the steam specimens tested in steam. Recall that this specimen produced the lowest compressive strength of a mere 55 MPa. These results suggest that monotonic loading at a slow rate in steam is detrimental to the compressive strength of N720/A. As matrix grain size increases and hydrothermal softening of the matrix occurs the matrix is significantly weakened. Next the fibers fail in shearing in a coordinated manner. The result is a smooth angled fracture surface that would be expected in a monolithic ceramic material. The fibers adhere to the matrix with such intensity it is almost difficult to distinguish two constituent materials with the naked eye.

One of the manifestations of matrix densification is the amount of matrix that remains attached to exposed fibers after failure. α-Alumina matrix in the as-processed specimen is porous. Therefore only very small pieces of matrix would remain bonded to the pulled-out fibers after specimen failure. However, as the matrix coarsens and densifies due to exposure to elevated temperature under sustained loading, larger and larger pieces of matrix adhere to the pulled-out fibers until the matrix densifies to such an extent as to inhibit fiber pull-out.

The images in Figure 48 and 49 show that all specimens exhibit some amount of matrix bonded to the exposed fibers. However, it is seen that each specimen exhibits a different amount of matrix bonded to its fibers. The specimen tested in compression to failure in air and the specimen tested in compression to failure in steam following 25 h of

aging at 1200°C in steam clearly show the least amount of matrix bonded to exposed fibers. This is a predictable observation due to the fact that it has been established that densification is accelerated when specimens are subjected to sustained loading. In the case of these specimens, neither experienced loading for more than twenty seconds. This indicates that although steam was present during the aging of the specimen in Figure 48(b), it had little effect on the densification experienced by the matrix during compression to failure.

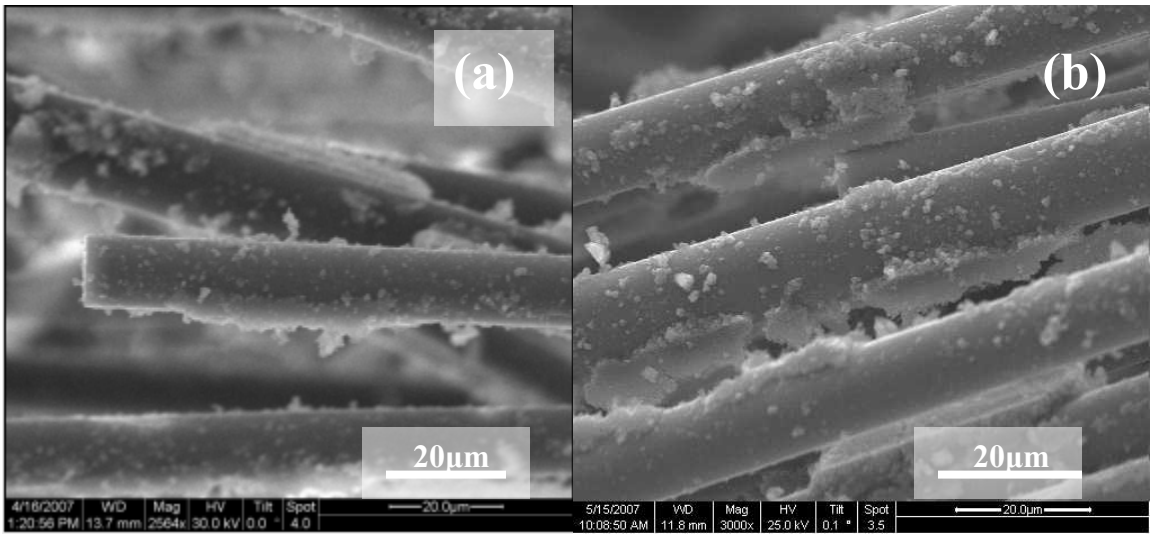

Figure 48. Fracture of N720/A specimens tested at 1200°C in: (a) compression to failure in air, (b) compression to failure in steam following 25 h of aging at 1200°C in steam.

Micrographs in Figure 49 show fracture surfaces of specimens tested in creep at -60 MPa in air and in steam as well as the fracture surface obtained in a load-controlled compression to failure test conducted in steam. Note that the fracture surfaces obtained in creep at -60 MPa shown in Figure 49(a) and 49(b) show considerably larger pieces of matrix bonded to the fibers than those in Figure 48. This observation suggests that matrix

densification occurred under sustained compressive loading in the case of the specimen subjected to creep in air at 1200°C. Further examination of the micrographs in Figure 49 reveal that the specimen subjected to creep in steam at 1200°C has the greatest amount of matrix attached to fibers of any specimen examined under the SEM in this study. This finding indicates that when a specimen is exposed to both steam and sustained loading its matrix densifies to a much greater degree. This matrix densification is due to both load and hydrothermal softening attributable to exposure to steam environment at 1200°C. These findings are confirmed by examining the fracture surface of the specimen tested at slow stress rate shown in Figure 49(c) which was exposed to a steam environment at 1200°C under monotonic compression, which exhibits a fairly large amount of matrix remaining bonded to the fibers.

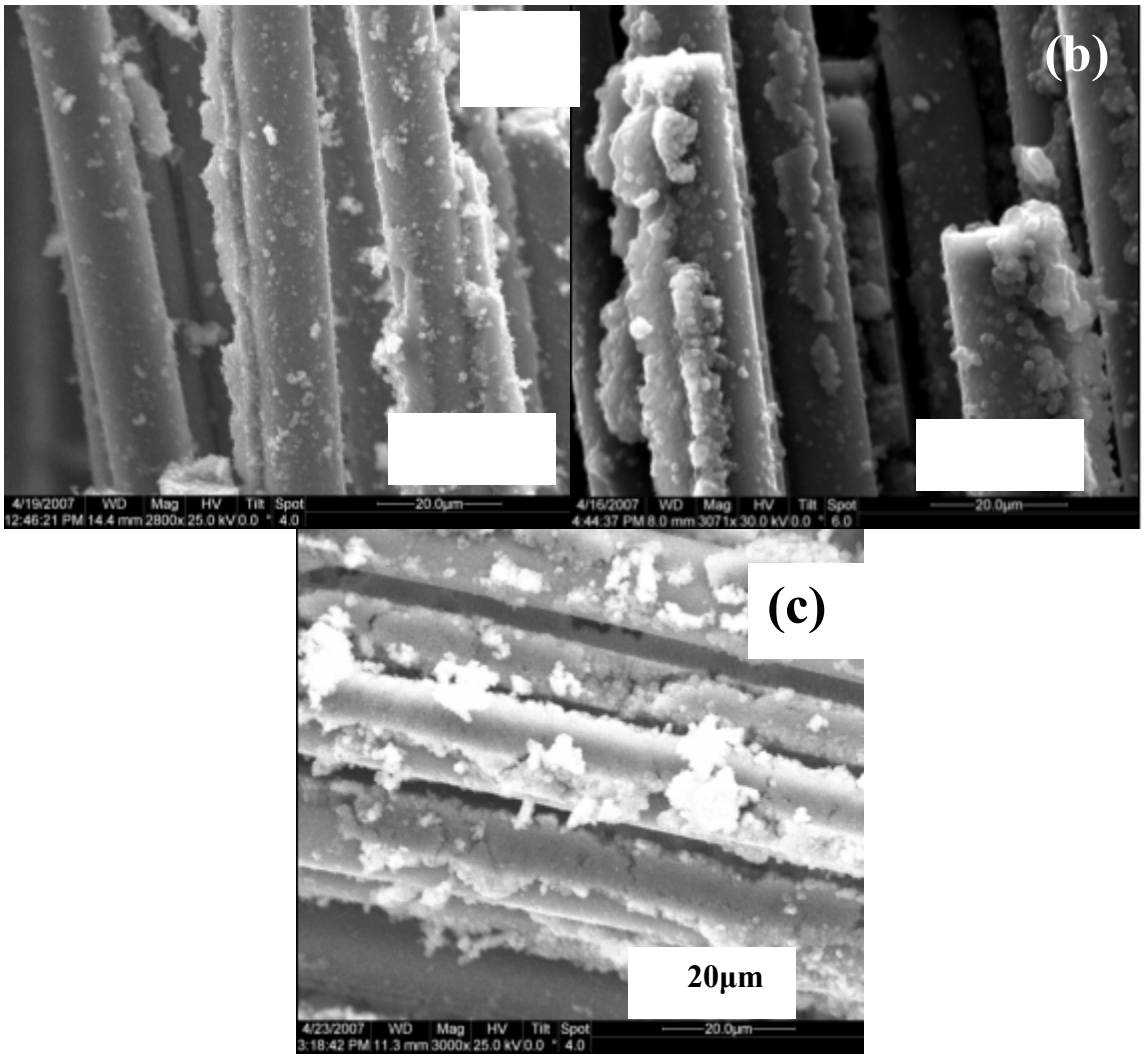

Figure 49. Fracture of N720/A specimens tested at 1200°C in: (a) creep in air at 60 MPa, (b) creep in steam at 60 MPa, (c) compression to failure at -0.0025 MPa/s in steam.

.

Results of this effort indicate that steam environment is a bad actor in regards to the compressive performance N720/A composite. Degrading effects of steam environment are exacerbated by sustained loading.

VI. Conclusions and Recommendations

This was the first research investigation exploring the compressive performance of Nextel^{TM} 720/Alumina CMC. Monotonic compression tests were performed in air and steam at 1200°C. The compressive modulus was 69 GPa, the compressive strength was -122 MPa, and failure strain was -0.207%. Additionally, compressive creep tests were also conducted at 1200°C in both air and steam. Tests conducted in air at stresses of -100, -80, and -60 MPa achieved run-out of 100 h. All creep strains accumulated in air were less than 0.41%. In steam creep tests were conducted at -100, -60, and -40 MPa. In steam, creep run-out was not achieved. Interestingly, the creep strains accumulated achieved in compressive creep tests performed in steam at 1200°C were massive: 0.188% at -100 MPa, 1.122% at -60 MPa, and 1.577% at -40 MPa.

Minimum creep rate was reached in all tests. Steady-state strain rates in air environment ranged from 10^{-8} to 10^{-7} s^{-1}. The presence of steam drastically accelerated creep, increasing creep rate magnitudes by as much as 5 orders of magnitude. In steam, creep strain rates ranged from 10^{-7} to 10^{-2} s^{-1}. In air, larger creep strains were accumulated at higher creep stress levels. In steam due to the fact that creep strain rates were so large at higher stress levels, specimens failed before they could accumulate creep strain. Therefore in steam, creep strain accumulation decreased with increasing creep stress.

Creep tests that achieved creep run-out were subjected to monotonic tests to failure in order to determine retained strength and stiffness. In this investigation only specimens tested in air achieved run-out. Specimens subjected to prior creep in air at -100 and -60 MPa were tested in compression to failure after creep run-out was achieved.

Both specimens exhibited an increase in compressive strength of .8% and 12.3%. However, the compressive modulus of both specimens was reduced by 34% and 24.7%. The specimen which survived compressive creep at -80 MPa was tested in tension to failure. Tensile strength was reduced by 30%, and elastic modulus was reduced by 20%.

Specimens tested in steam produced "smoother" and more coordinated fracture surfaces and shorter damage zones than those tested in air. The diagonal shearing of the specimens tested in steam indicated that matrix and fiber failed in a coordinated manner. As would be expected, areas of uncorrelated fiber fracture were more prevalent in fracture surfaces of specimens tested in air. It is noteworthy that the coordinated fracture surfaces were associated with a significant decrease in compressive strength. On the other hand, specimens tested in laboratory air actually gained strength.

Several factors are responsible for the aspects of compressive performance of N720/A at 1200°C observed in this study. First, the increase in the ultimate compressive strength of N720/A in specimens tested in creep in air can be attributed to a decrease in matrix porosity due to additional sintering of the matrix. However, the opposite trend is seen in tests conducted in a steam environment. Although the same matrix densification process that occurs in air appears to occur in steam, an additional factor causes weakening of the matrix. The steam environment introduces hydrogen and oxygen to the material system. The oxide/oxide fiber and matrix constituents found in N720/A were specifically designed to combat the effects of oxidation. However, hydrogen has a corrosive effect on the matrix material which is referred to as hydrothermal softening. This results in the weakening of the matrix and a significant loss of compressive strength.

Recommendations for future work include two additional microscopy methods that would be beneficial to fully understanding the compressive behavior of N720/A. The first method involves a Transmission Electron Microscope (TEM) analysis. This would allow examination of fracture surfaces at much higher magnifications than SEM imaging. The most applicable use of TEM in this research would be to quantify the actual grain size of N720/A matrix grains. SEM analysis only allows a qualitative comparison of grain size, therefore quantifying grain growth for associated stress levels and temperatures would be extremely valuable in understanding how much α-alumina matrix changes under compressive load at elevated temperature.

Additionally, a three-dimensional (3-D) SEM would allow a more detailed understanding of fracture surfaces. A third dimension would be valuable in truly understanding fracture surfaces and how different microstructure characteristics such as matrix troughs and matrix embedded on fibers are spatially related to each other in three dimensions. A 3-D SEM could accomplish this by incorporating a Focused Ion Beam (FIB) for real-time micro cross sectioning. These results would be useful in analyzing the effects of matrix densification and hydrothermal softening due to exposure to steam.

Appendix A. Additional SEM Micrographs

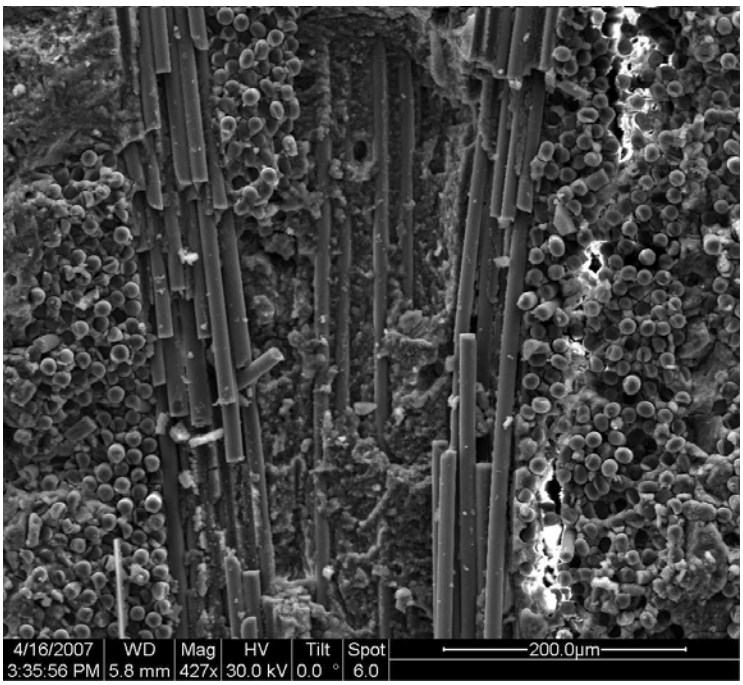

Figure 50. Fracture surface of N720/A specimen tested in compression to failure in displacement control at a rate of -0.05 mm/s in steam at 1200°C.

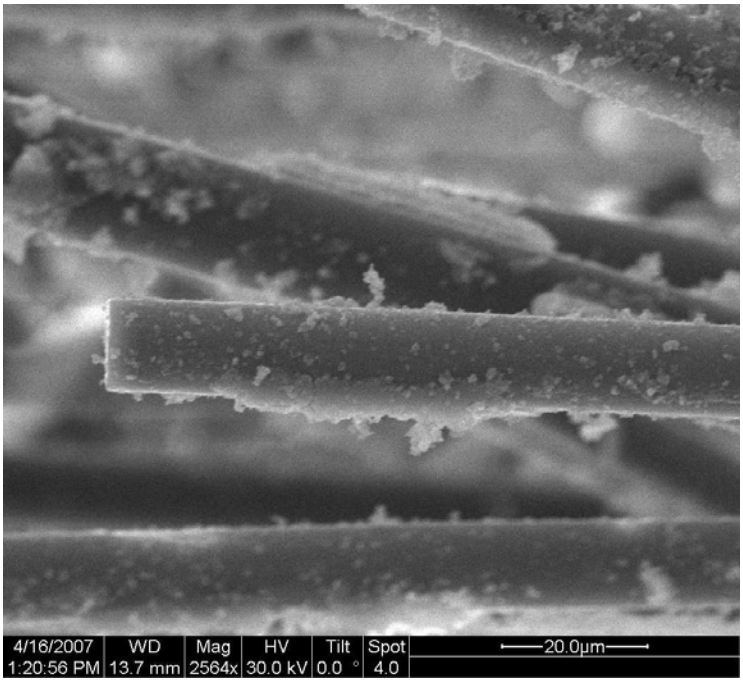

Figure 51. Fracture surface of N720/A specimen tested in compression to failure in displacement control at a rate of -0.05 mm/s in steam at 1200°C.

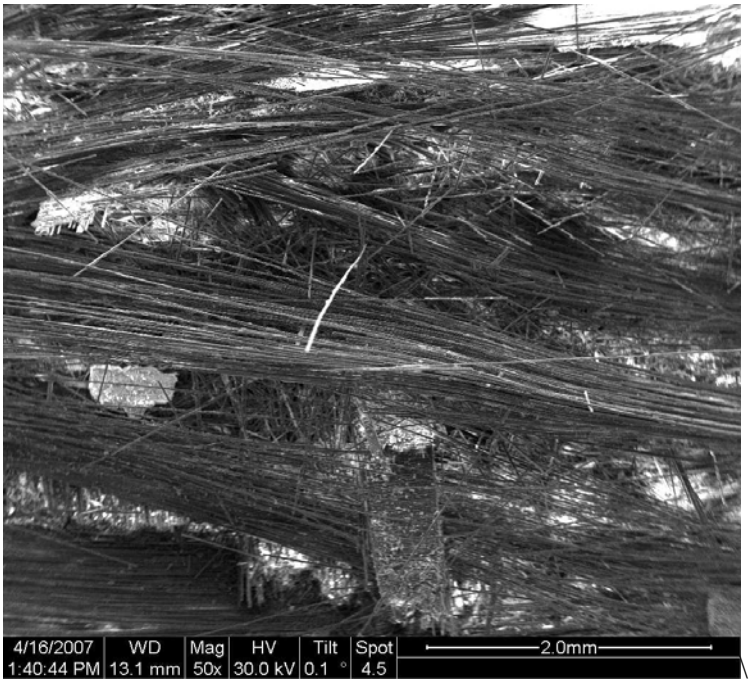

Figure 52. Fracture surface of N720/A specimen tested in compression to failure in displacement control at a rate of -0.05 mm/s in steam at 1200°C.

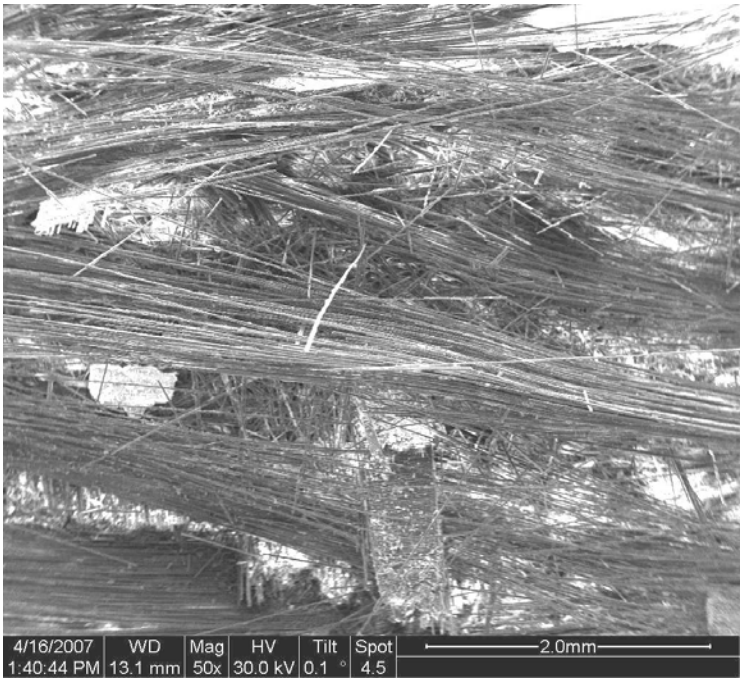

Figure 53. Fracture surface of N720/A specimen tested in compression to failure in displacement control at a rate of -0.05 mm/s in steam at 1200°C.

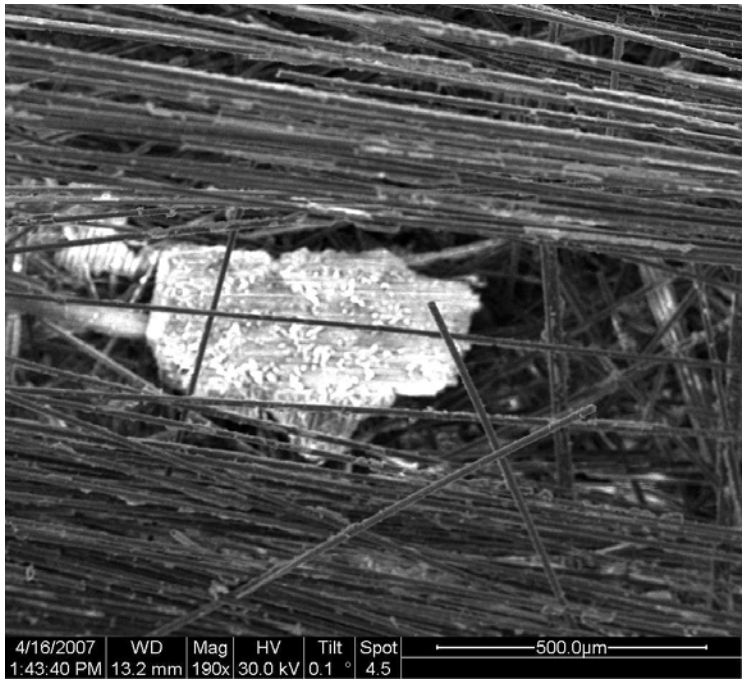

Figure 54. Fracture surface of N720/A specimen tested in compression to failure in displacement control at a rate of -0.05 mm/s in steam at 1200°C.

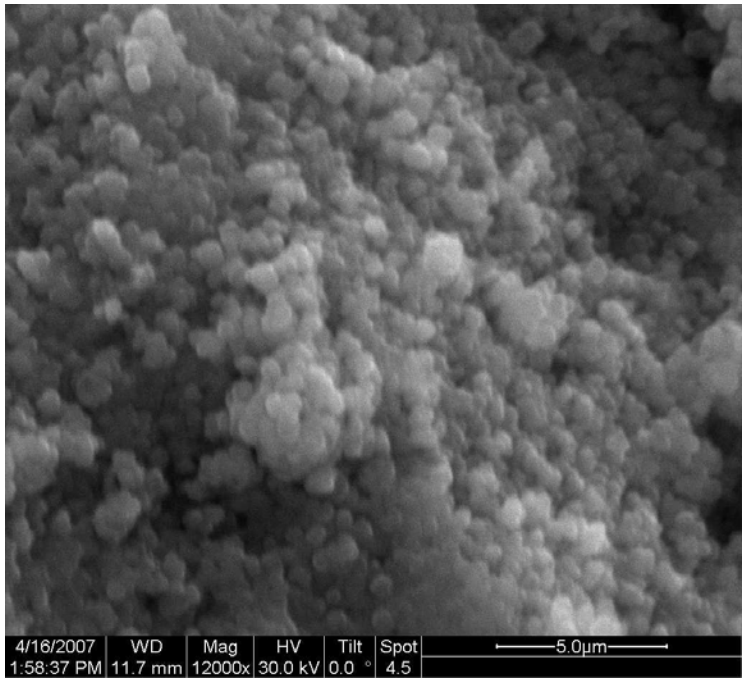

Figure 55. Fracture surface of N720/A specimen tested in compression to failure in displacement control at a rate of -0.05 mm/s in steam at 1200°C.

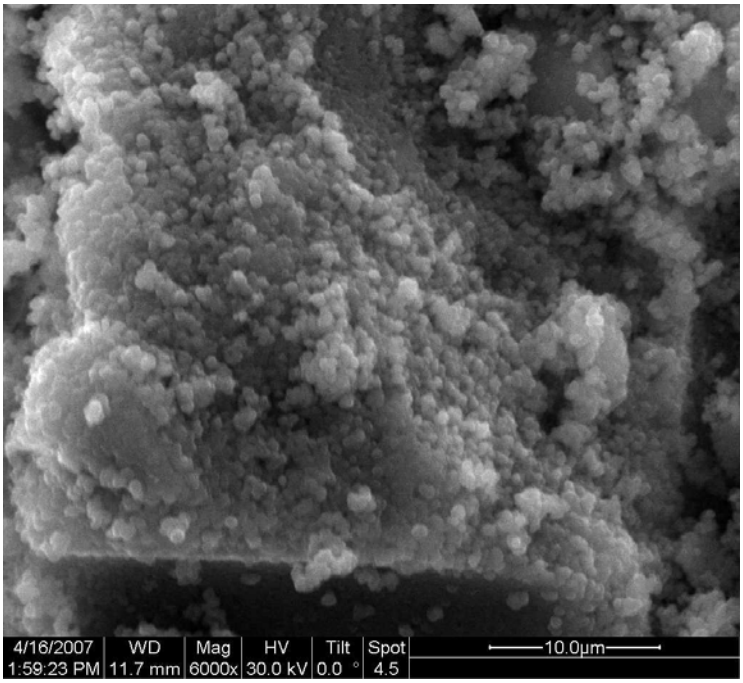

Figure 56. Fracture surface of N720/A specimen tested in compression to failure in displacement control at a rate of -0.05 mm/s in steam at 1200°C.

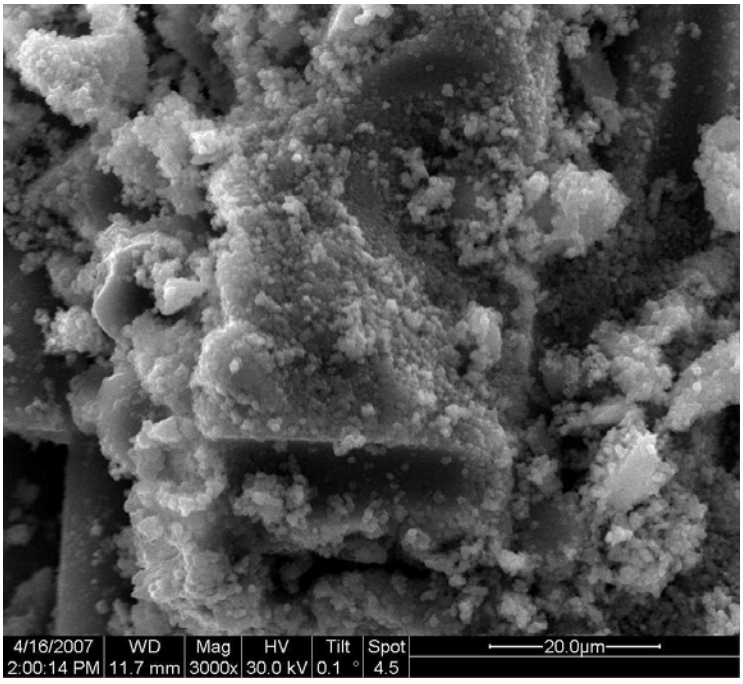

Figure 57. Fracture surface of N720/A specimen tested in compression to failure in displacement control at a rate of -0.05 mm/s in steam at 1200°C.

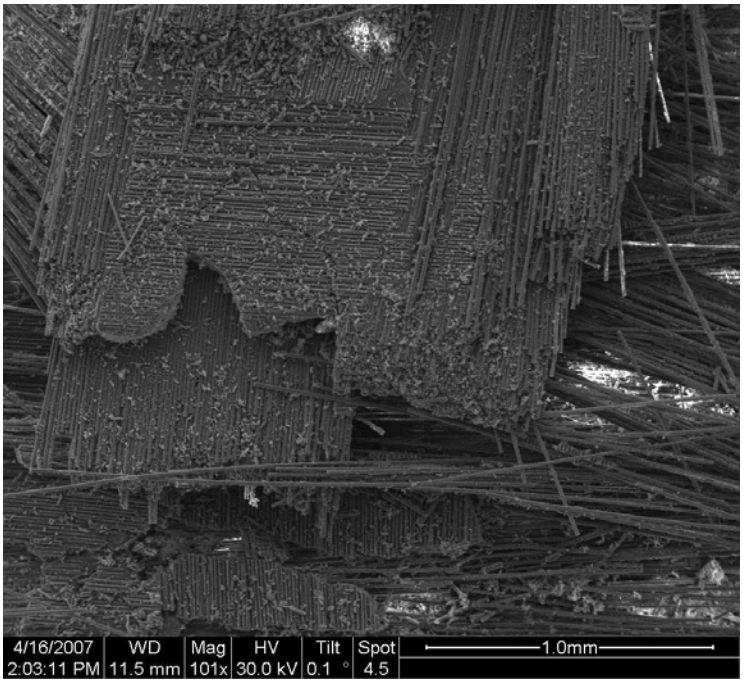

Figure 58. Fracture surface of N720/A specimen tested in compression to failure in displacement control at a rate of -0.05 mm/s in steam at 1200°C.

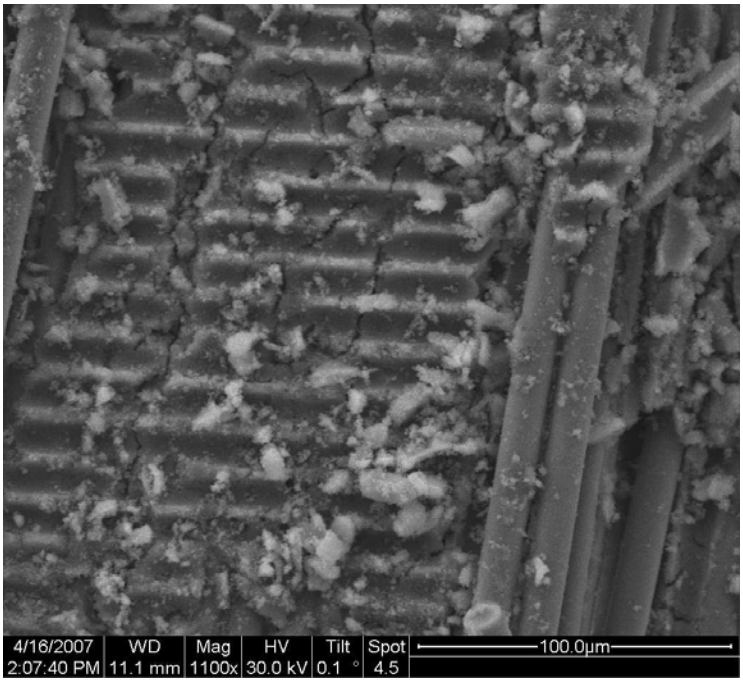

Figure 59. Fracture surface of N720/A specimen tested in compression to failure in displacement control at a rate of -0.05 mm/s in steam at 1200°C.

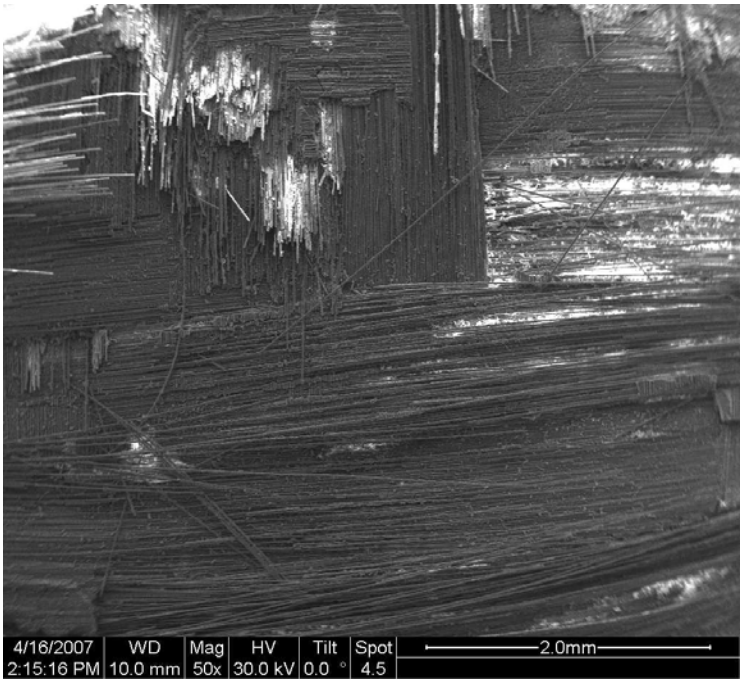

Figure 60. Fracture surface of N720/A specimen tested in compression to failure in displacement control at a rate of -0.05 mm/s in steam at 1200°C.

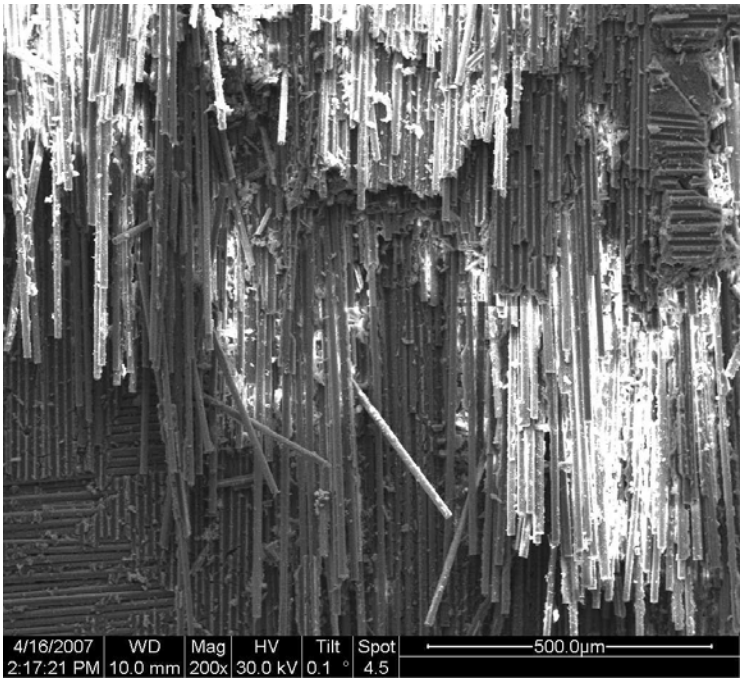

Figure 61. Fracture surface of N720/A specimen tested in compression to failure in displacement control at a rate of -0.05 mm/s in steam at 1200°C.

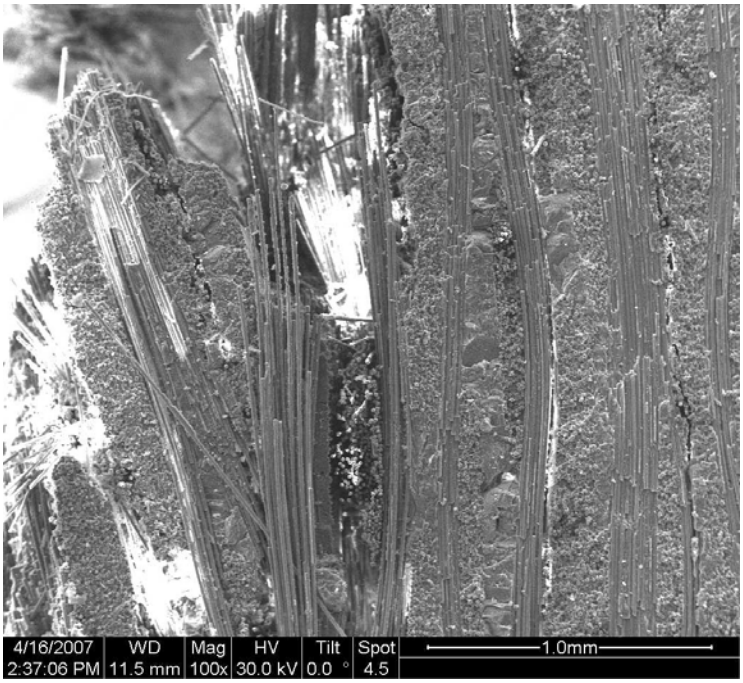

Figure 62. Fracture surface of N720/A specimen tested in compression to failure in displacement control at a rate of -0.05 mm/s in steam at 1200°C.

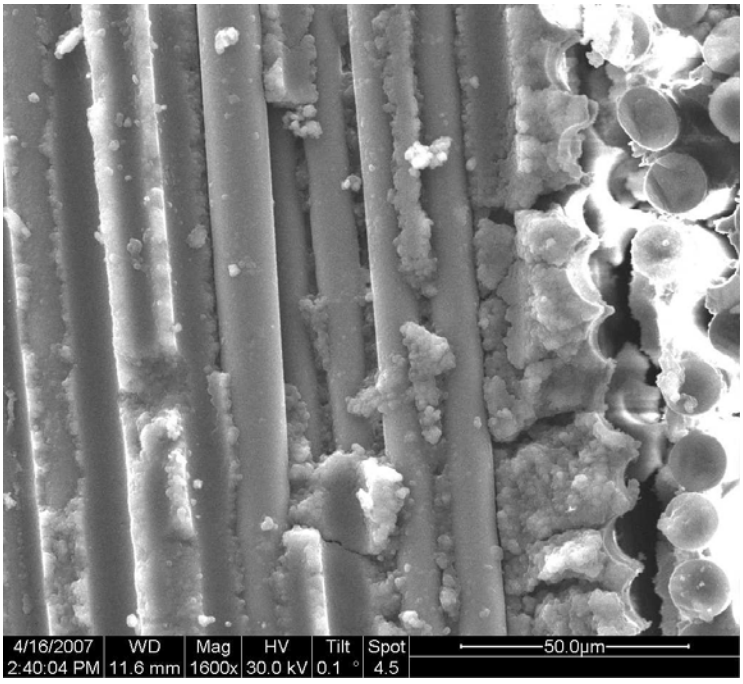

Figure 63. Fracture surface of N720/A specimen tested in compression to failure in displacement control at a rate of -0.05 mm/s in steam at 1200°C.

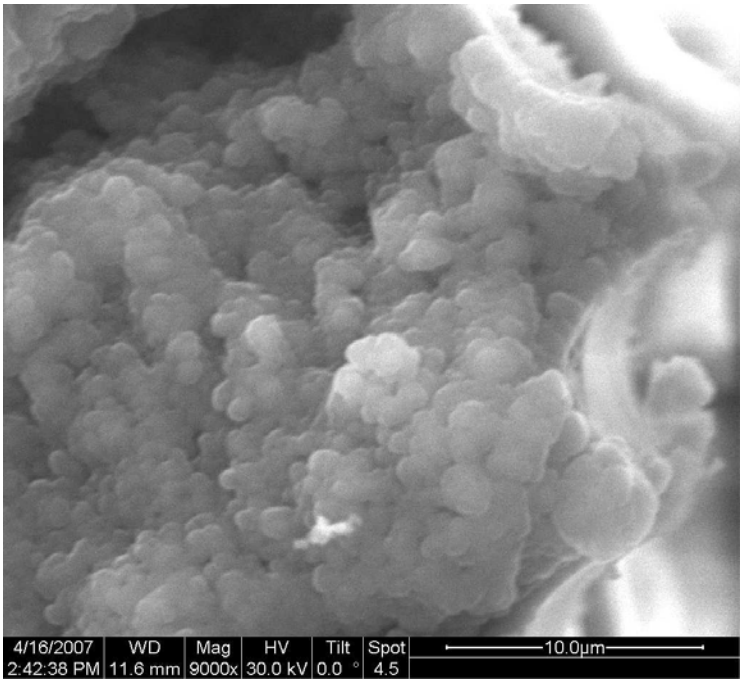

Figure 64. Fracture surface of N720/A specimen tested in compression to failure in displacement control at a rate of -0.05 mm/s in steam at 1200°C.

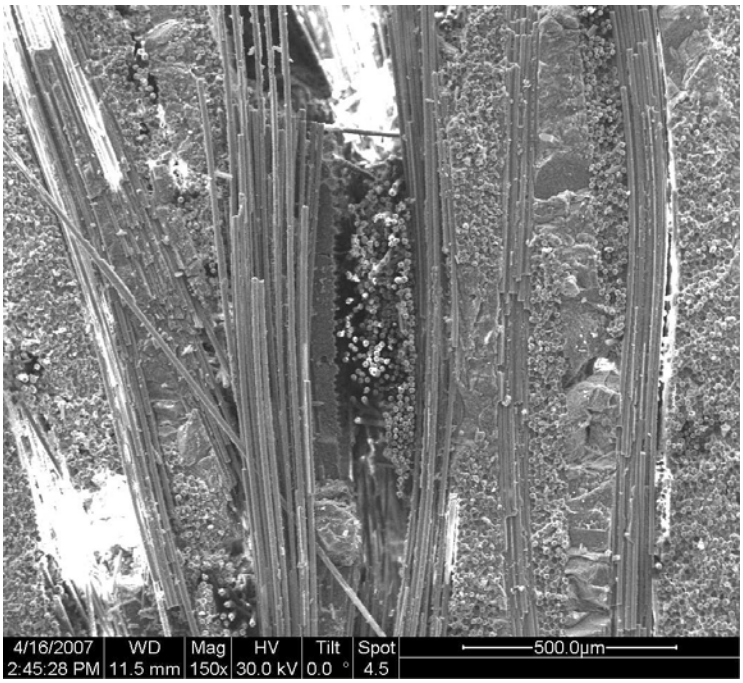

Figure 65. Fracture surface of N720/A specimen tested in compression to failure in displacement control at a rate of -0.05 mm/s in steam at 1200°C.

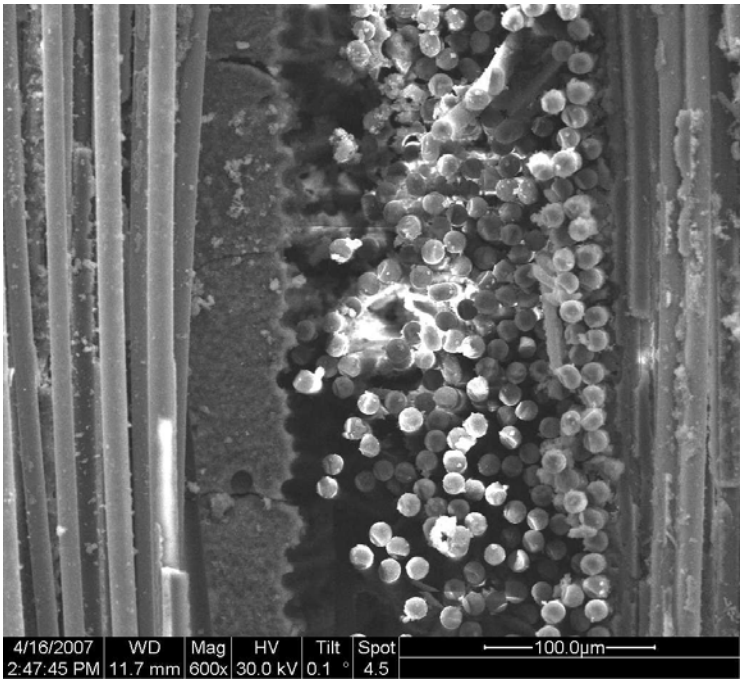

Figure 66. Fracture surface of N720/A specimen tested in compression to failure in displacement control at a rate of -0.05 mm/s in steam at 1200°C.

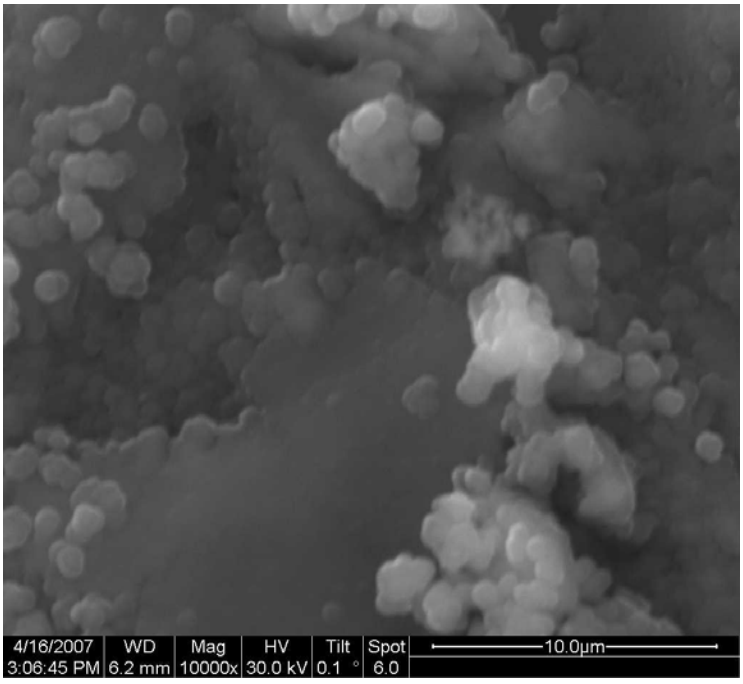

Figure 67. Fracture surface of N720/A specimen tested in compression to failure in displacement control at a rate of -0.05 mm/s in steam at 1200°C.

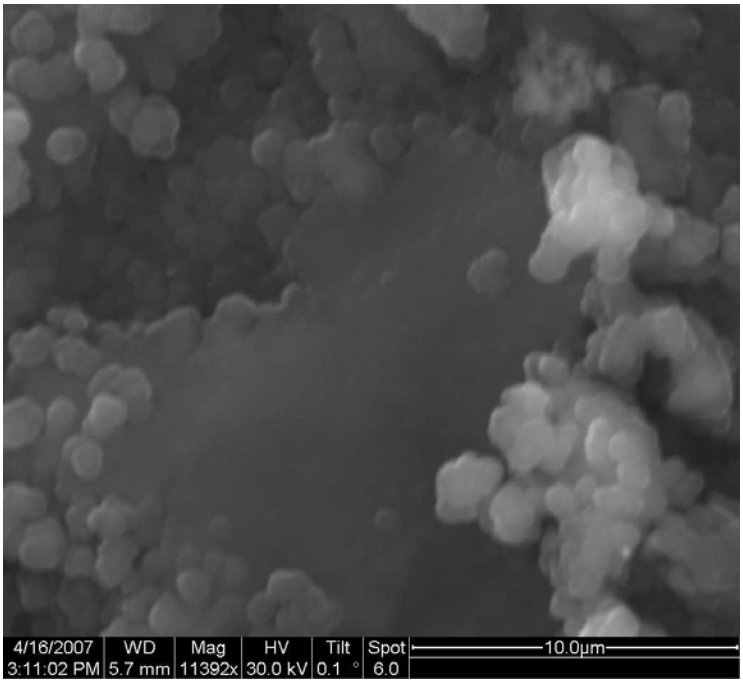

Figure 68. Fracture surface of N720/A specimen tested in compression to failure in displacement control at a rate of -0.05 mm/s in steam at 1200°C.

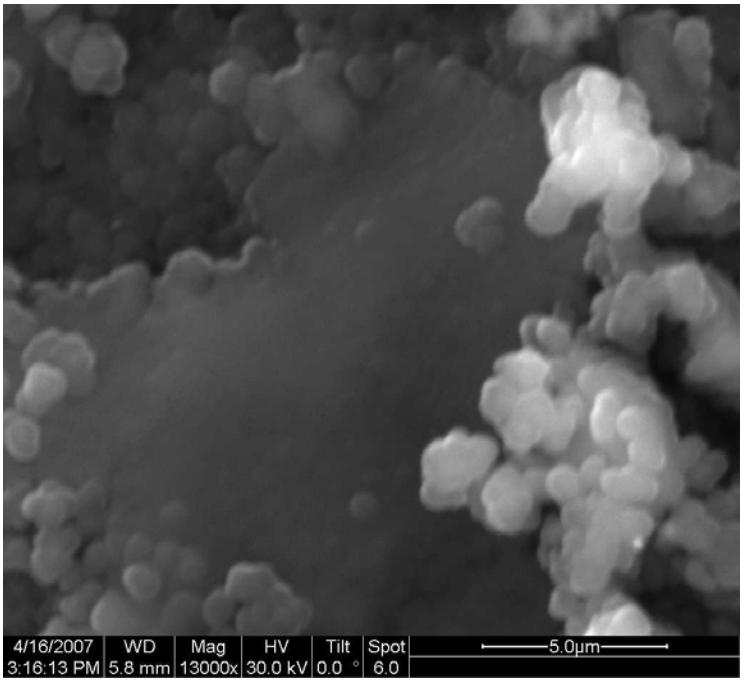

Figure 69. Fracture surface of N720/A specimen tested in compression to failure in displacement control at a rate of -0.05 mm/s in steam at 1200°C.

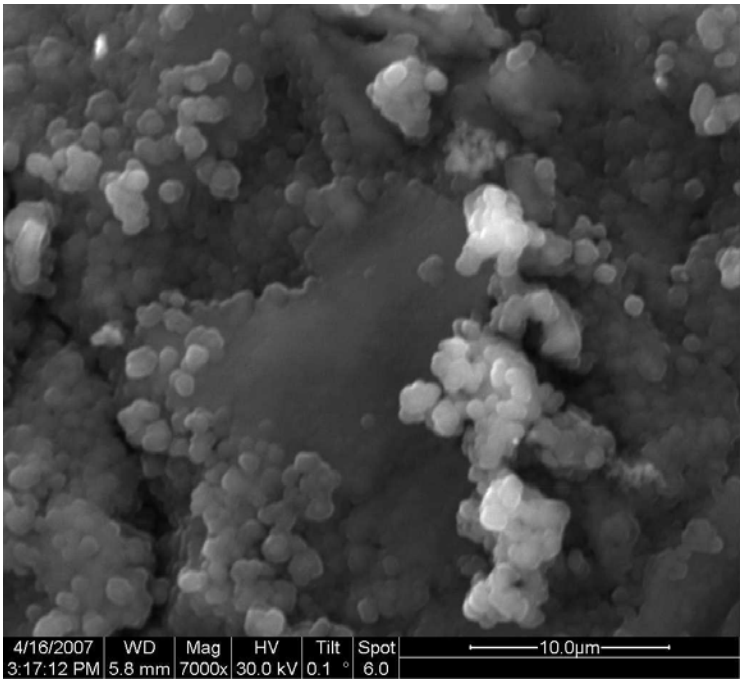

Figure 70. Fracture surface of N720/A specimen tested in compression to failure in displacement control at a rate of -0.05 mm/s in steam at 1200°C.

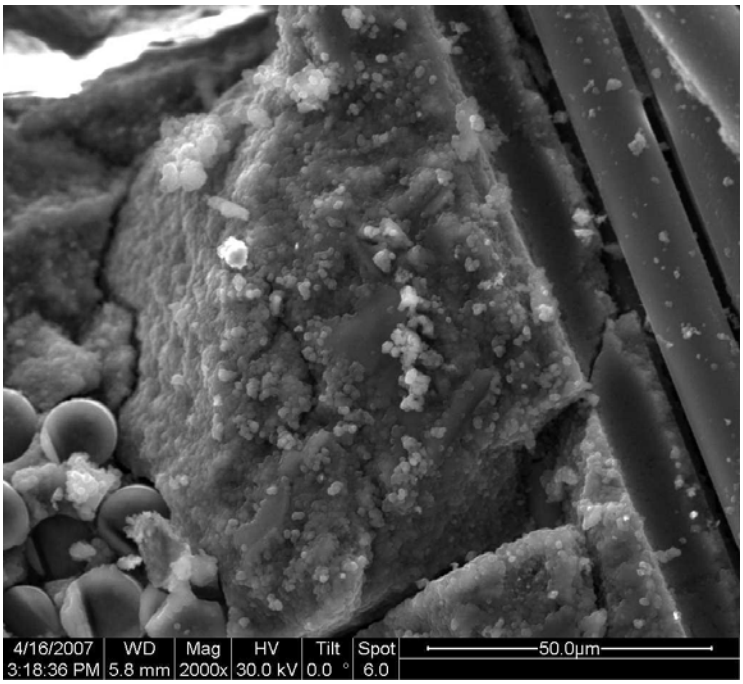

Figure 71. Fracture surface of N720/A specimen tested in compression to failure in displacement control at a rate of -0.05 mm/s in steam at 1200°C.

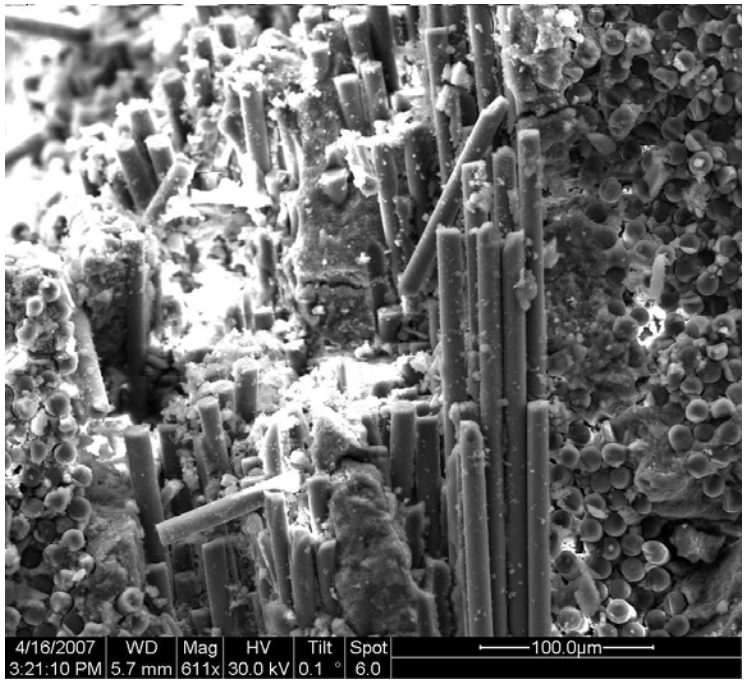

Figure 72. Fracture surface of N720/A specimen tested in compression to failure in displacement control at a rate of -0.05 mm/s in steam at 1200°C.

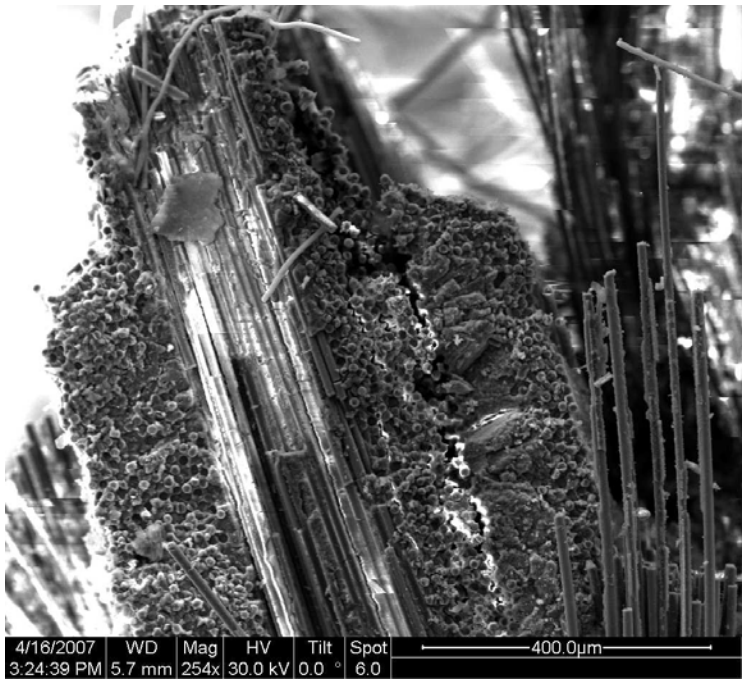

Figure 73. Fracture surface of N720/A specimen tested in compression to failure in displacement control at a rate of -0.05 mm/s in steam at 1200°C.

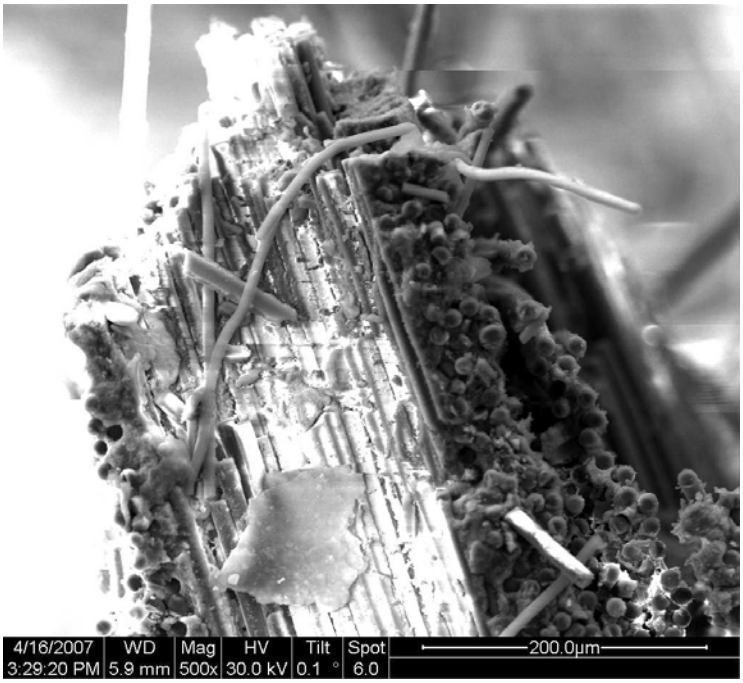

Figure 74. Fracture surface of N720/A specimen tested in compression to failure in displacement control at a rate of -0.05 mm/s in steam at 1200°C.

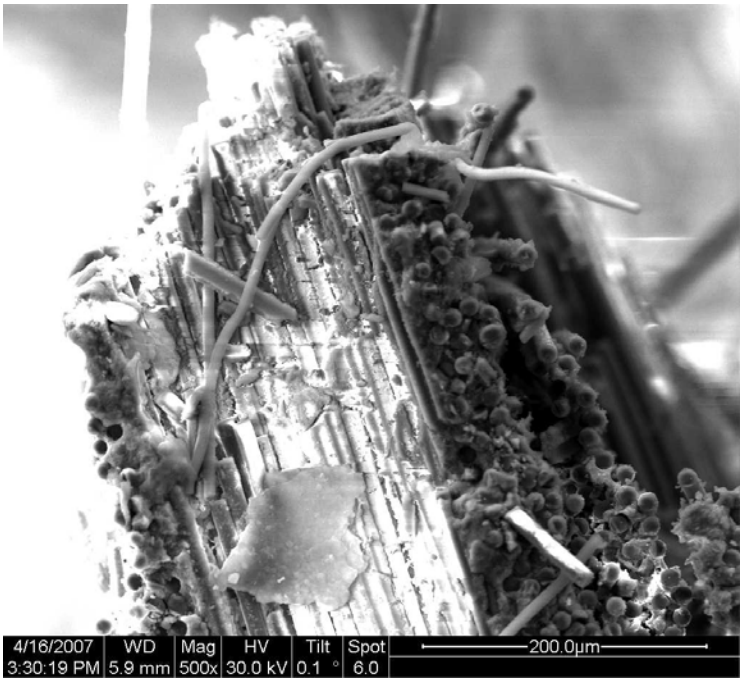

Figure 75. Fracture surface of N720/A specimen tested in compression to failure in displacement control at a rate of -0.05 mm/s in steam at 1200°C.

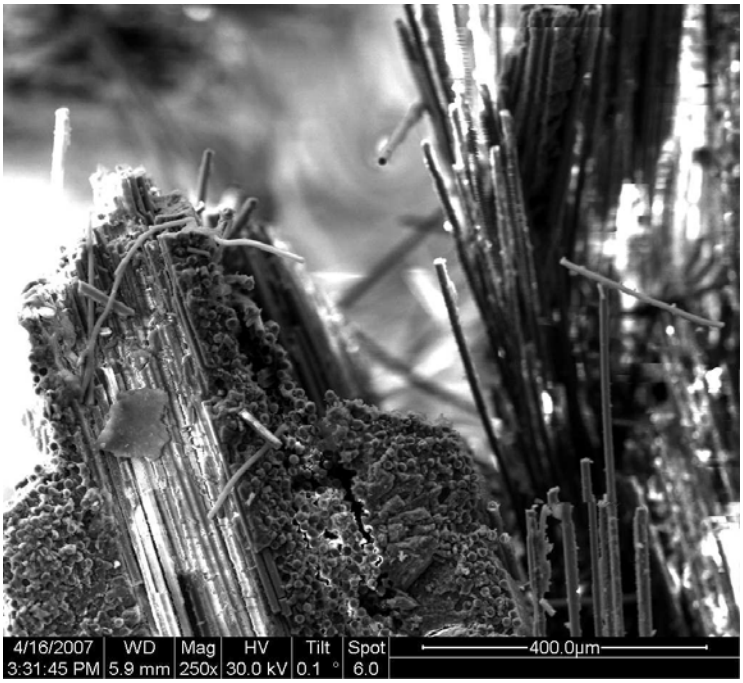

Figure 76. Fracture surface of N720/A specimen tested in compression to failure in displacement control at a rate of -0.05 mm/s in steam at 1200°C.

Figure 77. Fracture surface of N720/A specimen tested in compression to failure in displacement control at a rate of -0.05 mm/s in steam at 1200°C

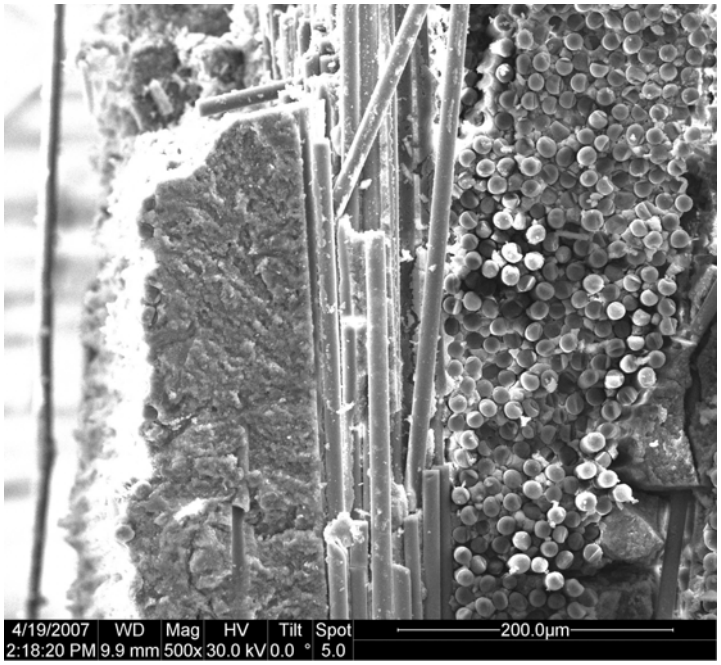

Figure 78. Fracture surface of N720/A specimen tested in creep at 60 MPa in air at 1200°C.

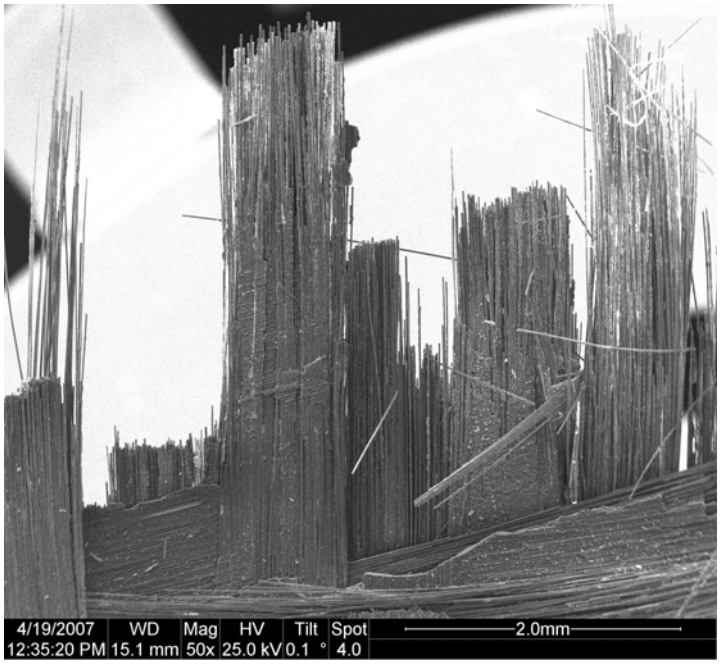

Figure 79. Fracture surface of N720/A specimen tested in creep at 60 MPa in air at 1200°C.

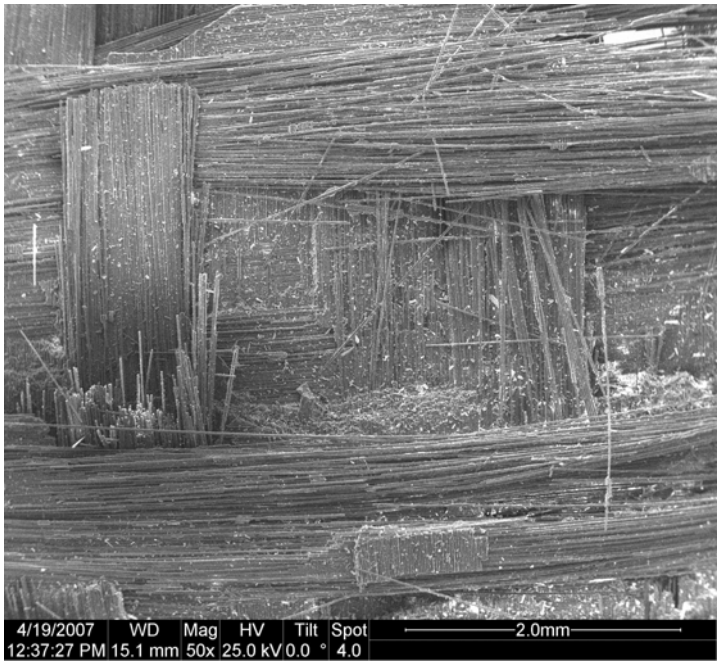

Figure 80. Fracture surface of N720/A specimen tested in creep at 60 MPa in air at 1200°C.

Figure 81. Fracture surface of N720/A specimen tested in creep at 60 MPa in air at 1200°C.

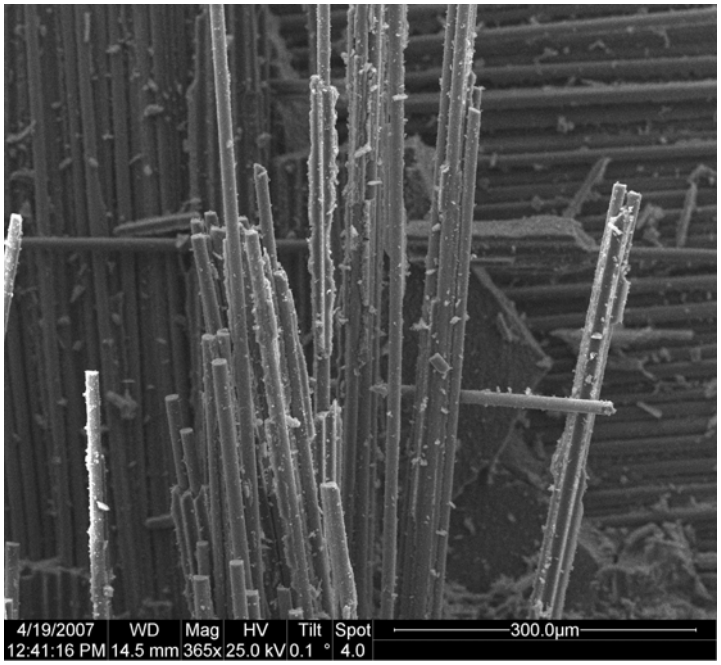

Figure 82. Fracture surface of N720/A specimen tested in creep at 60 MPa in air at 1200°C.

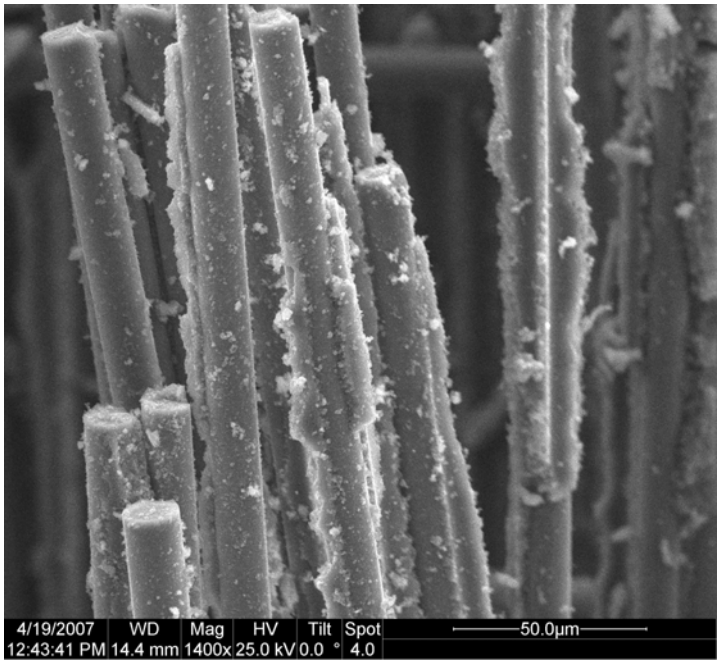

Figure 83. Fracture surface of N720/A specimen tested in creep at 60 MPa in air at 1200°C.

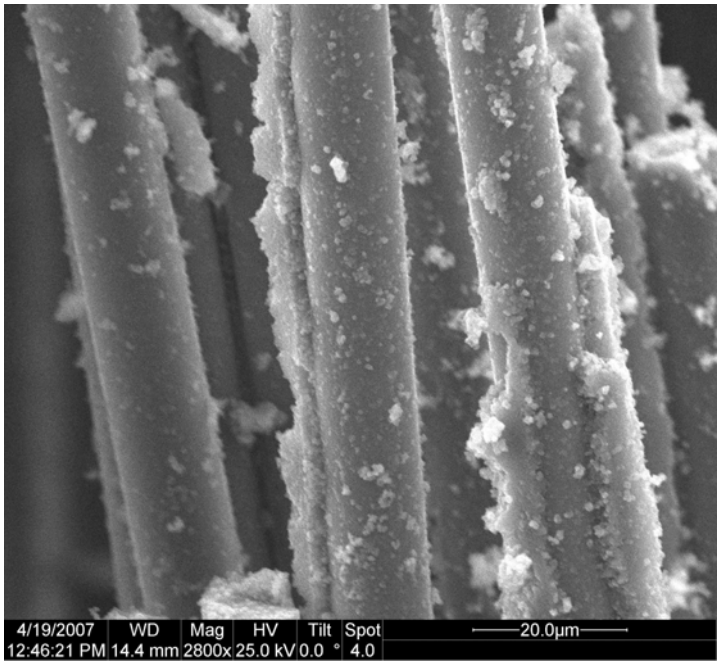

Figure 84. Fracture surface of N720/A specimen tested in creep at 60 MPa in air at 1200°C.

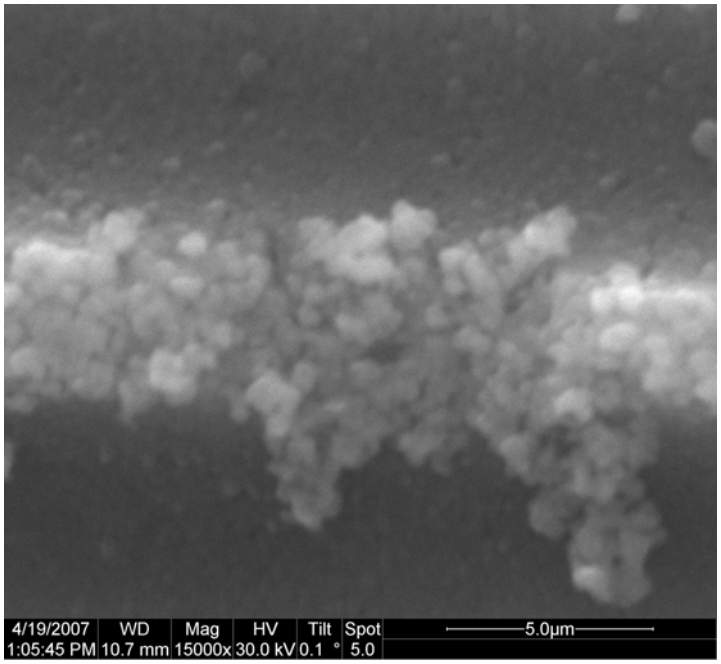

Figure 85. Fracture surface of N720/A specimen tested in creep at 60 MPa in air at 1200°C.

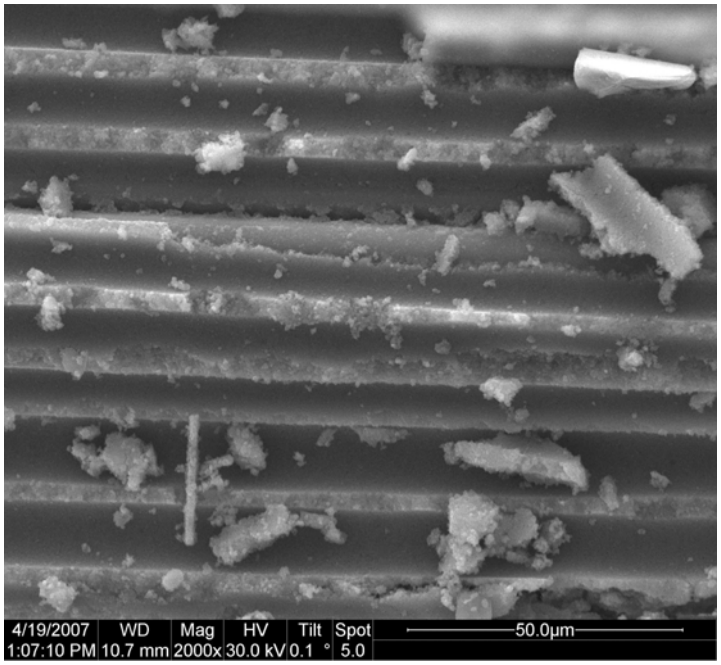

Figure 86. Fracture surface of N720/A specimen tested in creep at 60 MPa in air at 1200°C.

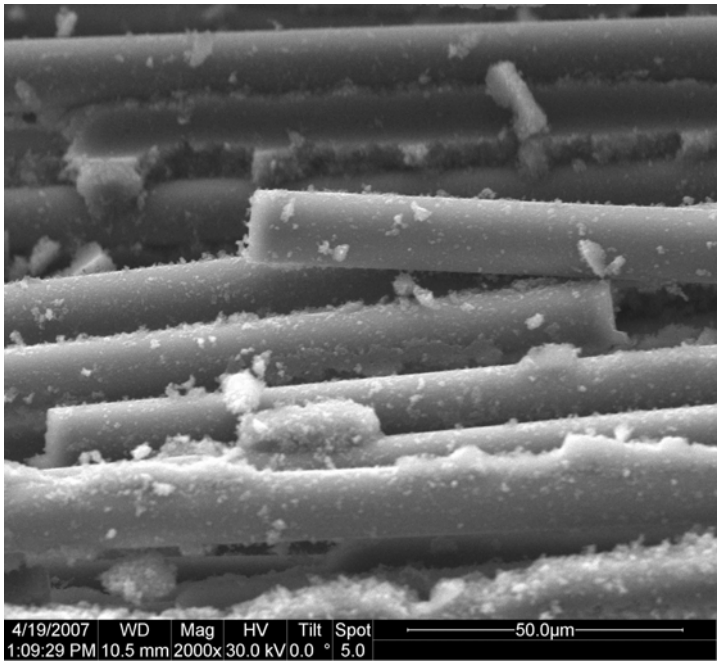

Figure 87. Fracture surface of N720/A specimen tested in creep at 60 MPa in air at 1200°C.

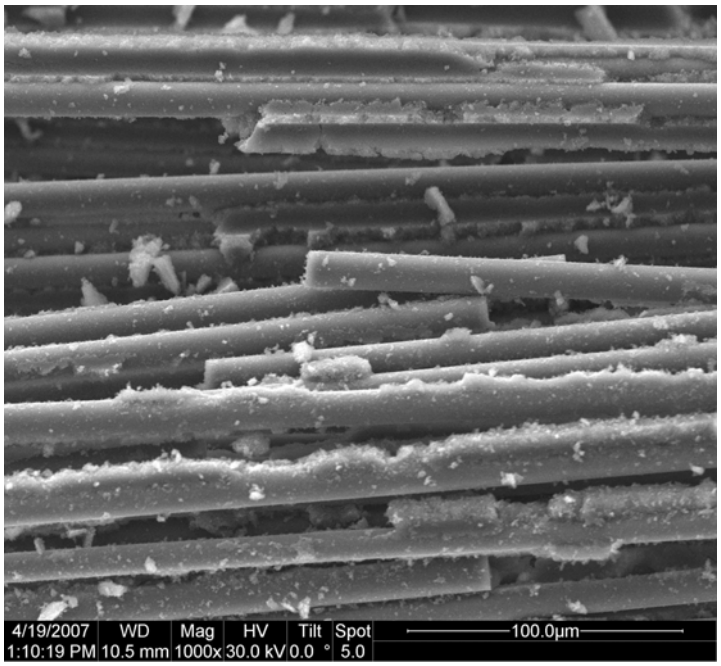

Figure 88. Fracture surface of N720/A specimen tested in creep at 60 MPa in air at 1200°C.

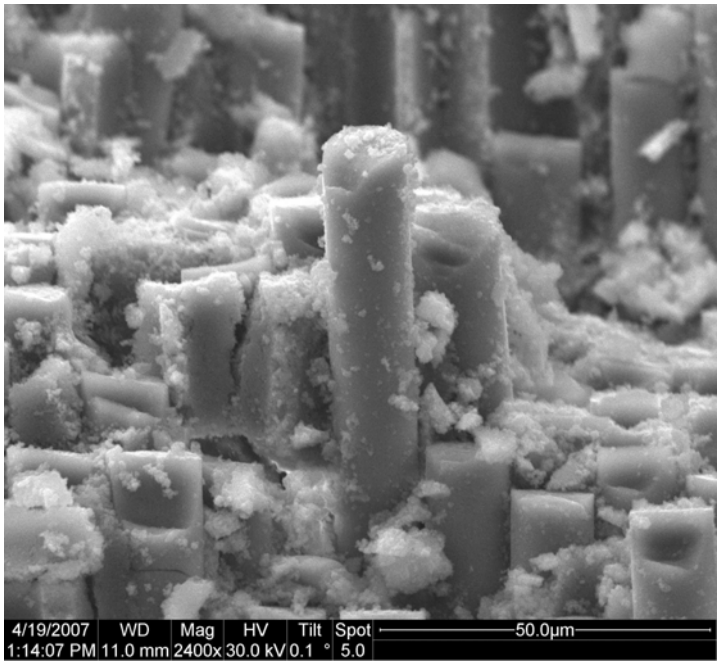

Figure 89. Fracture surface of N720/A specimen tested in creep at 60 MPa in air at 1200°C.

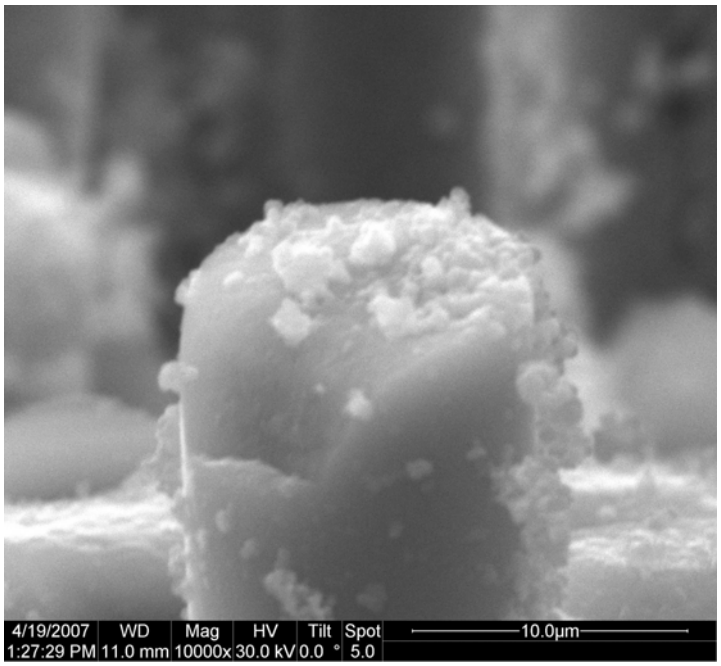

Figure 90. Fracture surface of N720/A specimen tested in creep at 60 MPa in air at 1200°C.

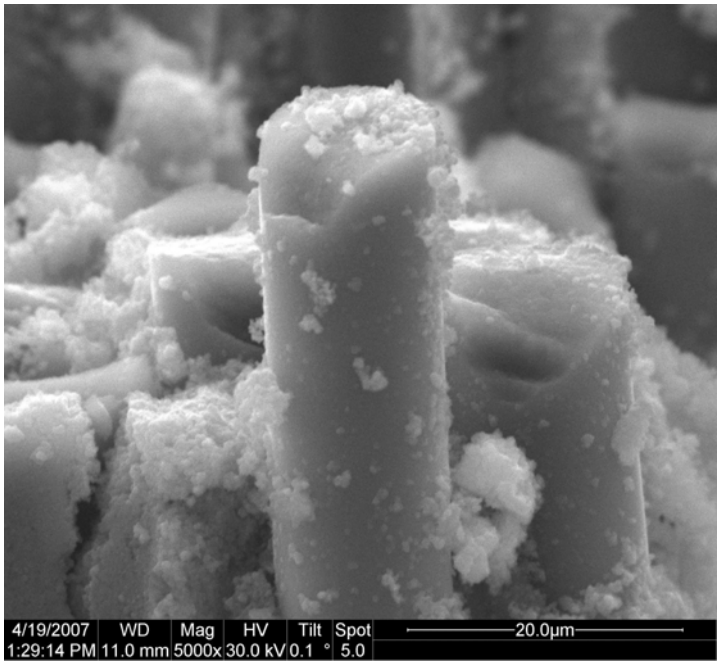

Figure 91. Fracture surface of N720/A specimen tested in creep at 60 MPa in air at 1200°C.

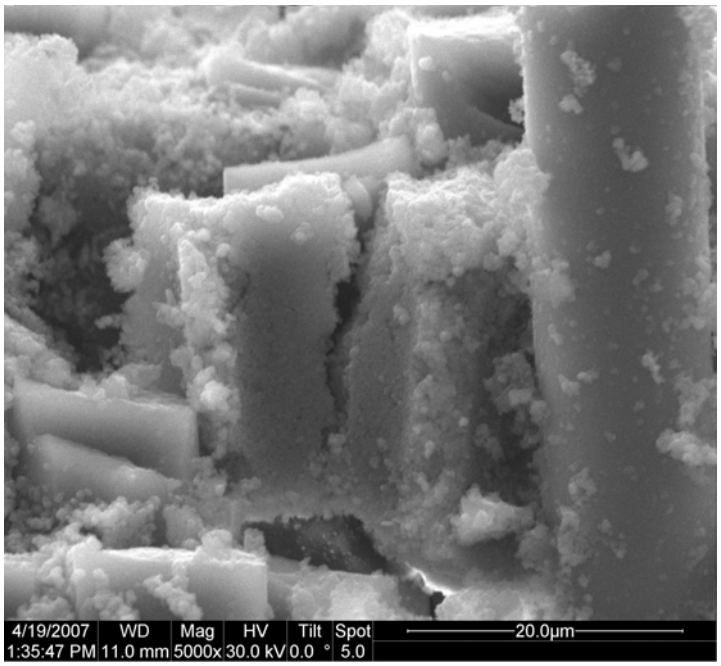

Figure 92. Fracture surface of N720/A specimen tested in creep at 60 MPa in air at 1200°C.

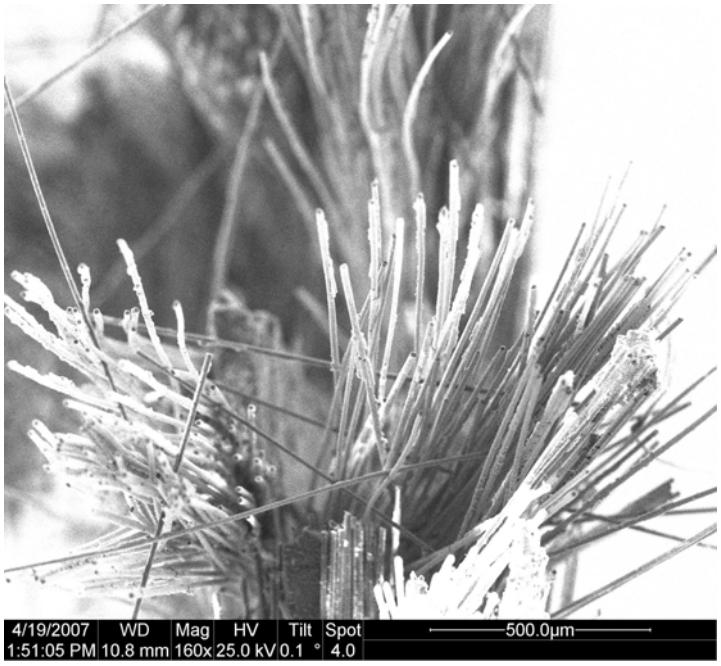

Figure 93. Fracture surface of N720/A specimen tested in creep at 60 MPa in air at 1200°C.

Figure 94. Fracture surface of N720/A specimen tested in creep at 60 MPa in air at 1200°C.

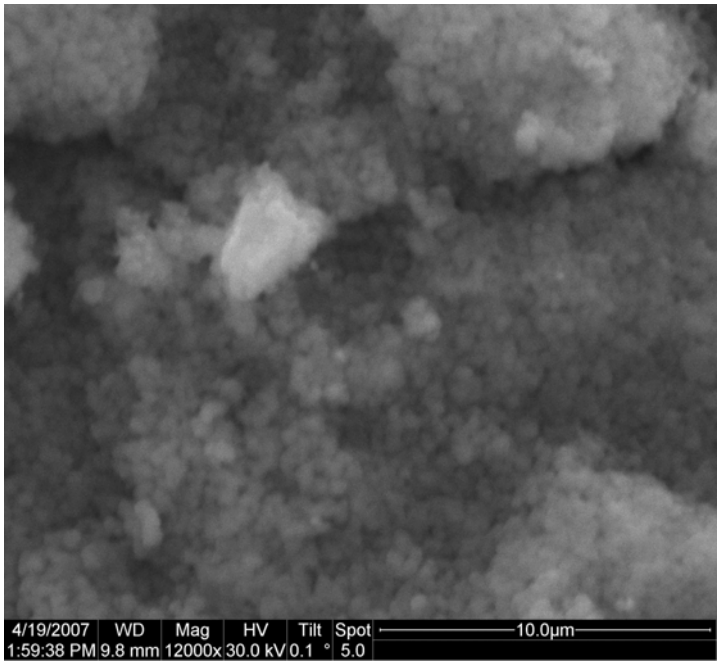

Figure 95. Fracture surface of N720/A specimen tested in creep at 60 MPa in air at 1200°C.

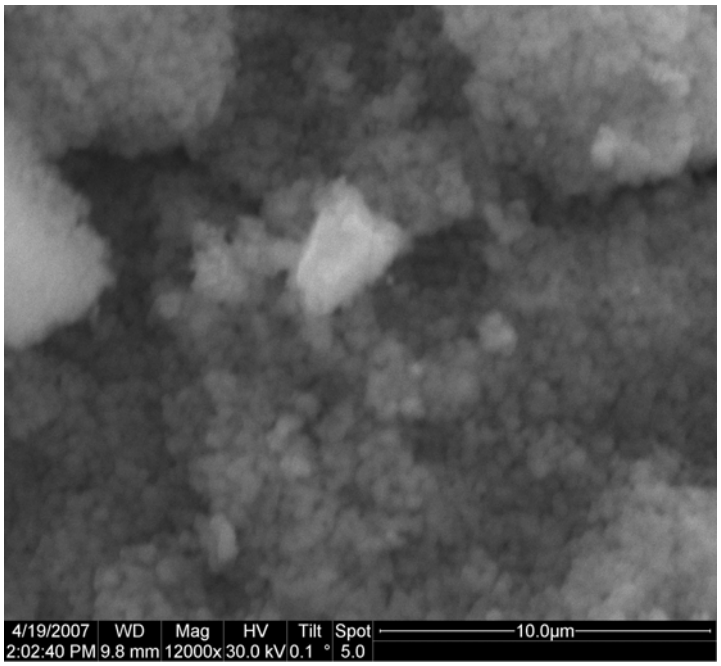

Figure 96. Fracture surface of N720/A specimen tested in creep at 60 MPa in air at 1200°C.

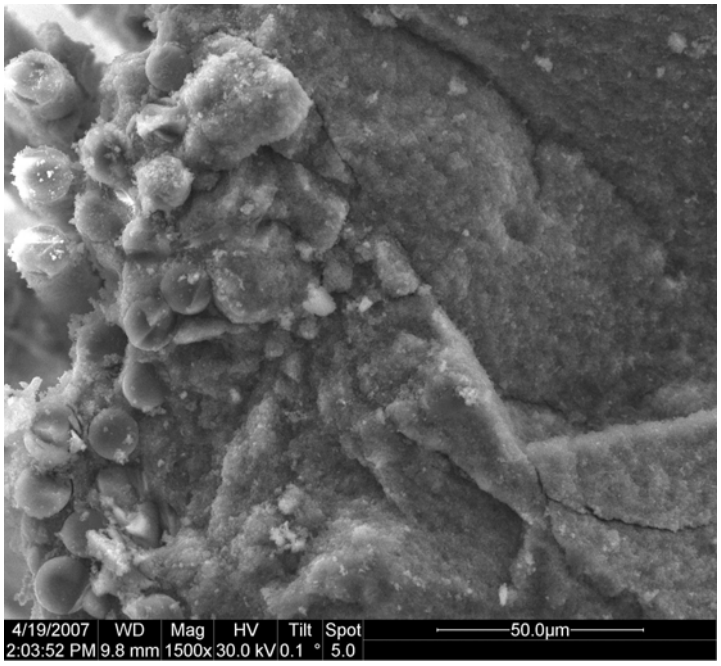

Figure 97. Fracture surface of N720/A specimen tested in creep at 60 MPa in air at 1200°C.

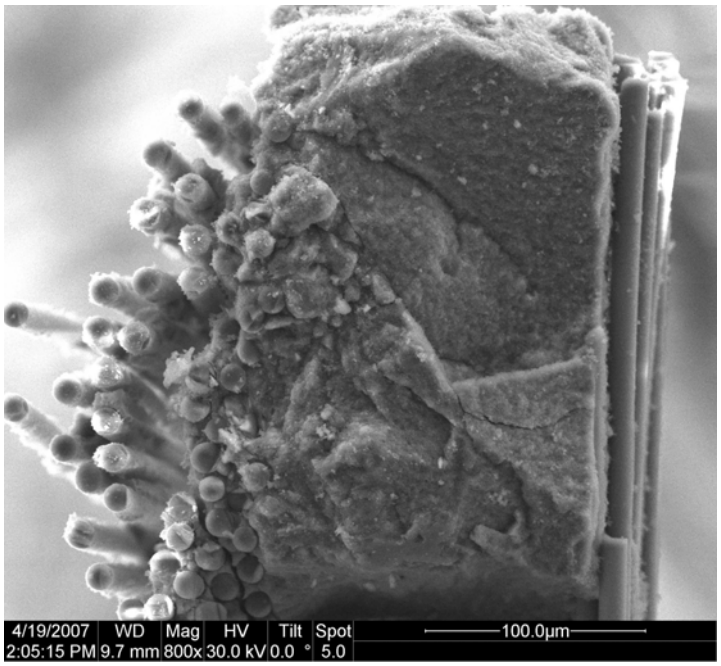

Figure 98. Fracture surface of N720/A specimen tested in creep at 60 MPa in air at 1200°C.

Figure 99. Fracture surface of N720/A specimen tested in creep at 60 MPa in air at 1200°C.

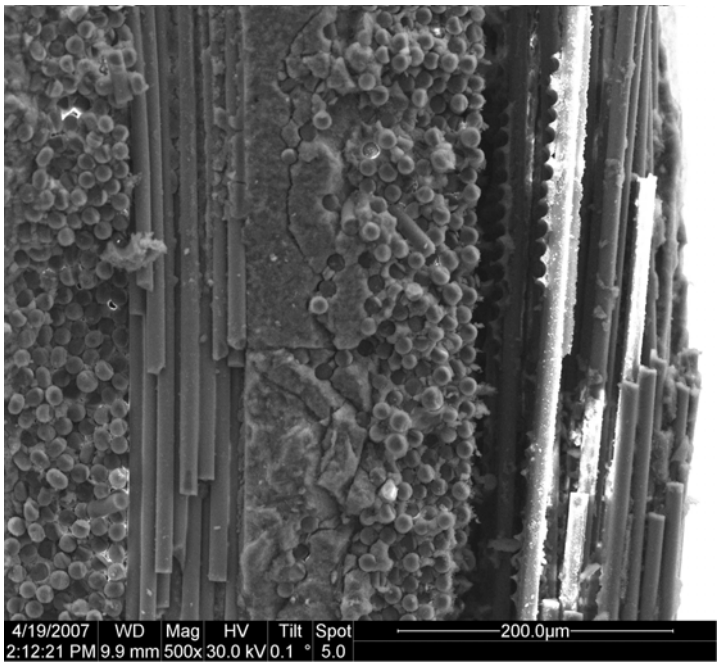

Figure 100. Fracture surface of N720/A specimen tested in creep at 60 MPa in air at 1200°C.

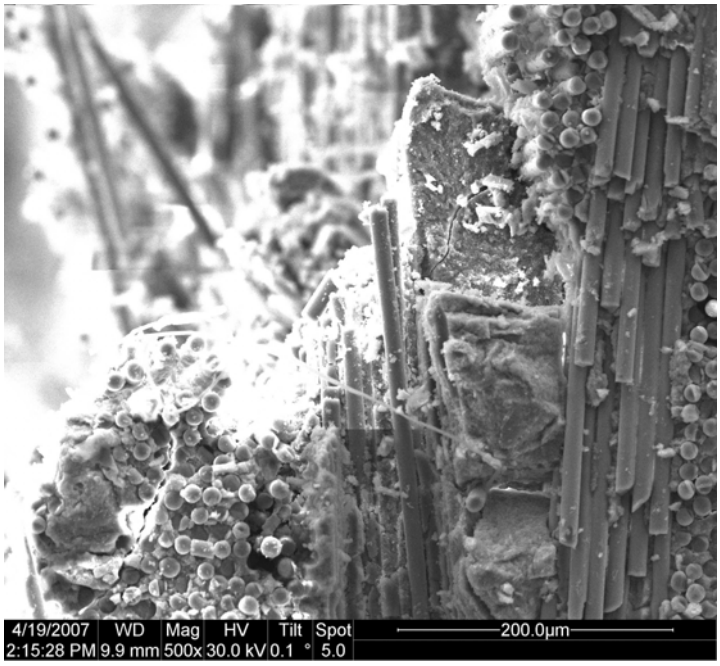

Figure 101. Fracture surface of N720/A specimen tested in creep at 60 MPa in air at 1200°C.

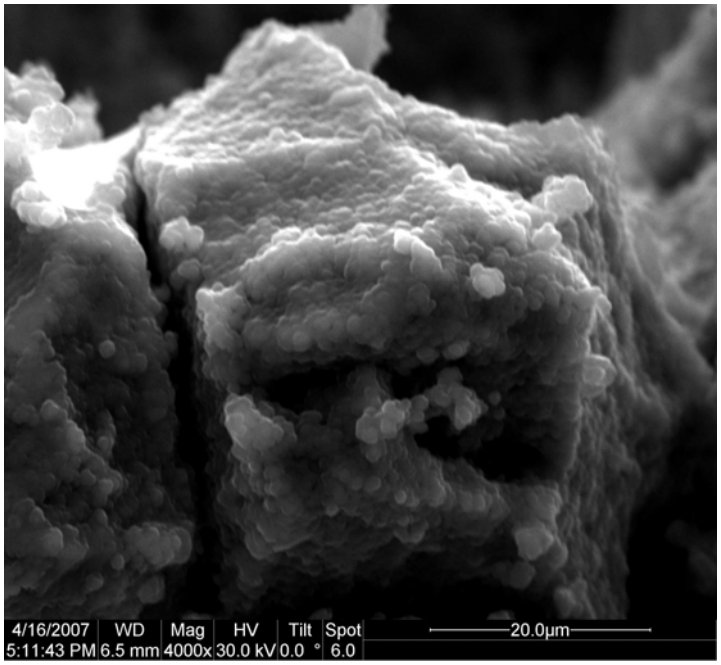

Figure 102. Fracture surface of N720/A specimen tested in creep at 60 MPa in steam at 1200°C.

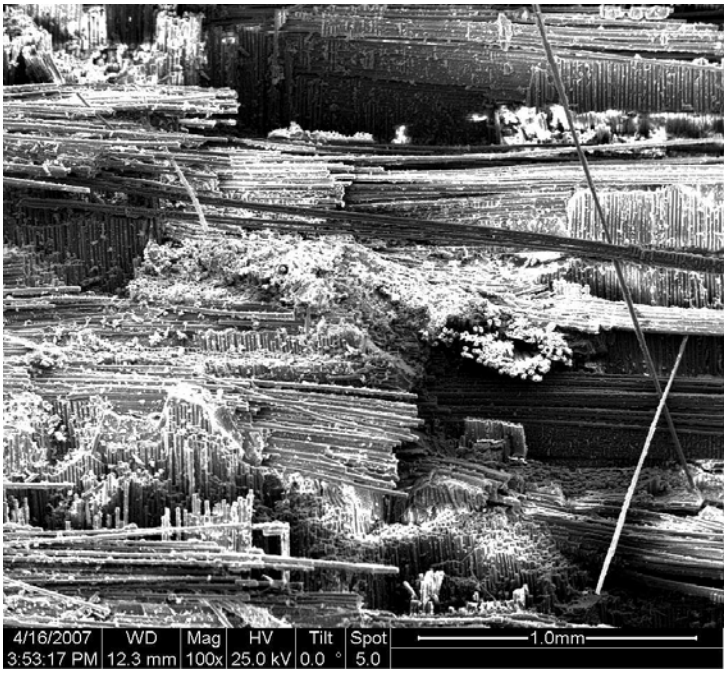

Figure 103. Fracture surface of N720/A specimen tested in creep at 60 MPa in steam at 1200°C.

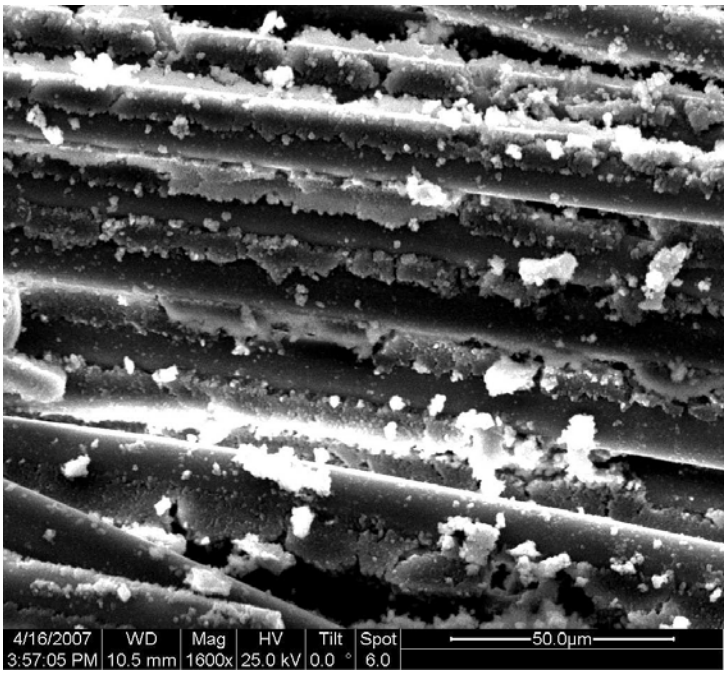

Figure 104. Fracture surface of N720/A specimen tested in creep at 60 MPa in steam at 1200°C.

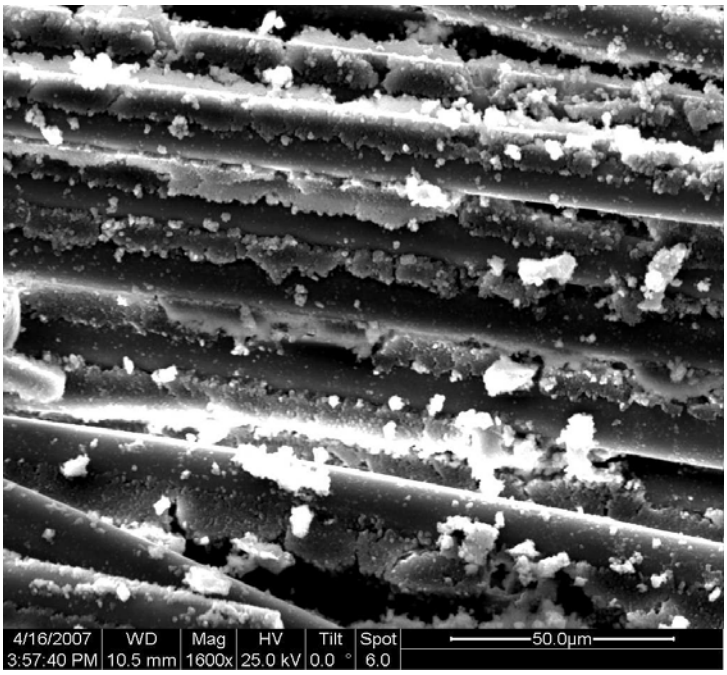

Figure 105. Fracture surface of N720/A specimen tested in creep at 60 MPa in steam at 1200°C.

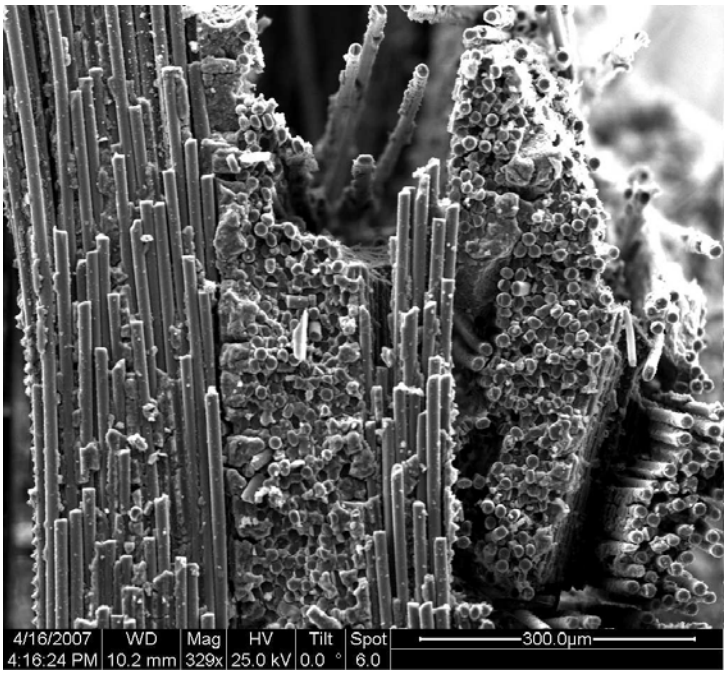

Figure 106. Fracture surface of N720/A specimen tested in creep at 60 MPa in steam at 1200°C.

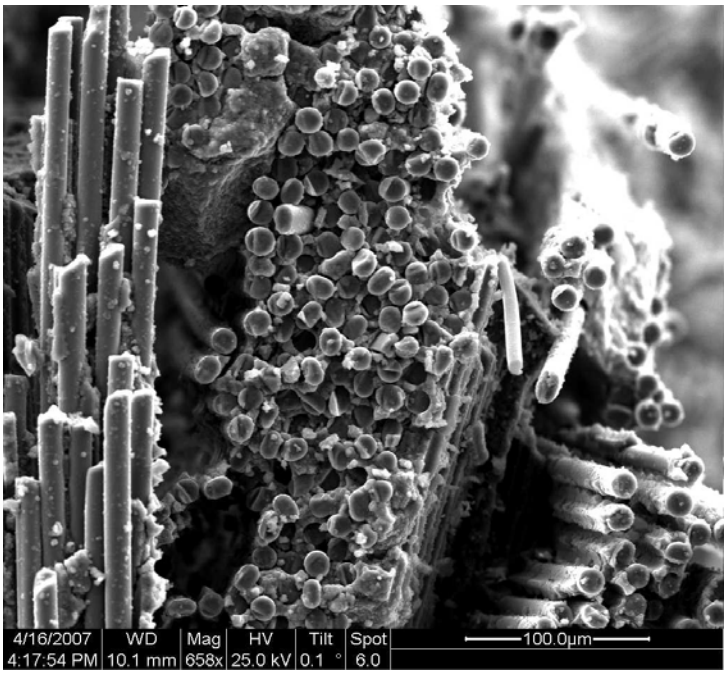

Figure 107. Fracture surface of N720/A specimen tested in creep at 60 MPa in steam at 1200°C.

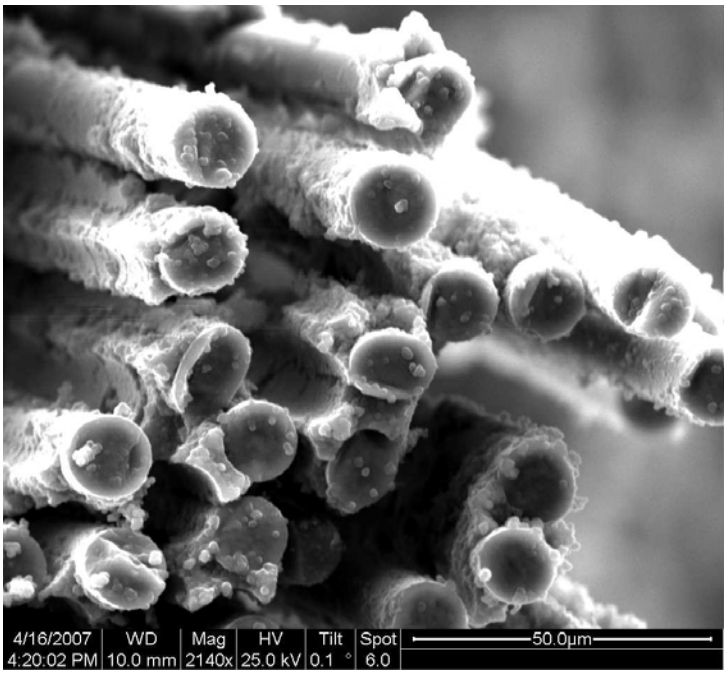

Figure 108. Fracture surface of N720/A specimen tested in creep at 60 MPa in steam at 1200°C.

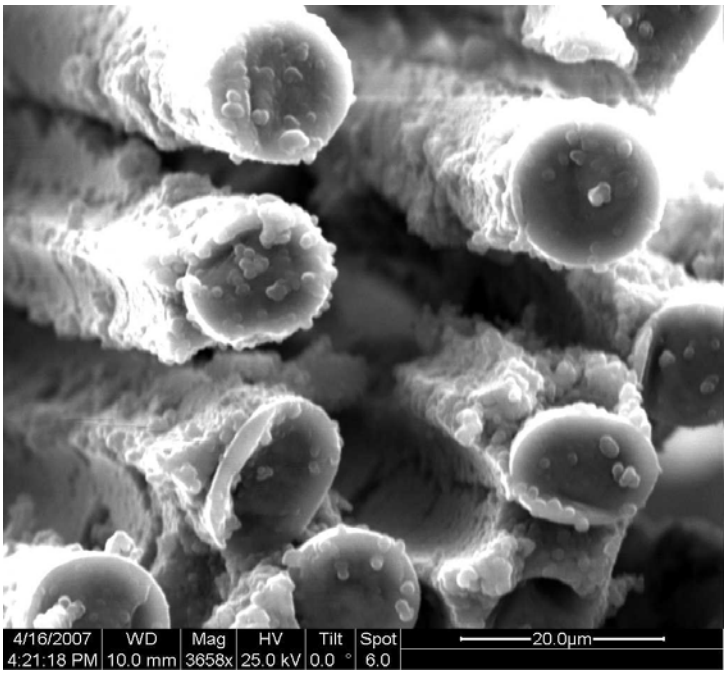

Figure 109. Fracture surface of N720/A specimen tested in creep at 60 MPa in steam at 1200°C.

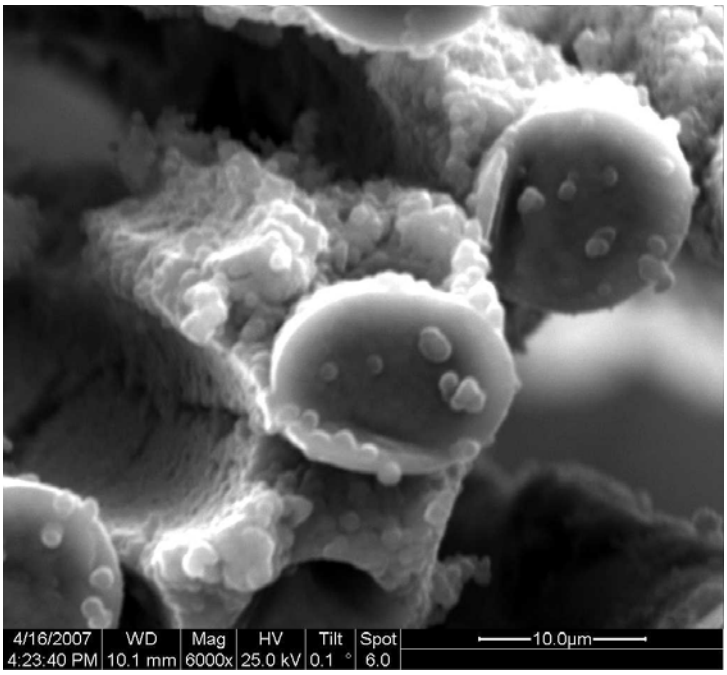

Figure 110. Fracture surface of N720/A specimen tested in creep at 60 MPa in steam at 1200°C.

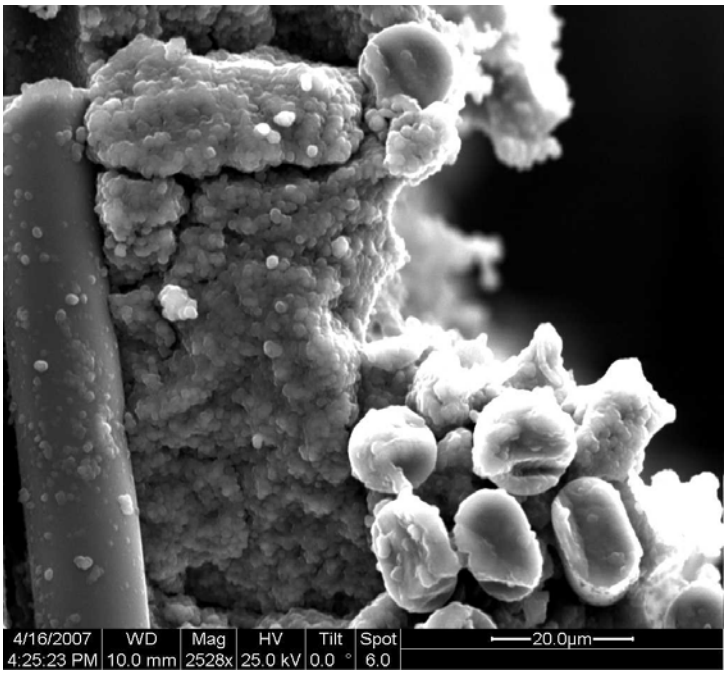

Figure 111. Fracture surface of N720/A specimen tested in creep at 60 MPa in steam at 1200°C.

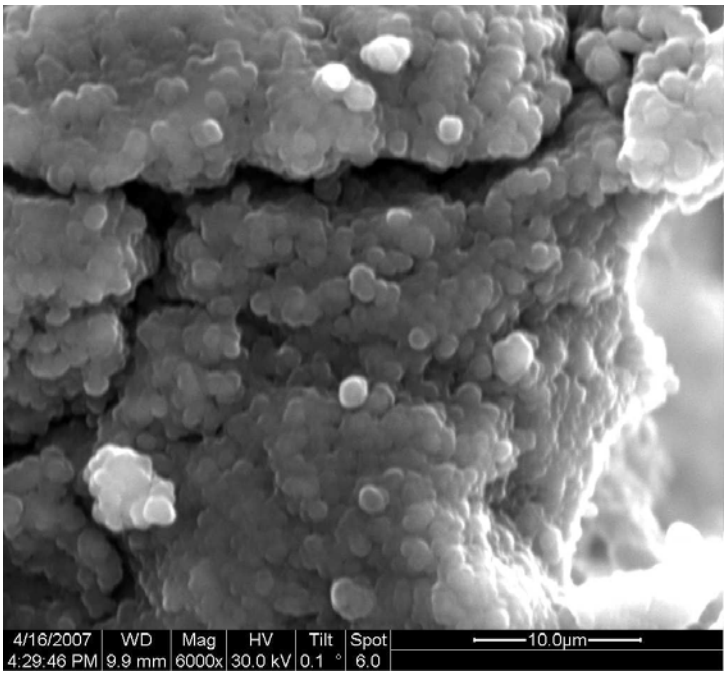

Figure 112. Fracture surface of N720/A specimen tested in creep at 60 MPa in steam at 1200°C.

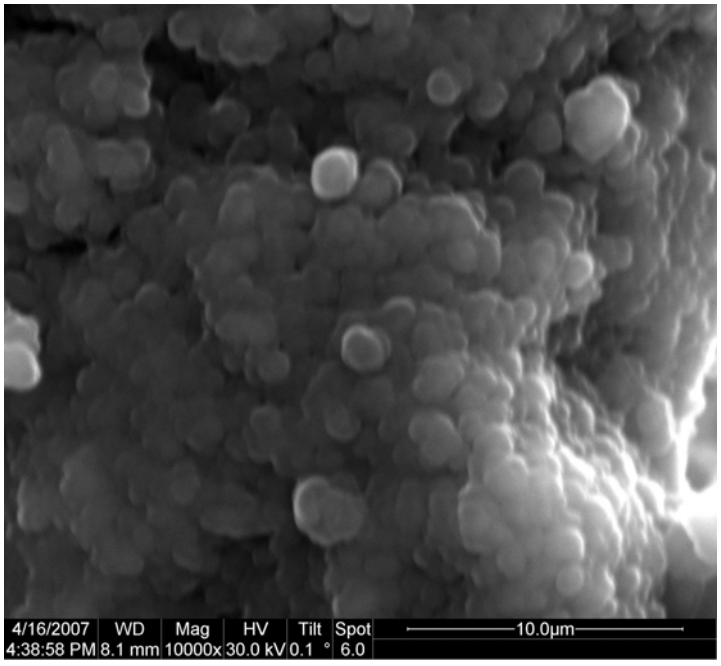

Figure 113. Fracture surface of N720/A specimen tested in creep at 60 MPa in steam at 1200°C.

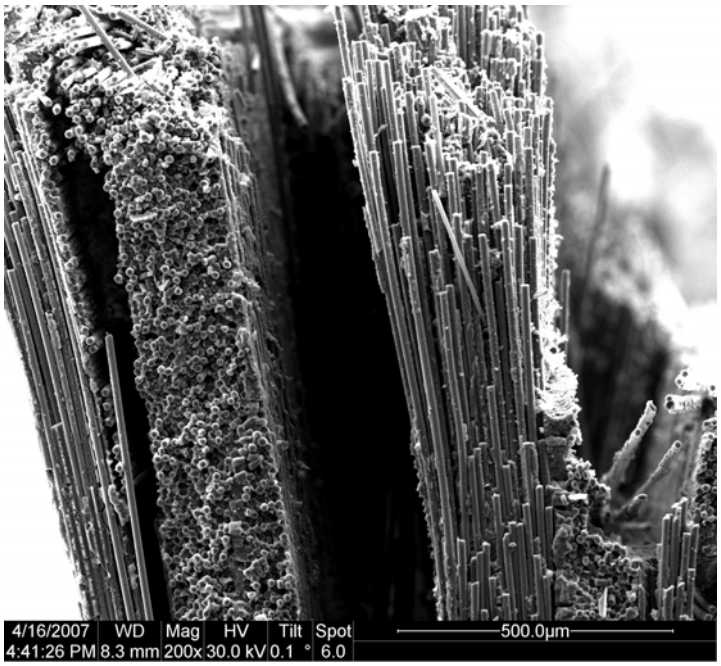

Figure 114. Fracture surface of N720/A specimen tested in creep at 60 MPa in steam at 1200°C.

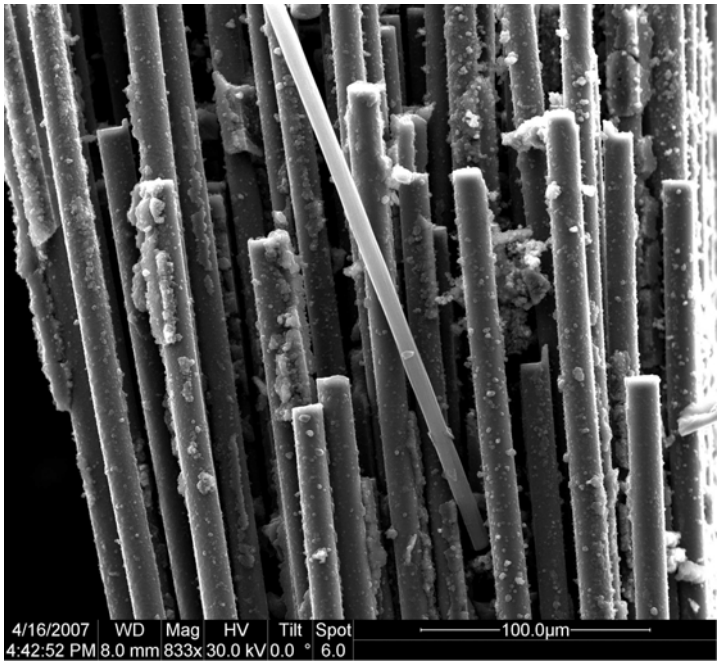

Figure 115. Fracture surface of N720/A specimen tested in creep at 60 MPa in steam at 1200°C.

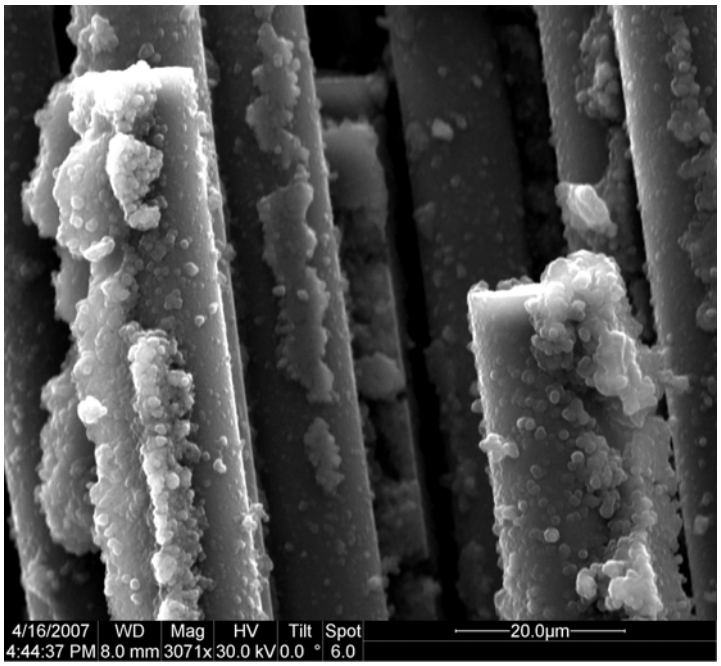

Figure 116. Fracture surface of N720/A specimen tested in creep at 60 MPa in steam at 1200°C.

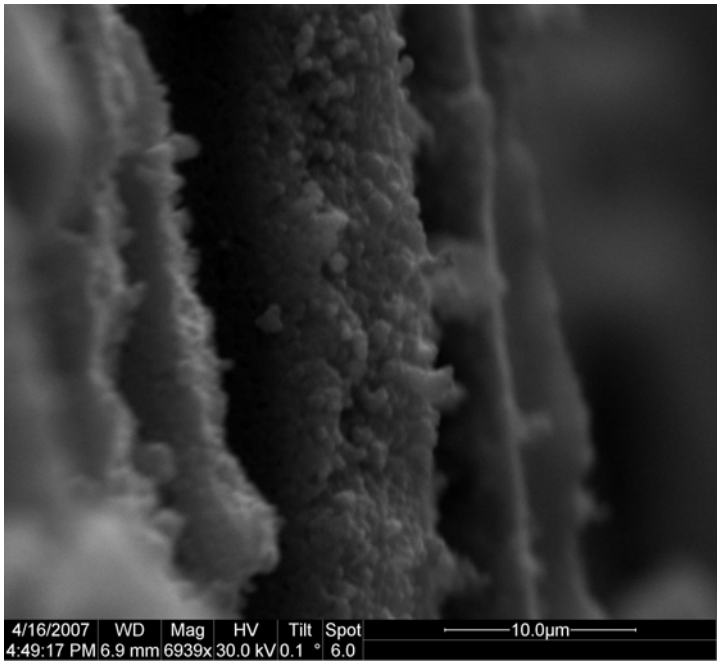

Figure 117. Fracture surface of N720/A specimen tested in creep at 60 MPa in steam at 1200°C.

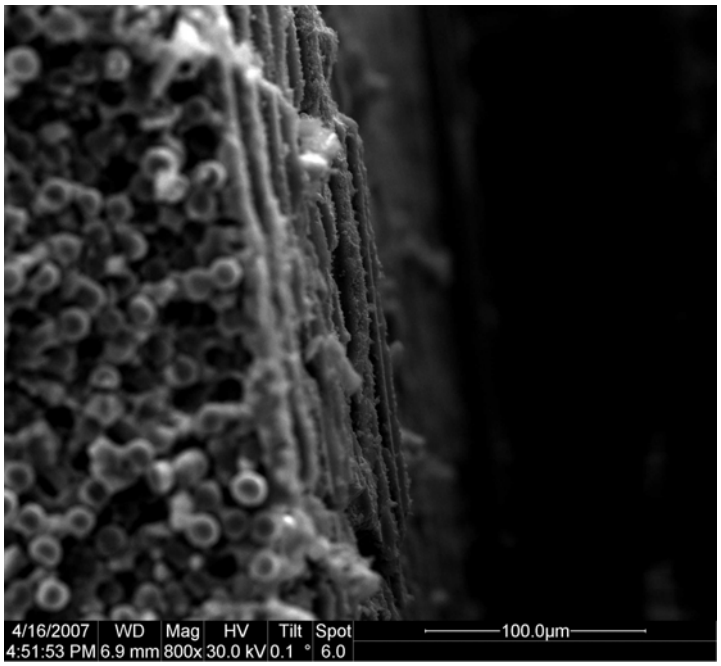

Figure 118. Fracture surface of N720/A specimen tested in creep at 60 MPa in steam at 1200°C.

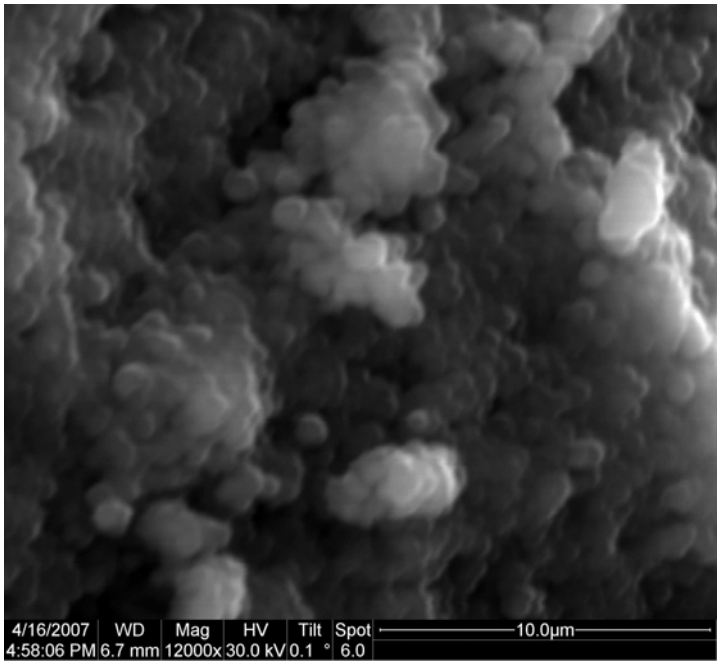

Figure 119. Fracture surface of N720/A specimen tested in creep at 60 MPa in steam at 1200°C.

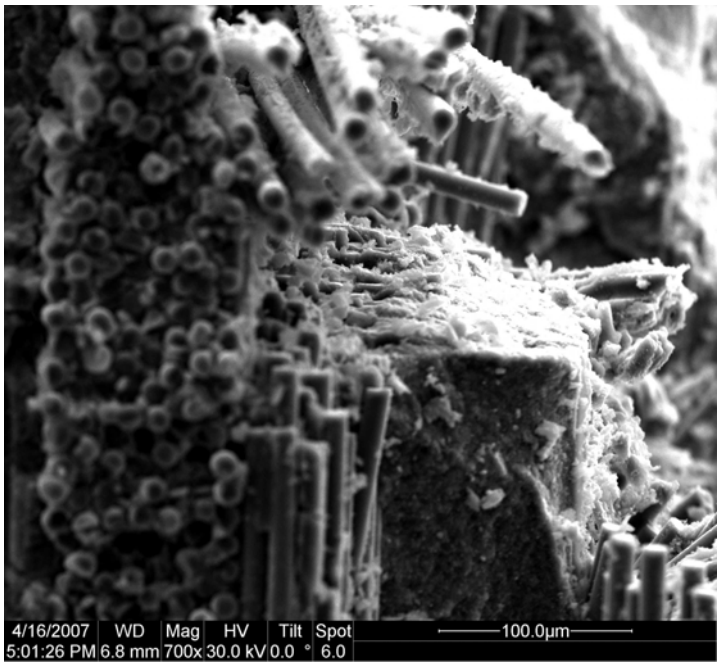

Figure 120. Fracture surface of N720/A specimen tested in creep at 60 MPa in steam at 1200°C.

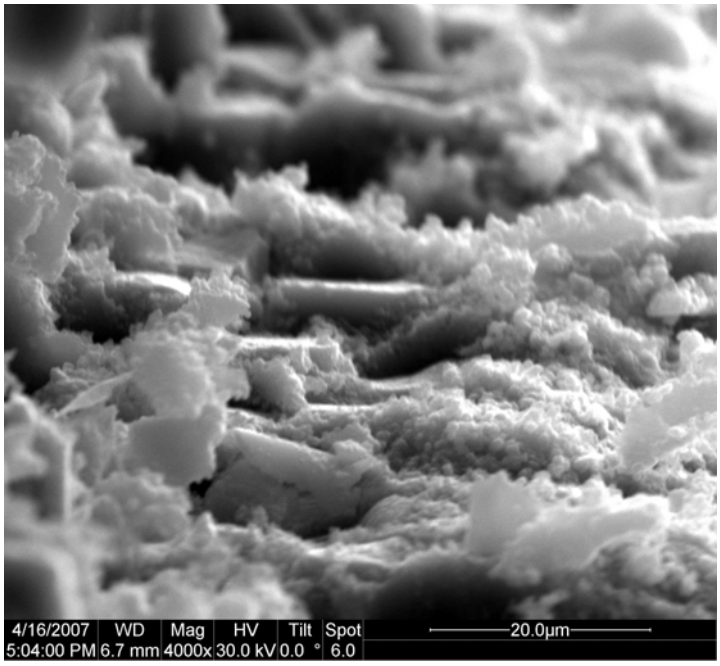

Figure 121. Fracture surface of N720/A specimen tested in creep at 60 MPa in steam at 1200°C.

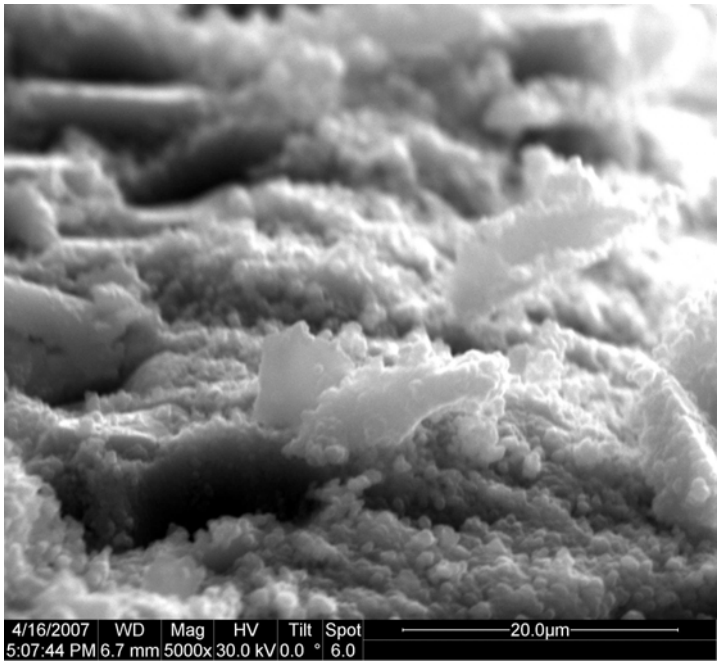

Figure 122. Fracture surface of N720/A specimen tested in creep at 60 MPa in steam at 1200°C.

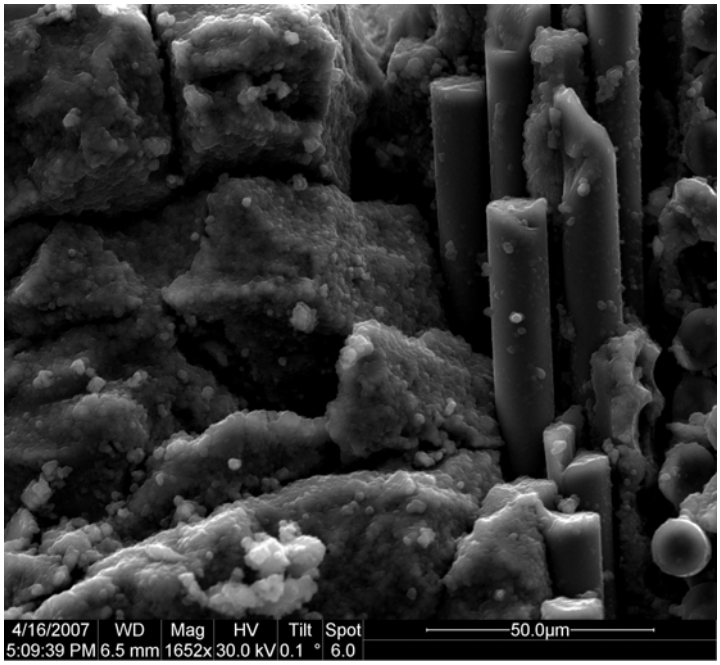

Figure 123. Fracture surface of N720/A specimen tested in creep at 60 MPa in steam at 1200°C.

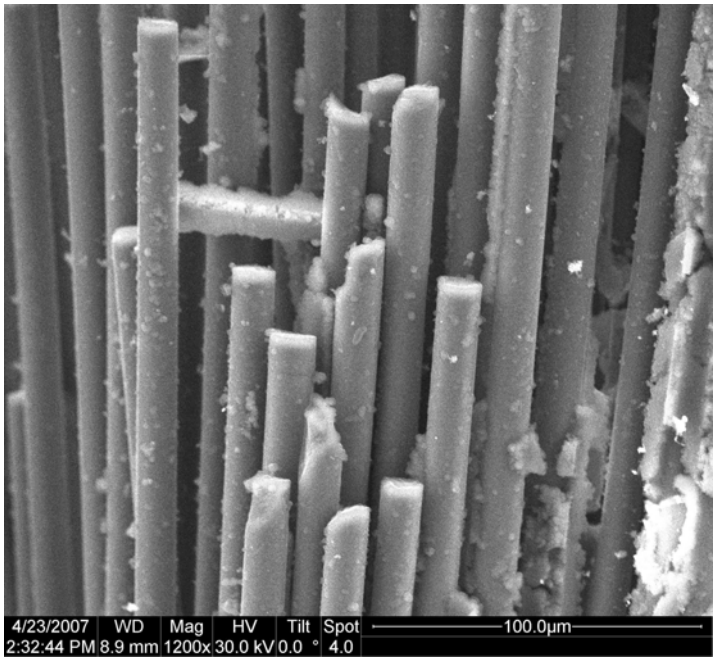

Figure 124. Fracture surface of N720/A specimen tested in compression to failure following aging in steam for 25 h.

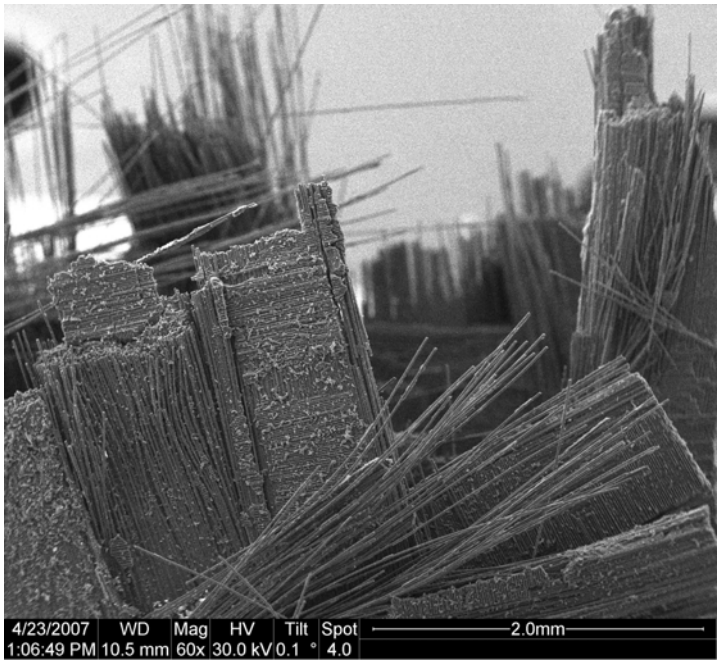

Figure 125. Fracture surface of N720/A specimen tested in compression to failure following aging in steam for 25 h.

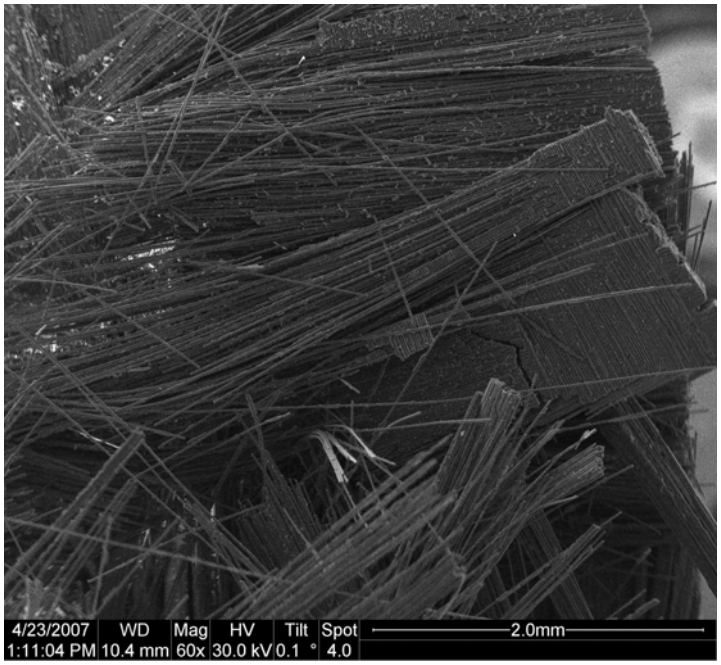

Figure 126. Fracture surface of N720/A specimen tested in compression to failure following aging in steam for 25 h.

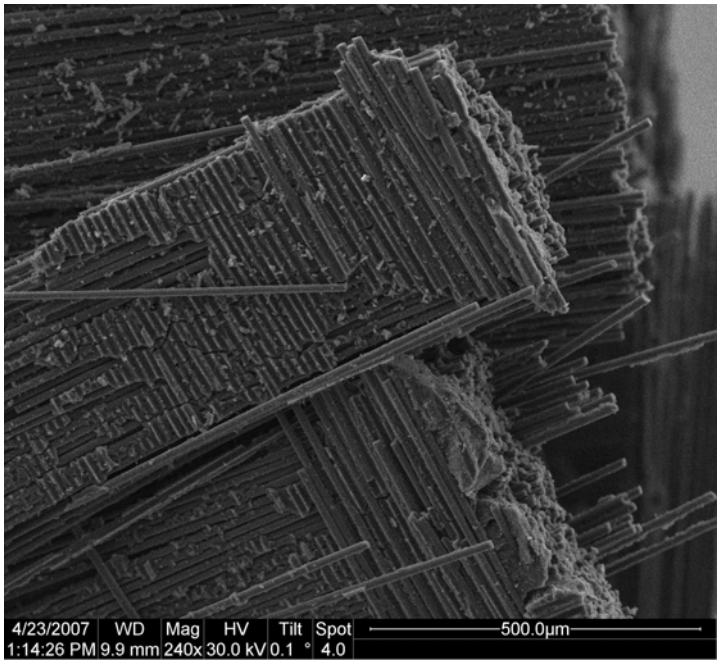

Figure 127. Fracture surface of N720/A specimen tested in compression to failure following aging in steam for 25 h.

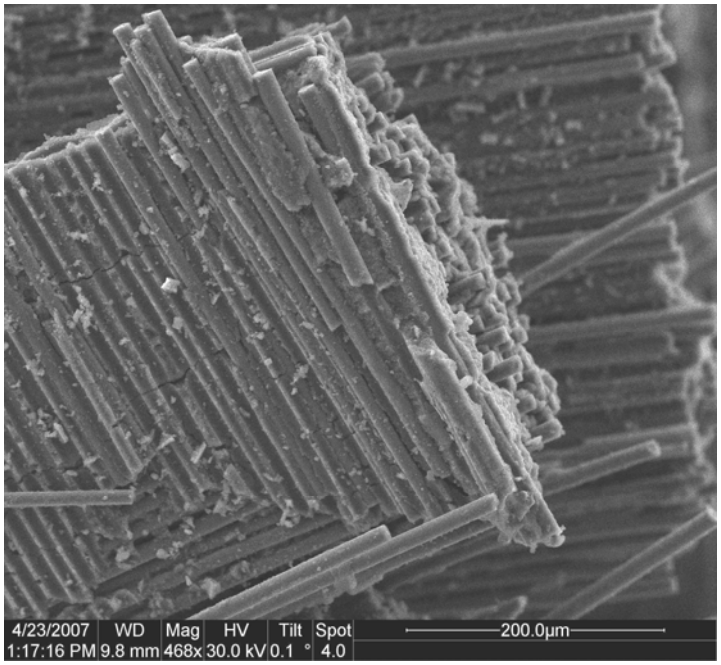

Figure 128. Fracture surface of N720/A specimen tested in compression to failure following aging in steam for 25 h.

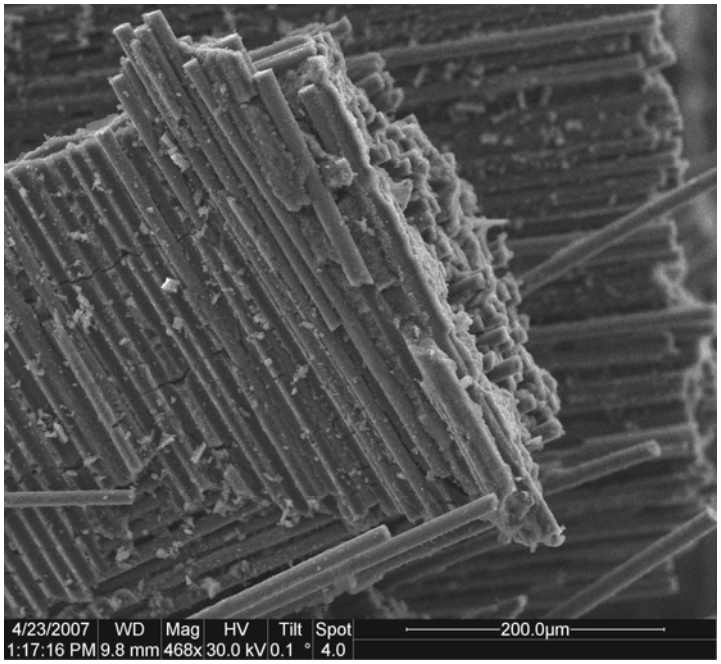

Figure 129. Fracture surface of N720/A specimen tested in compression to failure following aging in steam for 25 h.

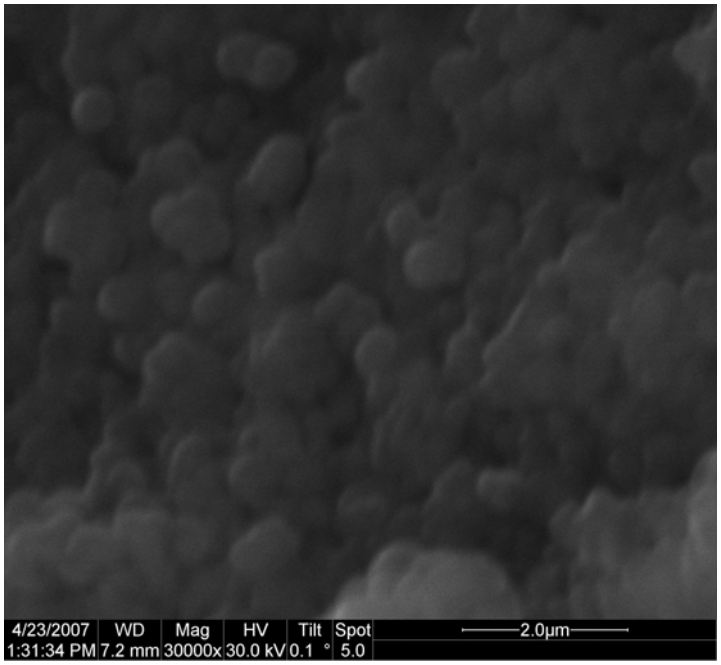

Figure 130. Fracture surface of N720/A specimen tested in compression to failure following aging in steam for 25 h.

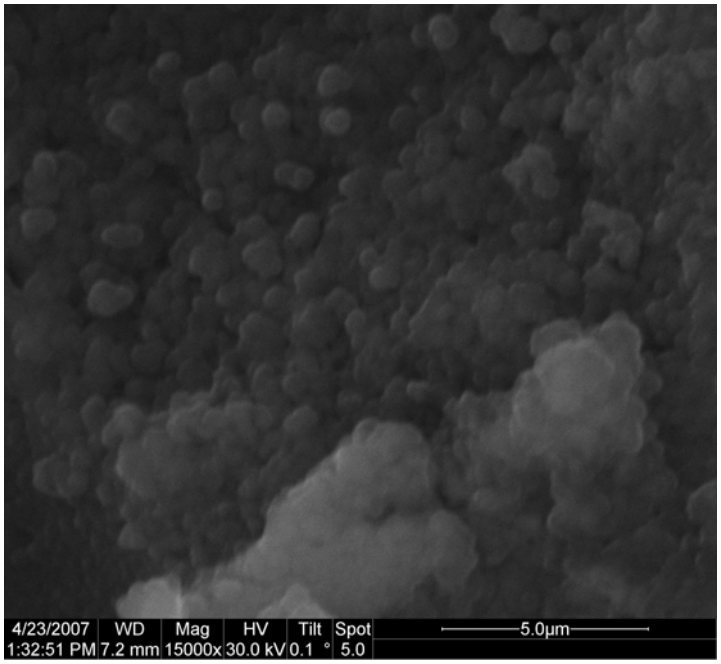

Figure 131. Fracture surface of N720/A specimen tested in compression to failure following aging in steam for 25 h.

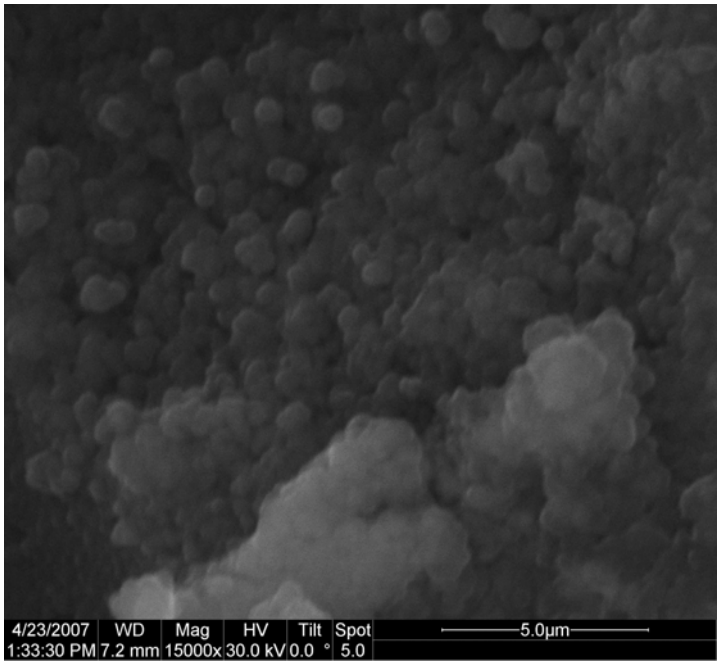

Figure 132. Fracture surface of N720/A specimen tested in compression to failure following aging in steam for 25 h.

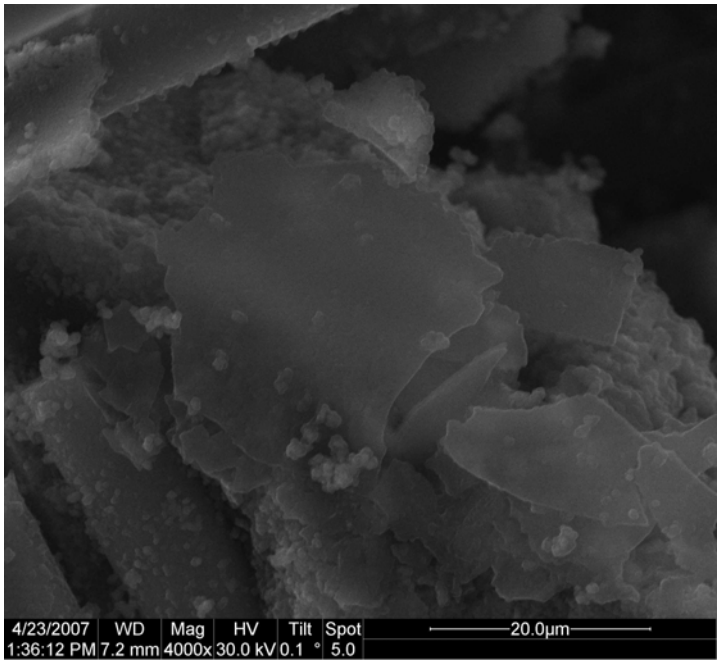

Figure 133. Fracture surface of N720/A specimen tested in compression to failure following aging in steam for 25 h.

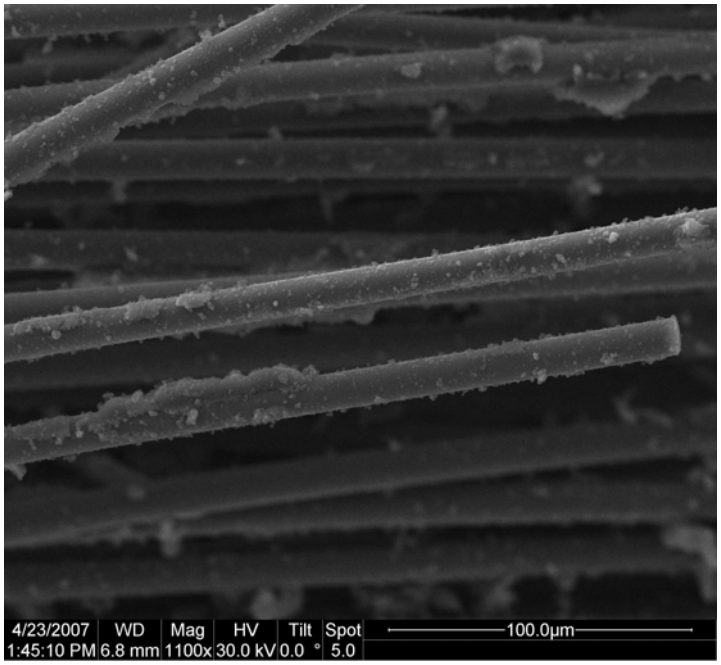

Figure 134. Fracture surface of N720/A specimen tested in compression to failure following aging in steam for 25 h.

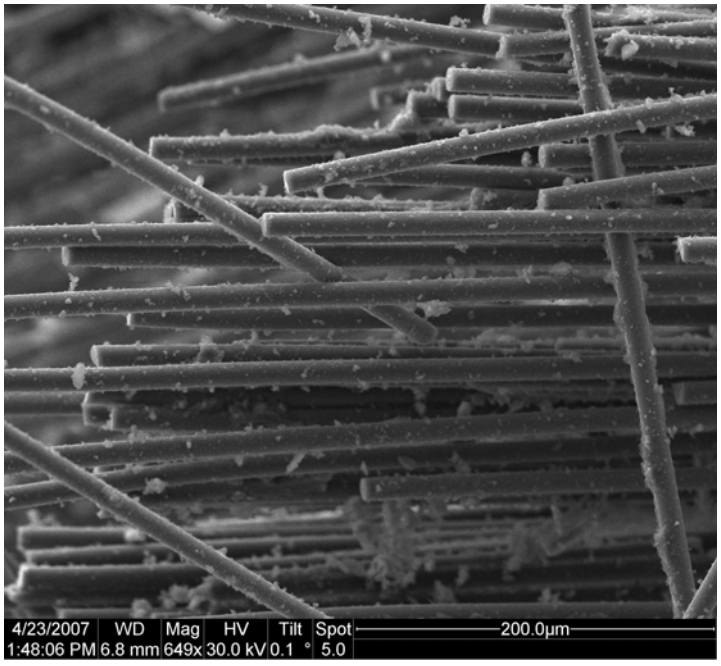

Figure 135. Fracture surface of N720/A specimen tested in compression to failure following aging in steam for 25 h.

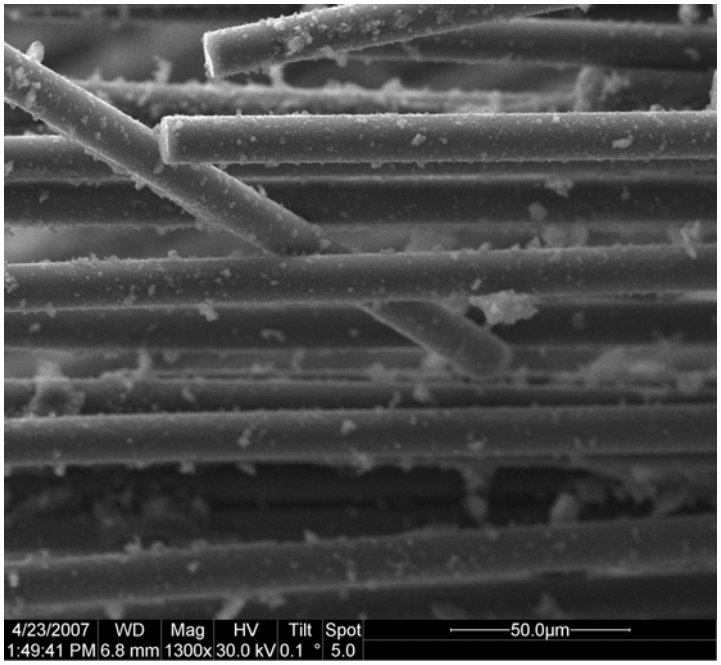

Figure 136.Fracture surface of N720/A specimen tested in compression to failure following aging in steam for 25 h.

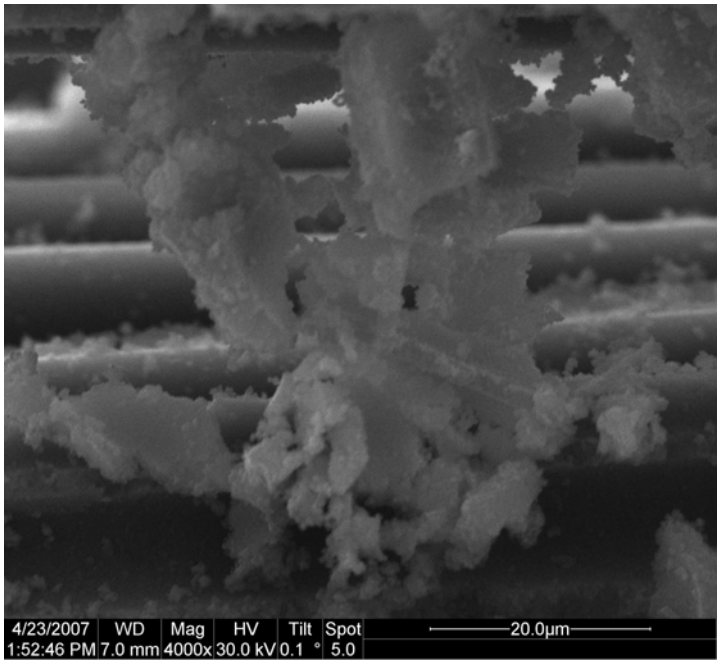

Figure 137. Fracture surface of N720/A specimen tested in compression to failure following aging in steam for 25 h.

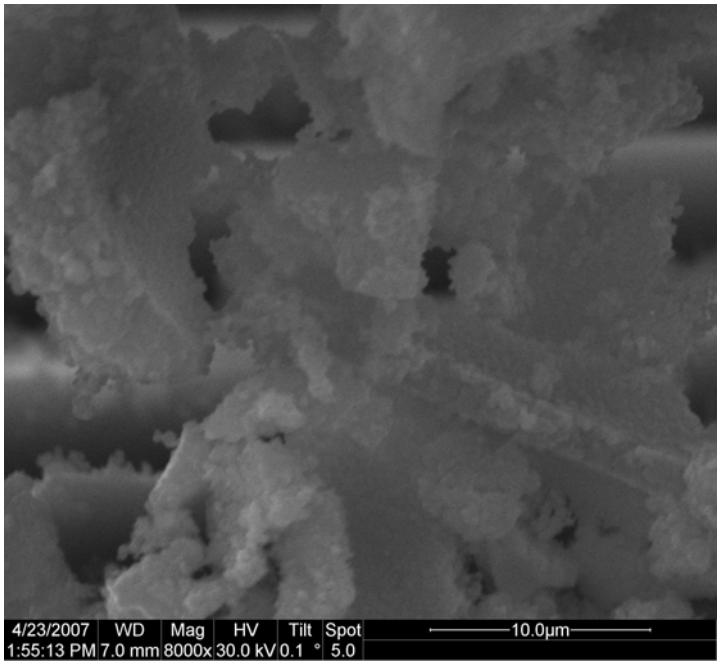

Figure 138. Fracture surface of N720/A specimen tested in compression to failure following aging in steam for 25 h.

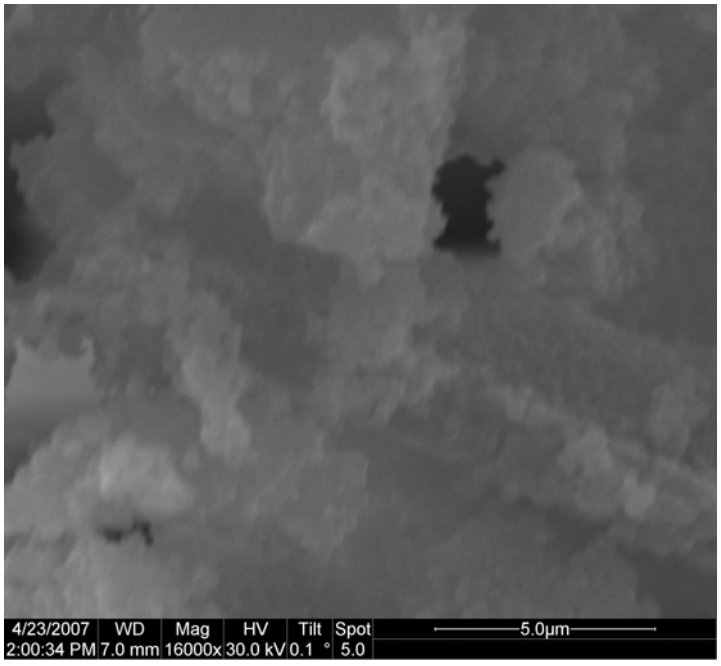

Figure 139. Fracture surface of N720/A specimen tested in compression to failure following aging in steam for 25 h.

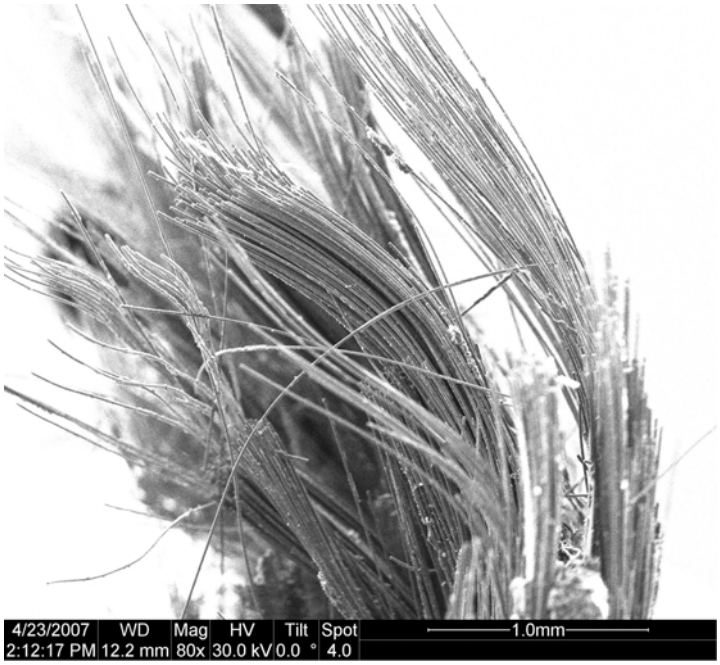

Figure 140. Fracture surface of N720/A specimen tested in compression to failure following aging in steam for 25 h.

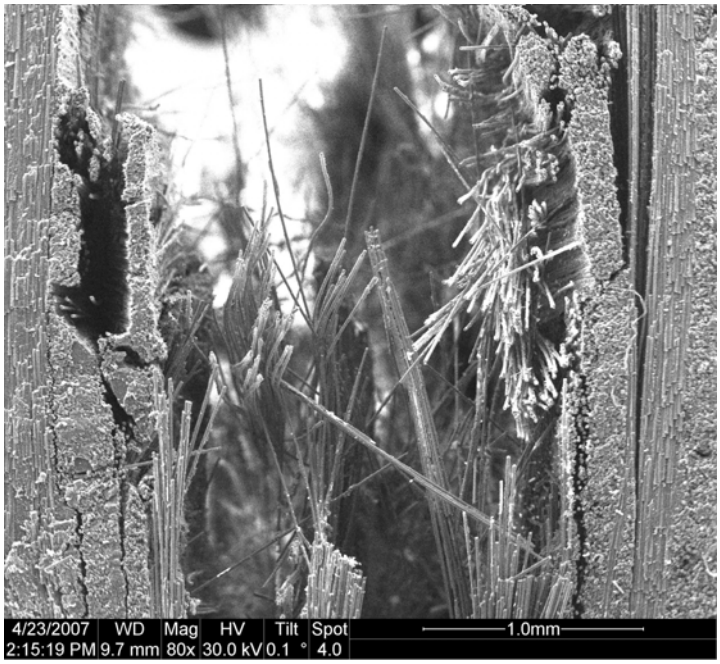

Figure 141. Fracture surface of N720/A specimen tested in compression to failure following aging in steam for 25 h.

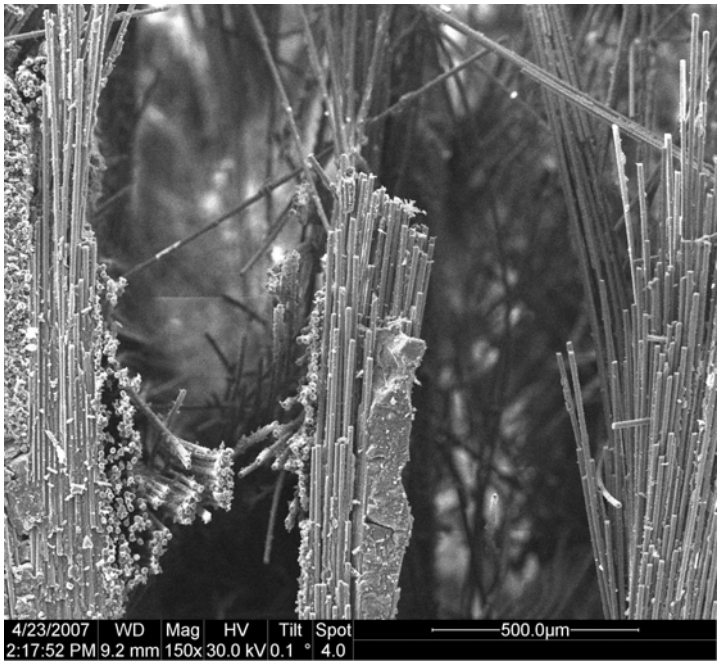

Figure 142. Fracture surface of N720/A specimen tested in compression to failure following aging in steam for 25 h.

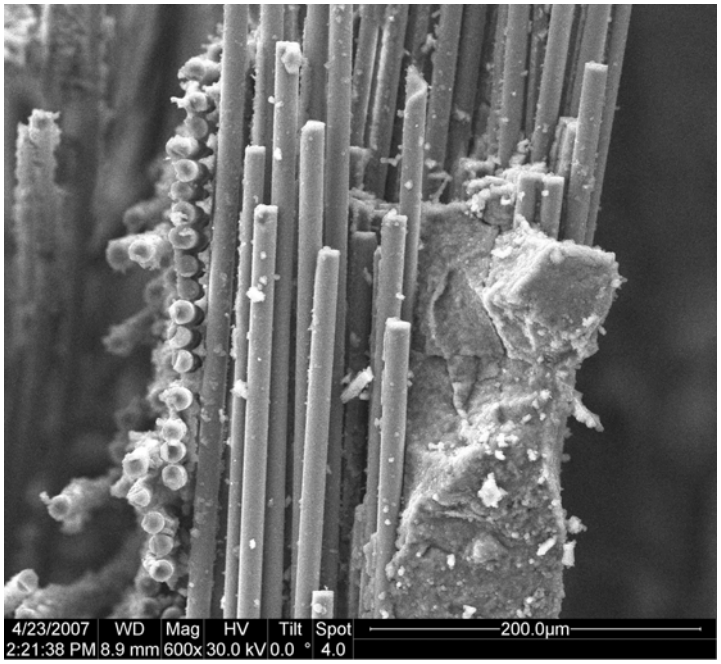

Figure 143. Fracture surface of N720/A specimen tested in compression to failure following aging in steam for 25 h.

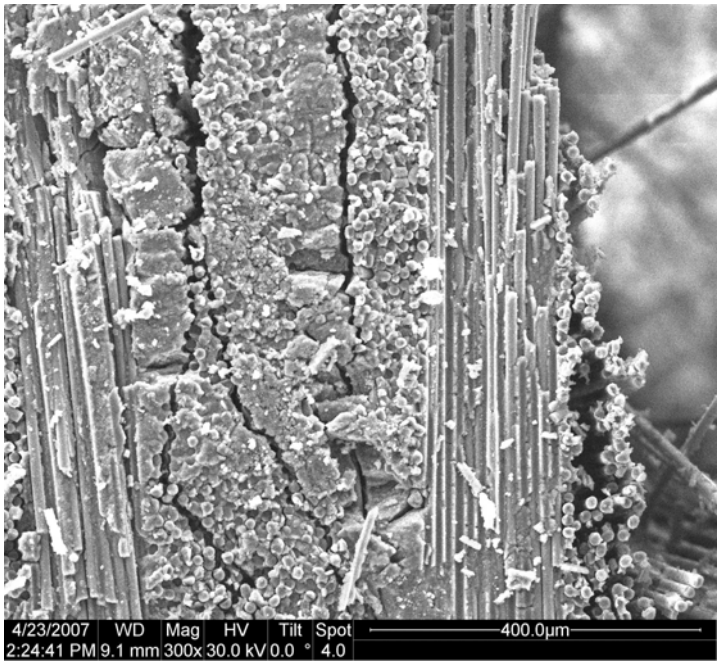

Figure 144. Fracture surface of N720/A specimen tested in compression to failure following aging in steam for 25 h.

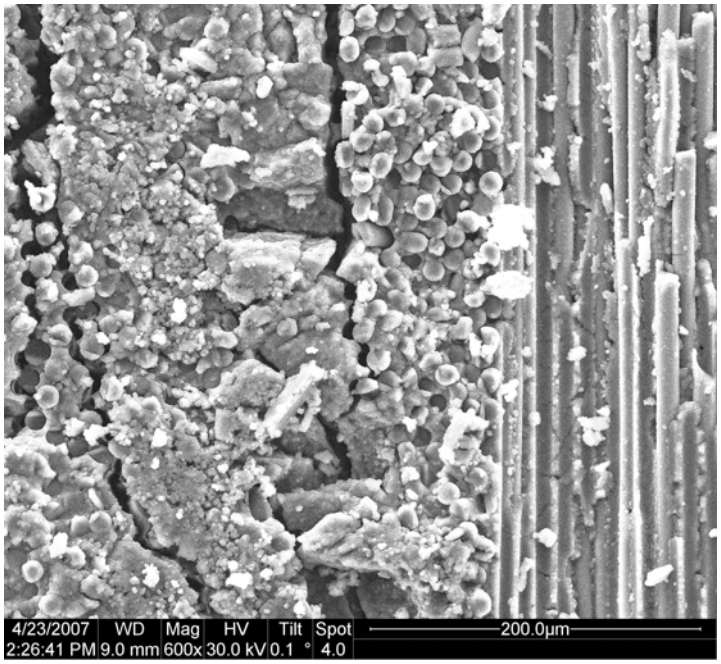

Figure 145. Fracture surface of N720/A specimen tested in compression to failure following aging in steam for 25 h.

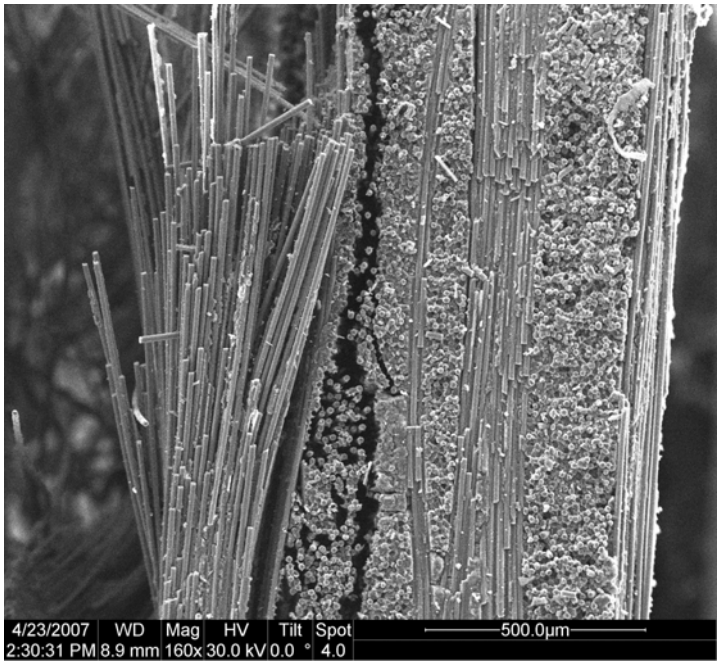

Figure 146. Fracture surface of N720/A specimen tested in compression to failure following aging in steam for 25 h.

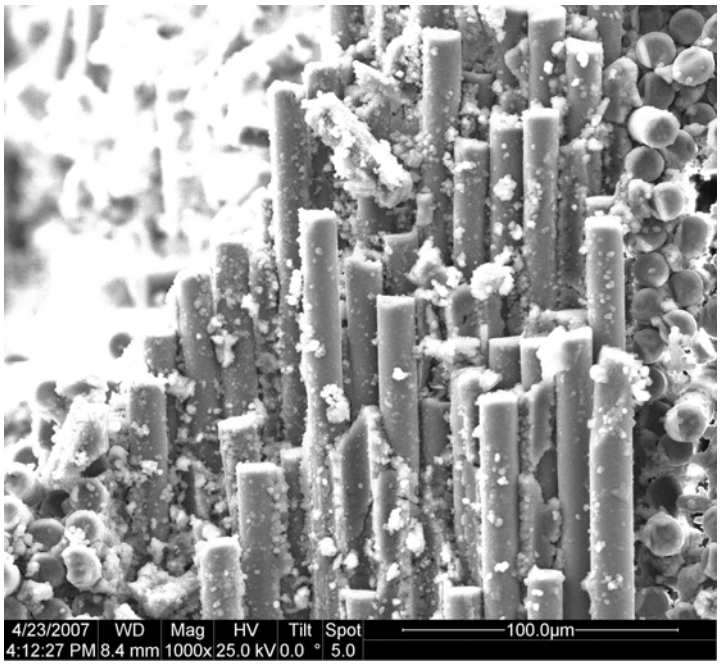

Figure 147. Fracture surface of N720/A specimen tested in compression to failure in load control at a rate of -0.0025 MPa/s in steam at 1200°C.

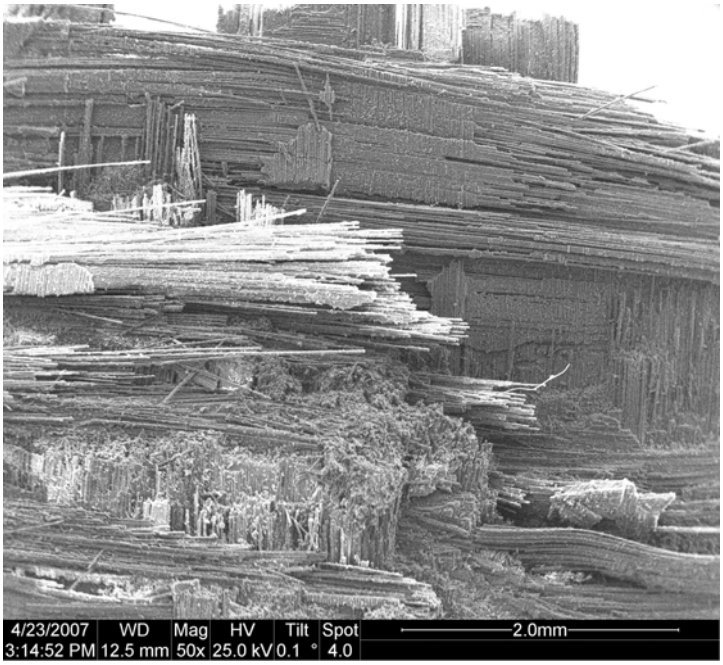

Figure 148. Fracture surface of N720/A specimen tested in compression to failure in load control at a rate of -0.0025 MPa/s in steam at 1200°C.

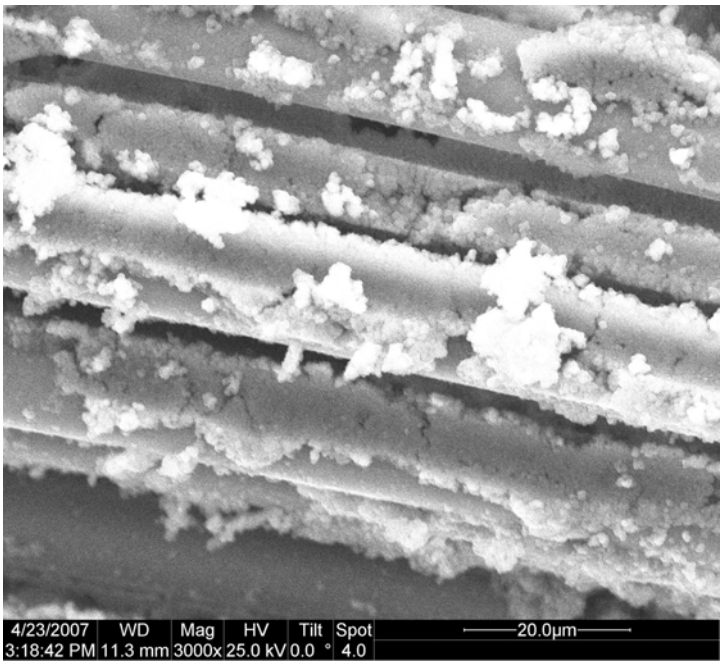

Figure 149. Fracture surface of N720/A specimen tested in compression to failure in load control at a rate of -0.0025 MPa/s in steam at 1200°C.

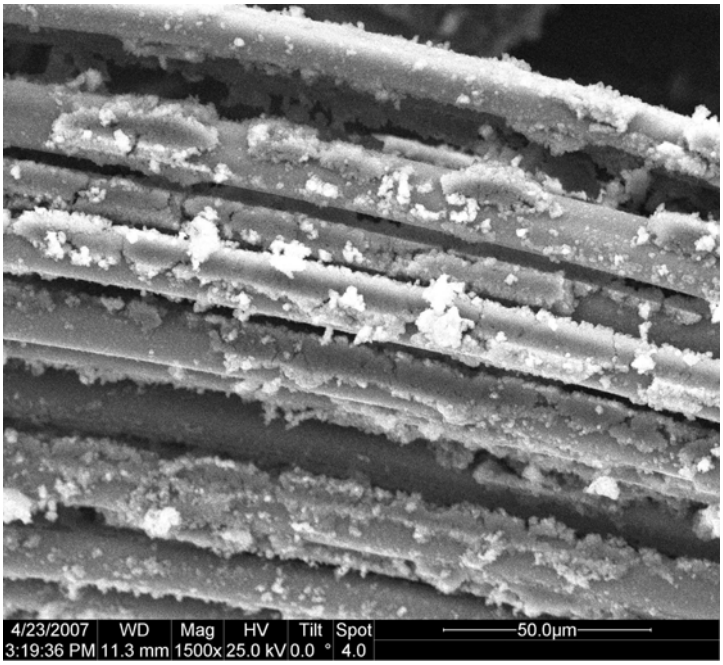

Figure 150. Fracture surface of N720/A specimen tested in compression to failure in load control at a rate of -0.0025 MPa/s in steam at 1200°C.

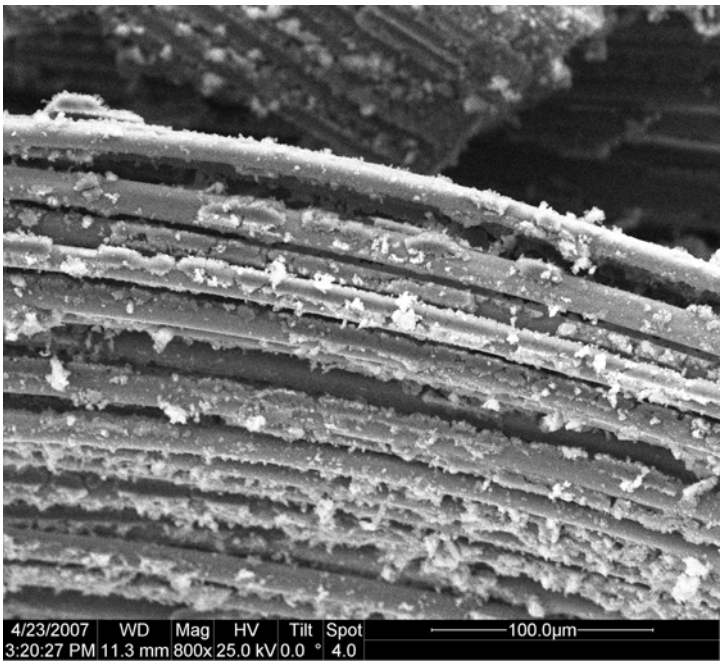

Figure 151. Fracture surface of N720/A specimen tested in compression to failure in load control at a rate of -0.0025 MPa/s in steam at 1200°C.

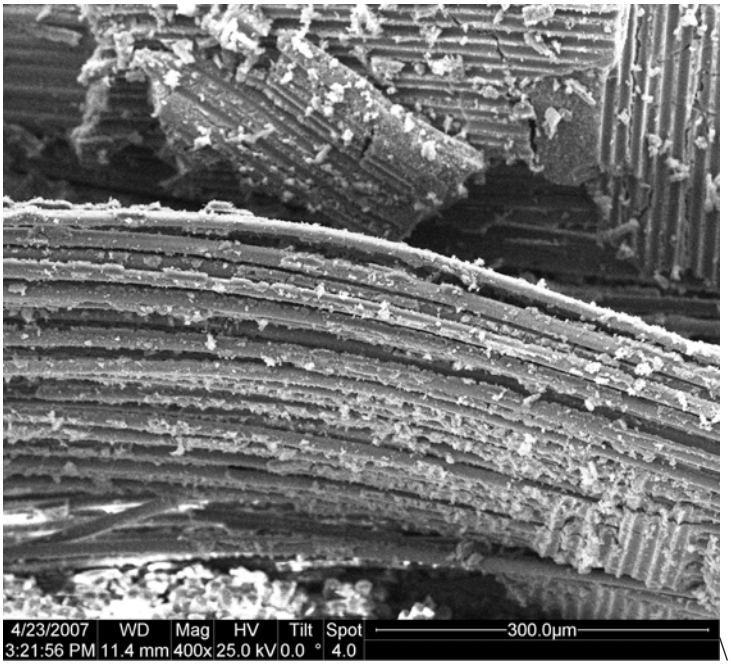

Figure 152. Fracture surface of N720/A specimen tested in compression to failure in load control at a rate of -0.0025 MPa/s in steam at 1200°C.

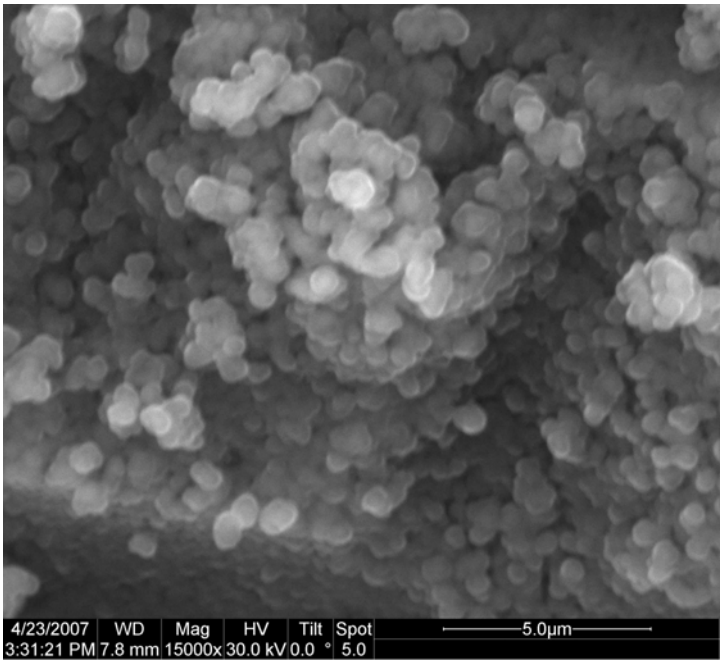

Figure 153. Fracture surface of N720/A specimen tested in compression to failure in load control at a rate of -0.0025 MPa/s in steam at 1200°C.

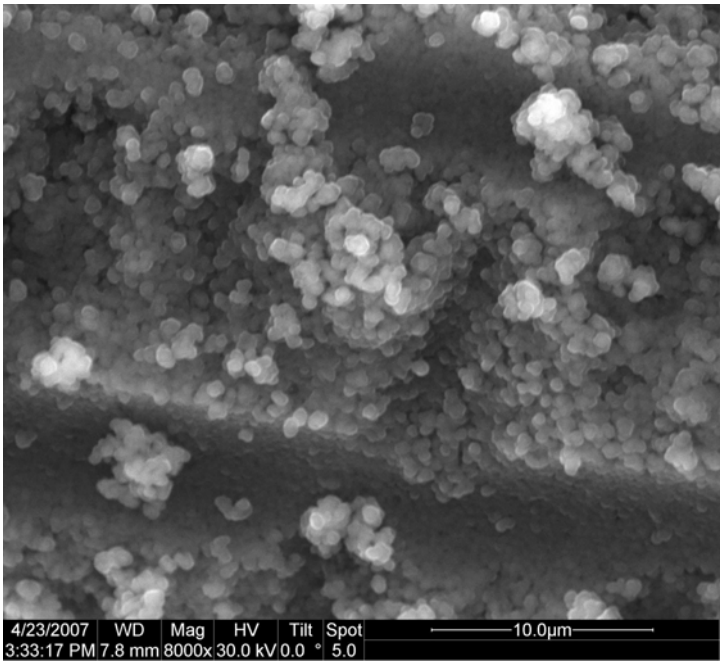

Figure 154. Fracture surface of N720/A specimen tested in compression to failure in load control at a rate of -0.0025 MPa/s in steam at 1200°C.

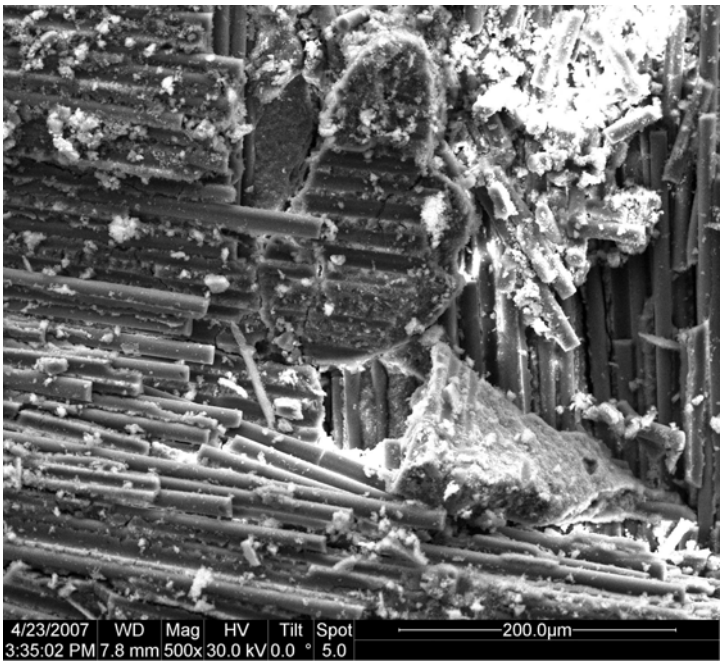

Figure 155. Fracture surface of N720/A specimen tested in compression to failure in load control at a rate of -0.0025 MPa/s in steam at 1200°C.

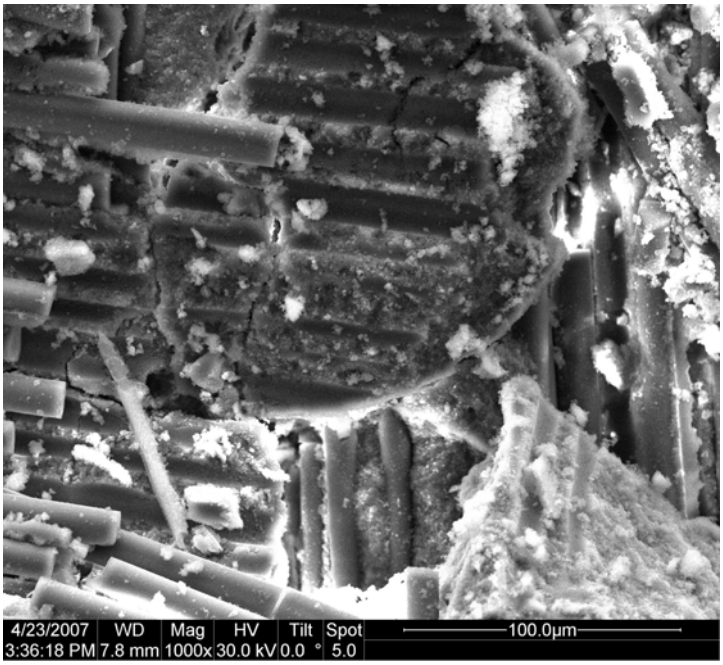

Figure 156. Fracture surface of N720/A specimen tested in compression to failure in load control at a rate of -0.0025 MPa/s in steam at 1200°C.

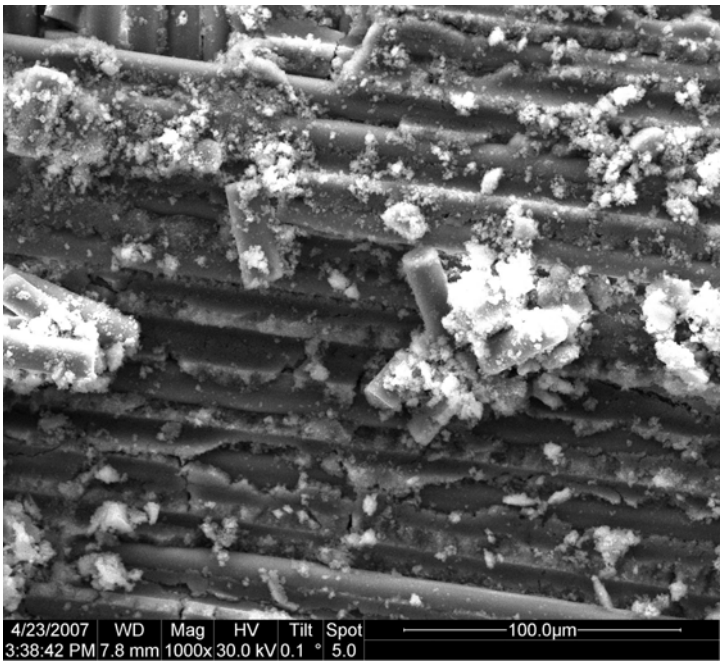

Figure 157. Fracture surface of N720/A specimen tested in compression to failure in load control at a rate of -0.0025 MPa/s in steam at 1200°C.

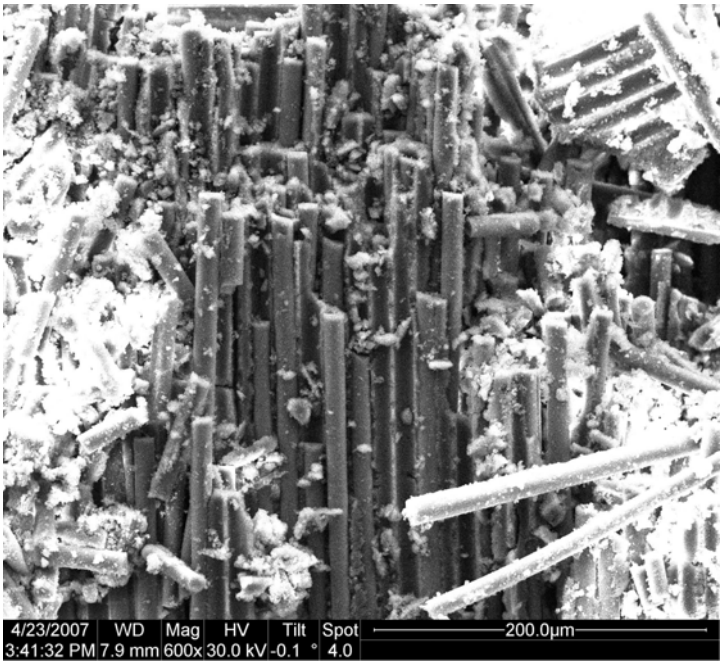

Figure 158. Fracture surface of N720/A specimen tested in compression to failure in load control at a rate of -0.0025 MPa/s in steam at 1200°C.

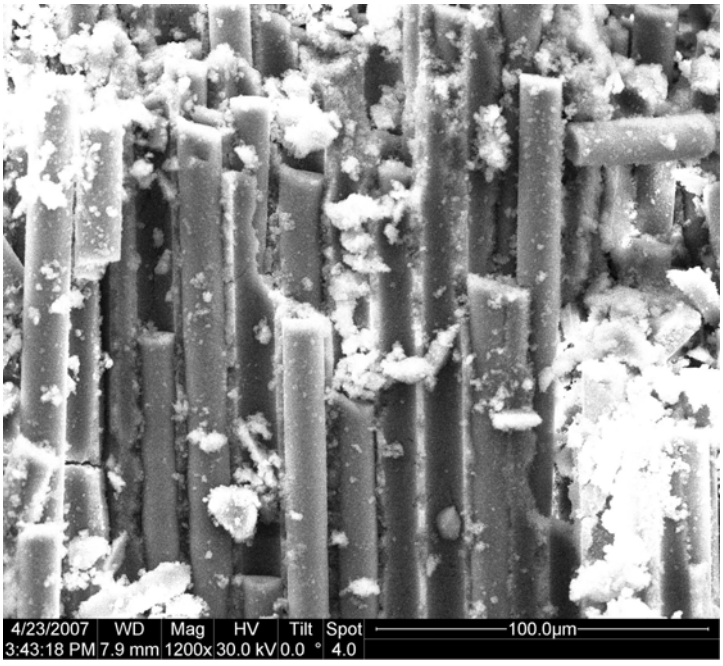

Figure 159. Fracture surface of N720/A specimen tested in compression to failure in load control at a rate of -0.0025 MPa/s in steam at 1200°C.

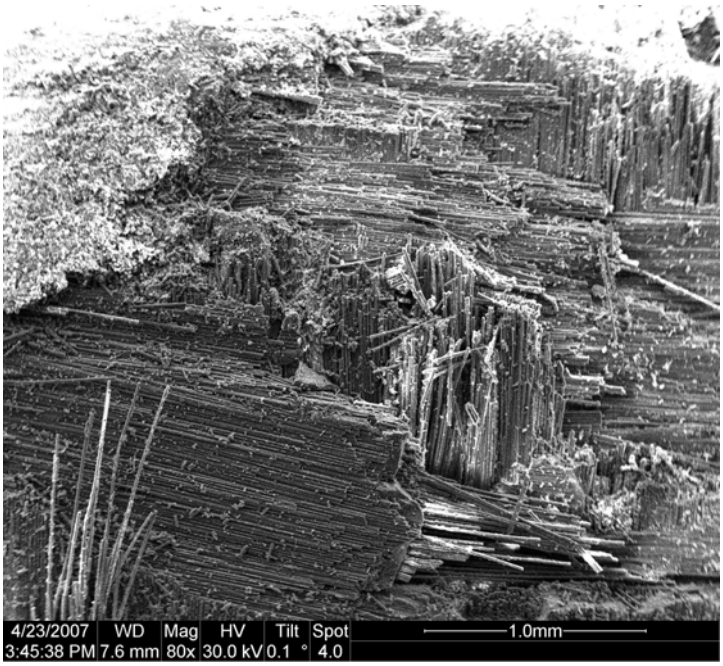

Figure 160. Fracture surface of N720/A specimen tested in compression to failure in load control at a rate of -0.0025 MPa/s in steam at 1200°C.

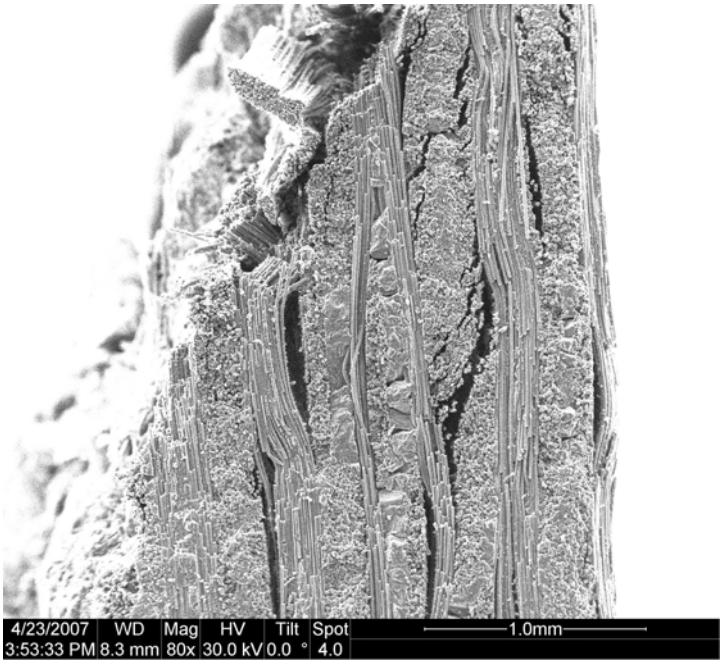

Figure 161. Fracture surface of N720/A specimen tested in compression to failure in load control at a rate of -0.0025 MPa/s in steam at 1200°C.

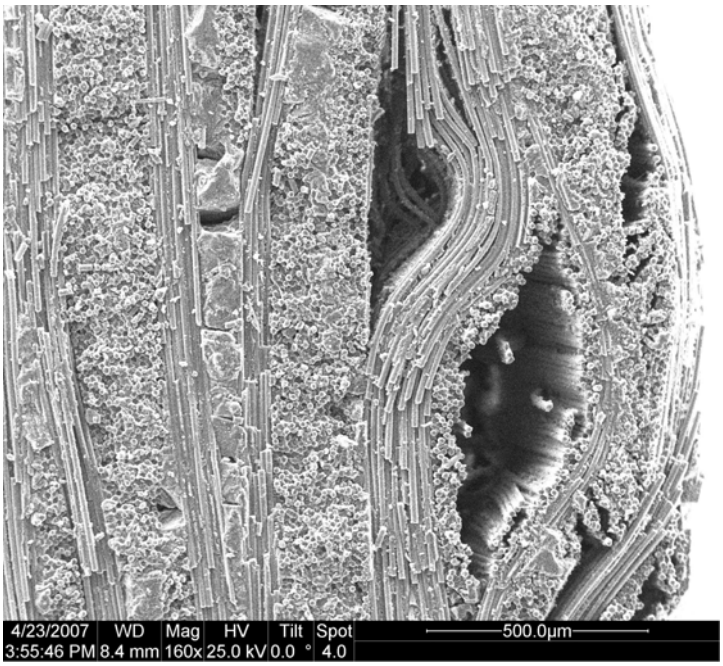

Figure 162. Fracture surface of N720/A specimen tested in compression to failure in load control at a rate of -0.0025 MPa/s in steam at 1200°C.

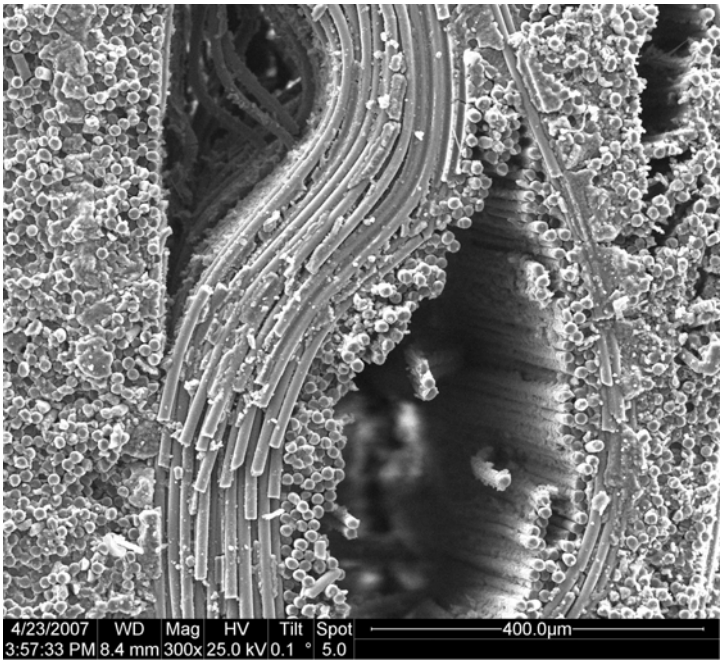

Figure 163. Fracture surface of N720/A specimen tested in compression to failure in load control at a rate of -0.0025 MPa/s in steam at 1200°C.

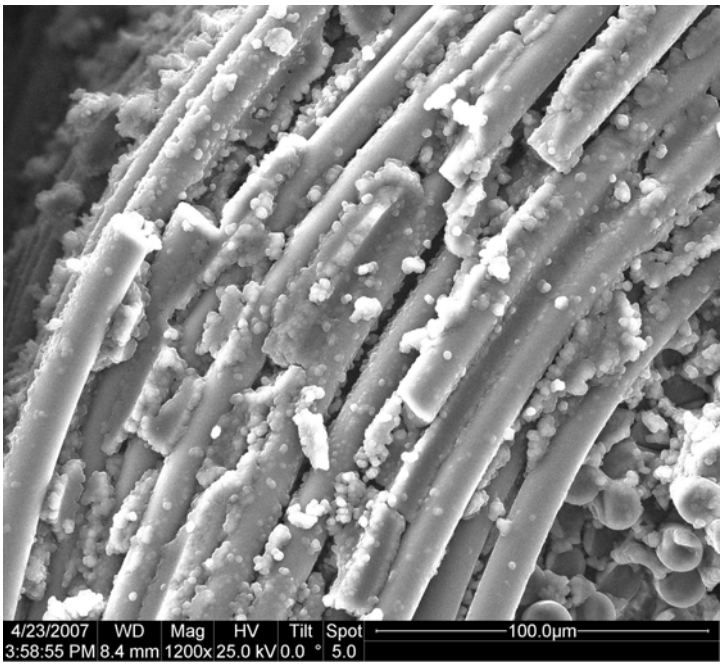

Figure 164. Fracture surface of N720/A specimen tested in compression to failure in load control at a rate of -0.0025 MPa/s in steam at 1200°C.

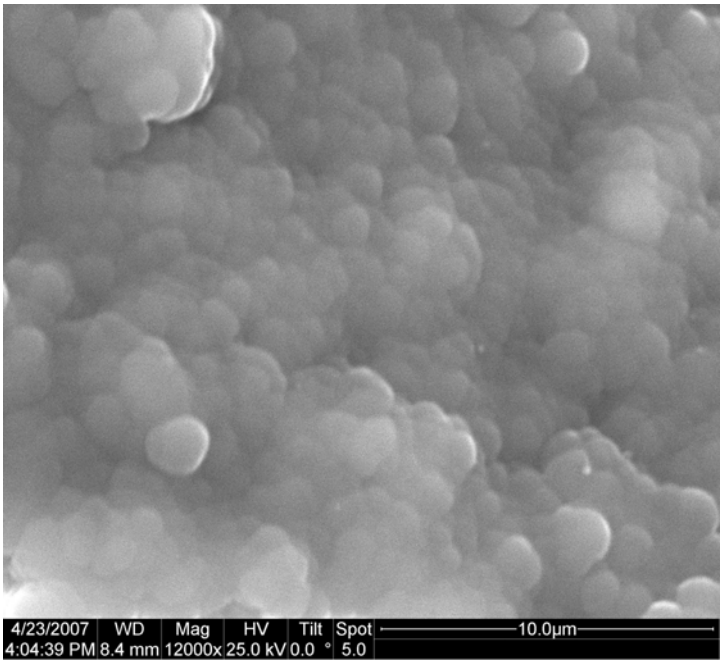

Figure 165. Fracture surface of N720/A specimen tested in compression to failure in load control at a rate of -0.0025 MPa/s in steam at 1200°C.

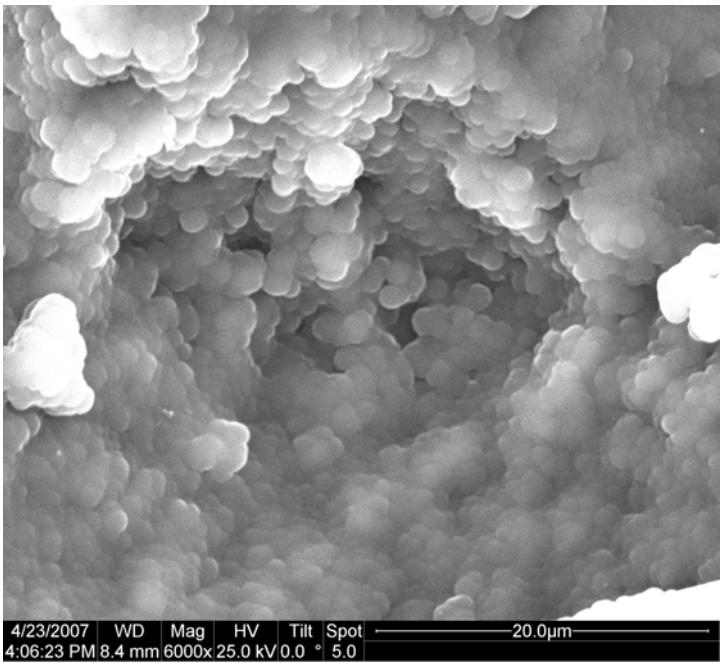

Figure 166. Fracture surface of N720/A specimen tested in compression to failure in load control at a rate of -0.0025 MPa/s in steam at 1200°C.

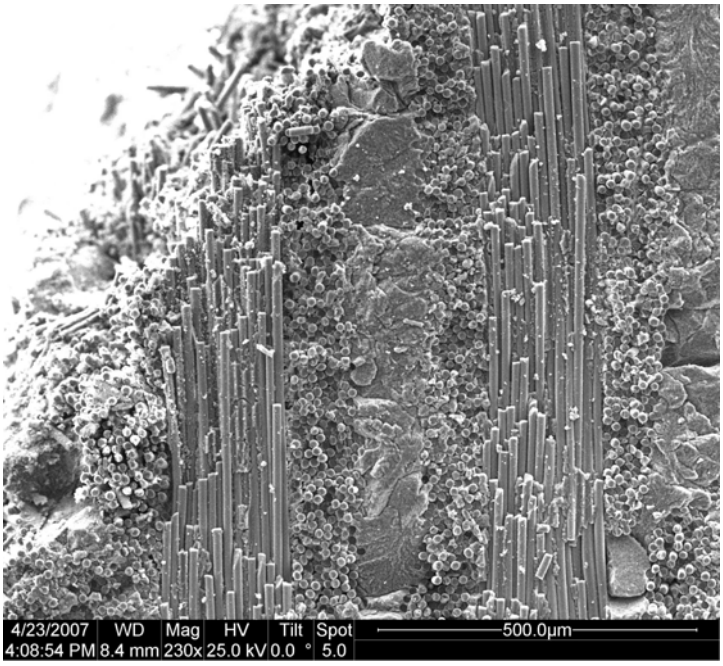

Figure 167. Fracture surface of N720/A specimen tested in compression to failure in load control at a rate of -0.0025 MPa/s in steam at 1200°C.

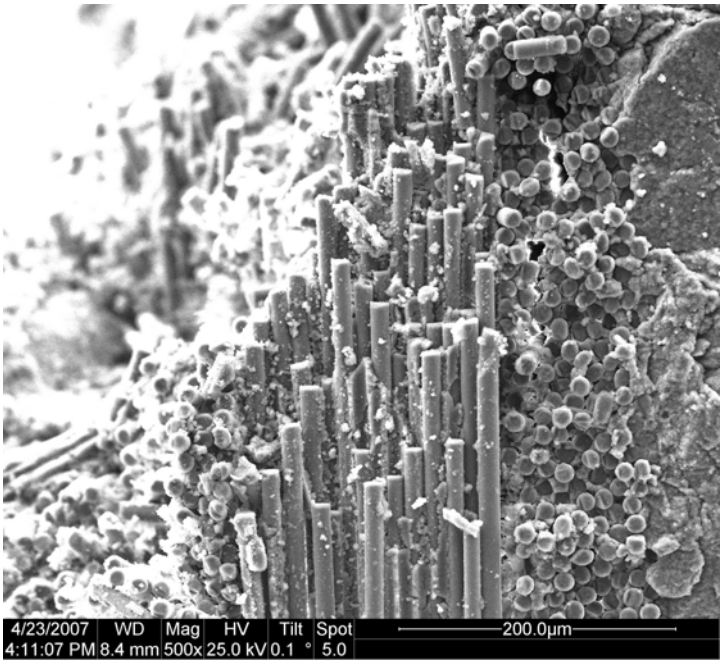

Figure 168. Fracture surface of N720/A specimen tested in compression to failure in load control at a rate of -0.0025 MPa/s in steam at 1200°C.

Appendix B. Additional Optical Micrographs

Figure 169. Fracture surface of N720/A specimen tested in compression to failure in displacement control at a rate of -0.05 mm/s in air at 1200°C.

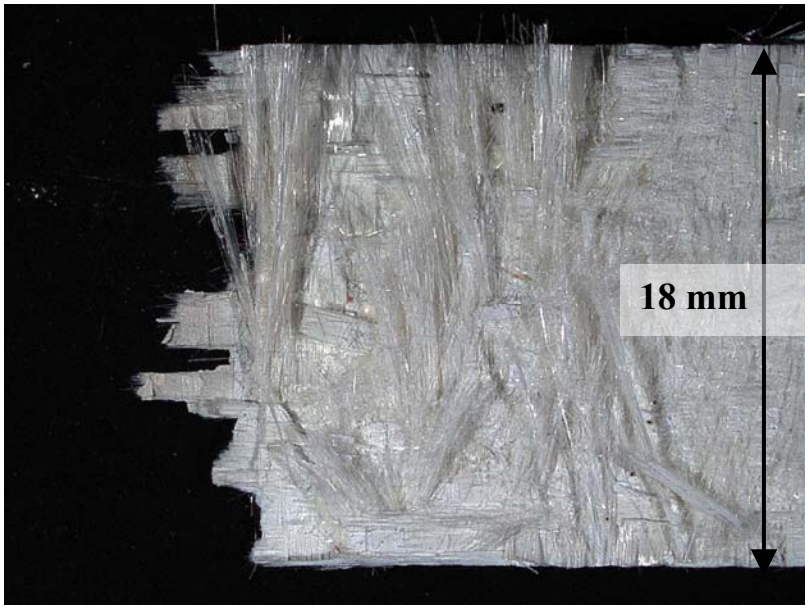

Figure 170. Fracture surface of N720/A specimen tested in compression to failure in displacement control at a rate of -0.05 mm/s in air at 1200°C.

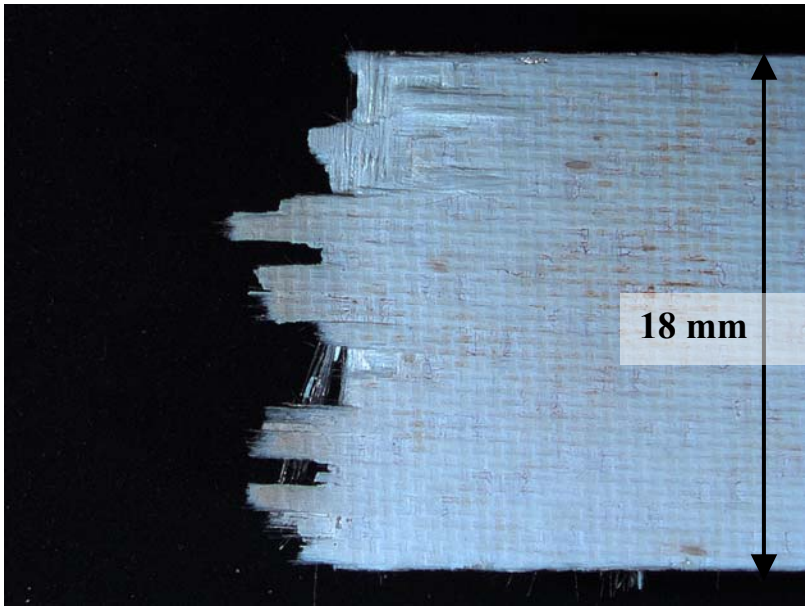

Figure 171. Fracture surface of N720/A specimen tested in compression to failure in displacement control at a rate of -0.05 mm/s in air at 1200°C.

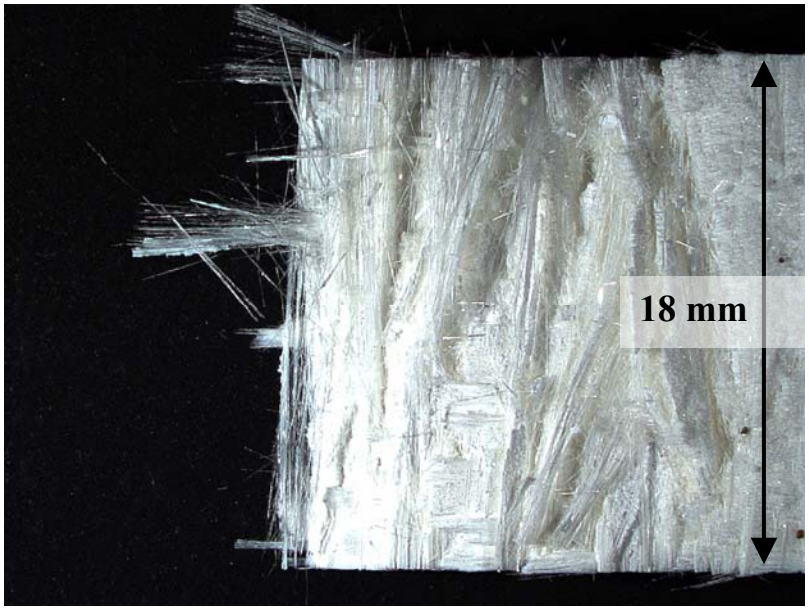

Figure 172. Fracture surface of N720/A specimen tested in compression to failure in displacement control at a rate of -0.05 mm/s in air at 1200°C.

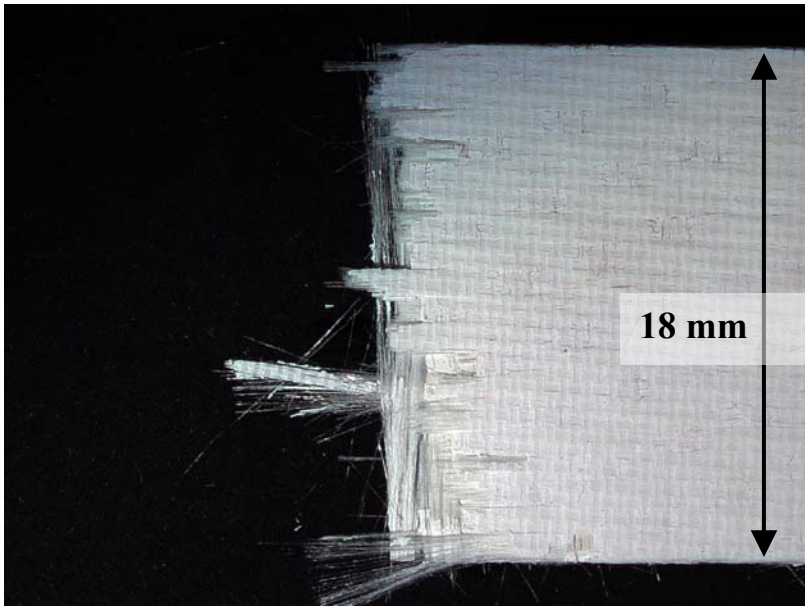

Figure 173. Fracture surface of N720/A specimen tested in compression to failure in displacement control at a rate of -0.05 mm/s in air at 1200°C.

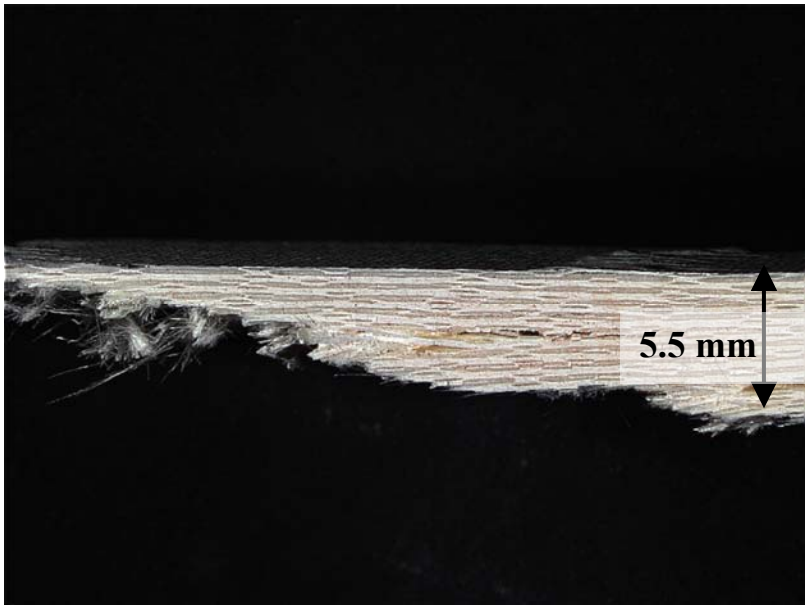

Figure 174. Fracture surface of N720/A specimen tested in compression to failure in displacement control at a rate of -0.05 mm/s in air at 1200°C.

Figure 175. Fracture surface of N720/A specimen tested in compression to failure in displacement control at a rate of -0.05 mm/s in air at 1200°C.

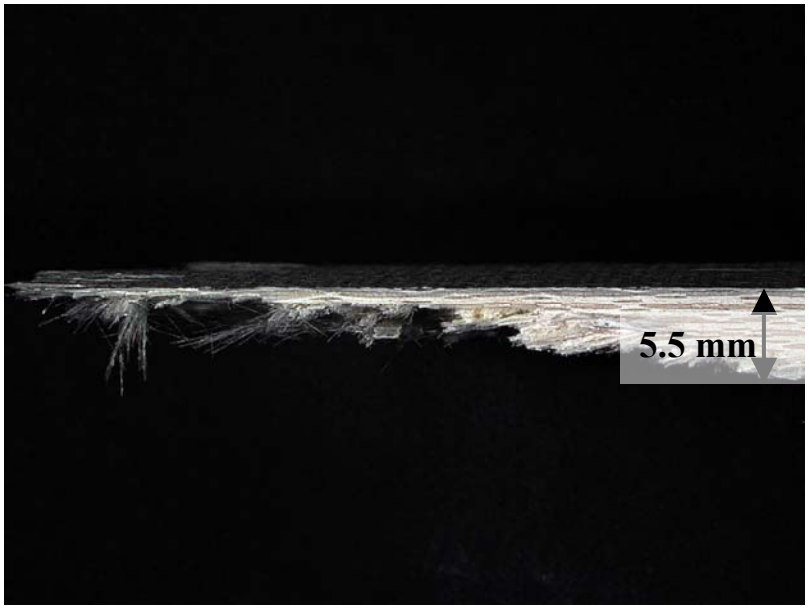

Figure 176. Fracture surface of N720/A specimen tested in compression to failure in displacement control at a rate of -0.05 mm/s in air at 1200°C.

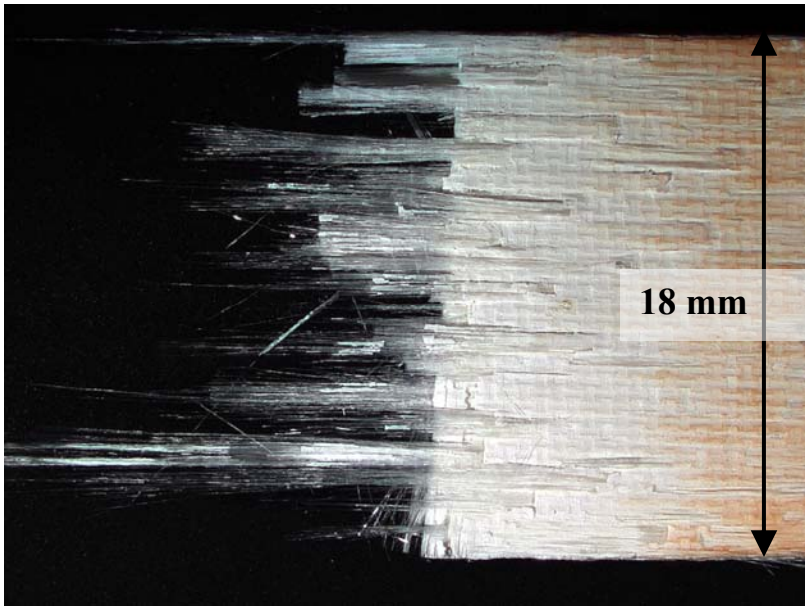

Figure 177. Fracture surface of N720/A specimen tested in compressive creep at -100 MPa for 100 h at 1200°C in air.

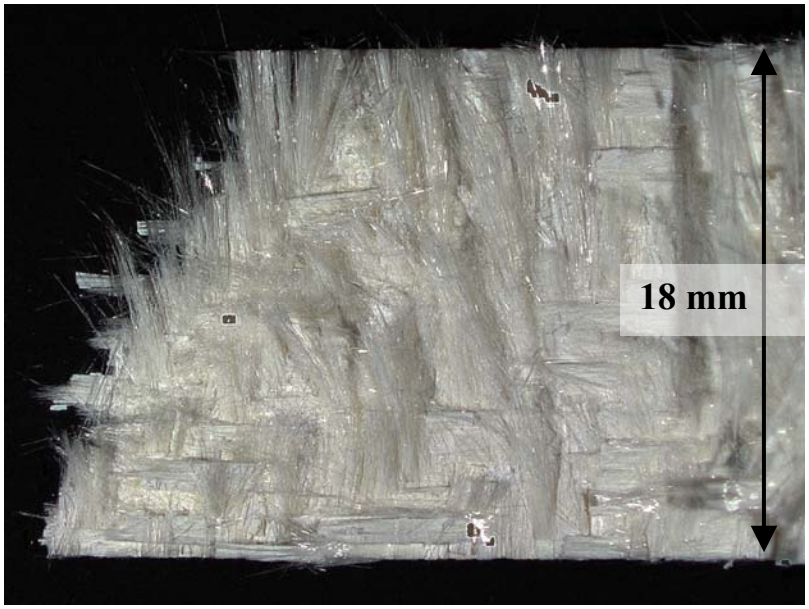

Figure 178. Fracture surface of N720/A specimen tested in compressive creep at -100 MPa for 100 h at 1200°C in air.

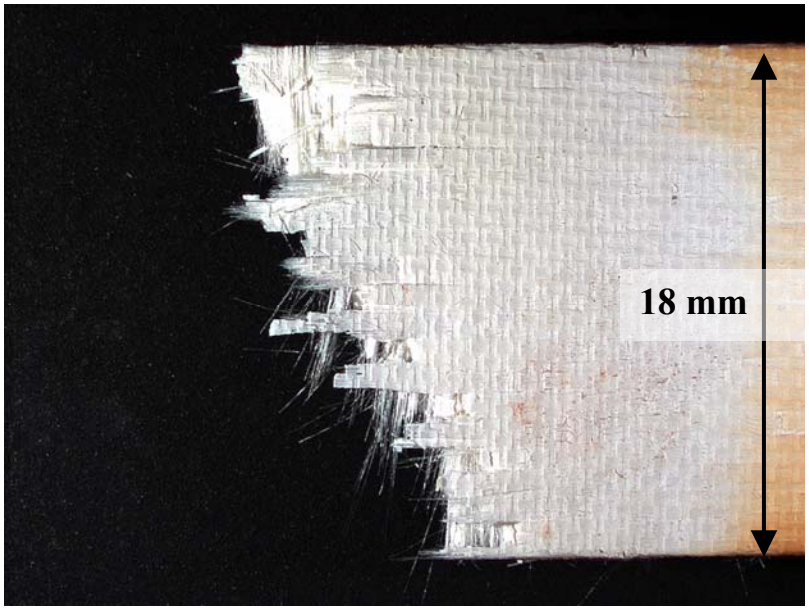

Figure 179. Fracture surface of N720/A specimen tested in compressive creep at -100 MPa for 100 h at 1200°C in air.

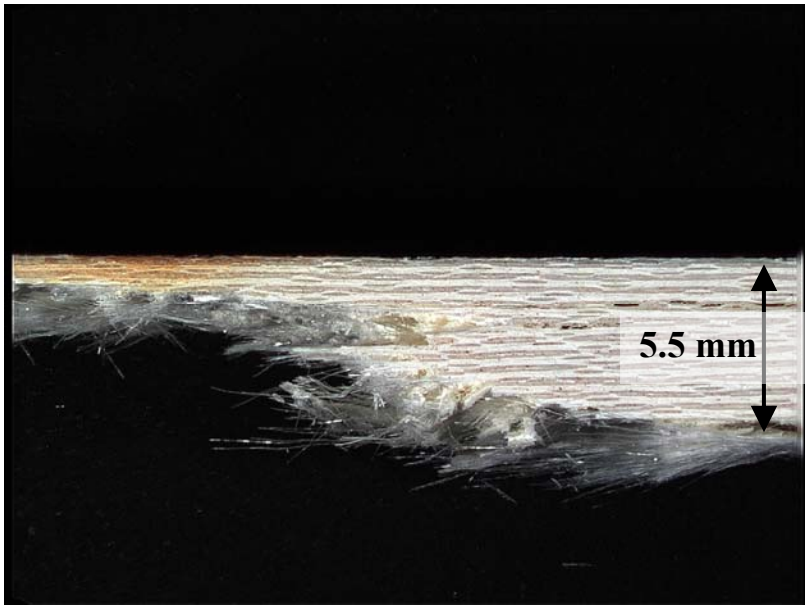

Figure 180. Fracture surface of N720/A specimen tested in compressive creep at -100 MPa for 100 h at 1200°C in air.

Figure 181. Fracture surface of N720/A specimen tested in compressive creep at -100 MPa for 100 h at 1200°C in air.

Figure 182. Fracture surface of N720/A specimen tested in compressive creep at -100 MPa for 100 h at 1200°C in air.

Figure 183. Fracture surface of N720/A specimen tested in compressive creep at -100 MPa for 100 h at 1200°C in air.

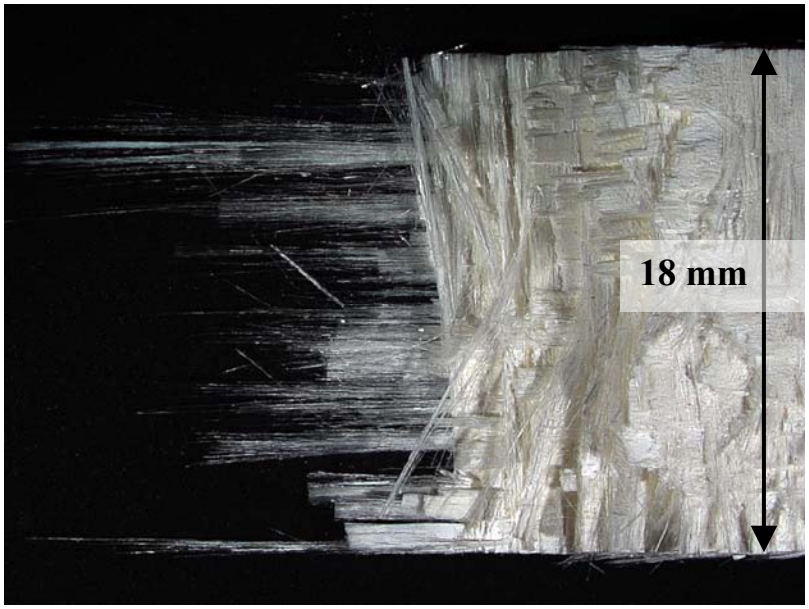

Figure 184. Fracture surface of N720/A specimen tested in compressive creep at -100 MPa for 100 h at 1200°C in air.

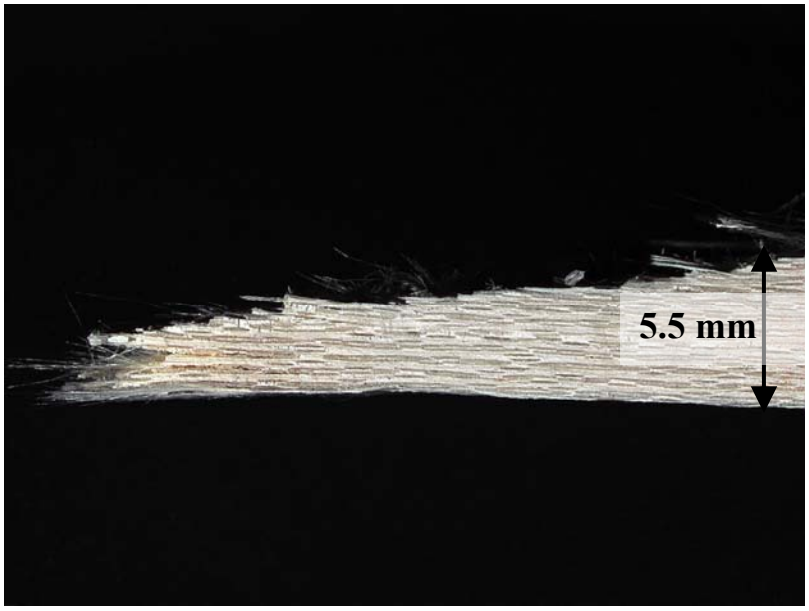

Figure 185. Fracture surface of N720/A specimen tested in compressive creep at -60 MPa for 100 h at 1200°C in air.

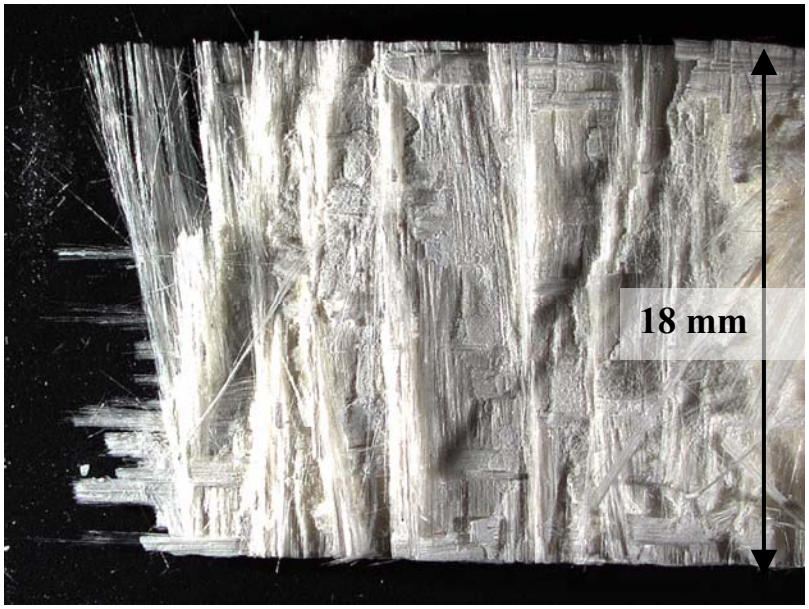

Figure 186. Fracture surface of N720/A specimen tested in compressive creep at -60 MPa for 100 h at 1200°C in air.

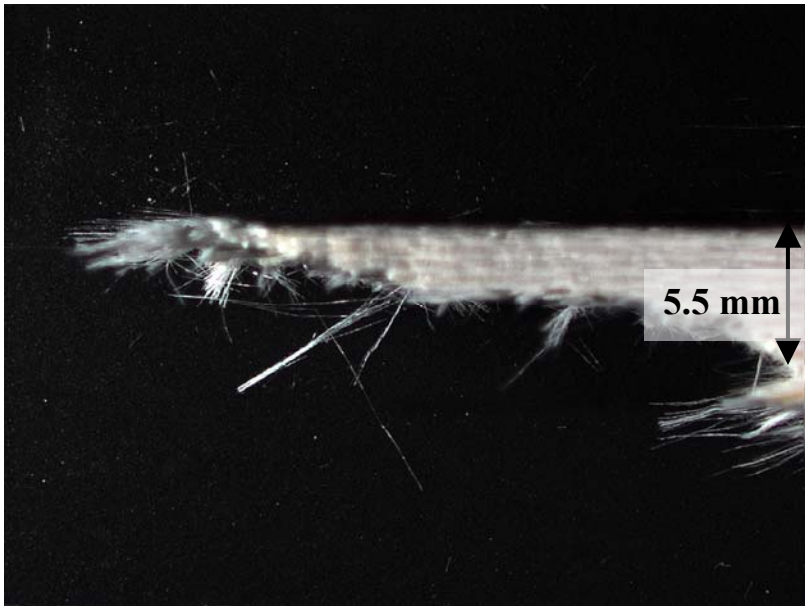

Figure 187. Fracture surface of N720/A specimen tested in compressive creep at -60 MPa for 100 h at 1200°C in air.

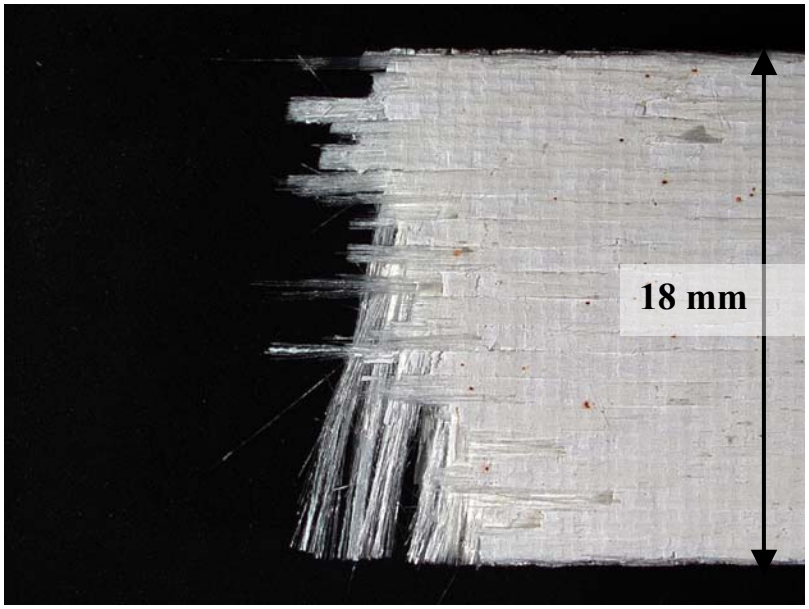

Figure 188. Fracture surface of N720/A specimen tested in compressive creep at -60 MPa for 100 h at 1200°C in air.

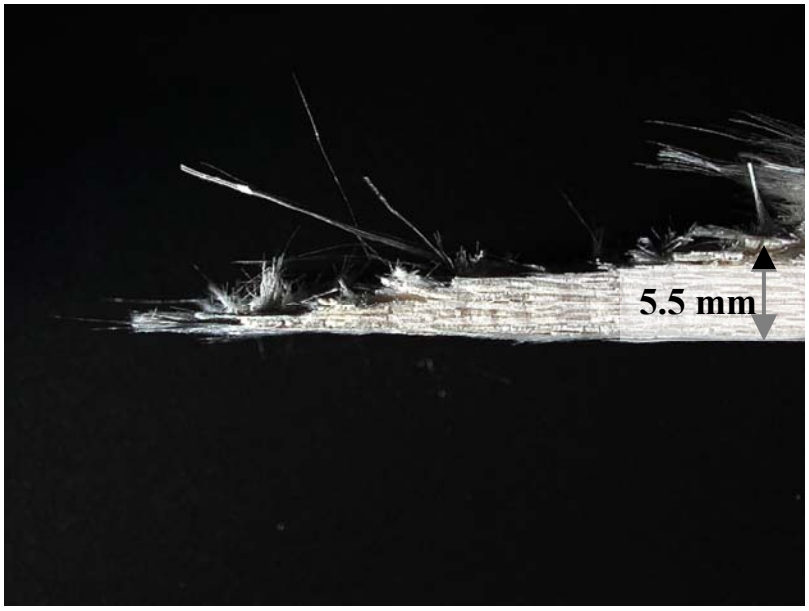

Figure 189. Fracture surface of N720/A specimen tested in compressive creep at -60 MPa for 100 h at 1200°C in air.

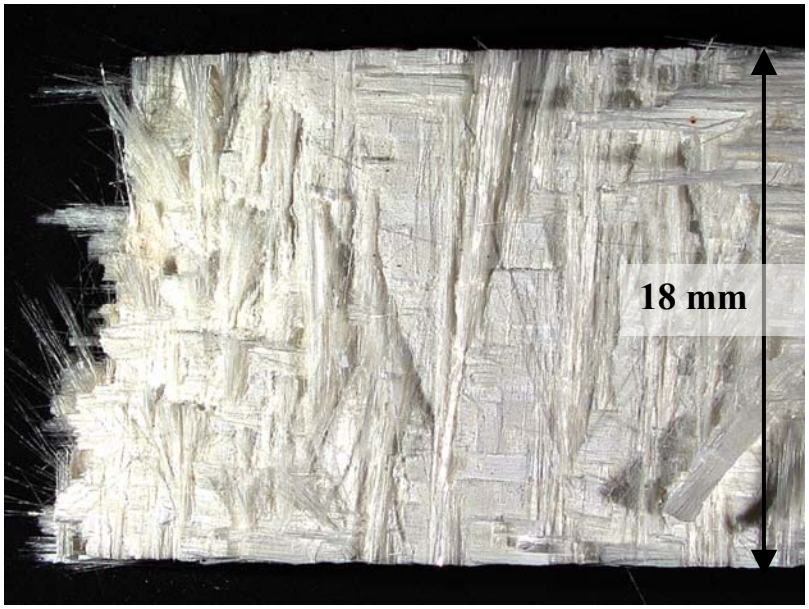

Figure 190. Fracture surface of N720/A specimen tested in compressive creep at -60 MPa for 100 h at 1200°C in air.

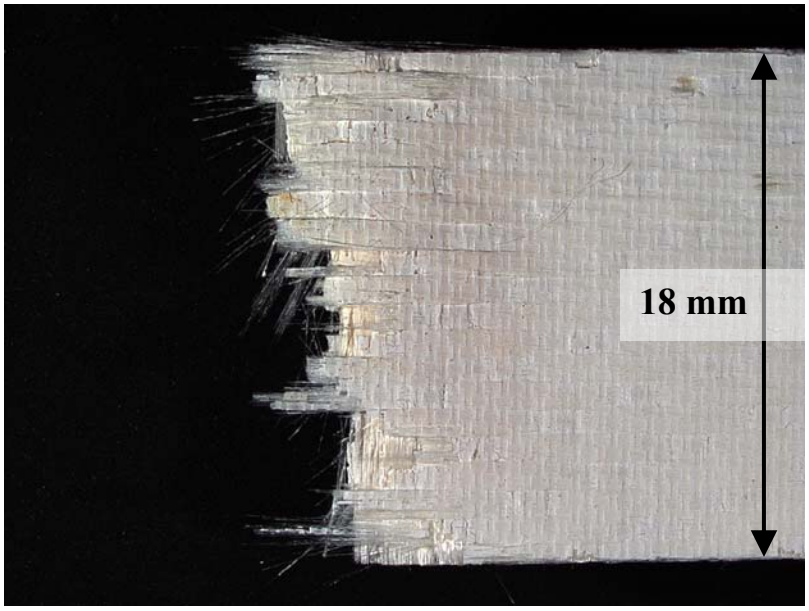

Figure 191. Fracture surface of N720/A specimen tested in compressive creep at -60 MPa for 100 h at 1200°C in air.

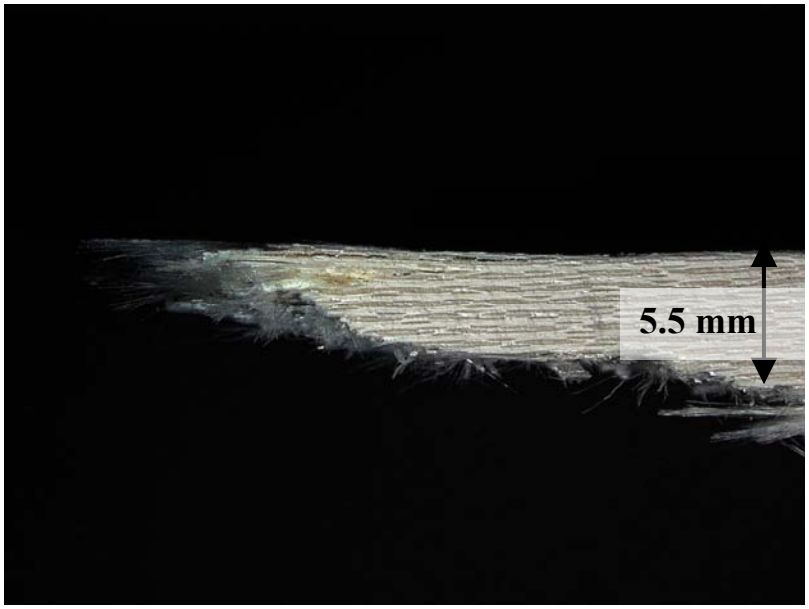

Figure 192. Fracture surface of N720/A specimen tested in compressive creep at -60 MPa for 100 h at 1200°C in air.

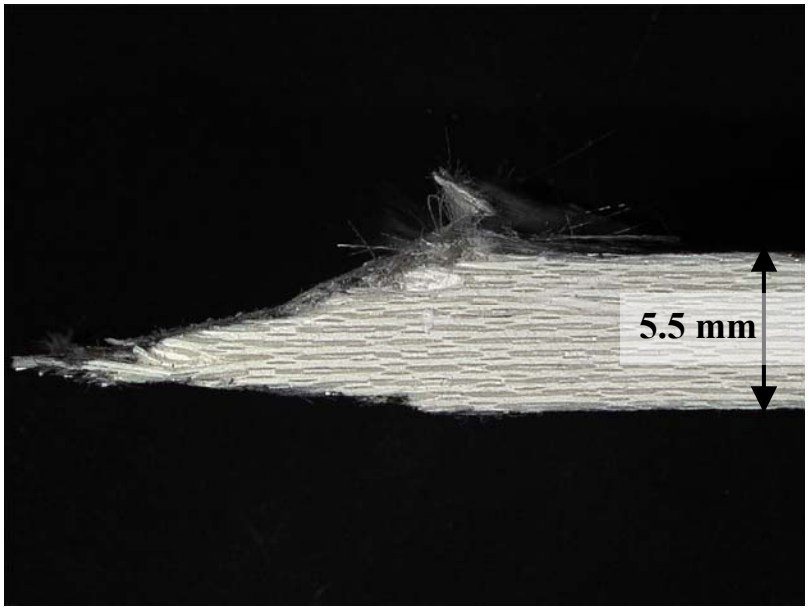

Figure 193. Fracture surface of N720/A specimen tested in compressive creep at -100 MPa for 100 h at 1200°C in steam.

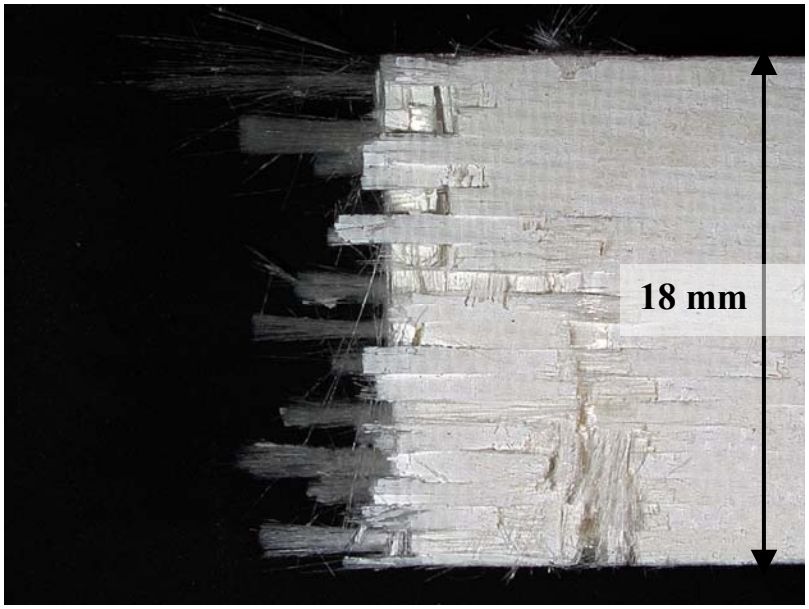

Figure 194. Fracture surface of N720/A specimen tested in compressive creep at -100 MPa for 100 h at 1200°C in steam.

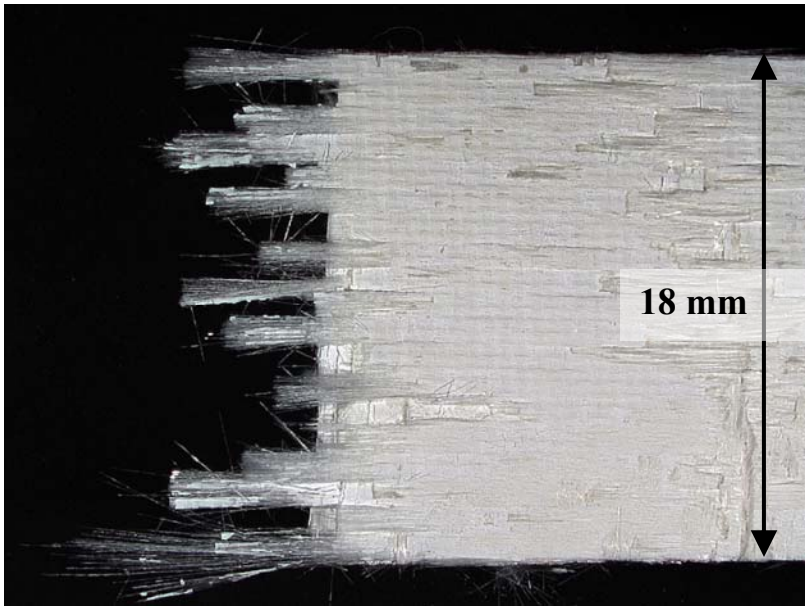

Figure 195. Fracture surface of N720/A specimen tested in compressive creep at -100 MPa for 100 h at 1200°C in steam.

Figure 196. Fracture surface of N720/A specimen tested in compressive creep at -100 MPa for 100 h at 1200°C in steam.

Figure 197. Fracture surface of N720/A specimen tested in compressive creep at -100 MPa for 100 h at 1200°C in steam.

Figure 198. Fracture surface of N720/A specimen tested in compressive creep at -100 MPa for 100 h at 1200°C in steam.

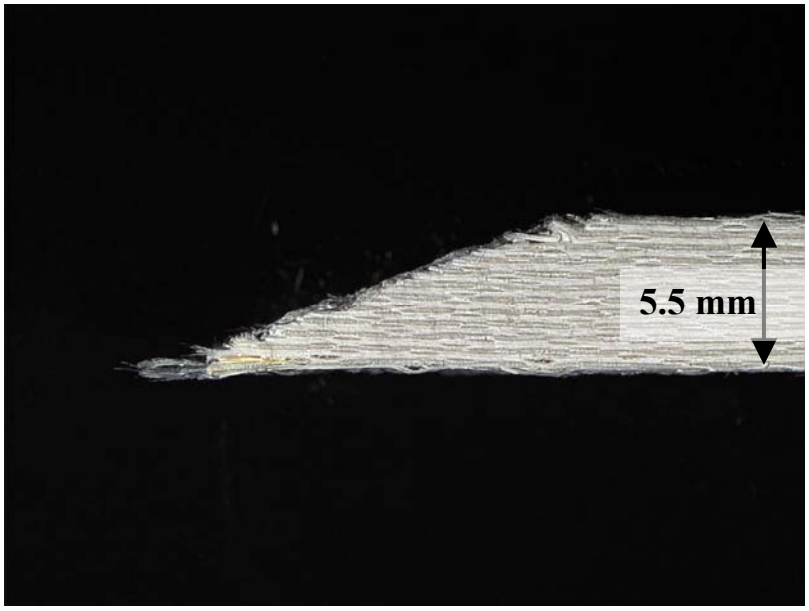

Figure 199. Fracture surface of N720/A specimen tested in compressive creep at -60 MPa for 100 h at 1200°C in steam.

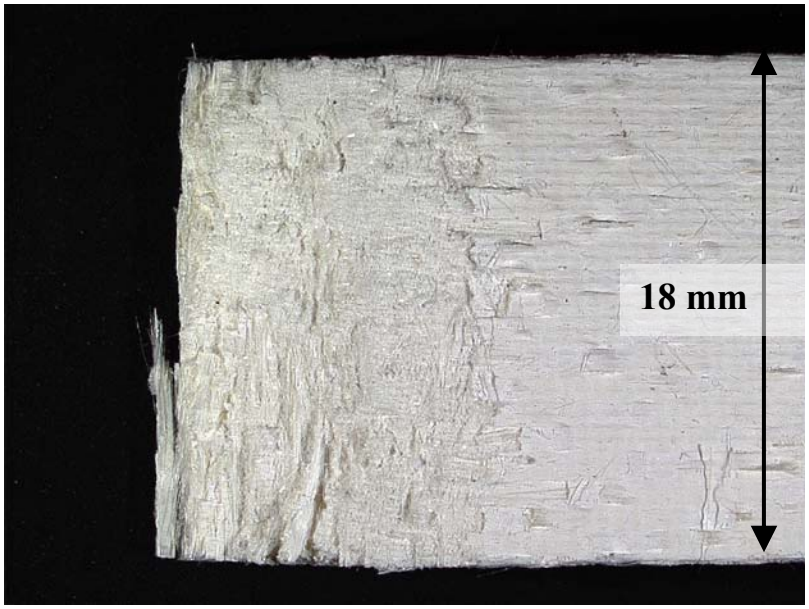

Figure 200. Fracture surface of N720/A specimen tested in compressive creep at -60 MPa for 100 h at 1200°C in steam.

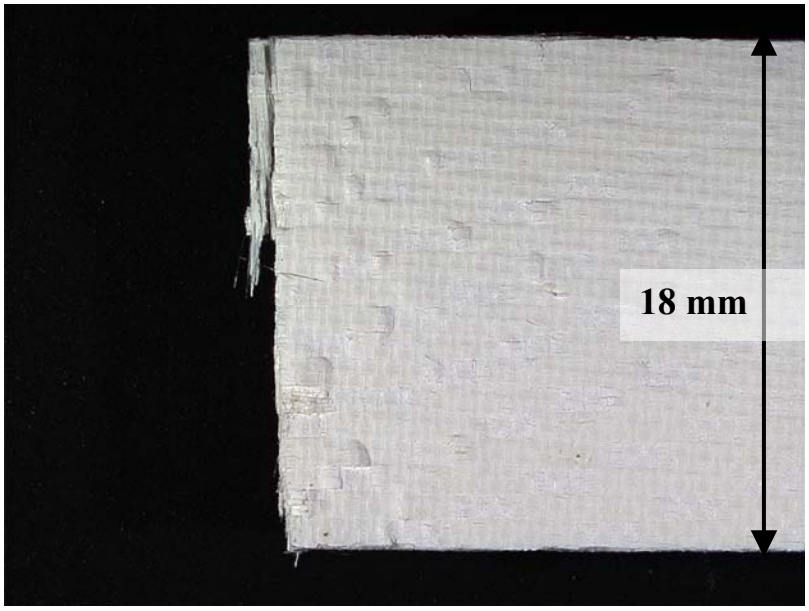

Figure 201. Fracture surface of N720/A specimen tested in compressive creep at -60 MPa for 100 h at 1200°C in steam.

Figure 202. Fracture surface of N720/A specimen tested in compressive creep at -60 MPa for 100 h at 1200°C in steam.

Figure 203. Fracture surface of N720/A specimen tested in compressive creep at -60 MPa for 100 h at 1200°C in steam.

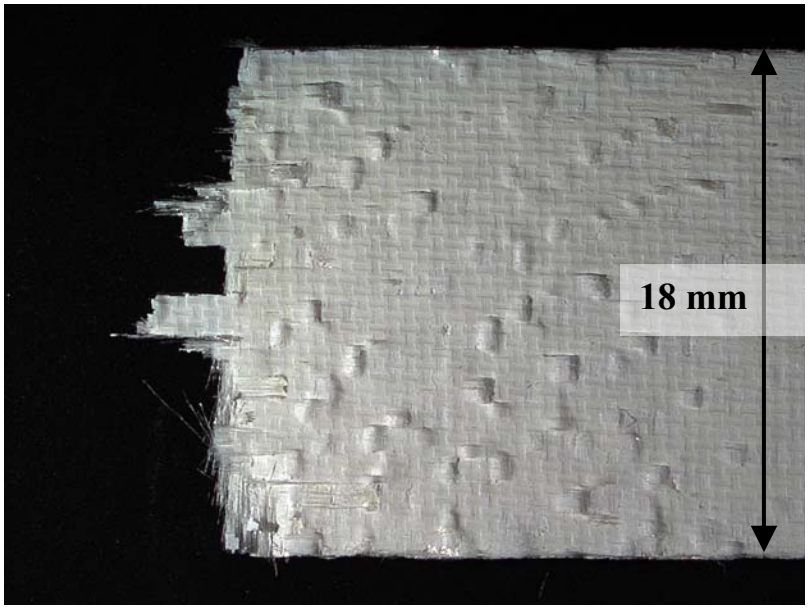

Figure 204. Fracture surface of N720/A specimen tested in compressive creep at -60 MPa for 100 h at 1200°C in steam.

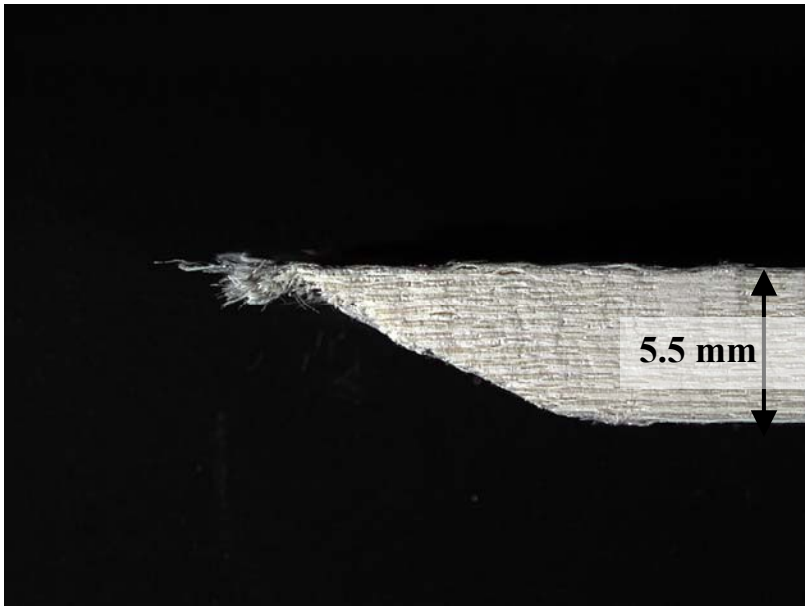

Figure 205 Fracture surface of N720/A specimen tested in compressive creep at -60 MPa for 100 h at 1200°C in steam.

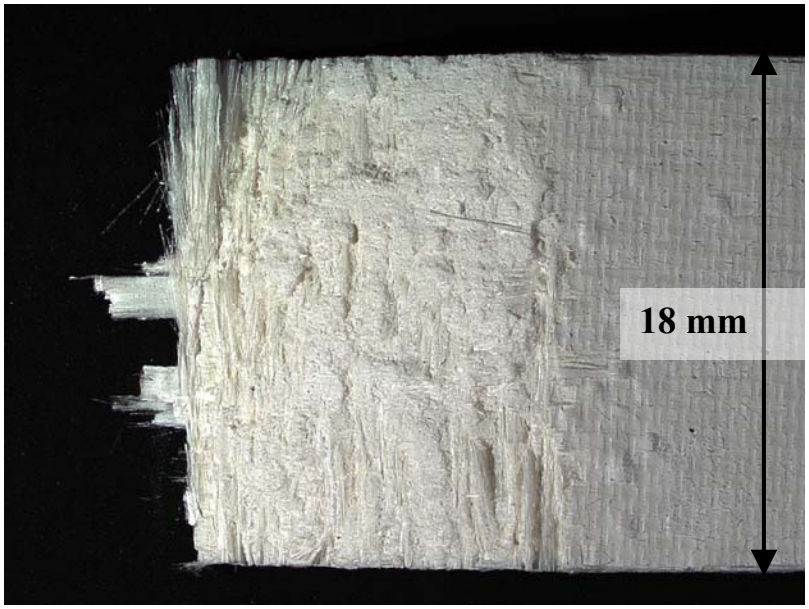

Figure 206. Fracture surface of N720/A specimen tested in compressive creep at -60 MPa for 100 h at 1200°C in steam.

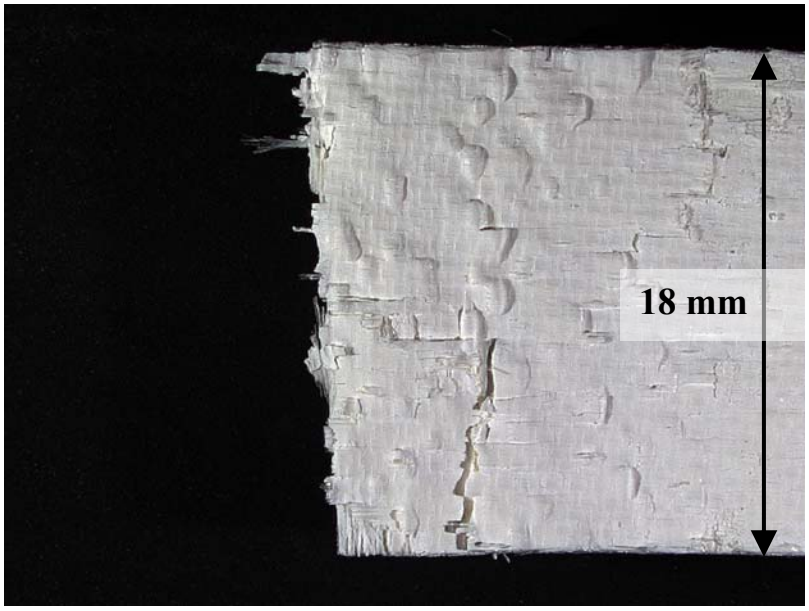

Figure 207. Fracture surface of N720/A specimen tested in compressive creep at -40 MPa for 100 h at 1200°C in steam.

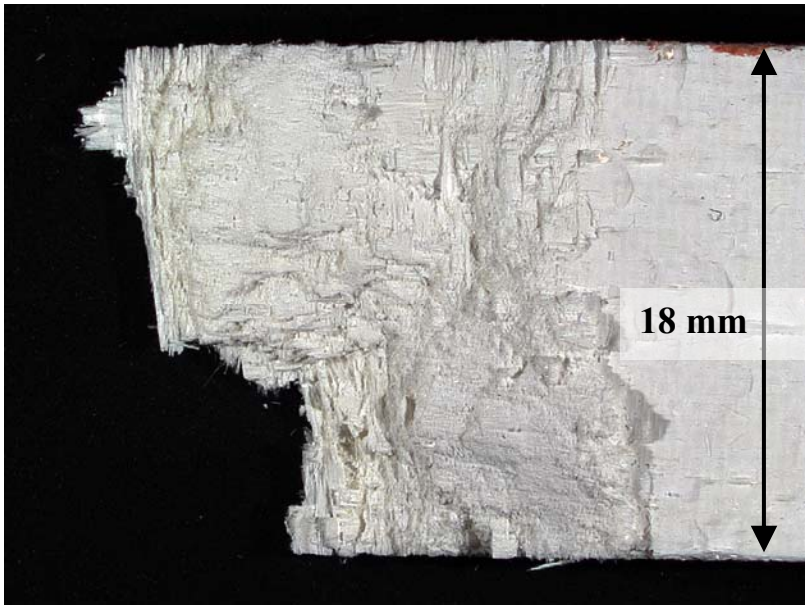

Figure 208. Fracture surface of N720/A specimen tested in compressive creep at -40 MPa for 100 h at 1200°C in steam.

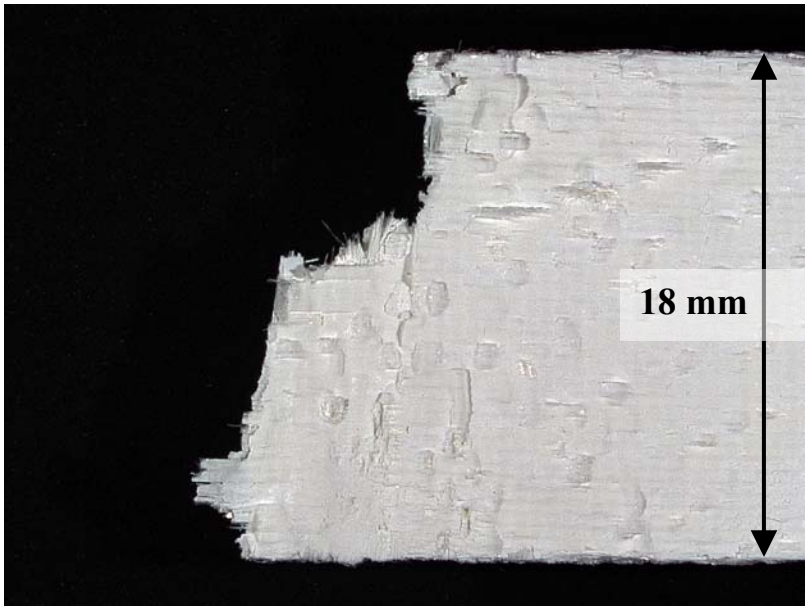

Figure 209. Fracture surface of N720/A specimen tested in compressive creep at -40 MPa for 100 h at 1200°C in steam.

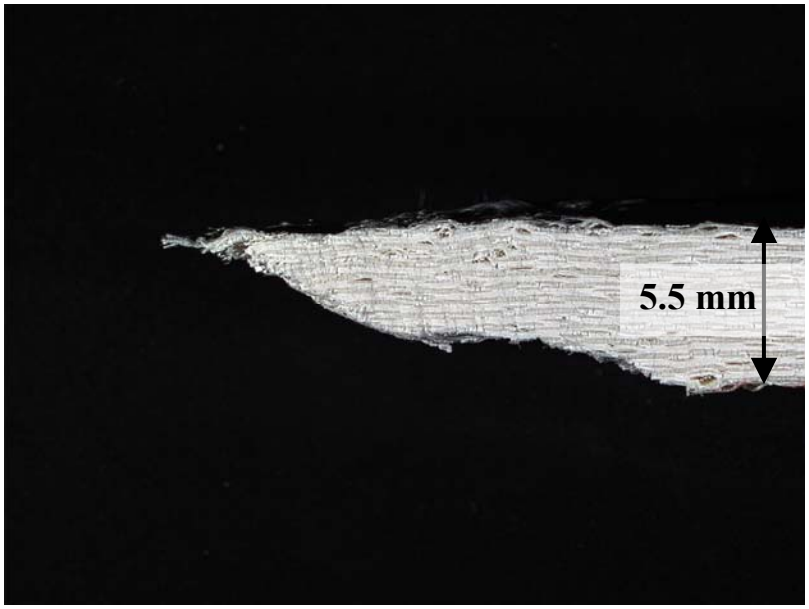

Figure 210. Fracture surface of N720/A specimen tested in compressive creep at -40 MPa for 100 h at 1200°C in steam.

Figure 211. Fracture surface of N720/A specimen tested in compressive creep at -40 MPa for 100 h at 1200°C in steam.

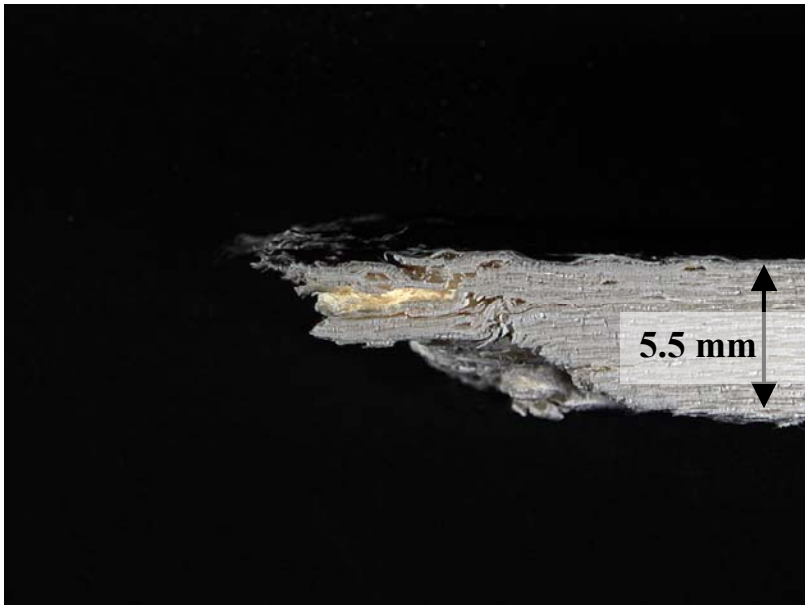

Figure 212. Fracture surface of N720/A specimen tested in compressive creep at -40 MPa for 100 h at 1200°C in steam.

Figure 213. Fracture surface of N720/A specimen tested in compressive creep at -40 MPa for 100 h at 1200°C in steam.

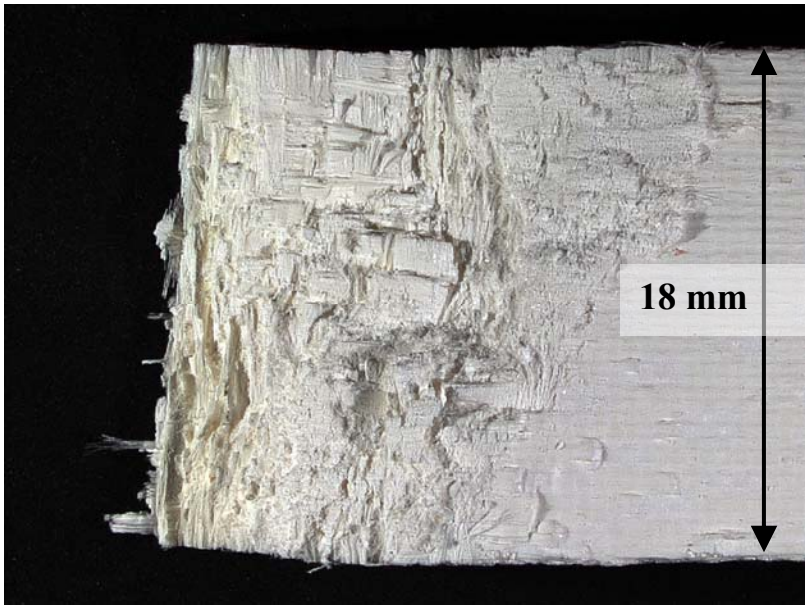

Figure 214. Fracture surface of N720/A specimen tested in compressive creep at -40 MPa for 100 h at 1200°C in steam.

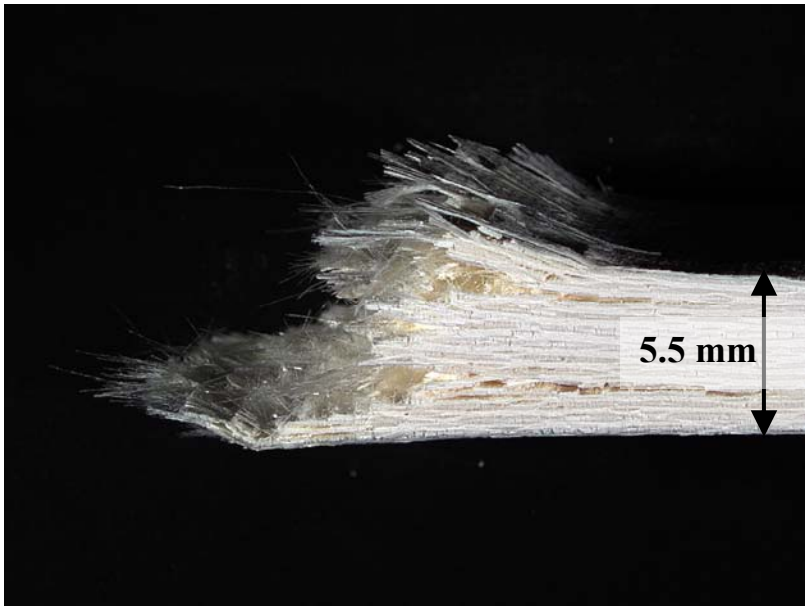

Figure 215. Fracture surface of N720/A specimen subjected to aging in steam at 1200°C for 25 h then failed in compression.

Figure 216. Fracture surface of N720/A specimen subjected to aging in steam at 1200°C for 25 h then failed in compression.

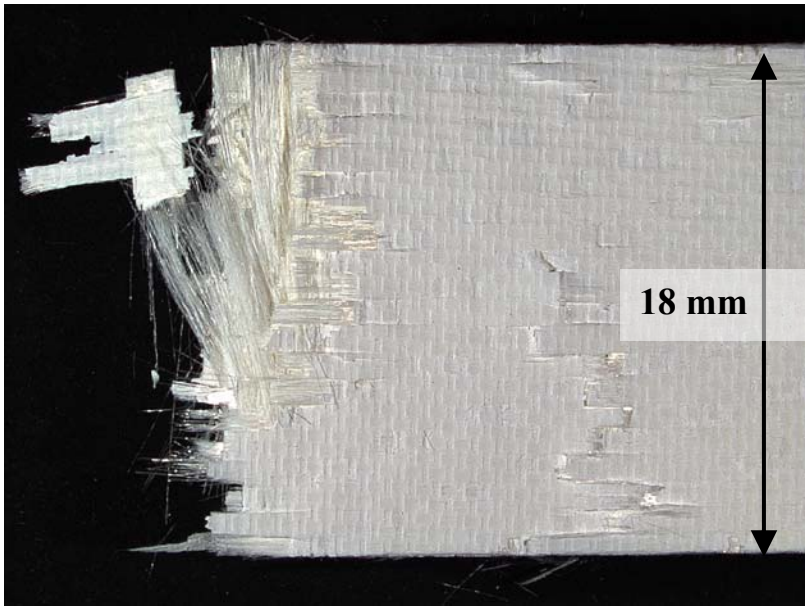

Figure 217. Fracture surface of N720/A specimen subjected to aging in steam at 1200°C for 25 h then failed in compression.

Figure 218. Fracture surface of N720/A specimen subjected to aging in steam at 1200°C for 25 h then failed in compression.

Figure 219. Fracture surface of N720/A specimen subjected to aging in steam at 1200°C for 25 h then failed in compression.

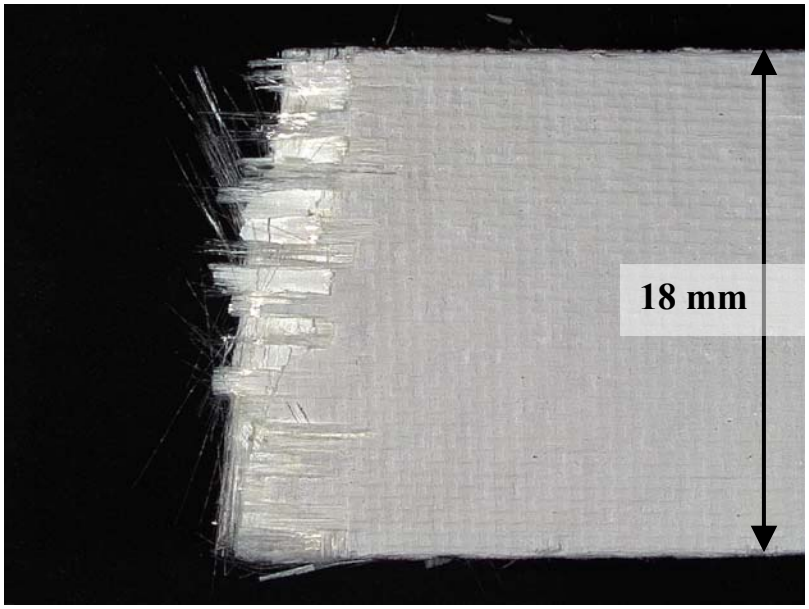

Figure 220. Fracture surface of N720/A specimen subjected to aging in steam at 1200°C for 25 h then failed in compression.

Figure 221. Fracture surface of N720/A specimen subjected to aging in steam at 1200°C for 25 h then failed in compression.

Figure 222. Fracture surface of N720/A specimen tested in compression to failure in steam at 1200°C in displacement control at -0.05 mm/s.

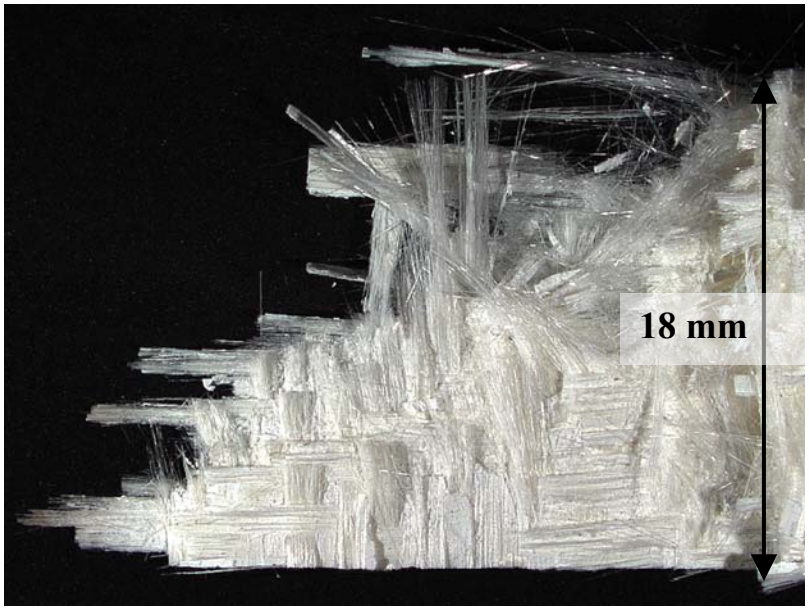

Figure 223. Fracture surface of N720/A specimen tested in compression to failure in steam at 1200°C in displacement control at -0.05 mm/s.

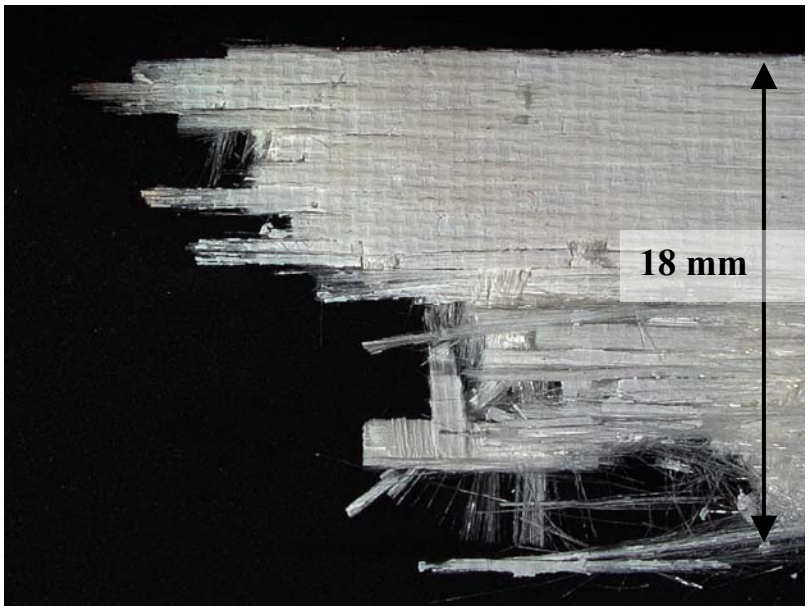

Figure 224. Fracture surface of N720/A specimen tested in compression to failure in steam at 1200°C in displacement control at -0.05 mm/s.

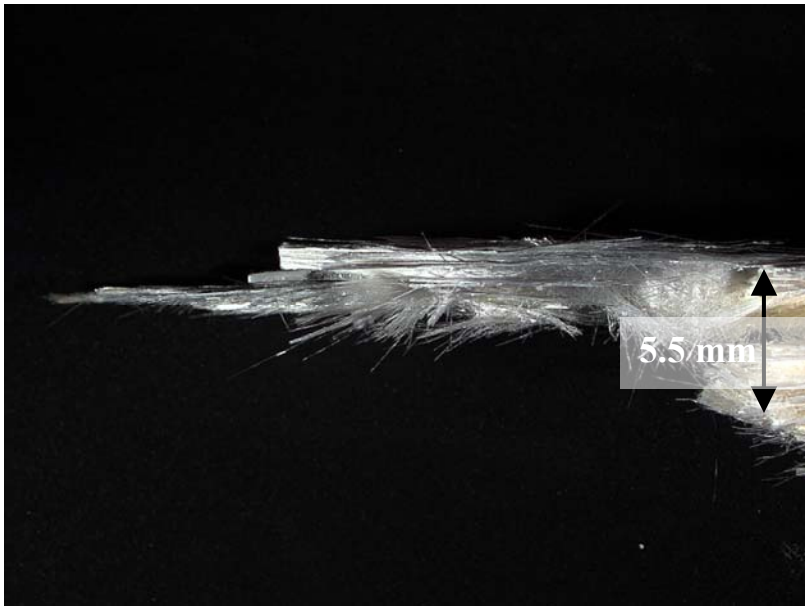

Figure 225. Fracture surface of N720/A specimen tested in compression to failure in steam at 1200°C in displacement control at -0.05 mm/s.

Figure 226. Fracture surface of N720/A specimen tested in compression to failure in steam at 1200°C in displacement control at -0.05 mm/s.

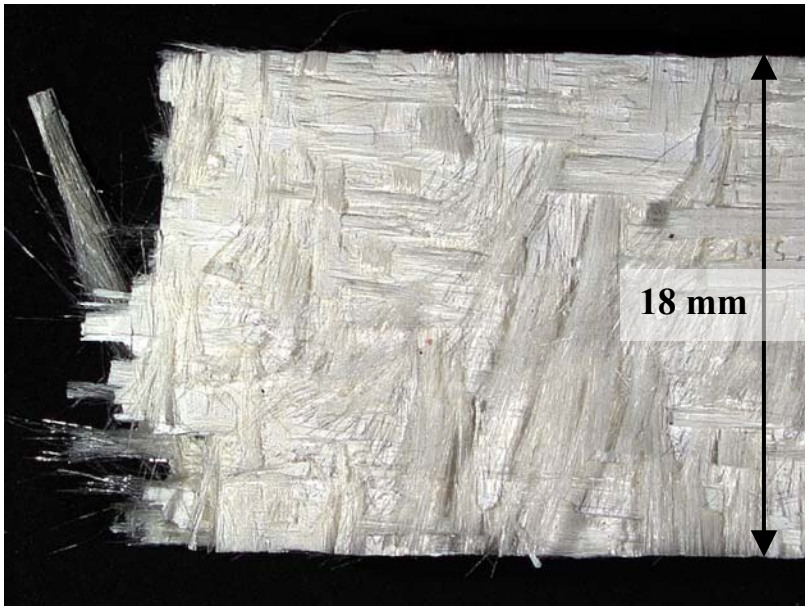

Figure 227. Fracture surface of N720/A specimen tested in compression to failure in steam at 1200°C in displacement control at -0.05 mm/s.

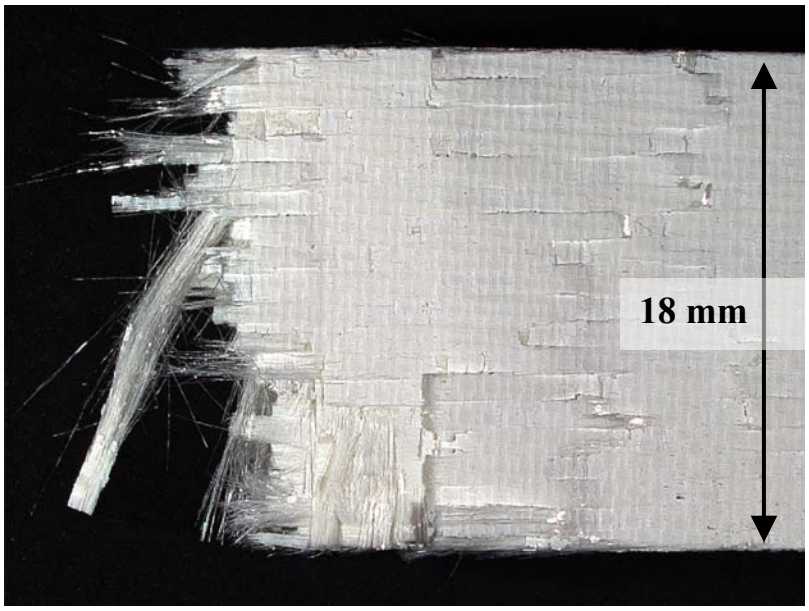

Figure 228. Fracture surface of N720/A specimen tested in compression to failure in steam at 1200°C in displacement control at -0.05 mm/s.

Figure 229. Fracture surface of N720/A specimen tested in compression to failure in steam at 1200°C in displacement control at -0.05 mm/s.

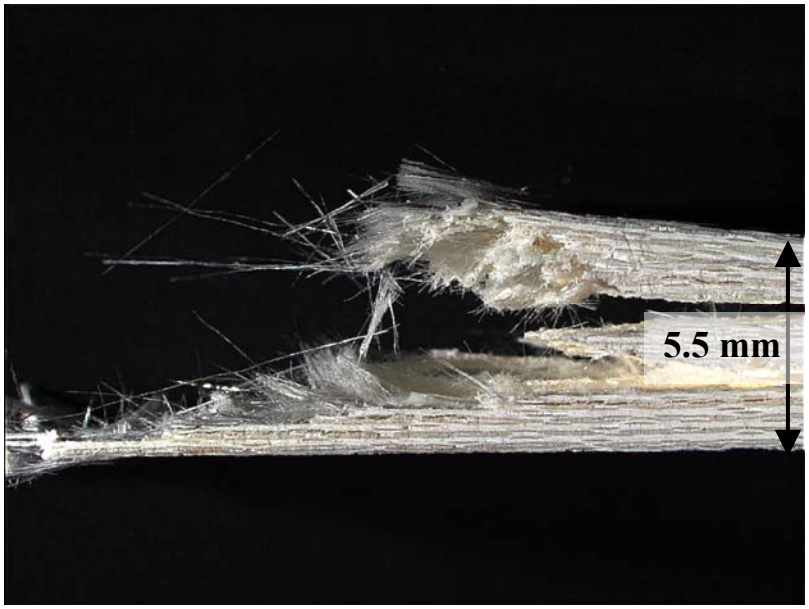

Figure 230. Fracture surface of N720/A specimen tested in compression to failure in air at 1200°C in stress control at -0.0025 MPa/s.

Figure 231. Fracture surface of N720/A specimen tested in compression to failure in air at 1200°C in stress control at -0.0025 MPa/s.

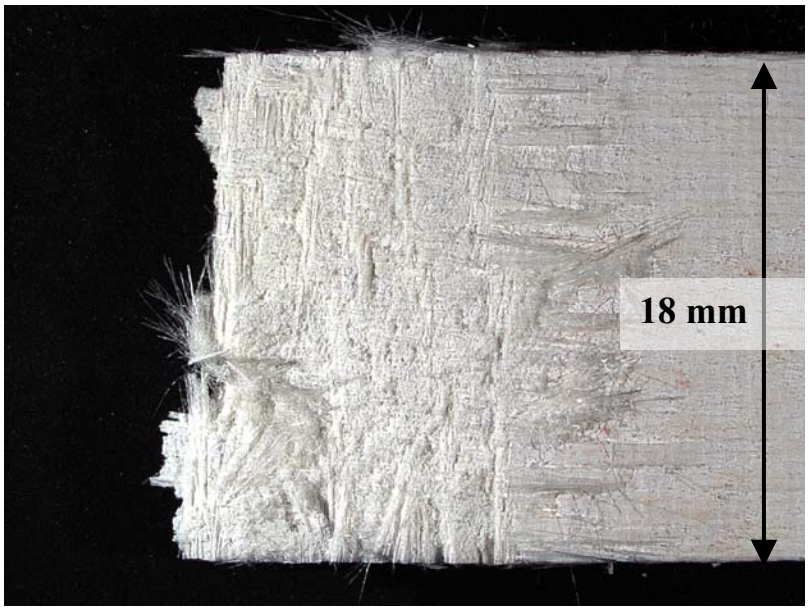

Figure 232. Fracture surface of N720/A specimen tested in compression to failure in air at 1200°C in stress control at -0.0025 MPa/s.

Figure 233. Fracture surface of N720/A specimen tested in compression to failure in air at 1200°C in stress control at -0.0025 MPa/s.

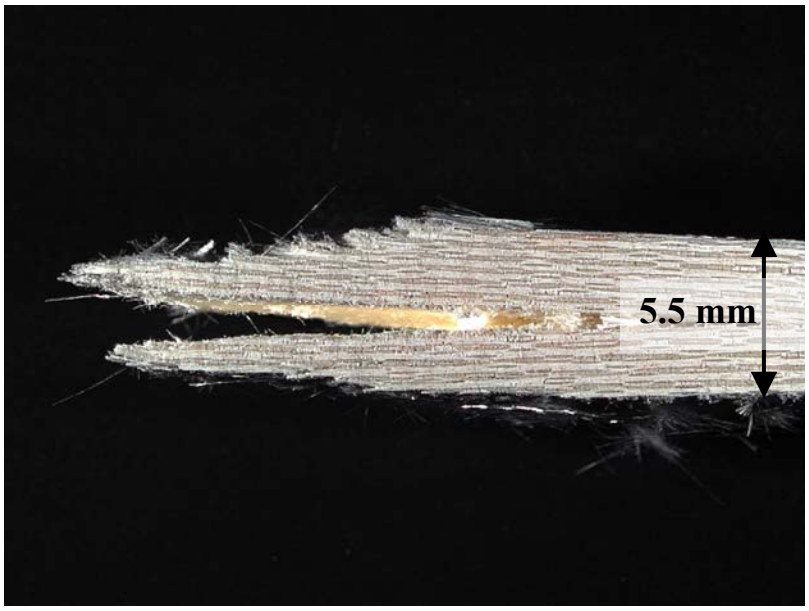

Figure 234. Fracture surface of N720/A specimen tested in compression to failure in air at 1200°C in stress control at -0.0025 MPa/s.

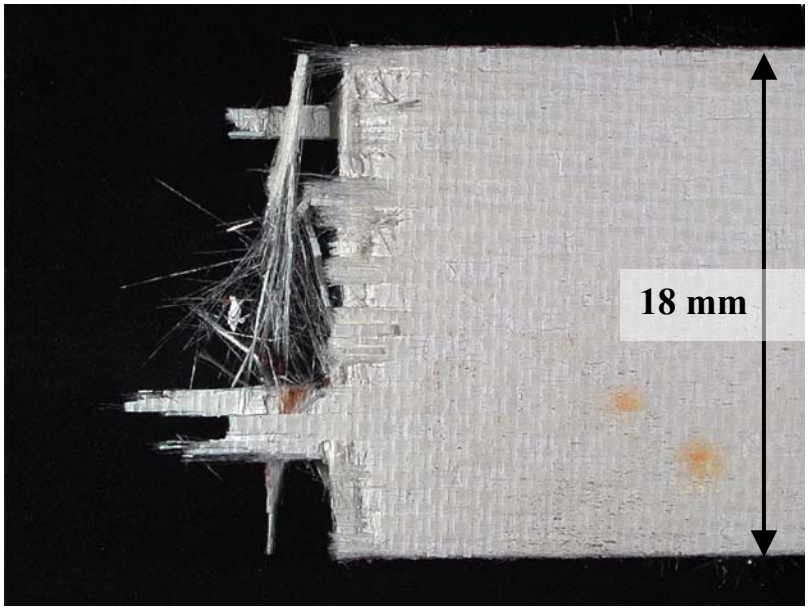

Figure 235. Fracture surface of N720/A specimen tested in compression to failure in air at 1200°C in stress control at -0.0025 MPa/s.

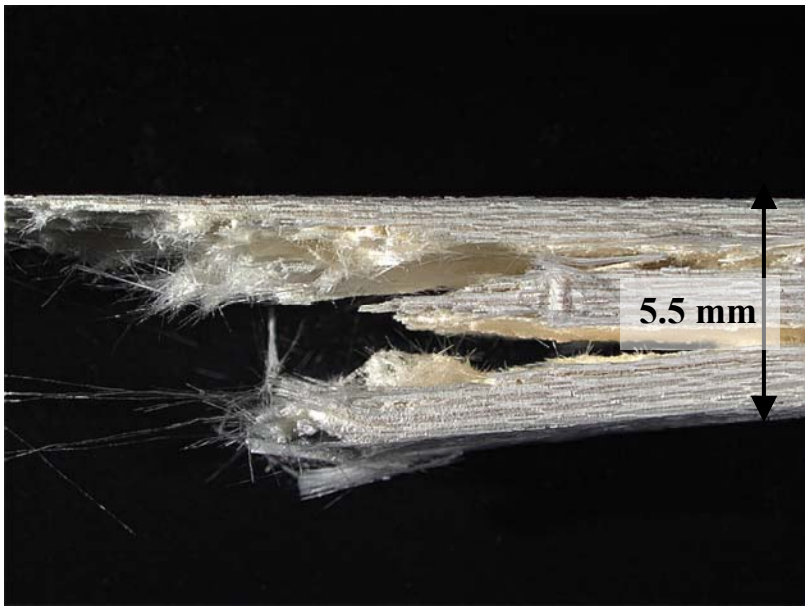

Figure 236. Fracture surface of N720/A specimen tested in compression to failure in air at 1200°C in stress control at -0.0025 MPa/s.

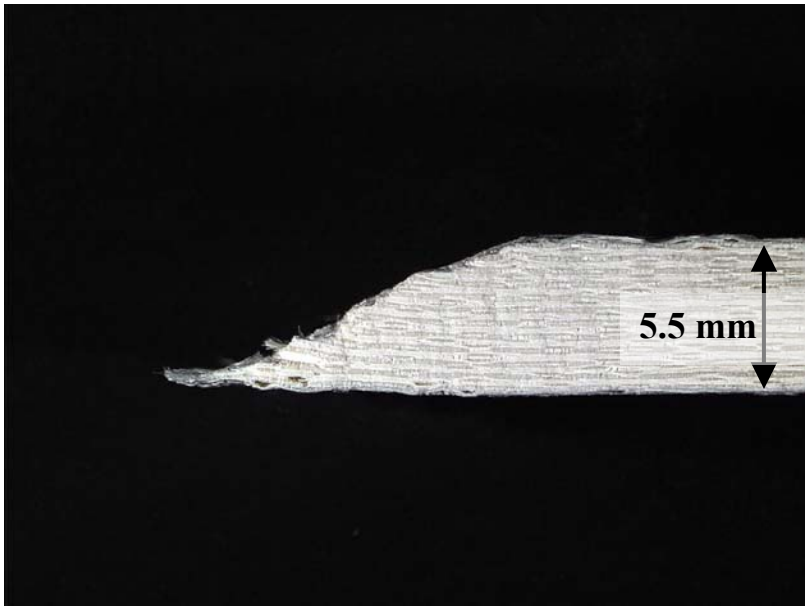

Figure 237. Fracture surface of N720/A specimen tested in compression to failure in steam at 1200°C in stress control at -0.0025 MPa/s.

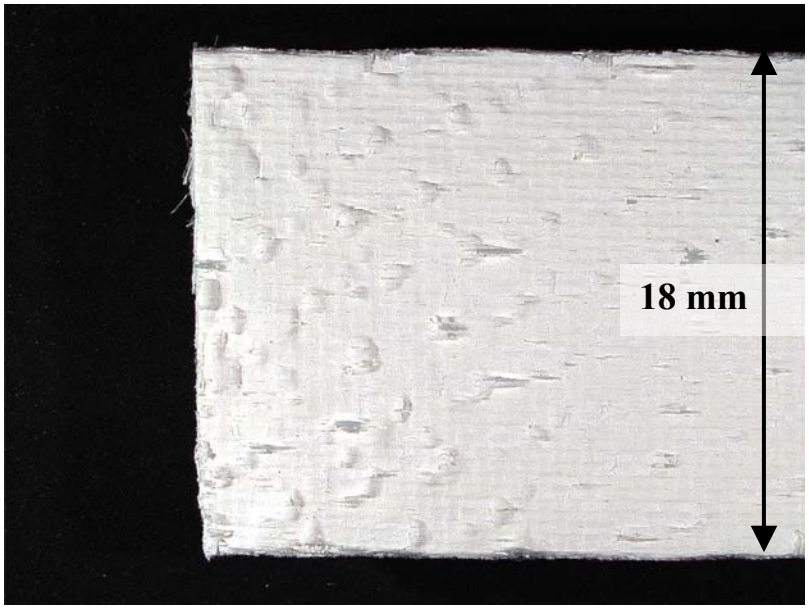

Figure 238. Fracture surface of N720/A specimen tested in compression to failure in steam at 1200°C in stress control at -0.0025 MPa/s.

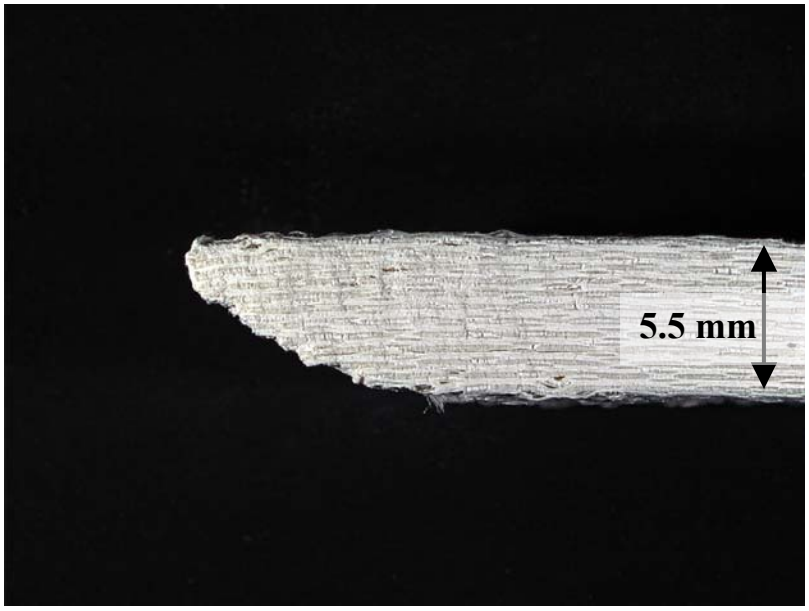

Figure 239. Fracture surface of N720/A specimen tested in compression to failure in steam at 1200°C in stress control at -0.0025 MPa/s.

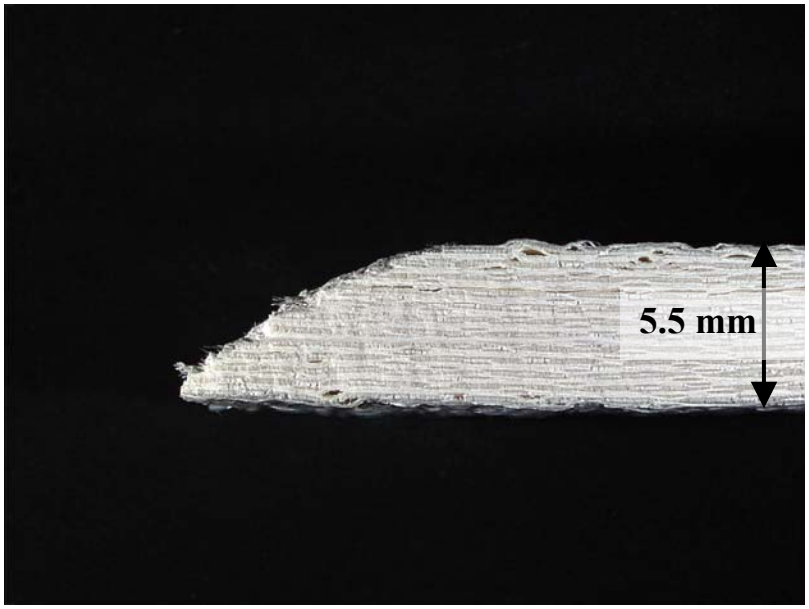

Figure 240. Fracture surface of N720/A specimen tested in compression to failure in steam at 1200°C in stress control at -0.0025 MPa/s.

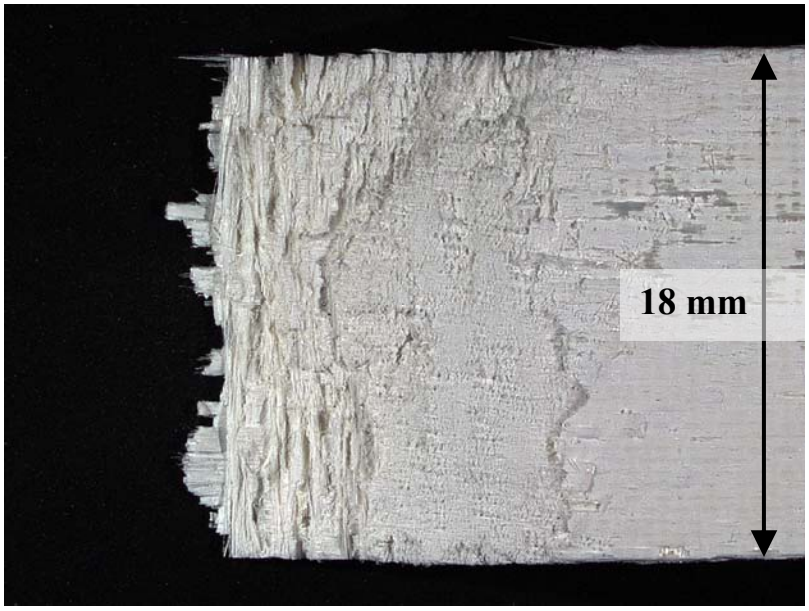

Figure 241. Fracture surface of N720/A specimen tested in compression to failure in steam at 1200°C in stress control at -0.0025 MPa/s.

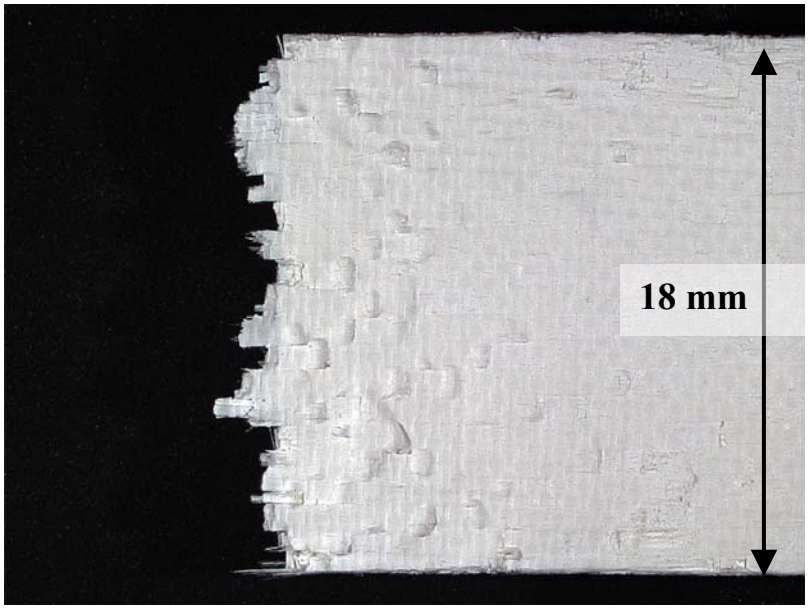

Figure 242. Fracture surface of N720/A specimen tested in compression to failure in steam at 1200°C in stress control at -0.0025 MPa/s.

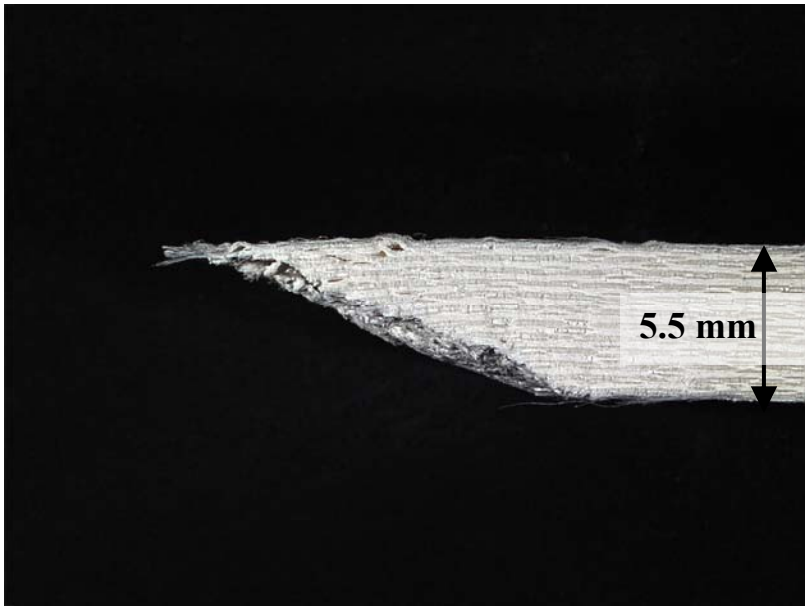

Figure 243. Fracture surface of N720/A specimen tested in compression to failure in steam at 1200°C in stress control at -0.0025 MPa/s.

Bibliography

1. All You Wanted to Know About Electron Microscopy…but Didn't Dare to Ask. Hillsboro, OR: FEI Company, no date. http//www.feicompany.com. 10 Feb 2006.

2. "F-22 Raptor Materials and Processes." Globalsecurity.Org. http://www.globalsecurity.org/military/systems/aircraft/f-22-mp.htm. 19 Dec. 2005.

3. "Report of the Committee on the Definition of the Term Ceramics," Journal of the American Ceramic Society, 3(7):526-542 (1920).

4. Antti, M-L, and Edgar Lara-Curzio. "Effect of Notches, Specimen Size, and Fiber Orientation on the Monotonic Tensile Behavior of Composites at Ambient and Elevated Temperatures," in 25th Annual Conference on Composites Advanced Ceramics Materials, and Structures: A. Ed. Mrityunjay Singh and Todd Jensen. Westerville, OH: The American Ceramic Society, 2001.

5. Baker, A., Dutton, S., Kelly, D. Composite Materials for Aircraft Structures (Second Edition). Virginia: AIAA, 2004.

6. Bernard-Granger, G. and Guizard, C. and Duclos, R. " Compressive Creep Behavior in Air of a Slightly Porous As-sintered Polycrystalline α-alumina material," Journal of Material Science, 42:2807-2819 (2007).

7. The Boeing Company, (Feb 2007), http://www.boeing.com

8. Buchanan, Dennis J., Reji John, and Larry P. Zawada. "Creep Rupture Behavior of ±45° Oxide/Oxide NextelTM720/AS Composite," in 25th Annual Conference on Composites Advanced Ceramics Materials, and Structures: A. Ed. Waltruad M. Kriven and Hau-Tay Lin. Westerville, OH: The American Ceramic Society, 2003.

9. Campbell, C.X., Carelli, E.V., More, K.L., Varghese, P., Seal, S., and V. H. Desai, "Effect of High-Temperature Water Vapor Exposure on Nextel 720 in an Alumina-Matrix CMC," Siemens Westinghouse Power Corporation Technical Document TP-02076.

10. Carelli, E.A., Fujita, H., Yang, J.Y., and Zok, F.W. "Effects of Thermal Aging on the Mechanical Properties of a Porous-Matrix Ceramic Composite," Journal of the American Ceramic Society, 85[3]: 595-602 (2002).

11. Casas, L., and Martínez-Esnaola J.M. "Microstructural characterization of an alumina/mullite composite tested in creep," Materials Science and Engineering, A368: 139-144 (2004).

12. Charles RJ, Hillig WB. “The kinetics of glass failure by stress corrosion,” in Symposium on Mechanical Strength of Glass and Ways of Improving It, Florence, Italy, September 25–29 (1961). Union Scientifique Continentale du Verre, Charleroi, Belgium, 1962. p. 511–527.

13. Charles R.J., and W.B. Hillig. “Surfaces, stress-dependent surface reactions, and strength,” in: High-strength materials. Ed. V.F. Zackey. New York, NY: Wiley, 1965. p. 682–705.

14. Chawla, K. K. Ceramic Matrix Composites (Second Edition). Boston: Kluwer Academic Publishers, 2003.

15. COI Ceramics, Unpublished Data.

16. Daniel, Isaac M. and Ori Ishai. Engineering Mechanics of Composite Materials. New York, NY: Oxford University Press, 1994.

17. DiCarlo, James A. and Sunil Dutta. “Continuous Ceramic Fibers for Ceramic Matrix Composites,” in Handbook on Continuous Fiber-Reinforced Ceramic Matrix Composites. Ed. Richard L. Lehman, Said K. El-Rahaiby, and John B. Wachtman, Jr.Westerville, OH: The American Ceramic Society, 1995.

18. Dowling, N.E. Mechanical Behavior of Materials (Second Edition). Upper Saddle River: Prentice-Hall, 1999.

19. Fujita, H., Levi, C. G., Zok, F. W., and G. Jefferson, “Controlling Mechanical Properties of Porous Mullite/Alumina Mixtures via Precursor-Derived Alumina,” Journal of the American Ceramic Society, 88[2]: 367-375 (2005).

20. Fujita, H., Jefferson, G., McMeeking, R.M., and F.W. Zok, “Mullite/Alumina Mixtures for Use as Porous Matrices in Oxide Fiber Composites,” Journal of the American Ceramic Society, 87[2]: 261-67 (2004).

21. Harada, Yoshihisa, Suzuki, Takayuki, and Hirano, Kazumi. “Influence of Moisture on Ultra-High-Temperature Tensile Creep Behavior of in Situ Single-Crystal Oxide Ceramic Alumina/Yttrium Aluminum Garnet Eutectic Composite,” Journal of the American Ceramic Society, 86: 951-958 (2003).

22. Harlan, Lee B. Creep-Rupture Behavior of an Oxide/Oxide Ceramic Matrix Composite at Elevated Temperatures in Air and Steam Environments. MS thesis, AFIT/GA/ENY/05-M05. School of Engineering and Management, Air Force Institute of Technology (AU), Wright-Patterson AFB OH, March 2005.

23. Haslam, J.J., Berroth, K.E., and Lange, F.F. “Processing and Properties of an all oxide composite with a porous matrix,” Journal of the European Ceramic Society, 20:607-618 (2000).

24. Haynes, J.A., Lance, M.J., Cooley, K.M., Ferber, M.K., Lowden, R.A., Stinton, D.P. “CVD Mullite Coating in High-Temperature, High-Pressure Air-H2O,” Journal of the American Ceramic Society, 83[3]:657-659 (2000).

25. Hetrick, Griffin. Effects of Frequency and Environment on Fatigue Behavior of an Oxide-Oxide Ceramic Matrix Composite at 1200 °C. MS thesis, AFIT/GA/ENY/06-J05. School of Engineering and Management, Air Force Institute of Technology (AU), Wright-Patterson AFB OH, June 2006.

26. Holmquist, M.G. and Lange, F.F. “Processing and Properties of a Porous Oxide Matrix Composite Reinforced with Continuous Oxide Fibers,” Journal of the American Ceramic Society, 86[10]:1799-40 (2003).

27. Jackson, Patrick R. Characterization of Compressive Creep Behavior of Oxide/Oxide Composite with Monazite Coating at Elevated Temperature. MS thesis, AFIT/GAE/ENY/06-M17. School of Engineering and Management, Air Force Institute of Technology (AU), Wright-Patterson AFB OH, March 2006.

28. Jackson P. R., Ruggles-Wrenn M. B., Baek S. S., K. A. Keller, “Tensile and Compressive Creep Behavior of an Oxide-Oxide Ceramic Composite with Monazite Fiber Coating at Elevated Temperatures”, Materials Science and Engineering A, Vol. 454-455, 2007, pp. 590-601.

29. Jacobson, N.S. “Corrosion of Silicon-Based Ceramics in Combustion Environments,” Journal of the American Ceramic Society, 76[1]:3-28 (1993).

30. Jacobson, N.S., Morscher, G.N., Bryant, D.R., Tressler, R.E. “High-Temperature Oxidation of Boron Nitride: II, Boron Nitride Layers in Composites,” Journal of the American Ceramic Society, 82[6]:1473-1482 (1999).

31. Jurf, R.A. and Butner, S.C. “Advances in Oxide-Oxide CMC”, Journal of Engineering for Gas Turbines and Engine Power, 122: 202-205 (April 2000).

32. Kaya, C., Butler, E.G., Selcuk, A., Boccaccini, A.R., and Lewis, M.H. “Mullite (Nextel™ 720) fibre-reinforced mullite matrix composites exhibiting favourable thermomechanical properties,” Journal of the European Ceramic Society, 22: 2333-2342 (2002).

33. Kerans, R.J. and Parthasarathy, T.A. “Crack deflection in ceramic composites and fiber coating design criteria,” Composites: Part A, 30:521-524 (1999).

34. Kooner, S., Westby, W.S., Watson, C.M.A., and Farries, P.M. “Processing of Nextel™720/mullite composition composite using electrophoretic deposition,” Journal of the European Ceramic Society, 20:631-638 (2000).

35. Korinek, L.M. and Castaing, J. “Slip and Twinning in Polycrystalline Alumina (α-Al_2O_3) Deformed under Hydrostatic Pressure between 600°C and 1000°C,” Journal of the American Ceramics Society, 4:566-573 (2003).

36. Lange, F.F., Tu, W.C., Evans, A.G. “Processing of damage-tolerant, oxidation resistant ceramic matrix composites by a precursor infiltration and pyrolysis method,” Materials Science and Engineering, A195:145-150 (1995).

37. LaRochelle, K.J. Tensile Stress Rupture Behavior of a Woven Ceramic Matrix Composite in Humid Environments at Intermediate Temperatures. Ph.D. dissertation, AFIT/DS/ENY/05-01. School of Engineering and Management, Air Force Institute of Technology (AU), Wright-Patterson AFB, OH March 2005.

38. Levi, Carlos G., James Y. Yang, Brian J. Dalgleish, Frank W. Zok, and Anthony G. Evans. “Processing and Performance of an All-Oxide Ceramic Composite,” Journal of the American Ceramic Society, 81[8]: 2077-86 (1998).

39. Lewis III, David. “Continuous Fiber-Reinforced Ceramic Matrix Composites: A Historical Overview,” in Handbook on Continuous Fiber-Reinforced Ceramic Matrix Composites. Ed. Richard L. Lehman, Said K. El-Rahaiby, and John B. Wachtman, Jr.Westerville, OH: The American Ceramic Society, 1995.

40. Mecham, Michael. "Composite Power." Aviation Week 17 Apr. 2006: 47-52.

41. Mehrman, J.M. Effect of Hold Times on Fatigue Behavior of Nextel™ 720/Alumina Ceramic Matrix Composite at 1200 °C in Air and in Steam Environment. MS thesis, AFIT/GA/ENY/06-M23. School of Engineering and Management, Air Force Institute of Technology (AU), Wright-Patterson AFB, OH March 2006.

42. Mehrman, J. M., Ruggles-Wrenn M. B., Baek S. S., “Influence of Hold Times on the Elevated-Temperature Fatigue Behavior of an Oxide-Oxide Ceramic Composite in Air and in Steam Environment”, Composites Science and Technology, Vol. 67, No. 7-8, 2007, pp. 1425-1438.

43. Michalske, T.A. and B.C. Bunker. “A chemical kinetics model for glass fracture,” Journal of the American Ceramic Society, 76[10]: 2613-2618 (1993).

44. Michalske, T.A., and S.W. Frieman. “A molecular mechanism for stress corrosion in vitreous silica,” Journal of the American Ceramic Society, 66[4]: 284-288 (1983).

45. Minnesota Mining and Manufacturing Company (3M™). “Nextel™ Ceramic Textiles Technical Notebook,” Company produced technical notebook. No date

46. Morscher, G.N., Bryant, D.R., Tressler, R.E. “Environmental Durability of BN Based (For SiC/SiC Composites) in H2O-Containing Atmospheres at Intermediate Temperatures,” Ceramic Engineering and Science Proceedings, 18[3]: 525-533 (1997).

47. Musikant, S. What Every Engineer Should Know About Ceramics. New York: Marcel Dekker, 1991.

48. Musil, Sean S. Characterization of Creep Behavior of Oxide/Oxide Composite with Monazite Coating at Elevated Temperature. MS thesis, AFIT/GAE/ENY/05-M14. School of Engineering and Management, Air Force Institute of Technology (AU), Wright-Patterson AFB OH, March 2005.

49. Nutt, S.R., “Environmental Effects on High Temperature Mechanical Behavior of Ceramic Matrix Composites,” High Temperature Mechanical Behavior of Ceramic Composites. Newton, MA: Butterworth-Heinemann, 1995.

50. Oates, G.C. Aerothermodynamics of Gas Turbine and Rocket Propulsion, 3rd Ed. Reston, VA: American Institute of Aeronautics and Astronautics, Inc 1997.

51. Ogbuji, L.U. “Degradation of SiC/BN/SiC Composite in the Burner Rig,” Ceramic Engineering and Science Proceedings, 19[4]: 257-264 (1998).

52. Ohnabe, H., Masaki, S., Onozuka, M., Miyahara, K., Sasa, T. “Potential application of ceramic matrix composites to aero-engine components,” Composites: Part A, Applied Science and Manufacturing 30: 489-496 (1999).

53. Parlier, M. and Ritti, M.H. “State of the art and perspectives for oxide/oxide composites,” Aerospace Science and Technology, 7: 211-221 (2003).

54. Parthasarathy, T.A., Zawada, L.P., John, R., Cinibulk, M. K., Kerans, R. J., and Zelina, J. “Evaluation of Oxide-Oxide Composites in a Novel Combustor Wall Application,” International Journal of Applied Ceramic Technology, 2 (2): 122-132 (2005).

55. Radsick, T., Saruhan, B., and Schneider, H. “Damage tolerant oxide/oxide fiber laminate composites,” Journal of the European Ceramic Society, 20: 545-550 (2000).

56. Radzicki, Andy T. Rate-Dependence of Tensile Properties and Stress-Strain Behavior of an Oxide/Oxide Ceramic Matrix Composite at Elevated Temperature and the Effects of Low-Magnitude Sustained Loading on Composite Microstructure. MS thesis, AFIT/GAE/ENY/06-S09. School of Engineering and Management, Air Force Institute of Technology (AU), Wright-Patterson AFB OH, September 2006.

57. Ramulu, M., Prasad, N.E., Malakondaiah, G. and Guo, Z. "Secondary Processing Effects and Damage Mechanisms in Continuous-Fiber Ceramic Composites," Thermal and Mechanical Test Methods and Behavior of Continuous-Fiber Ceramic Composites, ASTM STP 1309, Michael G. Jenkins, Stephan T. Gonczy, Edgar Lara-Curzio, Noel E. Ashbaugh, and Larry P. Zawada, Eds., American Society for Testing and Materials (1997).

58. Raymer, D.P. Aircraft Design: A Conceptual Approach, 3rd Edition. Reston, VA: American Institute of Aeronautics and Astronautics, Inc, 1999.

59. Ruggles-Wrenn M. B., Hetrick G., Baek S. S., "Effects of Frequency and Environment on Fatigue Behavior of an Oxide-Oxide Ceramic Composite at 1200 °C", International Journal of Fatigue, in press.

60. Ruggles-Wrenn M. B., Mall S., Eber C. A., Harlan L. B., "Effects of Steam Environment on High-Temperature Mechanical Behavior of Nextel™720/ Alumina (N720/A) Continuous Fiber Ceramic Composite", Composites Part A: Applied Science and Manufacturing, Vol. 37, No. 11, 2006, pp. 2029-2040.

61. Ruggles-Wrenn M. B., Musil S. S., Mall S., Keller K. A., "Creep-Rupture Behavior of Nextel™610/ Monazite/Alumina Composite at Elevated Temperatures", Composites Science and Technology, Vol. 66, No. 13, 2006, pp. 2089-2099.

62. Ruggles-Wrenn M. B., Siegert G. T., Baek S. S., "Creep Behavior of Nextel™720/Alumina Ceramic Composite with ±45° Fiber Orientation at 1200 °C", Composites Science and Technology, in press.

63. Saruhan, Bilge. Oxide-Based Fiber-Reinforced Ceramic Matrix Composites: Principles and Materials. Boston: Kluwer Academic Publishers, 2003.

64. Schmidt, S., Beyer, S., Knabe, H., Immich, H., Mestring, R., and Gessler, A. "Advanced ceramic matrix composite materials for current and future propulsion technology applications," Acta Astronautica, 55: 409-420 (2004).

65. Siegert, G. Effect of Environment on Creep Behavior of an Oxide/Oxide CFCC with ±45° Fiber Orientation. MS thesis, AFIT/GA/ENY/06-J15. School of Engineering and Management, Air Force Institute of Technology (AU), Wright-Patterson AFB, OH June 2006.

66. Steel, Steven G. Monotonic and Fatigue Loading Behavior of an Oxide/Oxide Ceramic Matrix Composite. MS thesis, AFIT/GMS/ENY/00M-02. School of Engineering and Management, Air Force Institute of Technology (AU), Wright-Patterson AFB OH, March 2000.

67. Tressler, R.E. “Recent developments in fibers and interphases for high temperature ceramic matrix composites,” Composites: Part A, 30: 429-437 (1999).

68. Tu, W.C., Lange, F.F., Evans, A.G. “Concept for a Damage-Tolerant Ceramic Composite with Strong Interfaces,” Journal of the American Ceramic Society, 79[2]: 417-424 (1996).

69. Wannaparhun S., Seal S., Desai V.H., Varghese P. Campbell, C.X. “A Combined Spectroscopic and Thermodynamic Investigation of Nextel-720/alumina Ceramic Matrix Composite in Air and Water Vapor at 1100 °C,” Journal of the American Ceramic Society, 86[9]: 1628-1630 (2003).

70. Wiederhorn, S.M.. “Influence of water vapor on crack propagation in soda-lime glass,” Journal of the American Ceramic Society, 50[8]: 407–14 (1967).

71. Wiederhorn S.M., and L.H. Bolz. “Stress corrosion and static fatigue of glass,” Journal of the American Ceramic Society, 53[10]: 543–8 (1970).

72. Wiederhorn S.M. “A chemical interpretation of static fatigue,” Journal of the American Ceramic Society, 55[2]: 81–85 (1972).

73. Wiederhorn, S. M. , Freiman S. W., Fuller, E. R. , and C. J. Simmons, “Effects of Water and Other Dielectrics on Crack Growth,” Journal of Material Science, 17: 3460-3478 (1982).

74. Wkipedia http://en.wikipedia.org/wiki/Airbus_A380

75. Wikipedia http://en.wikipedia.org/wiki/Composites

76. Wilson, D.M. and Visser, L.R. “High Performance Oxide Fibers for Metal and Ceramic Composites,” Composites: Part A, 32[8]: 1143-1153 (2001).

77. Wilson, D.M., Lieder, S.L., and D.C. Luenegurg, “Microstructure and high temperature properties of Nextel 720 fibers,” Ceramic Engineering and Science Proceedings, 16[5]: 1005–1014 (1995).

78. Zawada, L.P. “Longitudinal and transthickness tensile behavior of several oxide/oxide composites,” Ceramic Science and Engineering Proceedings, 19[3]: 327-340 (1998).

79. Zok, W. and Carlos G. Levi. “Mechanical Properties of Porous-Matrix Ceramic Composites,” Advanced Engineering Materials, 3[1-2]: 15-23 (2001).

Vita

Ensign Neil R. Szymczak graduated from Natick High School in Natick, Massachusetts. In 2002, he was appointed to the United States Naval Academy in Annapolis, Maryland. In 2006, he graduated with a Bachelor of Science degree in Ocean Engineering. He received a commission as a United States Naval Officer on 26 May 2006 through the United States Naval Academy.

His first assignment was at Wright Patterson Air Force Base in Dayton, Ohio. In summer 2006 he entered the Graduate School of Engineering and Management, Air Force Institute of Technology. Upon graduation, he will be assigned to NAS Whiting Field in Milton, Florida where he will commence United States Navy Primary Flight Training.

REPORT DOCUMENTATION PAGE

Form Approved
OMB No. 074-0188

1. REPORT DATE *(DD-MM-YYYY)*	2. REPORT TYPE	3. DATES COVERED *(From – To)*
17-06-2006	Master's Thesis	JUN 2006 – JUN 2007

4. TITLE AND SUBTITLE

Compressive Creep Behavior of NEXTEL™ 720/Alumina Ceramic Matrix Composite at 1200°C in Air and in Steam Environment

5a. CONTRACT NUMBER

5b. GRANT NUMBER

5c. PROGRAM ELEMENT NUMBER

6. AUTHOR(S)

Szymczak, Neil, R., Ensign, USN

5d. PROJECT NUMBER

5e. TASK NUMBER

5f. WORK UNIT NUMBER

7. PERFORMING ORGANIZATION NAMES(S) AND ADDRESS(S)

Air Force Institute of Technology
Graduate School of Engineering and Management (AFIT/EN)
2950 Hobson Way, Building 640
WPAFB OH 45433-8865

8. PERFORMING ORGANIZATION REPORT NUMBER

AFIT/GAE/ENY/07-J20

9. SPONSORING/MONITORING AGENCY NAME(S) AND ADDRESS(ES)

AFRL/PRTS
Attn: Dr. Ruth Sikorsky
1950 Fifth Street
WPAFB OH 45433-7251

AFRL/PRTS
Attn: Dr. Charles Cross
2977 P Street
WPAFB OH 45433-7734

10. SPONSOR/MONITOR'S ACRONYM(S)

11. SPONSOR/MONITOR'S REPORT NUMBER(S)

12. DISTRIBUTION/AVAILABILITY STATEMENT

APPROVED FOR PUBLIC RELEASE; DISTRIBUTION UNLIMITED.

13. SUPPLEMENTARY NOTES

14. ABSTRACT

The aerospace community continues to push the envelope in engineering aircraft that fly higher, faster, and safer while operating with a greater degree of efficiency. To meet these operational requirements innovative aerospace components must be designed to operate in aggressive environments. This research will investigate the ultimate compressive strength and the compressive creep behavior of Nextel™ 720/Alumina ceramic matrix composite at 1200°C in air and 100% steam environments. The effects of creep loading history on the tensile and compressive material behavior will also be examined. The primary strengths of the N720/A composite are its oxide/oxide composition which inherently resists oxidation and a porous matrix which enables crack deflection producing enhanced matrix damage tolerance.

Mechanical testing showed a significant decrease in the compressive performance of N720/A when exposed to steam environment. Conversely, N720/A specimens tested in compressive creep in air experienced an increase in compressive performance. SEM analysis showed that densification of the α-alumina matrix occurred in both test environments. In air densification sinters the matrix resulting in a strengthening effect. Whereas, in steam environment analysis shows the addition of hydrogen induces hydrothermal softening of the matrix resulting in a significant loss of the compressive performance of N720/A.

15. SUBJECT TERMS

Ceramic Matrix Composites, Composite Materials, Ceramic Fibers, Ceramic Materials, Fiber Reinforced Composites, Alumina, Mullite, Creep, Oxides, Nextel 720 ™ Fiber

16. SECURITY CLASSIFICATION OF:			17. LIMITATION OF ABSTRACT	18. NUMBER OF PAGES	19a. NAME OF RESPONSIBLE PERSON
REPORT	ABSTRACT	c. THIS PAGE			Dr. Marina B. Ruggles-Wrenn (ENY)
U	U	U	UU	231	19b. TELEPHONE NUMBER *(Include area code)* (937) 255-3636, ext 4641; email: marina.ruggles-wrenn@afit.edu